



Universiteit
Leiden
The Netherlands

Click-to-release for immune cell activation

Barendrecht, A.

Citation

Barendrecht, A. (2024, February 13). *Click-to-release for immune cell activation*. Retrieved from <https://hdl.handle.net/1887/3717016>

Version: Publisher's Version

License: [Licence agreement concerning inclusion of doctoral thesis in the Institutional Repository of the University of Leiden](#)

Downloaded from: <https://hdl.handle.net/1887/3717016>

Note: To cite this publication please use the final published version (if applicable).

Click-to-Release for Immune Cell Activation

Proefschrift

ter verkrijging van
de graad van doctor aan de Universiteit Leiden,
op gezag van rector magnificus prof.dr.ir. H. Bijl,
volgens besluit van het college voor promoties
te verdediging op dinsdag 13 februari 2024
klokke 15:00 uur
door

Amber Barendrecht
geboren te Dirksland
in 1994

Promotor:

Prof. dr. S. I. van Kasteren

Co-promotor:

Dr. Z. W. B. Armstrong

Promotiecommissie:

Prof. dr. M. Ubbink

Prof. dr. J. D. C. Codee

Prof. dr. L. J. C. Jeuken

Prof. dr. M. Travis (University of Manchester)

Dr. A. S. Wentink

Dr. M. Verdoes (Radboud Universiteit)

ISBN: 978-94-6483-704-9

Printed by Ridderprint

Cover design by Noëlle van Egmond

All rights reserved. No part of this book may be reproduced in any manner or by any means without permission.

Table of contents

List of Abbreviations	5
Chapter 0 General Introduction	7
Chapter 1 Mini-review – Immunocytokines: a New Tool in the Fight Against Cancer	13
Chapter 2 Chemical Inactivation and Reactivation of an IL-1 β -Based Immunocytokine using Click-to-Release Chemistry	35
Chapter 3 TNF- α : Chemical Inactivation and Reactivation of a Master Regulator Cytokine	77
Chapter 4 Towards Crystallization of Recombinant HLA-DR1	111
Chapter 5 Summary & Future Prospects	147
Nederlandse Samenvatting	161
List of Publications	164
<i>Curriculum Vitae</i>	165
Dankwoord	167

List of Abbreviations

ACN	acetonitrile
ADC	antibody-drug conjugate
AKT	protein kinase B
ANOVA	analysis of variance
BEVS	baculovirus expression vector system
Bp	base pair
BSA	bovine serum albumin
CCO	cis-cyclooctene
CEA	carcino-embryonic antigen
ciAP	cellular inhibitor of apoptosis protein
CM	carboxymethyl
CTLA	cytotoxic T-lymphocyte-associated protein
DEAE	diethylaminoethyl
DMEM	Dulbecco's Modified Eagle's Medium
DMSO	dimethylsulfoxide
DNA	deoxyribonucleic acid
dNTP	deoxyribose nucleoside triphosphate
DTT	dithiothreitol
EDA	extra-domain A of fibronectin
EDB	extra-domain B of fibronectin
EDTA	ethylenediaminetetraacetic acid
EGFR	epidermal growth factor receptor
ELISA	enzyme-linked immunosorbent assay
ER	endoplasmic reticulum
ESI	electrospray ionization
FA	formic acid
FAP	fibroblast activating protein
FCS	Fetal Calf Serum
GAG	glycosaminoglycan
GM-CSF	granulocyte-macrophage colony-stimulating factor
GnTI	<i>N</i> -acetylglucosaminyltransferase I
HEK	human embryonic kidney
HER2	human epidermal growth factor receptor 2
HLA	human leukocyte antigen
HRP	horseradish peroxidase
IC	immunocytokine
IEDDA	inverse-electron demand Diels-Alder
IFN	interferon
IL	interleukin
IL-1RAcP	interleukin-1 receptor accessory protein
IPTG	isopropyl β -D-thiogalactopyranoside
Iv	intravenous
kDa	kilodalton
LB	lysogeny broth
LC-MS	liquid chromatography-mass spectrometry
LUBAC	linear ubiquitin chain assembly complex
M	marker

MAPK	mitogen-activated protein kinase
MHC	major histocompatibility complex
MDSC	myeloid-derived suppressor cell
MLKL	mixed lineage kinase domain-like protein
MMP	matrix metalloproteinase
NCS	Newborn Calf Serum
NF- κ B	nuclear factor kappa B
Ni	nickel
NK	natural killer
OD	optical density
PAGE	polyacrylamide gel electrophoresis
PAMP	pathogen-associated molecular pattern
PBS	phosphate buffered saline
PCR	polymerase chain reaction
PD-L1	programmed death-ligand 1
PEI	polyethylenimine
PMSF	phenylmethylsulfonylfluoride
PRR	pattern recognition receptor
PSA	polysaccharide A1
rcf	relative centrifugal force
RIPK	receptor-interacting serine/threonine protein kinase
RNA	ribonucleic acid
rpm	revolutions per minute
scFv	single-chain variable fragment
SDS	sodium dodecyl sulfate
SEAP	secreted embryonic alkaline phosphatase
SEC	size-exclusion chromatography
SEC-MALS	size-exclusion chromatography multi-angle light scattering
SEM	standard error of the mean
SP1	<i>Streptococcus pneumoniae</i> 1
TBS	tert-butyldimethylsilyl
TCO	trans-cyclooctene
TEV	tobacco etch virus
TLR	Toll-like receptor
TME	tumour-microenvironment
TNF	tumour necrosis factor
TNFR	tumour necrosis factor receptor
TRADD	TNF receptor-associated death domain
TRAF	TNFR-associated factor
Treg	T-regulatory
Tz	tetrazine
VEGF	vascular endothelial growth factor
YFP	yellow fluorescence protein
ZPS	zwitterionic polysaccharide

0

General Introduction

Bioorthogonal Bond Making/Breaking Chemistry

In 2022 Carolyn Bertozzi, Morton Meldal and K. Barry Sharpless were rewarded the Nobel Prize in Chemistry for their work in the development of click chemistry and bioorthogonal chemistry.¹ This new chemistry can be defined as highly selective, mild chemistry that can be performed in a wide variety of solvents.² Bertozzi took this a step further and developed a set of reactions that are *bioorthogonal*, meaning that they were so mild and selective that they could be performed in biological samples; from cell lines to mice.^{3,4}

Initially, these reactions all focused on the making of new chemical bonds in the biological environment. However, in a reversal of this context, Meggers and co-workers described a bioorthogonal bond breaking reaction in 2006.^{5,6} Here they used a Ru-complex to remove an allyl group in a living cell. This new and exciting concept was further expanded by the introduction of a Staudinger reduction to cleave a bond, but – most relevant for this thesis – also the use of an inverse-electron demand Diels-Alder (IEDDA)-pyridazine mediated elimination reaction, developed by Robillard and co-workers.^{7,8} This reaction employs the highly selective ligation of electron-poor dienes and electron-rich/strained dienophiles to first ligate two reagents together (**Figure 1A**). Then by positioning a leaving group at the allylic position of the double bond, the 4,5-dihydropyridazine intermediate can rearrange to a 1,4-dihydropyridazine and eliminate this allylic substituent ‘releasing’ the pendant group and usually CO₂, although elimination of ethers has also been reported that does not employ the liberation of a gaseous by-product as a driving force (**Figure 1B**).^{8,10–12}

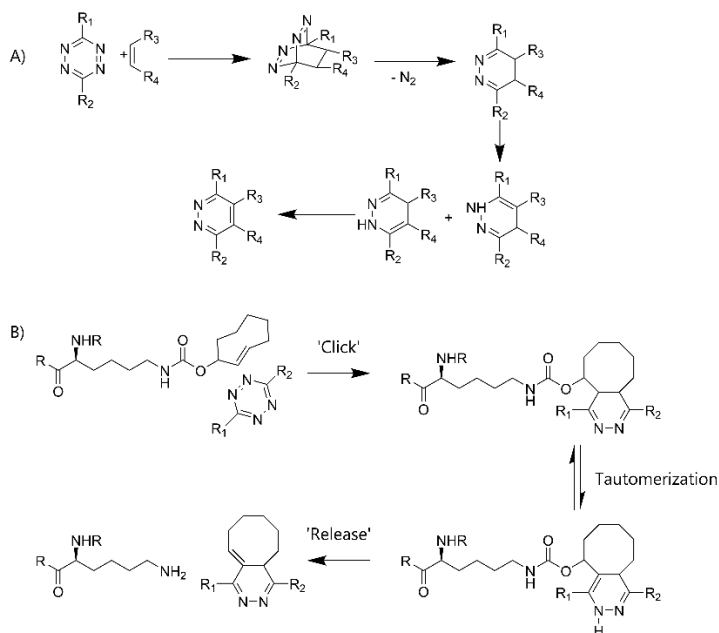


Figure 1 - Overview click-to-release chemistry based on the inverse-electron demand Diels-Alder reaction.

A) General principle of an inverse-electron demand Diels-Alder (IEDDA) reaction with an electron-poor diene and an electron-rich dienophile. This reaction releases nitrogen gas. B). The principle of click-to-release chemistry based on IEDDA with trans-cyclooctene (electron-poor) and tetrazine (electron-rich). Upon the IEDDA reaction ('click') the formed product can release CO₂ and regains its free amine.

The most notable application of this methodology has been in antibody drug conjugation.^{8,10,13} Robillard and co-workers designed antibody-drug conjugates (ADC) in which antibodies targeting tumour-specific antigens were coupled to highly toxic compounds via a TCO-linker. This meant that the drug could be released through reaction with a tetrazine (**Figure 2**).

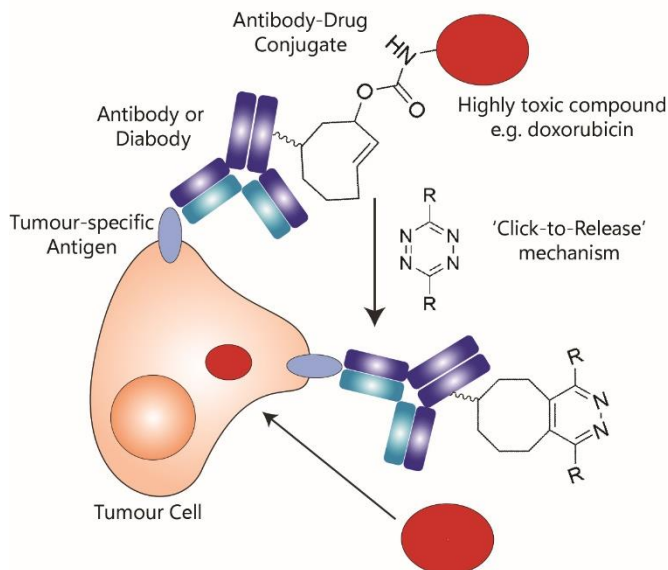


Figure 2 - Schematic overview of click-to-release chemistry applied in antibody-drug conjugates (ADCs).

Antibody-drug conjugates (ADCs) are based on a targeting moiety (antibody, diabody or single-chain variable fragments) coupled to a highly toxic compound to achieve targeted delivery of the drug to tumours. Using click-to-release chemistry Robillard and co-workers used a TCO-moiety to couple the drug to a targeting moiety. Upon reaching the target, tetrazine is applied, causing the release of the toxin, creating a local high concentration of the toxic compound or drug. This eliminates the essence of targeting an antigen that is internalized upon antibody binding. Figure was adapted from Rossin *et al.*

Click-to-release chemistry has also been used for temporal controlled T-cell activation.¹¹ Van der Gracht, De Geus *et al.* managed to modify the cross-presented epitope SIINFEKL at the Lys7 position with a solubilised TCO-group (**Figure 3**). This group prevented the T-cell from recognizing the peptide and no immune response was obtained. However, when treating cells *in vitro*¹¹ or mice *in vivo*¹⁴ with tetrazine, T-cell activation could be restored. In a similar approach, Van de Graaff, Oosenbrug *et al.* were able to control the interaction between a pathogen-associated molecular pattern (PAMP) and its cognate Toll-Like receptor (TLR).¹⁵ A TCO blocked ligand was incubated with various (primary) murine and human cell lines. Upon tetrazine addition, TLR activation could be observed.¹⁵

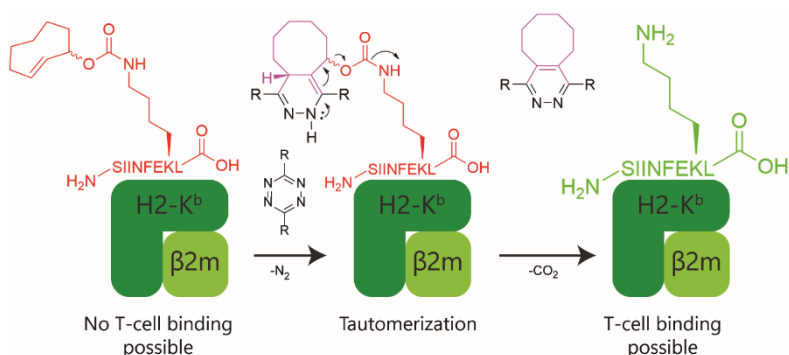


Figure 3 - Schematic overview of the use of clickable peptides in T-cell activity control.

The lysine at position 7 (K7) was modified with a TCO-molecules. This blocked the T-cell receptor from recognizing the epitope. Upon addition of tetrazine and the following tautomerization, N_2 and CO_2 are released as well as the TCO-molecule recovering the native amine of the lysine side chain. T-cell receptors can interact with the MHC-peptide complex again. Figure was adapted from Van de Gracht, De Geus *et al.*

In this research, click-to-release chemistry is used, not to control the activity of a small molecule, but to switch off/on the activity of whole proteins. This is a difficult feat, as multiple lysine residues per protein have to be modified and released. As the yields of the click-to-release are not quantitative, a fine balance has to be found between under- and over-modification.

Aim and outline

The aim of this work is to use click-to-release chemistry as a means to get spatiotemporal control over the (toxic) activity of immunocytokines and as a tool to research MHC-TCR interactions.

Chapter 1 describes the need for immunocytokines (ICs), the different combinations of antibody formats and cytokines and gives a broad overview of most immunocytokines currently in (pre-) clinical trials. Most of these ICs still cause systemic toxicities ranging from manageable to severe toxicities. Various groups have tried to prevent these toxicities in an IC-specific manner using point mutations, local assembly of the cytokine or using tumour-specific enzymes. This chapter introduces the current problem in the immunocytokine field which is that cytokines can be very potent anti-cancer therapeutics, but are until date too toxic to have a broad therapeutic window.

In **Chapter 2** the cytokine IL-1 β is described. This is one of the master regulator cytokines which can have both pro- and anti-inflammatory properties. However, in cancer treatment it is of limited use as it is strongly believed that it has a general tumour-growth promoting function. Nevertheless, as IL-1 β contains various lysines that are essential for receptor interaction, this cytokine can function as a prototype for applying a new free-amine based tool. This chapter introduces click-to-release chemistry as a tool to control IL-1 β activity *in vitro*. Upon bacterial overexpression, recombinant IL-1 β was obtained with a C-terminal sortase A recognition site, which allowed for the formation of a covalent IC after inactivation with the TCO-ester. Using tetrazine, IL-1 β activity was restored, showing a proof-of-principle of this method for IC design.

As IL-1 β is not a commonly used cytokine in cancer research **Chapter 3** applies the same principle on a different, more clinically relevant cytokine, TNF- α . TNF- α , a very important regulator cytokine, is known to be a promising anti-cancer therapeutic. Various research groups have tried to make use of its high toxicity in cancer treatment in a controlled manner. Until now, this proved to be rather difficult, but not impossible. ICs based on TNF- α have been designed and are currently in late stage clinical trials. Here, the proof-of-principle experiments on IL-1 β were translated to TNF- α , using TCO to inactivate the cytokine and tetrazine to regain its activity. As lysines are not essential for TNF- α , this proved to be more difficult. Inactivation was established using similar conditions as for IL-1 β . However, regaining its activity proved hard to translate from *in vitro* experiments to cellular environment.

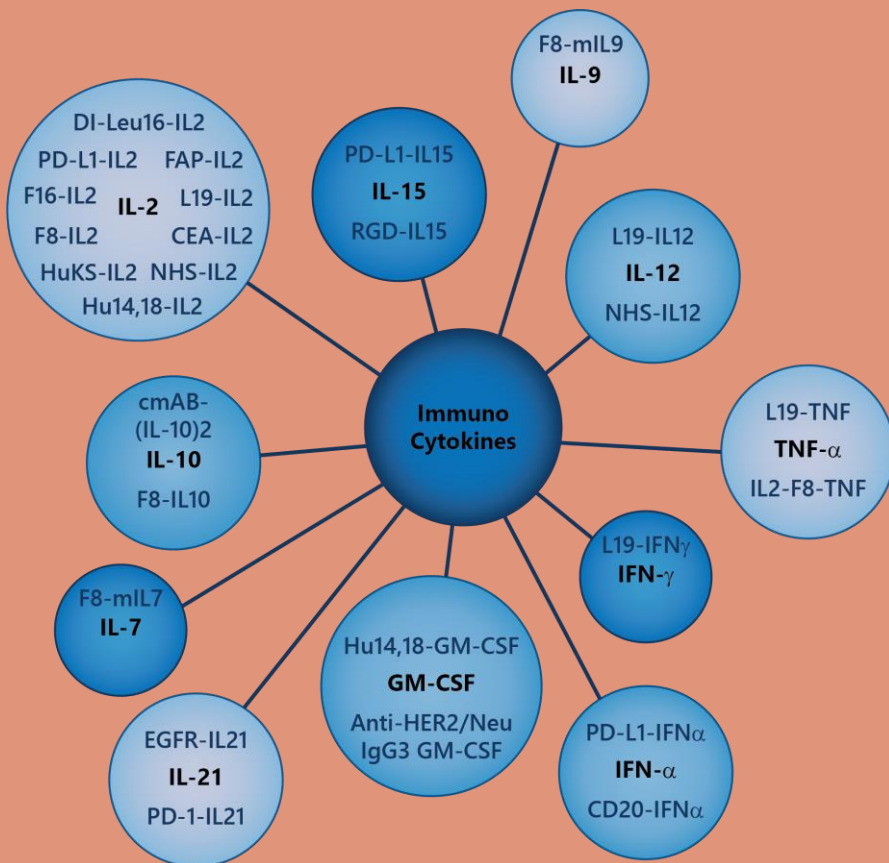
Chapter 4 describes a different use for click-to-release chemistry, as the aim here is to use it to get more insight into the processes and binding of antigenic peptides to MHC-molecules and T-cell receptors. Here, the human leukocyte antigen (HLA) complex class II was expressed using a variety of expression systems: bacteria, insect cells and mammalian cells. The purified, folded complex of HLA-DR1 was used for an initial crystallization screen with the native CLIP peptide in the binding groove. Comparison experiments with different (clickable) peptides would give more insight in how these peptides bind and why minor changes introduced in these peptides, like click-handles, cause the abolishment of T-cell activation.

Chapter 5 gives an overview of the results described in this work as well as an outlook, giving the experiments that have to be performed to completely underline the use of click-to-release chemistry in immunocytokines. Finally, the follow-up experiments regarding HLA-DR1 co-crystallization with (clickable) peptides are further elaborated.

References

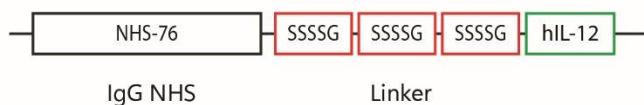
- (1) The Nobel Committee for Chemistry. Scientific Background on the Nobel Prize in Chemistry 2022 - Click Chemistry and Bioorthogonal Chemistry. *Kungl. Vetenskaps-Akademien*. 2022, pp 1–18.
- (2) Kolb, H. C.; Finn, M. G.; Sharpless, K. B. Click Chemistry: Diverse Chemical Function from a Few Good Reactions. *Angewandte Chemie International Edition* **2001**, *40* (11), 2004–2021. [https://doi.org/10.1002/1521-3773\(20010601\)40:11<2004::AID-ANIE2004>3.0.CO;2-5](https://doi.org/10.1002/1521-3773(20010601)40:11<2004::AID-ANIE2004>3.0.CO;2-5).
- (3) Chang, P. V.; Prescher, J. A.; Sletten, E. M.; Baskin, J. M.; Miller, I. A.; Agard, N. J.; Lo, A.; Bertozzi, C. R. Copper-Free Click Chemistry in Living Animals. *Proceedings of the National Academy of Sciences* **2010**, *107* (5), 1821–1826. <https://doi.org/10.1073/pnas.0911116107>.
- (4) Xiao, H.; Woods, E. C.; Vukojicic, P.; Bertozzi, C. R. Precision Glycocalyx Editing as a Strategy for Cancer Immunotherapy. *Proceedings of the National Academy of Sciences* **2016**, *113* (37), 10304–10309. <https://doi.org/10.1073/pnas.1608069113>.
- (5) Streu, C.; Meggers, E. Ruthenium-Induced Allylcarbamate Cleavage in Living Cells. *Angewandte Chemie International Edition* **2006**, *45* (34), 5645–5648. <https://doi.org/10.1002/anie.200601752>.
- (6) Wang, J.; Wang, X.; Fan, X.; Chen, P. R. Unleashing the Power of Bond Cleavage Chemistry in Living Systems. *ACS Cent Sci* **2021**, *7* (6), 929–943. <https://doi.org/10.1021/acscentsci.1c00124>.
- (7) Blackman, M. L.; Royzen, M.; Fox, J. M. Tetrazine Ligation: Fast Bioconjugation Based on Inverse-Electron-Demand Diels–Alder Reactivity. *J Am Chem Soc* **2008**, *130* (41), 13518–13519. <https://doi.org/10.1021/ja8053805>.
- (8) Versteegen, R. M.; Rossin, R.; Ten Hoeve, W.; Janssen, H. M.; Robillard, M. S. Click to Release: Instantaneous Doxorubicin Elimination upon Tetrazine Ligation. *Angewandte Chemie - International Edition* **2013**, *52* (52), 14112–14116. <https://doi.org/10.1002/anie.201305969>.
- (9) Oliveira, B. L.; Guo, Z.; Bernardes, G. J. L. Inverse Electron Demand Diels–Alder Reactions in Chemical Biology. *Chem Soc Rev* **2017**, *46* (16), 4895–4950. <https://doi.org/10.1039/C7CS00184C>.
- (10) Rossin, R.; van Duijnhoven, S. M. J.; ten Hoeve, W.; Janssen, H. M.; Kleijn, L. H. J.; Hoebe, F. J. M.; Versteegen, R. M.; Robillard, M. S. Triggered Drug Release from an Antibody–Drug Conjugate Using Fast “Click-to-Release” Chemistry in Mice. *Bioconjug Chem* **2016**, *27* (7), 1697–1706. <https://doi.org/10.1021/acs.bioconjchem.6b00231>.
- (11) Van Der Gracht, A. M. F.; De Geus, M. A. R.; Camps, M. G. M.; Ruckwardt, T. J.; Sarris, A. J. C.; Bremmers, J.; Maurits, E.; Pawlak, J. B.; Posthoorn, M. M.; Bongers, K. M.; Filippov, D. V.; Overkleeft, H. S.; Robillard, M. S.; Ossendorp, F.; Van Kasteren, S. I. Chemical Control over T-Cell Activation in Vivo Using Deprotection of Trans-Cyclooctene-Modified Epitopes. *ACS Chem Biol* **2018**, *13* (6), 1569–1576. <https://doi.org/10.1021/acscchembio.8b00155>.
- (12) de Geus, M. A. R.; Groenewold, G. J. M.; Maurits, E.; Araman, C.; van Kasteren, S. I. Synthetic Methodology towards Allylic Trans -Cyclooctene-Ethers Enables Modification of Carbohydrates: Bioorthogonal Manipulation of the Lac Repressor. *Chem Sci* **2020**, *11* (37), 10175–10179. <https://doi.org/10.1039/D0SC03216F>.
- (13) Rossin, R.; Versteegen, R. M.; Wu, J.; Khasanov, A.; Wessels, H. J.; Steenbergen, E. J.; Ten Hoeve, W.; Janssen, H. M.; Van Onzen, A. H. A. M.; Hudson, P. J.; Robillard, M. S. Chemically Triggered Drug Release from an Antibody–Drug Conjugate Leads to Potent Antitumour Activity in Mice. *Nat Commun* **2018**, *9* (1). <https://doi.org/10.1038/s41467-018-03880-y>.
- (14) Lahav-van der Gracht, A. M. F. Bioorthogonal Deprotection Strategy to Study T-Cell Activation and Cross-Presentation, Universiteit Leiden, Leiden, 2020.
- (15) van de Graaff, M. J.; Oosenbrug, T.; Marqvorsen, M. H. S.; Nascimento, C. R.; de Geus, M. A. R.; Manoury, B.; Rensing, M. E.; van Kasteren, S. I. Conditionally Controlling Human TLR2 Activity via Trans-Cyclooctene Caged Ligands. *Bioconjug Chem* **2020**, *31* (6), 1685–1692. <https://doi.org/10.1021/acs.bioconjchem.0c00237>.

Minireview – Immunocytokines: a New Tool in the Fight Against Cancer

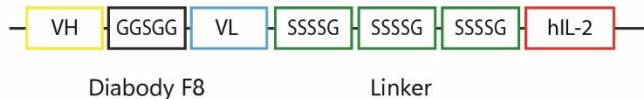


Immunocytokines (ICs) are a potent new class of therapeutics for the treatment of cancer.¹⁻³ These protein constructs consist of a tumour-targeting moiety, like an antibody, a diabody or a single-chain variable fragment (scFv), linked via a flexible linker consisting of serines and glycines, to an immunological messenger molecule (IL-12, IL-2 or TNF- α) in a single genetic construct (**Figure 1A**). They were first described by Gillies *et al.* as an attempt to increase the therapeutic window and clinical access of cytokines.⁴ These are small protein regulators of the immune response. As such, they can in principle be very potent in activating an anti-tumour response, but also have major on-target toxic side-effects; with the cytokine activating the immune system in the whole body, leading to a potentially lethal cytokine storm.^{5,6}

A) NHS-IL12



F8-IL2



L19-TNF



B)

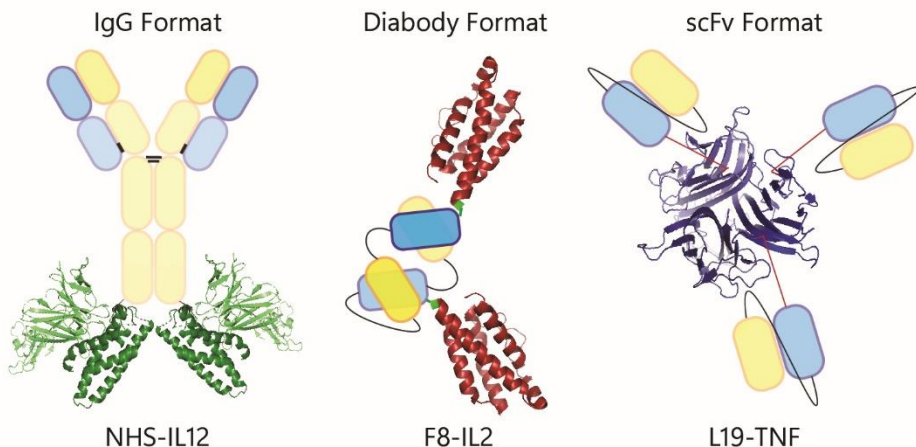


Figure 1 - Summary of genetically engineered fusion protein based immunocytokines.

A) Construct design of three immunocytokines differing in targeting moiety (antibody (IgG), diabody, single-chain variable fragment (scFv)) and cytokine payload (IL-12, IL-2 and TNF- α). B) Visual representation of three ICs currently in (pre-)clinical trials. Crystal structures were modified from Yoon *et al.* (IL-12; PDB: 1F45)⁷, Arkin *et al.* (IL-2; PDB:1M47)⁸ and Baeyens *et al.* (TNF- α ; PDB:2tnf)⁹.

Immunocytokines aim to circumvent these side-effects by conjugating the cytokine to a tumour-targeting antibody. This will lead to accumulation of the cytokine in the tumour, resulting in lower systemic toxicity. This approach has reduced, but not completely eliminated, the intrinsic toxicity of cytokines to the patient, allowing for an altered dosage compared to a non-targeted cytokine injection.^{2,10} In this chapter, I will give an overview of the progress that has been made in this field, starting with clinical examples and ending with the pre-clinical examples.

Immunocytokines – Formats and Payloads

Many variations of ICs are currently in clinical trials (**Table 1**), with most of the ICs diverging in the cytokine used or the antigenic target of the antibody (**Figure 1B**). The latter is usually a tumour or microenvironment-targeting antibody reagent that is then genetically linked to interleukin-2 (IL-2)^{1,4,11–13}, tumour necrosis factor α (TNF- α)^{2,14,15} or interleukin-12 (IL-12).^{16,17} Various antibody formats are used in these ICs (e.g. diabody, IgG, scFv). These are beyond the scope of this chapter and have been reviewed elsewhere.^{18–20}

IL-2-based immunocytokines

Interleukin-2 (IL-2) is a 15-16 kDa cytokine that is involved in the activation but also homeostasis of the immune system.²¹ It is mainly expressed upon activation of T-cells, natural killer (NK) cells, NKT cells and dendritic cells.²² It interacts with the IL-2 receptor (IL-2R) which can consist of one to three subunits, IL-2R α , IL-2R β and IL-2R γ . Interaction with IL-2R α does not lead to signalling which therefore acts as a scavenger, regulating the amount of active IL-2.²³ The dimer formed by IL-2R β and IL-2R γ has a low affinity for IL-2 whereas the trimeric IL-2R which includes IL-2R α as well has a high affinity for IL-2.²⁴ Upon triggering either the dimeric or trimeric IL-2R, various (de)phosphorylation processes encompass the signalling pathways which will not be discussed further here.^{22,25} IL-2 is predominantly involved in promoting the T-cell dependent immune response, in particular promoting T-cell proliferation and clonal expansion leading up to an immune response.^{21,26} As such IL-2 has been used as a drug for the treatment of invasive cancer²⁶ or, at low dose, for treatment of auto-immune diseases by stimulating regulatory T-cells.²⁷

Hu14.18-IL-2

IL-2 was the first cytokine used in the immunocytokine format. It was coupled to humanized ch14.18 (hu14.18)⁴, which targets ganglioside GD2 expressed on neuroblastoma²⁸ and melanoma tumours.²⁹ A phase I clinical trial in stage III and stage IV melanoma patients showed that the reoccurrence-free survival was a median of 5.7 months for the 18 treated patients.³⁰ Following a phase II clinical study in the combinational treatment with hu14.18-IL2 plus GM-CSF and isotretinoin showed mixed results. No responses were observed in the first stratum. However, in the second stratum involving 31 neuroblastoma patients, 5 objective responses were observed, 3 being complete, the other 2 being partial responses. Unfortunately, the majority of the participants suffered from adverse-effects (fever, anorexia among others) even though these were reversible.³¹

L19-IL2

L19-IL2 is also one of the first described ICs, in which IL-2 was coupled to the L19 antibody, targeting EDB (extra-domain B, angiogenesis-associated isoform of fibronectin). This conjugate resulted in a 10 fold reduction in tumour mass in mice compared to IL-2 or saline treated mice.¹ L19-IL2 was tested as well in a phase I clinical trial (NCT01058538), resulting in 1.38 mg iv 3 times per week administration to be recommended resulting in stable disease for the majority of the participants without unmanageable side-effects.³² Various phase I and phase II clinical studies are still being set-up to research the potential of L19-IL2 either as monotherapy or in combination with other ICs (L19TNF) or other drugs such as Rituximab.

F16-IL2

F16-IL2 is an IC based on a single-chain variable fragment (scFv) targeting the A1 domain of tenascin-C which is only expressed during tissue remodelling and therefore a suitable target for immune-based cancer therapy. F16-IL2 was examined in a phase Ib/II trial with patients bearing solid tumours (19) or metastatic breast cancer (10), respectively. Combinational treatment with doxorubicin resulted in over 50% (57% and 67% respectively) disease control after 8 weeks which decreased to 30-40% after 12 weeks. The treatment resulted in some side-effects like constipation and asthenia but these were reversible.³³

NHS-IL2LT

NHS-IL2LT is an IC containing a mutated IL-2 (D20T) which has similar activity as the wild type IL-2 but reduced binding to intermediate IL-2 receptor α , thereby reducing its systemic toxicity.³⁴ This IL-2LT was fused to an antibody (NHS76) which targets DNA/histone complexes which are present in the tumour necrotic core.³⁵ Mice models for non-small cell lung metastasis showed up to 90% reduction in metastasis surface when treated with 80 μ g/day for 5 days.³⁴

Pre-clinical study in combination with radiotherapy and cisplatin administration in a lung carcinoma mouse model showed that this combined treatment resulted in complete regression of tumour growth in 80-100% of the mice.³⁶ Following, a phase Ib trial (NCT00879866) with non-small cell lung carcinoma patients indicated no objective responses but the occurrence of adverse effects like fatigue, skin disorders and respiratory symptoms. Nevertheless 2/13 patients had long-term survival with one patient having long-term control over the tumour.³⁶

A phase IIa clinical trial with advanced melanoma patients (NCT01973608) was terminated early as the decision was made to discontinue the development of the drug for financial reasons. The results until that moment showed no safety or efficacy problems.³⁷

FAP-IL2

FAP-IL2 is based on an antibody against fibroblast activation protein α (FAP) coupled to an IL-2 variant that has abolished affinity for the IL-2 receptor α .³⁸ FAP is barely present in normal healthy human tissue, but very common in cancer-associated fibroblasts.³⁹ This IC was mainly designed to increase the potency of already existing cancer therapies based on the immune system. Waldhauer *et al.* showed that FAP-IL2 activated different immune effector cells, NK cells and CD4+/CD8+ T-cells with minimal activation of undesired T-regulatory (Treg) cells. Combinational treatment with cetuximab (anti-EGFR) increased tumour lysis in various mouse models.³⁸

A high-risk neuroblastoma mouse model showed that combinational treatment with an anti-GD₂ antibody (Dinutuximab beta) resulted in similar increase of NK- and T-cell activation as described by Waldhauer *et al.* together with minimal regulatory T-cell (Treg) induction. Mice treated with this combination had stable tumour volume for 25 days and over 80% of the mice had event free survival.⁴⁰

F8-IL2

As with L19, the F8 antibody targets the extra-domain of fibronectin, extra-domain A⁴¹ which is common in various types of cancer and nearly absent in normal tissue.⁴² The diabody format of this antibody was coupled to IL-2 and analysed initially in renal cell carcinoma mouse model as monotherapy or in combination with sunitinib⁴³ (kinase inhibitor). The monotherapy was not more effective than sunitinib monotherapy. However, combination with sunitinib resulted in 2/7 mice being cured, mostly because of increased NK-cell infiltration in the tumour mass.⁴³

Another pre-clinical assessment of this IC involving non-small cell lung carcinoma showed changes in the immune cell population in the tumour micro-environment.⁴⁴ Hutchmacher *et al.* showed that only administration in combination with a checkpoint inhibitor for CTLA-4 resulted in a complete response (5/5) in colon carcinoma mouse models. This was caused by the increased NK-cell activation by the IC and altered CD8+ T-cell activity by the CTLA-4 checkpoint inhibitor.⁴⁵ Finally, administration of F8-IL2 together with F8-TNF resulted in a 50% survival rate in a melanoma mice model.⁴⁶

IL2-F8-TNFmut

F8-IL2 has also been used in a dual immunocytokine format together with a mutated form of TNF- α (IL2-F8-TNFmut). By mutating human TNF- α at one position (R108A or mTNF- α R108W) to reduce its potency and match it to IL-2, this construct caused *in vivo* durable complete responses in all mice (5/5) bearing WEHI-164 sarcomas, which was not the case when these were treated with conventional doxorubicin or the individual immunocytokines. This treatment also completely prevented tumour growth upon re-injecting the cured mice. Finally mouse models for colon cancer and leukemia showed complete responses, 2/4 and 3/4 mice respectively, when treated with this dual IC.⁴⁷ This dual IC was also used in combination with blocking PD-L1, which also induced complete responses in two different mouse models and partial responses in two other mouse models.⁴⁸

A variant of this dual immunocytokine, IL2-XE114-TNFmut recognizing carbonic anhydrase IX, was designed by the same group. This dual IC targets renal cell carcinoma and was oriented to inhibit tumour growth in mice although this was accompanied by significant changes in body weight. However, these body weight changes were less severe when compared to treatments with the non-relevant targeting control. Although this compound did not show the staggering results as IL2-F8-TNFmut, there is potential in using this dual IC for treatment of metastasis renal cell carcinoma.⁴⁹

TNF- α -based immunocytokines

TNF has been the other cytokine used extensively, due to its ability to induce potent anti-tumour responses (for more background information see *Chapter 3*). However this has been hampered by the very toxic side-effect profile. L19mTNF α was one of the first murine TNF- α (mTNF- α)-based immunocytokines. It showed that a 4-fold decrease in dose of L19mTNF α in mouse models, had a similar effect as in the control groups treated with either non-conjugated TNF- α or TNF- α conjugated to a non-relevant antibody.² Phase I/II clinical trials regarding monotherapy of L19-TNF α concluded that L19-TNF α monotherapy did not cause the opted tumour regression in patients with advanced solid tumours.¹⁰ However, combinational therapy with doxorubicin resulted in a lower recommended dose for doxorubicin (60 mg/m² instead of 75 mg/m²) when administered in combination with 13 μ g/kg L19-TNF α in patients with soft-tissue sarcomas, previously treated with doxorubicin only.⁵⁰

Another study showed that the combination of isolated limb perfusion therapy with L19-TNF α treatment resulted in a complete response rate in 50% of the patients (5/10) in an early clinical trial (NCT01213732) even though severe side-effects still proved dose-limiting for some patients.⁵¹ Unfortunately, monotherapy of L19-TNF α in solid tumour patients did not result in the desired tumour response. Nonetheless, a different phase I/II trial with grade III/IV glioma patients had different results (NCT03779230). Three patients treated with 10 μ g/kg every 21 days did not show signs of severe toxicity. This study also showed that 2/3 patients had stable disease 6 months after treatment with an increase necrotic area around in the tumour environment.⁵²

Finally, a phase II clinical study involving melanoma patients showed that intralesional administration of both ICs resulted in complete responses in 32/105 lesions in 20 patients. Complete responses were also observed in 7/13 untreated lesions suggesting the activation of the immune system in a systemic matter. Unfortunately, some grade 2/3 adverse events (injection site reaction, oedema and cutaneous rash among others) remained, suggesting that the therapy could be further improved.⁵³

IL-12-based immunocytokines

Interleukin-12 (IL-12) is a heterodimeric cytokine composed of IL-12A (p35) and IL-12B (p40).⁵⁴ It is known as a proinflammatory cytokine which promotes proliferation and cytotoxicity of NK-, NKT- and CD8+ T-cells.⁵⁵ Upon activation by IL-12, T-cells increase the production of TNF- α and IFN- γ , while at the same time it reduces the suppression of IFN- γ caused by IL-4 secretion.⁵⁶ Next to that it causes the change from innate to adaptive immunity and stimulation of cell-mediated immunity via Th1-cells, among other things.^{57,58} The effect of IL-12 on the activation of Th1-cells made them a target in treatment of autoimmune diseases such as multiple sclerosis.⁵⁹ However, it has also been shown that IL-12 has beneficial effects when administered to melanoma and renal cancer patients, even though the side-effects were severe at an effective dose.⁶⁰

NHS-IL12

Further researching the use of IL-12 as a cancer treatment has resulted in the design of NHS-IL12 which is an immunocytokine based on two IL-12 molecules that are coupled C-terminally to the human NHS76¹⁶ antibody targeting DNA/histone complexes, commonly exposed in necrotic parts of tumours.¹⁶ Pre-clinical data in B16- or MC38-tumour bearing mice showed increased activation of tumour-infiltrating CD8+ T-cells and NK-cells. MB49^{luc}-bladder tumour bearing mice also showed that NHS-IL12 treatment reduced myeloid-derived suppressor cells (MDSCs), which cleared the way for immunotherapy even more.⁶¹

Various other pre-clinical trials with NHS-IL12 in combination with Avelumab (anti-PD-L1) showed complete regression in 7/8 breast cancer tumour bearing mice which were also protected from reoccurring tumours.⁶² Also in mice with bladder cell carcinoma, the combination Avelumab/NHS-IL12 significantly reduced tumour growth.⁶³ The first phase I clinical trial with NHS-IL12 in melanoma patients resulted in an increased number of activated or mature NK- and NKT-cells. NHS-IL12 was tolerated up until a dose of 16.8 $\mu\text{g/kg}$.⁶⁴

L19-IL12

Similar to IL-2 and TNF- α , also IL-12 has been fused to the L19 antibody. Various forms of this combination have been designed but Gafner *et al.* suggested a format in which each subunit of IL-12 was coupled to its own scFv L19, creating a 2-L19-IL12 immunocytokine. This variant showed increased tumour penetration with comparable distribution throughout the rest of the body with L19-IL12.⁶⁵ Mice bearing F9 tumour treated with either of these constructs showed delayed tumour growth for 2-L19-IL12 compared to L19-IL12 in all treatment regimes. 3x40 μg application of 2-L19-IL12 extended tumour growth inhibition up until 23 days after tumour grafting, compared to 14 days for L19-IL12. Yet another research done by Ongaro *et al.* showed that placing a 15-amino acid linker (GSADGGSSAGGSADAG) between the IL-12 heterodimer and L19 also improved the tumour infiltrating properties.⁶⁶

Finally, a glioblastoma mouse model showed that a complete cure in 2/5 mice was established using a tandem diabody L19-IL12 which was superior to either L19-TNF α (1/5) and L19-IL2 (0/5) over a 60 days course. Rechallenging these mice with the same tumour showed that memory was built during the previous challenge, resulting in protection against reoccurring tumours.⁵²

IL-15-based immunocytokines

Interleukin-15 (IL-15) is a widely studied cytokine in the quest of suitable cancer treatment.⁶⁷ It belongs to the IL-2 family, activating NK-cells and T-cells but is, unlike IL-2, not involved in cell death activation or regulatory T-cell maintenance.^{68,69} It also interacts partly with the same receptor subunits IL-2/15R β and IL-2/15R γ . The IL-15R α is uniquely for IL-15 interaction.⁷⁰ As with many cytokines, IL-15 has also been associated with different diseases. IL-15 is believed to play an important role in the development of rheumatoid arthritis⁷¹ due to its function as T-cell attractant. But also other autoimmune diseases such as inflammatory bowel disease⁷² have been associated with IL-15 functioning. Also in cancer research it has been shown that IL-15 can be involved in the development or maintenance of cancer (adult T-cell leukemia).^{73,74} However studies have also shown that IL-15 can be beneficial in cancer treatment^{75,76} as it promotes CD8+ T-cell and NK-cell growth and stimulates their tumour-infiltrating properties.⁷⁷ This makes it a target for IC development.

RGD-IL15

PFC-1 is an immunocytokine based on IL-15, having IL-15 coupled to IL-15 receptor α (IL-15R α), an FC domain to increase half-life and an Arg-Gly-Asp (RGD)-peptide.⁷⁸ This construct showed *in vitro* stimulation of both NK- and T-cells in a similar fashion as recombinant human IL-15 and was able to target integrin $\alpha\beta 3$ -positive tissue. *In vivo* studies in C57BL/6 mice with B16F10 melanoma cells showed inhibition of tumour growth, and even reduced tumour volume with 54% after three treatments. This tumour volume reduction was accompanied with increased CD8+ T-cell and NK-cell numbers in the blood, spleen and tumour, which were also more activated. Finally, metastasis was also decreased by 80% compared to the vehicle control group.⁷⁸

BJ-001, another IL-15 immunocytokine based on IL-15, IL-15R α , the Fc-domain and RGD for targeting, was assessed in a phase I clinical trial in patients with solid tumours. Data until January 2021, suggested that this immunocytokine is safe at least at 6 $\mu\text{g/kg}$ dose, although escalation to 10 $\mu\text{g/kg}$ was ongoing. Until date 2/7 patients experienced stable disease and are still receiving BJ-001. Nevertheless, some (severe) side-effects like anorexia and cytokine release syndrome were also observed.⁷⁹

PD-L1-IL15

PD-L1 targeting is one of the many strategies applied nowadays in the fight against cancer. Therefore multiple immunocytokines have been developed using anti-PD-L1 antibodies or scFvs. N-809 is a IL-15/IL-15R α containing immunocytokine combined with a N-803 Fc domain and two scFvs for PD-L1, thereby combining three methods to fight tumour cells. *In vitro* assays showed increased activation of CD4+ T-, CD8+ T- and NK-cells together with increased lysis of tumour cells. Mice bearing bladder cancer cells were treated with N-809 and showed increased localization at the tumour site. When treated with N-809, 60% of the mice bearing colon cancer tumours were cured within 15 days after treatment.⁸⁰ Later studies with N-809 indicated higher tumour infiltration and activation of CD8+ T-cells and NK-cells compared to co-administration of N-803 with anti-PD-L1 in mouse models for both breast and colon cancer. Although survival of these mice was rather low (8%) rechallenging these mice did not cause tumour growth again and all mice survived.⁸¹

Li *et al.* designed a similar immunocytokine, anti-PD-L1-CD16a-IL15/IL15R α which also allowed for T-cell and NK-cell activation and proliferation. *In vivo* studies including mice injected with colorectal cancer cells showed that mice treated with this IC were completely cured from the formed tumour, while alternative forms of this IC, lacking the CD16a or IL-15 itself had less promising results. No clear toxicities were observed in these studies including body weight loss.⁸² More ICs are being designed nowadays, like LH01, which are based on the combination of IL-15/IL-15R α with anti-PD-L1 in the search for the ideal combination.⁸³ No clinical data has been published so far.

IL-21-based immunocytokines

Interleukin-21 (IL-21) is mostly expressed by CD4⁺ T- and NK-cells and assists in the maturation and increasing cytotoxicity of present CD8⁺ T- and NK-cells.⁸⁴ IL-21 interacts with the IL-21 receptor (IL-21R) which has structural similarities with IL-2R/IL-15R. It also requires, similar to these receptors the interaction with the γ -chain for signal transduction, which is performed by the Jak/STAT pathway.⁸⁵ IL-21 has been tested in various clinical trials for melanoma and renal cell carcinoma patients.⁸⁶ Phase I clinical trials showed complete responses for 2/47 melanoma patients. Most side-effects were flu-like symptoms such as fever but also dose-limiting toxicities were observed such as thrombocytopenia and increased liver enzymes.⁸⁷ This trial suggested the use for IL-21 as immunotherapy against cancer which also resulted into the development of various ICs.

EGFR-IL21

Targeting IL-21 to cEGFR with a known EGFR antibody resulted *in vivo* in tumour eradication while at the same time no apparent toxicities were observed. Erb-IL21 largely functions via already existing CD8⁺ T-cells in the tumour micro-environment instead of attracting new CD8⁺ T-cells into this environment. Besides that, it does not activate Treg cells which caused it to be less toxic compared to Erb-IL2 ICs.⁸⁸

PD-1-IL21

Just like PD-L1, PD-1 is often targeted during cancer treatment. Shen *et al.* designed a PD-1 targeting IL-21 in which the IL-21 is coupled to one of the C-termini of the heavy chain of the antibody. Furthermore, they designed IL-21 carrying two mutations (R9E5, R76A) causing it to have increased attenuation and prolonged exposure to increase its functionality. Melanoma mouse models showed that administration of this anti-PD-1-IL21 mutein resulted in reduced tumour growth compared to anti-PD-1 treatment only.⁸⁹ Li *et al.* designed PD-1ab21, which consists of an anti-PD-1 diabody fused to IL-21. In melanoma tumour-bearing mice, this compound showed increased memory-stem T-cell numbers and expansion of CD8⁺ T-cells.⁹⁰

Attempts by Di Nitto *et al.* to target IL-21 via an F8 single chain diabody format towards the tumour micro-environment did not result in preferential localization of IL-21 in the tumour.⁹¹

Other cytokines in the immunocytokine format

Interleukin-7 (IL-7) -based immunocytokines are not commonly researched. The 25 kDa protein is expressed by T-cell, pre-B cells and bone marrow macrophages.⁹² It signals via the heterodimeric receptor IL-7R which consists of the alpha chain (IL-7R α or CD127) and

the gamma chain (IL-7R γ).⁹³ IL-7 is known to assist in T- and B-cell development⁹⁴ and its role in cancer regression was first examined in mice with Renca cell carcinoma.⁹⁵ Systemic administration of human IL-7 (hIL-7) reduced pulmonary metastases with 50-70%. A clinical trial concerning patients with metastasis resulted in several (severe) side-effects after hIL-7 administration.⁹⁶ Pasche *et al.* examined functioning of F8-mIL7 and its derivative F8-mIL7-F8.⁹⁷ Both variants were able to reduce F9 tumour growth in immunocompetent mice. Surprisingly, targeting of this immunocytokine to the tumour did not seem to be necessary for this effect.⁹⁷

Immunocytokines can also be used in other diseases than cancer. Interleukin-9 (IL-9) is expressed by various cell types including Tregs, NKT-cells and CD4+ T-cells.⁹⁸ IL-9 is associated with activation of, among others, T-cells, B-cells and mast cells.⁹⁹ It prevents apoptosis¹⁰⁰ and stimulates cell growth. Although IL-9 has been shown to prevent melanoma growth in mice¹⁰¹, it is also known to be important in asthma development.¹⁰² In pulmonary hypertension. Heiss *et al.* fused IL-9 with both a full IgG (F8IgGIL9) and an scFv (F8IL9F8) F8 targeting moiety.¹⁰³ Mice treated with F8IL9F8 had less lung tissue damage and elevated systolic right ventricular pressure, which was absent in the untreated animals. Even so the number of Tregs increased in the treated population.¹⁰³

Interleukin-10 (IL-10) is known as an immune suppressive cytokine as it reduces expression of MHC-II molecules¹⁰⁴ and co-stimulatory molecules on macrophages, among other things.¹⁰⁵ It functions via its IL-10 receptor (IL-10R) which is a dimer of the high-affinity IL-10R α and IL-10R β .¹⁰⁵ Upon binding signalling proceeds via the Jak/Stat pathway.¹⁰⁵ Although IL-10 anti-tumour activity has been recognized, as it reduces tumour metastasis in mice¹⁰⁶, it is more known for its link with auto-immune diseases and inflammatory diseases.¹⁰⁷ Nonetheless, Qiao *et al.* designed an IC which was based on Cetuximab, targeting epidermal growth factor receptor (EGFR), in which one arm was replaced with an IL-10 homodimer. Hereby they managed to prevent tumour growth in a melanoma mouse model by reducing dendritic cell-mediated apoptosis of tumour infiltrated CD8+ T-cells. Specifically, it reduces IFN- γ production by dendritic cells which get activated by IL-10 receptor interaction rather than IFN- γ production by activated CD8+ T-cells.¹⁰⁸

As IL-10 has a more immune suppressive function, its use in auto-immune diseases has been recognized as well. Schager *et al.* used an F8-IL10 or DEKAVIL IC, targeting extra-domain A of fibronectin which is commonly expressed in tumour neovascular tissue but also arthritic lesions.⁴¹ This IC inhibited collagen-induced arthritis in the respective mouse-model. Both a reduction in expression of the immune activating cytokine IL-6 and anti-collagen II immunoglobulin molecule numbers would be responsible for this inhibition. Pre-clinical safety examinations concluded that humans could be safely treated with 20 μ g/kg of F8-IL10.⁴¹

Nowadays, immunocytokines based on interferon- α (IFN- α)^{109,110}, interferon- γ (IFN- γ)¹¹¹ and granulocyte-macrophage colony-stimulating factor (GM-CSF)^{112,113} have also been developed and are currently under pre-clinical evaluation. Despite this progress, immunocytokines are still too toxic to be used as a monotherapy. ICs are, therefore, often administered in combination therapies with other immunocytokines^{3,49}, radiotherapy¹¹⁴ or monoclonal antibodies.¹¹⁵

Table 1 - Overview immunocytokines in (pre-) clinical trials.

An overview of most immunocytokines that have been or are being tested in (pre-) clinical tests. Table was based on reviews by Gout *et al.* and Zheng *et al.* and added with different immunocytokines.^{20,116}

Name	Antigen	Antibody Format	Cytokine Payload	Disease	Clinical status	Reference/source
FAP-IL2v	Fibroblast Activating Protein (FAP)	IgG	IL-2v	Solid tumours, melanoma, pancreatic cancer	Phase I/II	NCT02627274 NCT03875079 NCT03193190 NCT03386721 NCT03063762
CEA-IL2v	Carcino-Embryonic Antigen (CEA)	IgG	IL-2	CEA-positive solid tumours	Phase I	NCT02350673 NCT02004106 NCT02957032
F16-IL2	Extra-domain A1 of tenascin-C	scFv	IL-2	Relapsed acute myeloid leukemia	Phase I	NCT01131364 NCT01134250 NCT02054884 NCT03207191
F8-IL2	Extra-domain A (EDA)	Diabody	IL-2	Renal cancer carcinoma, lung adenocarcinoma, colon carcinoma	Pre-clinical	Ref. [43-45]
NHS-IL2LT	Histone complex	IgG	(D20T) IL-2	Advanced solid tumours	Phase I/II	NCT00879866 NCT01032681 NCT01973608
DI-Leu16-IL2	CD20	IgG	IL-2	Blood tumours	Phase I/II	NCT0215903 NCT1874288 NCT00720135
Hu14.18-IL2	GD2 or disialoganglioside	IgG	IL-2	Neuroblastoma/Osteosarcoma	Phase I/II (ended)	NCT03209869 NCT03958383 NCT00003750 NCT00109863 NCT00082758 NCT00590824 NCT01334515
huKS-IL2	GD2 or disialoganglioside	IgG	IL-2	Solid tumours	Phase I	NCT00132522
L19-IL2	Extra-domain B (EDB)	scFv	IL-2	Metastatic melanoma IV, diffuse large B-cell lymphoma, NSCLC	Phase I/II	NCT02076646 NCT02957019 NCT03705403 NCT01198522 NCT01058538 NCT02086721 NCT01253096 NCT01055522
L19-IL2 + L19-TNF α	Extra-domain B (EDB)	scFv	IL-2/TNF α	Basal cell carcinoma, cutaneous squamous cell carcinoma, stage III B/C melanoma	Phase II/III	NCT04362722 NCT02938299N CT03567889
IL-2-F8-TNFmut	Alternatively spliced EDA	scFv	IL-2/TNF α mut	Solid tumours	Pre-clinical	Ref. [47,48]
L19-TNF α	Extra-domain B (EDB)	scFv	Monomer TNF- α	Grade III/IV glioma, glioblastoma, STS	Phase I/II/III	NCT03779230 NCT04573192 NCT04443010 NCT04733183 NCT03420014 NCT04650984
F8-mIL7	Alternatively spliced EDA	scFv	mIL-7	Teratocarcinoma	Pre-clinical	Ref. [97]
F8-IL9	Alternatively spliced EDA	scFv	mIL-9	Pulmonary hypertension	Pre-clinical	Ref. [103]

Chapter 1

cmAB-(IL-10)2	Epidermal Growth Factor receptor	IgG	IL-10	Lung cancer	Phase I	Ref.[¹⁰⁸]
DEKAVIL (F8-IL10)	Extra-domain A (EDA)	scFv	IL-10	Rheumatoid arthritis	Pre-clinical	Ref.[⁴⁴¹]
NHS-IL12	DNA/histone complex	IgG	IL-12	Stage IV breast cancer, metastatic non-prostate genitourinary cancers, Kaposi sarcoma, colorectal cancers, solid tumours	Phase I/II	NCT04756505 NCT04235777 NCT04633252 NCT04303117 NCT04491955 NCT01417546
L19-IL12	Extra-domain B (EDB)	scFv	IL-12	Advanced or metastatic carcinoma, diffuse large B-cell lymphoma	Phase I	NCT04471987
PD-L1-IL15	PD-L1	IgG	IL-15 (N72D)	Lung cancer	Pre-clinical	Ref.[⁸¹]
RGD-IL15	Integrins	RGD	IL-15 (N72D)	Advanced or metastatic solid tumours	Phase I	Ref.[⁷⁹]
EGFR-IL21	Epidermal Growth Factor Receptor	IgG	IL-21	Lung cancer	Pre-clinical	Ref.[⁸⁸]
PD-1-IL21	PD-1	IgG	IL-21	Solid tumours	Pre-clinical	Ref.[^{89,90}]
CD20-IFN α	CD-20	IgG	IFN- α	B-cell lymphoma	Pre-clinical	Ref.[¹⁰⁹]
PD-L1-IFN α	PD-L1	IgG	IFN- α	B-cell lymphoma	Pre-clinical	Ref.[¹¹⁰]
L19-IFN γ	Extra-domain B	scFv	IFN- γ	Colon adenocarcinoma	Pre-clinical	Ref.[¹¹¹]
Hu14.18/GM-CSF	GD2 or disialoganglioside	IgG	GM-CSF	Neuroblastoma	<i>In vitro</i>	Ref.[¹¹²]
Anti-HER2/neu IgG3 (GM-CSF)	HER2/Neu	IgG	GM-CSF	Colon adenocarcinoma	Pre-clinical	Ref.[¹¹³]

Immunocytokines – Strategies to reduce toxicity

Unfortunately, the residual toxicity does remain⁵³ and is the result of the fact that the cytokine-part of the protein remains capable of binding its target receptor in this conjugated construct. This is despite it being targeted to the tumour. Although targeting localizes the toxicity mostly to the tumour location, intermediate- or high-binding cytokine receptors present in the body can still interact with the cytokine moiety leading to on target/off tumour toxicity. Increasing the therapeutic window of ICs by reducing this on-target/off-tumour toxicity has been attempted by altering the intrinsic toxicity of the cytokine.

Introducing mutations

Some of these attempts were based on introducing mutations into the cytokine to reduce the binding capacity of the cytokine to low or intermediate-binding receptors. Gillies *et al.*³⁴ modified the endothelial low affinity IL-2 receptor binding motif of IL-2, by mutating the aspartic acid residue at position 20 (D20) to a threonine. This IL-2 mutant showed a loss in binding to intermediate-binding vascular IL-2 receptors, while maintaining binding ability to the high-binding IL-2 receptors present on activated (and/or regulatory) T-cells.¹³ The toxicity was reduced; the immunocytokine based on the native IL-2 was 20 times more toxic (50 µg/mouse for 5 days) compared to the immunocytokine based on the D20T mutated IL-2 (1 mg/mouse for 5 days), but other side-effects such as Treg upregulation remained.³⁴

Klein *et al.* designed a CEA-targeting IL-2 variant (CEA-IL2v), targeting a carcinoembryonic antigen (CEA) using an IL-2 variant with three point mutations; F42A, Y45A and L72G¹¹⁷. These mutations allowed for IL-2 to interact with the IL-2 receptor $\beta\gamma$ (IL-2R $\beta\gamma$), but prevented binding to IL-2 receptor α (CD25 or IL-2R α). As IL-2R α has high affinity for IL-2 but is not essential for signalling and IL-2R $\beta\gamma$ mediate signalling¹¹⁸, targeting the later receptor concept could reduce intrinsic toxicity of IL-2. Pre-clinical safety tests in cynomolgus monkey were performed using a CEA-homolog as CEA did not cross react with monkey CEA. No hepatotoxicity was observed outside of the CEA-targeted area.¹¹⁷

Introducing steric hindrance

Another strategy applied to reduce off-target IL-2R binding described by Gillies¹¹⁹ was to change the architecture of the IC. By genetically fusing the *N*-terminus of IL-2 to the light chain of the antibody instead of coupling to the heavy chain, interaction with intermediate-binding IL-2 receptors (ED₅₀ 65-70 ng/mL) was reduced 8 to 10 fold compared to heavy chain coupled IL-2 (ED₅₀ 7.0-9.0 ng/mL). This was also due to the fact that the *N*-terminus of IL-2 was shortened, thereby limiting the access of intermediate-binding IL-2Rs to the critical aspartic acid 20 (Asp20), which has been identified to be important for interactions with intermediate-binding receptors.³⁴ Additionally, the use of cytokine-light chain fusion, as opposed to a cytokine heavy chain fusion, improved the biological properties, such as increased circulating half-life and uptake rate, and improved antibody effector activities such as antibody-dependent cytotoxic activity and complement-dependent cytotoxicity.

Recently, a new concept was described by Hsu *et al.*¹²⁰, who generated constructs in which IL-2 was inactivated by the (genetic) attachment of an IL-2 receptor to IL-2 linked via a peptide, sensitive to proteases upregulated in the tumour micro-environment (**Figure 2**). In this manner, they could activate their IL-2 preferentially in the tumour, without even the need for targeting it with an antibody. One issue, however, is the presence of the activating proteases elsewhere in the body, making this construct not fully tumour-specific.

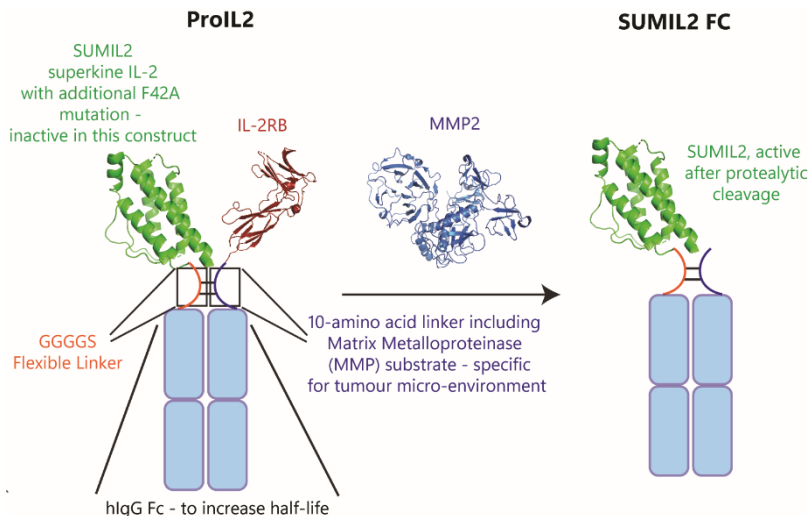


Figure 2 - Overview of MMP activity activated ProIL2 to SUMIL2 FC.

Superkine IL-2, further modified by a F42A mutation was coupled to the N-terminal of one Fc domain via a flexible GGGGS linker. The other Fc domain was N-terminally coupled to extracellular IL-2 receptor B (IL-2RB) to prevent interactions with intermediate affinity receptors throughout the body. This coupling was established using a linker sequence combined with a substrate sequence for matrix metalloproteinases (MMP) which predominantly expressed in the tumour micro-environment. The presence of the human IgG Fc (hlgG Fc) increased IL-2 half-life in the body. Crystals were modified from Arkin *et al.* (IL-2; PDB:1M47)⁸, Stauber *et al.* (IL-2RB; PDB:2ERJ)¹²¹ and Morgunova *et al.* (MMP2; PDB:1CK7)¹²².

Local multimerization

Venetz *et al.* focused on the use of IL-12 - a very potent Th1-polarizing cytokine - to activate T-cells in tumours.¹⁷ This cytokine is a heterodimer consisting of two inactive monomers, IL-12A (p35) and IL-12B (p40).^{123,124} Rather than delivering the cytokine to the tumour intact, they opted to deliver each of the parts to the tumour using its antibody vehicle. Only in the tumour did the cytokine then reassemble to form the active cytokine. Despite the elegance of the approach, it was of limited use in reducing toxicity. It was found that IL12A subunit on its own already can stimulate T-cells and natural killer cells in the Sv129 mouse model, which can cause part of the parental cytokine toxicity.

Outlook

Although all these methods result in a decrease in (systemic) toxicity, the methods applied are cytokine-specific. A more general method to deliver an inactive cytokine to the tumour micro-environment (TME) has not yet been designed. In this thesis, I show work towards the design of such a method, applicable to multiple cytokines to keep them (almost) inactive until they reach the TME. This method is based on *click-to-release* bioorthogonal chemistry which was described in *Chapter 0*. By using the reaction between free amines and *trans cyclo-octene* in the first step to block cytokine activity and the reaction between tetrazine and the *cyclo-octene* in the second step, obtaining spatiotemporal control over cytokine activity was attempted. *Chapter 2* and *Chapter 3* will focus on the cytokines IL-1 β and TNF- α , respectively. More (future) work will be described in the future prospects (*Chapter 5*). *Chapter 4* will focus on a different aspect of T-cell activation in the TME, using this caging strategy to selectively activate T-cells by peptide-presenting HLADR1 molecules, which is explained more extensively in *Chapter 0* of this work.

References

- (1) Carnemolla, B.; Borsi, L.; Balza, E.; Castellani, P.; Meazza, R.; Berndt, A.; Ferrini, S.; Kosmehl, H.; Neri, D.; Zardi, L. Enhancement of the Antitumor Properties of Interleukin-2 by Its Targeted Delivery to the Tumor Blood Vessel Extracellular Matrix. *Blood* **2002**, 99 (5), 1659–1665. <https://doi.org/10.1182/blood.V99.5.1659>.
- (2) Borsi, L.; Balza, E.; Carnemolla, B.; Sassi, F.; Castellani, P.; Berndt, A.; Kosmehl, H.; Birò, A.; Siri, A.; Orecchia, P.; Grassi, J.; Neri, D.; Zardi, L. Selective Targeted Delivery of TNF α to Tumor Blood Vessels. *Blood* **2003**, 102 (13), 4384–4392. <https://doi.org/10.1182/blood-2003-04-1039>.
- (3) Schwager, K.; Hemmerle, T.; Aebischer, D.; Neri, D. The Immunocytokine L19-IL2 Eradicates Cancer When Used in Combination with CTLA-4 Blockade or with L19-TNF. *Journal of Investigative Dermatology* **2013**, 133 (3), 751–758. <https://doi.org/10.1038/jid.2012.376>.
- (4) Gillies, S. D.; Reilly, E. B.; Lo, K.-M.; Reisfeld, R. A. Antibody-Targeted Interleukin 2 Stimulates T-Cell Killing of Autologous Tumor Cells (Recombinant Antibody/Cytokine Fusion Protein/Tumor-Infiltrating Lymphocytes); 1992; Vol. 89.
- (5) Panelli, M. C.; White, R.; Foster, M.; Martin, B.; Wang, E.; Smith, K.; Marincola, F. M. Forecasting the Cytokine Storm Following Systemic Interleukin (IL)-2 Administration. *J Transl Med* **2004**, 2 (17).
- (6) Jia, F.; Wang, G.; Xu, J.; Long, J.; Deng, F.; Jiang, W. Role of Tumor Necrosis Factor- α in the Mortality of Hospitalized Patients with Severe and Critical COVID-19 Pneumonia. *Aging* **2021**, 13 (21), 23895–23912. <https://doi.org/10.18632/aging.203663>.
- (7) Yoon, C.; Johnston, S. C.; Tang, J.; Stahl, M.; Tobin, J. F.; Somers, W. S. Charged Residues Dominate a Unique Interlocking Topography in the Heterodimeric Cytokine Interleukin-12. *EMBO J* **2000**, 19 (14), 3530–3541. <https://doi.org/10.1093/emboj/19.14.3530>.
- (8) Arkin, M. R.; Randal, M.; DeLano, W. L.; Hyde, J.; Luong, T. N.; Oslob, J. D.; Raphael, D. R.; Taylor, L.; Wang, J.; McDowell, R. S.; Wells, J. A.; Braisted, A. C. Binding of Small Molecules to an Adaptive Protein–Protein Interface. *Proceedings of the National Academy of Sciences* **2003**, 100 (4), 1603–1608. <https://doi.org/10.1073/pnas.252756299>.
- (9) Baeyens, K. J.; De Bondt, H. L.; Raeymaekers, A.; Fiers, W.; De Ranter, C. J. The Structure of Mouse Tumour-Necrosis Factor at 1.4 Å Resolution: Towards Modulation of Its Selectivity and Trimerization. *Acta Crystallogr D Biol Crystallogr* **1999**, 55 (4), 772–778. <https://doi.org/10.1107/S0907444998018435>.
- (10) Spitaleri, G.; Berardi, R.; Pierantoni, C.; de Pas, T.; Noberasco, C.; Libbra, C.; González-Iglesias, R.; Giovannoni, L.; Tasciotti, A.; Neri, D.; Menssen, H. D.; de Braud, F. Phase I/II Study of the Tumour-Targeting Human Monoclonal Antibody-Cytokine Fusion Protein L19-TNF in Patients with Advanced Solid Tumours. *J Cancer Res Clin Oncol* **2013**, 139 (3), 447–455. <https://doi.org/10.1007/s00432-012-1327-7>.
- (11) Sabzevari, H.; Gillies, S. D.; Mueller, B. M.; Pancook, J. D.; Reisfeld, R. A. A Recombinant Antibody-Interleukin 2 Fusion Protein Suppresses Growth of Hepatic Human Neuroblastoma Metastases in Severe Combined Immunodeficiency Mice. *Proc Natl Acad Sci U S A* **1994**, 91 (20), 9626–9630. <https://doi.org/10.1073/pnas.91.20.9626>.
- (12) Lode, H. N.; Xiang, R.; Pertl, U.; Förster, E.; Schoenberger, S. P.; Gillies, S. D.; Reisfeld, R. A. Melanoma Immunotherapy by Targeted IL-2 Depends on CD4 T-Cell Help Mediated by CD40-CD40L Interaction. *Journal of Clinical Investigation* **2000**, 105 (11), 1623–1630. <https://doi.org/10.1172/JCI9177>.
- (13) Becker, J. C.; Pancook, J. D.; Gillies, S. D.; Furukawaf, K.; Reisfeld, R. A. T Cell-Mediated Eradication of Murine Metastatic Melanoma Induced by Targeted Interleukin 2 Therapy. *Journal of experimental medicine* **1996**, 183 (5), 2361–2366. <https://doi.org/10.1084/jem.183.5.2361>.
- (14) Hoogenboom, H. R.; Volckaert, G.; M Raust, J. C. Construction and Expression of Antibody-Tumor Necrosis Factor Fusion Proteins. *Mol Immunol* **1991**, 28 (9), 1027–1037. [https://doi.org/10.1016/0161-5890\(91\)90189-Q](https://doi.org/10.1016/0161-5890(91)90189-Q).
- (15) Gillies, S. D.; Young, D.; Lo, K.-M.; Roberts, S. Biological Activity and in Vivo Clearance of Antitumor Antibody/ Cytokine Fusion Proteins. *Bioconjug Chem* **1993**, 4 (3), 230–235.
- (16) Gillies, S. D.; Lan, Y.; Wesolowski, J. S.; Qian, X.; Reisfeld, R. A.; Holden, S.; Super, M.; Lo, K. M. Antibody-IL-12 Fusion Proteins Are Effective in SCID Mouse Models of Prostate and Colon Carcinoma Metastases. *J Immunol* **1998**, 160 (12), 6195–6203.
- (17) Venetz, D.; Koovely, D.; Weder, B.; Neri, D. Targeted Reconstitution of Cytokine Activity upon Antigen Binding Using Split Cytokine Antibody Fusion Proteins. *Journal of Biological Chemistry* **2016**, 291 (35), 18139–18147. <https://doi.org/10.1074/jbc.M116.737734>.
- (18) Asaadi, Y.; Jouneghani, F. F.; Janani, S.; Rahbarizadeh, F. A Comprehensive Comparison between Camelid Nanobodies and Single Chain Variable Fragments. *Biomark Res* **2021**, 9 (1), 87. <https://doi.org/10.1186/s40364-021-00332-6>.
- (19) Bathula, N. V.; Bommadevara, H.; Hayes, J. M. Nanobodies: The Future of Antibody-Based Immune Therapeutics. *Cancer Biother Radiopharm* **2021**, 36 (2), 109–122. <https://doi.org/10.1089/cbr.2020.3941>.

- (20) Gout, D. Y.; Groen, L. S.; van Egmond, M. The Present and Future of Immunocytokines for Cancer Treatment. *Cellular and Molecular Life Sciences* **2022**, *79* (10). <https://doi.org/10.1007/s00018-022-04514-9>.
- (21) Arenas-Ramirez, N.; Woytschak, J.; Boyman, O. Interleukin-2: Biology, Design and Application. *Trends Immunol* **2015**, *36* (12), 763–777. <https://doi.org/10.1016/j.it.2015.10.003>.
- (22) Boyman, O.; Sprent, J. The Role of Interleukin-2 during Homeostasis and Activation of the Immune System. *Nat Rev Immunol* **2012**, *12* (3), 180–190. <https://doi.org/10.1038/nri3156>.
- (23) Létourneau, S.; Krieg, C.; Pantaleo, G.; Boyman, O. IL-2– and CD25-Dependent Immunoregulatory Mechanisms in the Homeostasis of T-Cell Subsets. *Journal of Allergy and Clinical Immunology* **2009**, *123* (4), 758–762. <https://doi.org/10.1016/j.jaci.2009.02.011>.
- (24) Taniguchi, T. The IL-2/IL-2 Receptor System: A Current Overview. *Cell* **1993**, *73* (1), 5–8. [https://doi.org/10.1016/0092-8674\(93\)90152-G](https://doi.org/10.1016/0092-8674(93)90152-G).
- (25) Liao, W.; Lin, J.-X.; Leonard, W. J. Interleukin-2 at the Crossroads of Effector Responses, Tolerance, and Immunotherapy. *Immunity* **2013**, *38* (1), 13–25. <https://doi.org/10.1016/j.immuni.2013.01.004>.
- (26) Geng, X.; Zhang, R.; Yang, G.; Jiang, W.; Xu, C. Interleukin-2 and Autoimmune Disease Occurrence and Therapy. *Eur Rev Med Pharmacol Sci* **2012**, *16* (11), 1462–1467.
- (27) Ye, C.; Brand, D.; Zheng, S. G. Targeting IL-2: An Unexpected Effect in Treating Immunological Diseases. *Signal Transduct Target Ther* **2018**, *3* (1), 2. <https://doi.org/10.1038/s41392-017-0002-5>.
- (28) Schulz, G.; Cheresch, D. A.; Varki, N. M.; Yu, A.; Staffileno, L. K.; Reisfeld R.A. Detection of Ganglioside GD2 in Tumor Tissues and Sera of Neuroblastoma Patients. *Cancer Res* **1984**, *44* (12), 5914–5920.
- (29) Cheresch, D. A.; Harper, J. R.; Schulz, G.; Reisfeld, R. A. Localization of the Gangliosides GD2 and GD3 in Adhesion Plaques and on the Surface of Human Melanoma Cells. *Proceedings of the National Academy of Sciences* **1984**, *81* (18), 5767–5771. <https://doi.org/10.1073/pnas.81.18.5767>.
- (30) Albertini, M. R.; Yang, R. K.; Ranheim, E. A.; Hank, J. A.; Zuleger, C. L.; Weber, S.; Neuman, H.; Hartig, G.; Weigel, T.; Mahvi, D.; Henry, M. B.; Quale, R.; McFarland, T.; Gan, J.; Carmichael, L.; Kim, K. M.; Loibner, H.; Gillies, S. D.; Sondel, P. M. Pilot Trial of the Hu14.18-IL2 Immunocytokine in Patients with Completely Resectable Recurrent Stage III or Stage IV Melanoma. *Cancer Immunology, Immunotherapy* **2018**, *67* (10), 1647–1658. <https://doi.org/10.1007/s00262-018-2223-z>.
- (31) Shusterman, S.; Naranjo, A.; van Ryn, C.; Hank, J. A.; Parisi, M. T.; Shulkin, B. L.; Servaes, S.; London, W. B.; Shimada, H.; Gan, J.; Gillies, S. D.; Maris, J. M.; Park, J. R.; Sondel, P. M. Antitumor Activity and Tolerability of Hu14.18-IL2 with GMCSF and Isotretinoin in Recurrent or Refractory Neuroblastoma: A Children's Oncology Group Phase II Study. *Clinical Cancer Research* **2019**, *25* (20), 6044–6051. <https://doi.org/10.1158/1078-0432.CCR-19-0798>.
- (32) Johannsen, M.; Spitaleri, G.; Curigliano, G.; Roigas, J.; Weikert, S.; Kempkensteffen, C.; Roemer, A.; Kloeters, C.; Rogalla, P.; Pecher, G.; Miller, K.; Berndt, A.; Kosmehl, H.; Trachsel, E.; Kaspar, M.; Lovato, V.; González-Iglesias, R.; Giovannoni, L.; Menssen, H. D.; Neri, D.; De Braud, F. The Tumour-Targeting Human L19-IL2 Immunocytokine: Preclinical Safety Studies, Phase I Clinical Trial in Patients with Solid Tumours and Expansion into Patients with Advanced Renal Cell Carcinoma. *Eur J Cancer* **2010**, *46* (16), 2926–2935. <https://doi.org/10.1016/j.ejca.2010.07.033>.
- (33) Catania, C.; Maur, M.; Berardi, R.; Rocca, A.; Di Giacomo, A. M.; Spitaleri, G.; Masini, C.; Pierantoni, C.; González-Iglesias, R.; Zigon, G.; Tasciotti, A.; Giovannoni, L.; Lovato, V.; Elia, G.; Menssen, H. D.; Neri, D.; Cascinu, S.; Conte, P. F.; De Braud, F. The Tumor-Targeting Immunocytokine F16-IL2 in Combination with Doxorubicin: Dose Escalation in Patients with Advanced Solid Tumors and Expansion into Patients with Metastatic Breast Cancer. *Cell Adh Migr* **2015**, *9* (1–2), 14–21. <https://doi.org/10.4161/19336918.2014.983785>.
- (34) Gillies, S. D.; Lan, Y.; Hettmann, T.; Brunkhorst, B.; Sun, Y.; Mueller, S. O.; Lo, K. M. A Low-Toxicity IL-2-Based Immunocytokine Retains Antitumor Activity despite Its High Degree of IL-2 Receptor Selectivity. *Clinical Cancer Research* **2011**, *17* (11), 3673–3685. <https://doi.org/10.1158/1078-0432.CCR-10-2921>.
- (35) Sharifi, J.; Khawli, L. A.; Hu, P.; King, S.; Epstein, A. L. Characterization of a Phage Display-Derived Human Monoclonal Antibody (NHS76) Counterpart to Chimeric TNT-1 Directed Against Necrotic Regions of Solid Tumors. *Hybrid Hybridomics* **2001**, *20* (5–6), 305–312. <https://doi.org/10.1089/15368590152740707>.
- (36) van den Heuvel, M. M.; Verheij, M.; Boshuizen, R.; Belderbos, J.; Dingemans, A. M. C.; De Ruyscher, D.; Laurent, J.; Tighe, R.; Haanen, J.; Quarantino, S. NHS-IL2 Combined with Radiotherapy: Preclinical Rationale and Phase Ib Trial Results in Metastatic Non-Small Cell Lung Cancer Following First-Line Chemotherapy. *J Transl Med* **2015**, *13* (1). <https://doi.org/10.1186/s12967-015-0397-0>.
- (37) EMD Serono. *MSB0010445 and Stereotactic Body Radiation Therapy in Advanced Melanoma*. Clinicaltrials.gov.
- (38) Waldhauer, I.; Gonzalez-Nicolini, V.; Freimoser-Grundschober, A.; Nayak, T. K.; Fahrmi, L.; Hosse, R. J.; Gerrits, D.; Geven, E. J. W.; Sam, J.; Lang, S.; Bommer, E.; Steinhart, V.; Husar, E.; Colombetti, S.; Van Puijnenbroek, E.; Neubauer, M.; Cline, J. M.; Garg, P. K.; Dugan, G.; Cavallo, F.; Acuna, G.; Charo, J.

- Teichgräber, V.; Evers, S.; Boerman, O. C.; Bacac, M.; Moessner, E.; Umaña, P.; Klein, C. Simlukafusp Alfa (FAP-IL2v) Immunocytokine Is a Versatile Combination Partner for Cancer Immunotherapy. *MAbs* **2021**, *13* (1). <https://doi.org/10.1080/19420862.2021.1913791>.
- (39) Brennen, W. N.; Isaacs, J. T.; Denmeade, S. R. Rationale Behind Targeting Fibroblast Activation Protein–Expressing Carcinoma-Associated Fibroblasts as a Novel Chemotherapeutic Strategy. *Mol Cancer Ther* **2012**, *11* (2), 257–266. <https://doi.org/10.1158/1535-7163.MCT-11-0340>.
- (40) Siebert, N.; Leopold, J.; Zumpe, M.; Troschke-Meurer, S.; Biskupski, S.; Zikoridse, A.; Lode, H. N. The Immunocytokine FAP-IL-2v Enhances Anti-Neuroblastoma Efficacy of the Anti-GD2 Antibody Dinutuximab Beta. *Cancers (Basel)* **2022**, *14* (19). <https://doi.org/10.3390/cancers14194842>.
- (41) Schwager, K.; Kaspar, M.; Bootz, F.; Marcolongo, R.; Paresce, E.; Neri, D.; Trachsel, E. Preclinical Characterization of DEKAVIL (F8-IL10), a Novel Clinical-Stage Immunocytokine Which Inhibits the Progression of Collagen-Induced Arthritis. *Arthritis Res Ther* **2009**, *11* (5). <https://doi.org/10.1186/ar2814>.
- (42) Rybak, J.-N.; Roesli, C.; Kaspar, M.; Villa, A.; Neri, D. The Extra-Domain A of Fibronectin Is a Vascular Marker of Solid Tumors and Metastases. *Cancer Res* **2007**, *67* (22), 10948–10957. <https://doi.org/10.1158/0008-5472.CAN-07-1436>.
- (43) Frey, K.; Schliemann, C.; Schwager, K.; Giavazzi, R.; Johannsen, M.; Neri, D. The Immunocytokine F8-IL2 Improves the Therapeutic Performance of Sunitinib in a Mouse Model of Renal Cell Carcinoma. *J Urol* **2010**, *184*, 2540–2548. <https://doi.org/10.1016/j.juro.2010.07.030>.
- (44) Wieckowski, S.; Hemmerle, T.; Prince, S. S.; Schlienger, B. D.; Hillinger, S.; Neri, D.; Zippelius, A. Therapeutic Efficacy of the F8-IL2 Immunocytokine in a Metastatic Mouse Model of Lung Adenocarcinoma. *Lung Cancer* **2015**, *88* (1), 9–15. <https://doi.org/10.1016/j.lungcan.2015.01.019>.
- (45) Huttmacher, C.; Nuñez, N. G.; Luzzi, A. R.; Becher, B.; Neri, D. Targeted Delivery of IL2 to the Tumor Stroma Potentiates the Action of Immune Checkpoint Inhibitors by Preferential Activation of NK and CD8⁺ T Cells. *Cancer Immunol Res* **2019**, *7* (4), 572–583. <https://doi.org/10.1158/2326-6066.CIR-18-0566>.
- (46) Pretto, F.; Elia, G.; Castioni, N.; Neri, D. Preclinical Evaluation of IL2-Based Immunocytokines Supports Their Use in Combination with Dacarbazine, Paclitaxel and TNF-Based Immunotherapy. *Cancer Immunology, Immunotherapy* **2014**, *63* (9), 901–910. <https://doi.org/10.1007/s00262-014-1562-7>.
- (47) De Luca, R.; Soltermann, A.; Pretto, F.; Pemberton-Ross, C.; Pellegrini, G.; Wulhfard, S.; Neri, D. Potency-Matched Dual Cytokine–Antibody Fusion Proteins for Cancer Therapy. *Mol Cancer Ther* **2017**, *16* (11), 2442–2451. <https://doi.org/10.1158/1535-7163.MCT-17-0211>.
- (48) de Luca, R.; Neri, D. Potentiation of PD-L1 Blockade with a Potency-Matched Dual Cytokine–Antibody Fusion Protein Leads to Cancer Eradication in BALB/c-Derived Tumors but Not in Other Mouse Strains. *Cancer Immunology, Immunotherapy* **2018**, *67* (9), 1381–1391. <https://doi.org/10.1007/s00262-018-2194-0>.
- (49) de Luca, R.; Gouyou, B.; Ongaro, T.; Villa, A.; Ziffels, B.; Sannino, A.; Buttinoni, G.; Galeazzi, S.; Mazzacuvu, M.; Neri, D. A Novel Fully-Human Potency-Matched Dual Cytokine-Antibody Fusion Protein Targets Carbonic Anhydrase IX in Renal Cell Carcinomas. *Front Oncol* **2019**, *9* (November), 1–11. <https://doi.org/10.3389/fonc.2019.01228>.
- (50) Schliemann, C.; Hemmerle, T.; Berdel, A. F.; Angenendt, L.; Kerkhoff, A.; Hering, J. P.; Heindel, W.; Hartmann, W.; Wardelmann, E.; Chawla, S. P.; de Braud, F.; Lenz, G.; Neri, D.; Kessler, T.; Berdel, W. E. Dose Escalation and Expansion Phase I Studies with the Tumour-Targeting Antibody-Tumour Necrosis Factor Fusion Protein L19TNF plus Doxorubicin in Patients with Advanced Tumours, Including Sarcomas. *Eur J Cancer* **2021**, *150*, 143–154. <https://doi.org/10.1016/j.ejca.2021.03.038>.
- (51) Papadia, F.; Basso, V.; Patuzzo, R.; Maurichi, A.; Di Florio, A.; Zardi, L.; Ventura, E.; González-Iglesias, R.; Lovato, V.; Giovannoni, L.; Tasciotti, A.; Neri, D.; Santinami, M.; Menssen, H. D.; De Cian, F. Isolated Limb Perfusion with the Tumor-Targeting Human Monoclonal Antibody-Cytokine Fusion Protein L19-TNF plus Melphalan and Mild Hyperthermia in Patients with Locally Advanced Extremity Melanoma. *J Surg Oncol* **2013**, *107* (2), 173–179. <https://doi.org/10.1002/jso.23168>.
- (52) Weiss, T.; Puca, E.; Silginer, M.; Hemmerle, T.; Pazahr, S.; Bink, A.; Weller, M.; Neri, D.; Roth, P. Immunocytokines Are a Promising Immunotherapeutic Approach against Glioblastoma. *Sci Transl Med* **2020**, *12* (564), 2311. <https://doi.org/https://doi.org/10.1126/scitranslmed.abb2311>.
- (53) Danielli, R.; Patuzzo, R.; Di Giacomo, A. M.; Gallino, G.; Maurichi, A.; Di Florio, A.; Cutaia, O.; Lazzeri, A.; Fazio, C.; Miracco, C.; Giovannoni, L.; Elia, G.; Neri, D.; Maio, M.; Santinami, M. Intralesional Administration of L19-IL2/L19-TNF in Stage III or Stage IVM1a Melanoma Patients: Results of a Phase II Study. *Cancer Immunology, Immunotherapy* **2015**, *64* (8), 999–1009. <https://doi.org/10.1007/s00262-015-1704-6>.
- (54) Trinchieri, G.; Pflanz, S.; Kastelein, R. A. The IL-12 Family of Heterodimeric Cytokines. *Immunity* **2003**, *19* (5), 641–644. [https://doi.org/10.1016/S1074-7613\(03\)00296-6](https://doi.org/10.1016/S1074-7613(03)00296-6).
- (55) Brunda, M. J.; Luistro, L.; Rummennik, L.; Wright, R. B.; Dvornozniak, M.; Aglione, A.; Wigginton, J. M.; Wilttrout, R. H.; Hendrzak, J. A.; Palleroni, A. V.; Dvornozniak, M.; Aglione, A.; Hendrzak, J. A.; Palleroni, A. V.; Wigginton,

- J. M.; Wilttrout, R. H. Antitumor Activity of Interleukin 12 in Preclinical Models. *Cancer Chemother Pharmacol* **1996**, *38*, 16–21. <https://doi.org/https://doi.org/10.1007/s002800051031>.
- (56) Zheng, H.; Ban, Y.; Wei, F.; Ma, X. Regulation of Interleukin-12 Production in Antigen-Presenting Cells; 2016; pp 117–138. https://doi.org/10.1007/978-94-024-0921-5_6.
- (57) Nakajima, C.; Uekusa, Y.; Iwasaki, M.; Yamaguchi, N.; Mukai, T.; Gao, P.; Tomura, M.; Ono, S.; Tsujimura, T.; Fujiwara, H.; Hamaoka, T. A Role of Interferon-Gamma (IFN-Gamma) in Tumor Immunity: T Cells with the Capacity to Reject Tumor Cells Are Generated but Fail to Migrate to Tumor Sites in IFN-Gamma-Deficient Mice. *Cancer Res* **2001**, *61* (8), 3399–3405.
- (58) Nastala, C. L.; Edington, H. D.; McKinney, T. G.; Tahara, H.; Nalesnik, M. A.; Brunda, M. J.; Gately, M. K.; Wolf, S. F.; Schreiber, R. D.; Storkus, W. J. Recombinant IL-12 Administration Induces Tumor Regression in Association with IFN-Gamma Production. *J Immunol* **1994**, *153* (4), 1697–1706.
- (59) Balashov, K. E.; Smith, D. R.; Khoury, S. J.; Hafler, D. A.; Weiner, H. L. Increased Interleukin 12 Production in Progressive Multiple Sclerosis: Induction by Activated CD4⁺ T Cells via CD40 Ligand. *Proceedings of the National Academy of Sciences* **1997**, *94* (2), 599–603. <https://doi.org/10.1073/pnas.94.2.599>.
- (60) Atkins, M. B.; Robertson, M. J.; Gordon, M.; Lotze, M. T.; DeCoste, M.; DuBois, J. S.; Ritz, J.; Sandler, A. B.; Edington, H. D.; Garzone, P. D.; Mier, J. W.; Canning, C. M.; Battiato, L.; Tahara, H.; Sherman, M. L. Phase I Evaluation of Intravenous Recombinant Human Interleukin 12 in Patients with Advanced Malignancies. *Clin Cancer Res* **1997**, *3* (3), 409–417.
- (61) Stromnes, I. M.; Brockenbrough, J. S.; Izeradjene, K.; Carlson, M. A.; Cuevas, C.; Simmons, R. M.; Greenberg, P. D.; Hingorani, S. R. Targeted Depletion of an MDSC Subset Unmasks Pancreatic Ductal Adenocarcinoma to Adaptive Immunity. *Gut* **2014**, *63* (11), 1769–1781. <https://doi.org/10.1136/gutjnl-2013-306271>.
- (62) Xu, C.; Zhang, Y.; Alexander Rolfe, P.; Hernández, V. M.; Guzman, W.; Kradjian, G.; Marelli, B.; Qin, G.; Qi, J.; Wang, H.; Yu, H.; Tighe, R.; Lo, K. M.; English, J. M.; Radvanyi, L.; Lan, Y. Combination Therapy with NHS-MuL12 and Avelumab (Anti-PD-L1) Enhances Antitumor Efficacy in Preclinical Cancer Models. *Clinical Cancer Research* **2017**, *23* (19), 5869–5880. <https://doi.org/10.1158/1078-0432.CCR-17-0483>.
- (63) Fallon, J. K.; Vandeveer, A. J.; Schlom, J.; Greiner, J. W. Enhanced Antitumor Effects by Combining an IL-12/Anti-DNA Fusion Protein with Avelumab, an Anti-PD-L1 Antibody. *Oncotarget* **2017**, *8* (13), 20558–20571. <https://doi.org/10.18632/oncotarget.16137>.
- (64) Strauss, J.; Heery, C. R.; Kim, J. W.; Jochems, C.; Donahue, R. N.; Montgomery, A. S.; McMahon, S.; Lamping, E.; Marte, J. L.; Madan, R. A.; Bilusic, M.; Silver, M. R.; Bertotti, E.; Schlom, J.; Gulley, J. L. First-in-Human Phase I Trial of a Tumor-Targeted Cytokine (NHS-IL12) in Subjects with Metastatic Solid Tumors. *Clinical Cancer Research* **2019**, *25* (1), 99–109. <https://doi.org/10.1158/1078-0432.CCR-18-1512>.
- (65) Gafner, V.; Trachsel, E.; Neri, D. An Engineered Antibody-Interleukin-12 Fusion Protein with Enhanced Tumor Vascular Targeting Properties. *Int J Cancer* **2006**, *119* (9), 2205–2212. <https://doi.org/10.1002/ijc.22101>.
- (66) Ongaro, T.; Matasci, M.; Cazzamalli, S.; Gouyou, B.; De Luca, R.; Neri, D.; Villa, A. A Novel Anti-Cancer L19-Interleukin-12 Fusion Protein with an Optimized Peptide Linker Efficiently Localizes in Vivo at the Site of Tumors. *J Biotechnol* **2019**, *297*, 17–25. <https://doi.org/10.1016/j.jbiotec.2018.12.004>.
- (67) Cheever, M. A. Twelve Immunotherapy Drugs That Could Cure Cancers. *Immunol Rev* **2008**, *222*, 357–368. <https://doi.org/10.1111/j.1600-065X.2008.00604.x>.
- (68) Rochman, Y.; Spolski, R.; Leonard, W. J. New Insights into the Regulation of T Cells by γ c Family Cytokines. *Nat Rev Immunol* **2009**, *9* (7), 480–490. <https://doi.org/10.1038/nri2580>.
- (69) Kermer, V.; Baum, V.; Hornig, N.; Kontermann, R. E.; Müller, D. An Antibody Fusion Protein for Cancer Immunotherapy Mimicking IL-15 Trans-Presentation at the Tumor Site. *Mol Cancer Ther* **2012**, *11* (6), 1279–1288. <https://doi.org/10.1158/1535-7163.MCT-12-0019>.
- (70) Fehniger, T. A.; Caligiuri, M. A. Interleukin 15: Biology and Relevance to Human Disease. *Blood* **2001**, *97* (1), 14–32. <https://doi.org/10.1182/blood.V97.1.14>.
- (71) McInnes, I. B.; Al-Mughales, J.; Field, M.; Leung, B. P.; Huang, F.; Dixon, R.; Sturrock, R. D.; Wilkinson, P. C.; Liew, F. Y. The Role of Interleukin-15 in T-Cell Migration and Activation in Rheumatoid Arthritis. *Nat Med* **1996**, *2* (2), 175–182. <https://doi.org/10.1038/nm0296-175>.
- (72) Kirman, I.; Nielsen, O. H. Increased Numbers of Interleukin-15-Expressing Cells in Active Ulcerative Colitis. *Am J Gastroenterol* **1996**, *91* (9), 1789–1794.
- (73) Bamford, R. N.; Battiat, A. P.; Burton, J. D.; Sharma, H.; Waldmann, T. A. Interleukin (IL) 15/IL-T Production by the Adult T-Cell Leukemia Cell Line HuT-102 Is Associated with a Human T-Cell Lymphotropic Virus Type I Region /IL-15 Fusion Message That Lacks Many Upstream AUGs That Normally Attenuates IL-15 mRNA Translation. *Proceedings of the National Academy of Sciences* **1996**, *93* (7), 2897–2902. <https://doi.org/10.1073/pnas.93.7.2897>.
- (74) Maeda, M.; Arima, N.; Daitoku, Y.; Kashiwara, M.; Okamoto, H.; Uchiyama, T.; Shirono, K.; Matsuoka, M.; Hattori, T.; Takatsuki, K. Evidence for the Interleukin-2 Dependent Expansion of Leukemic Cells in Adult T Cell Leukemia. *Blood* **1987**, *70* (5), 1407–1411.

- (75) Klebanoff, C. A.; Finkelstein, S. E.; Surman, D. R.; Lichtman, M. K.; Gattinoni, L.; Theoret, M. R.; Grewal, N.; Spiess, P. J.; Antony, P. A.; Palmer, D. C.; Tagaya, Y.; Rosenberg, S. A.; Waldmann, T. A.; Restifo, N. P. IL-15 Enhances the *in Vivo* Antitumor Activity of Tumor-Reactive CD8⁺ T Cells. *Proceedings of the National Academy of Sciences* **2004**, *101* (7), 1969–1974. <https://doi.org/10.1073/pnas.0307298101>.
- (76) Kobayashi, H.; Dubois, S.; Sato, N.; Sabzevari, H.; Sakai, Y.; Waldmann, T. A.; Tagaya, Y. Role of Trans-Cellular IL-15 Presentation in the Activation of NK Cell-Mediated Killing, Which Leads to Enhanced Tumor Immunosurveillance. *Blood* **2005**, *105* (2), 721–727. <https://doi.org/10.1182/blood-2003-12-4187>.
- (77) Bergamaschi, C.; Stravokefalou, V.; Stellas, D.; Karaliota, S.; Felber, B. K.; Pavlakis, G. N. Heterodimeric IL-15 in Cancer Immunotherapy. *Cancers (Basel)* **2021**, *13* (4), 837. <https://doi.org/10.3390/cancers13040837>.
- (78) Chen, S.; Huang, Q.; Liu, J.; Xing, J.; Zhang, N.; Liu, Y.; Wang, Z.; Li, Q. A Targeted IL-15 Fusion Protein with Potent Anti-Tumor Activity. *Cancer Biol Ther* **2015**, *16* (9), 1415–1421. <https://doi.org/10.1080/15384047.2015.1071739>.
- (79) Chung, K. Y.; Park, H.; Muhsin Abdul-Karim, R.; Blythe Doroshov, D.; Chaves, J.; Coleman, T. A.; Nakai, K.; Patel, P.; Wang, J.; Zhang, H.; Leijun, H. Phase I Study of BJ-001, a Tumor-Targeting Interleukin-15 Fusion Protein, in Patients with Solid Tumor. *Journal of Clinical Oncology* **2021**, *39* (15).
- (80) Jochems, C.; Tritsch, S. R.; Knudson, K. M.; Gameiro, S. R.; Rumfield, C. S.; Pellom, S. T.; Morillon, Y. M.; Newman, R.; Marcus, W.; Szeto, C.; Rabizadeh, S.; Wong, H. C.; Soon-Shiong, P.; Schlom, J. The Multi-Functionality of N-809, a Novel Fusion Protein Encompassing Anti-PD-L1 and the IL-15 Superagonist Fusion Complex. *Oncoimmunology* **2019**, *8* (2). <https://doi.org/10.1080/2162402X.2018.1532764>.
- (81) Knudson, K. M.; Hicks, K. C.; Ozawa, Y.; Schlom, J.; Gameiro, S. R. Functional and Mechanistic Advantage of the Use of a Bifunctional Anti-PD-L1/IL-15 Superagonist. *J Immunother Cancer* **2020**, *8* (1). <https://doi.org/10.1136/jitc-2019-000493>.
- (82) Li, Y.; Wu, L.; Liu, Y.; Ma, S.; Huang, B.; Feng, X.; Wang, H. A Novel Multifunctional Anti-PD-L1-CD16a-IL15 Induces Potent Cancer Cell Killing in PD-L1-Positive Tumour Cells. *Transl Oncol* **2022**, *21*. <https://doi.org/10.1016/j.tranon.2022.101424>.
- (83) Shi, W.; Lv, L.; Liu, N.; Wang, H.; Wang, Y.; Zhu, W.; Liu, Z.; Zhu, J.; Lu, H. A Novel Anti-PD-L1/IL-15 Immunocytokine Overcomes Resistance to PD-L1 Blockade and Elicits Potent Antitumor Immunity. *Molecular Therapy* **2023**, *31* (1), 66–77. <https://doi.org/10.1016/j.ymthe.2022.08.016>.
- (84) Leonard, W. J.; Spolski, R. Interleukin-21: A Modulator of Lymphoid Proliferation, Apoptosis and Differentiation. *Nature Reviews Immunology*. September 2005, pp 688–698. <https://doi.org/10.1038/nri1688>.
- (85) Habib, T.; Senadheera, S.; Weinberg, K.; Kaushansky, K. The Common γ Chain (Fc) Is a Required Signaling Component of the IL-21 Receptor and Supports IL-21-Induced Cell Proliferation via JAK3. *Biochemistry* **2002**, *41* (27), 8725–8731. <https://doi.org/10.1021/bi0202023>.
- (86) Søndergaard, H.; Skak, K. IL-21: Roles in Immunopathology and Cancer Therapy. *Tissue Antigens* **2009**, *74* (6), 467–479. <https://doi.org/10.1111/j.1399-0039.2009.01382.x>.
- (87) Davis, I. D.; Skrmsager, B. K.; Cebon, J.; Nicholaou, T.; Barlow, J. W.; Moller, N. P. H.; Skak, K.; Lundsgaard, D.; Frederiksen, K. S.; Thygesen, P.; McArthur, G. A. An Open-Label, Two-Arm, Phase I Trial of Recombinant Human Interleukin-21 in Patients with Metastatic Melanoma. *Clinical Cancer Research* **2007**, *13* (12), 3630–3636. <https://doi.org/10.1158/1078-0432.CCR-07-0410>.
- (88) Deng, S.; Sun, Z.; Qiao, J.; Liang, Y.; Liu, L.; Dong, C.; Shen, A.; Wang, Y.; Tang, H.; Fu, Y. X.; Peng, H. Targeting Tumors with IL-21 Reshapes the Tumor Microenvironment by Proliferating PD-1^{int}Tim-3-CD8⁺ T Cells. *JCI Insight* **2020**, *5* (7). <https://doi.org/10.1172/JCI.INSIGHT.132000>.
- (89) Shen, S.; Sckisel, G.; Sahoo, A.; Lalani, A.; Otter, D. Den; Pearson, J.; DeVoss, J.; Cheng, J.; Casey, S. C.; Case, R.; Yang, M.; Low, R.; Daris, M.; Fan, B.; Agrawal, N. J.; Ali, K. Engineered IL-21 Cytokine Muteins Fused to Anti-PD-1 Antibodies Can Improve CD8⁺ T Cell Function and Anti-Tumor Immunity. *Front Immunol* **2020**, *11*. <https://doi.org/10.3389/fimmu.2020.00832>.
- (90) Li, Y.; Cong, Y.; Jia, M.; He, Q.; Zhong, H.; Zhao, Y.; Li, H.; Yan, M.; You, J.; Liu, J.; Chen, L.; Hang, H.; Wang, S. Targeting IL-21 to Tumor-Reactive T Cells Enhances Memory T Cell Responses and Anti-PD-1 Antibody Therapy. *Nat Commun* **2021**, *12* (1). <https://doi.org/10.1038/s41467-021-21241-0>.
- (91) Di Nitto, C.; Neri, D.; Weiss, T.; Weller, M.; De Luca, R. Design and Characterization of Novel Antibody-Cytokine Fusion Proteins Based on Interleukin-21. *Antibodies* **2022**, *11* (1). <https://doi.org/10.3390/antib11010019>.
- (92) Chen, D.; Tang, T.-X.; Deng, H.; Yang, X.-P.; Tang, Z.-H. Interleukin-7 Biology and Its Effects on Immune Cells: Mediator of Generation, Differentiation, Survival, and Homeostasis. *Front Immunol* **2021**, *12*. <https://doi.org/10.3389/fimmu.2021.747324>.
- (93) Barata, J. T.; Durum, S. K.; Seddon, B. Flip the Coin: IL-7 and IL-7R in Health and Disease. *Nat Immunol* **2019**, *20* (12), 1584–1593. <https://doi.org/10.1038/s41590-019-0479-x>.

- (94) Namen, A. E.; Lupton, S.; Hjerrild, K.; Wignall, J.; Mochizuki, D. Y.; Schmierer, A.; Mosley, B.; March, C. J.; Urdal, D. Stimulation of B-Cell Progenitors by Cloned Murine Interleukin-7. *Nature* **1988**, *333*, 571–573. <https://doi.org/10.1038/333571a0>.
- (95) Komschlies, K. L.; Gregorio, T. M.; Gruys, M. E.; Back, T. C.; Faltynek, C. R.; Wilttrout, R. H. Administration of Recombinant Human IL-7 to Mice Alters the Composition of B-Lineage Cells and T Cell Subsets, Enhances T Cell Function, and Induces Regression of Established Metastases. *Journal of immunology* **1994**, *152* (12), 5776–5784.
- (96) Sportès, C.; Babb, R. R.; Krumlauf, M. C.; Hakim, F. T.; Steinberg, S. M.; Chow, C. K.; Brown, M. R.; Fleisher, T. A.; Noel, P.; Maric, I.; Stetler-Stevenson, M.; Engel, J.; Buffet, R.; Morre, M.; Amato, R. J.; Pecora, A.; Mackall, C. L.; Gress, R. E. Phase I Study of Recombinant Human Interleukin-7 Administration in Subjects with Refractory Malignancy. *Clinical Cancer Research* **2010**, *16* (2), 727–735. <https://doi.org/10.1158/1078-0432.CCR-09-1303>.
- (97) Pasche, N.; Woytschak, J.; Wulhfard, S.; Villa, A.; Frey, K.; Neri, D. Cloning and Characterization of Novel Tumor-Targeting Immunocytokines Based on Murine IL7. *J Biotechnol* **2011**, *154* (1), 84–92. <https://doi.org/10.1016/j.jbiotec.2011.04.003>.
- (98) Rojas-Zuleta, W. G.; Sanchez, E. IL-9: Function, Sources, and Detection; 2017; pp 21–35. https://doi.org/10.1007/978-1-4939-6877-0_2.
- (99) Yazdani, R.; Shapoori, S.; Rezaeipoor, M.; Sanaei, R.; Ganjalikhani-Hakemi, M.; Azizi, G.; Rae, W.; Aghamohammadi, A.; Rezaei, N. Features and Roles of T Helper 9 Cells and Interleukin 9 in Immunological Diseases. *Allergol Immunopathol (Madr)* **2019**, *47* (1), 90–104. <https://doi.org/10.1016/j.aller.2018.02.003>.
- (100) Bauer, J. H.; Liu, K. D.; You, Y.; Lai, S. Y.; Goldsmith, M. A. Heteromerization of the Γ c Chain with the Interleukin-9 Receptor α Subunit Leads to STAT Activation and Prevention of Apoptosis. *Journal of Biological Chemistry* **1998**, *273* (15), 9255–9260. <https://doi.org/10.1074/jbc.273.15.9255>.
- (101) Purwar, R.; Schlappbach, C.; Xiao, S.; Kang, H. S.; Elyaman, W.; Jiang, X.; Jetten, A. M.; Khoury, S. J.; Fuhlbrigge, R. C.; Kuchroo, V. K.; Clark, R. A.; Kupper, T. S. Robust Tumor Immunity to Melanoma Mediated by Interleukin-9-Producing T Cells. *Nat Med* **2012**, *18* (8), 1248–1253. <https://doi.org/10.1038/nm.2856>.
- (102) Doherty, T. A.; Broide, D. H. Insights into the Biology of IL-9 in Asthma. *Journal of Allergy and Clinical Immunology* **2022**, *150* (3), 585–586. <https://doi.org/10.1016/j.jaci.2022.05.015>.
- (103) Heiss, J.; Grün, K.; Tempel, L.; Matasci, M.; Schreppe, A.; Schwarzer, M.; Bauer, R.; Förster, M.; Berndt, A.; Jung, C.; Schulze, P. C.; Neri, D.; Franz, M. Targeted Interleukin-9 Delivery in Pulmonary Hypertension: Comparison of Immunocytokine Formats and Effector Cell Study. *Eur J Clin Invest* **2022**. <https://doi.org/10.1111/eci.13907>.
- (104) de Waal Malefyt, R.; Haanen, J.; Spits, H.; Roncarolo, M. G.; te Velde, A.; Figdor, C.; Johnson, K.; Kastelein, R.; Yssel, H.; de Vries, J. E. Interleukin 10 (IL-10) and Viral IL-10 Strongly Reduce Antigen-Specific Human T Cell Proliferation by Diminishing the Antigen-Presenting Capacity of Monocytes via Downregulation of Class II Major Histocompatibility Complex Expression. *Journal of Experimental Medicine* **1991**, *174* (4), 915–924. <https://doi.org/10.1084/jem.174.4.915>.
- (105) Saraiva, M.; Vieira, P.; O'Garra, A. Biology and Therapeutic Potential of Interleukin-10. *Journal of Experimental Medicine* **2020**, *217* (1). <https://doi.org/10.1084/jem.20190418>.
- (106) Zheng, L. M.; Ojcius, D. M.; Garaud, F.; Roth, C.; Maxwell, E.; Li, Z.; Rong, H.; Chen, J.; Wang, X. Y.; Catino, J. J.; King, I. Interleukin-10 Inhibits Tumor Metastasis through an NK Cell-Dependent Mechanism. *Journal of Experimental Medicine* **1996**, *184* (2), 579–584. <https://doi.org/10.1084/jem.184.2.579>.
- (107) Asadullah, K.; Sterry, W.; Volk, H. D. Interleukin-10 Therapy—Review of a New Approach. *Pharmacol Rev* **2003**, *55* (2), 241–269. <https://doi.org/10.1124/pr.55.2.4>.
- (108) Qiao, J.; Liu, Z.; Dong, C.; Luan, Y.; Zhang, A.; Moore, C.; Fu, K.; Peng, J.; Wang, Y.; Ren, Z.; Han, C.; Xu, T.; Fu, Y. X. Targeting Tumors with IL-10 Prevents Dendritic Cell-Mediated CD8+ T Cell Apoptosis. *Cancer Cell* **2019**, *35* (6), 901–915.e4. <https://doi.org/10.1016/j.ccell.2019.05.005>.
- (109) Rossi, E. A.; Goldenberg, D. M.; Cardillo, T. M.; Stein, R.; Chang, C. H. CD20-Targeted Tetrameric Interferon- α , a Novel and Potent Immunocytokine for the Therapy of B-Cell Lymphomas. *Blood* **2009**, *114* (18), 3864–3871. <https://doi.org/10.1182/blood-2009-06-228890>.
- (110) Liang, Y.; Tang, H.; Guo, J.; Qiu, X.; Yang, Z.; Ren, Z.; Sun, Z.; Bian, Y.; Xu, L.; Xu, H.; Shen, J.; Han, Y.; Dong, H.; Peng, H.; Fu, Y. X. Targeting IFN α to Tumor by Anti-PD-L1 Creates Feedforward Antitumor Responses to Overcome Checkpoint Blockade Resistance. *Nat Commun* **2018**, *9* (1). <https://doi.org/10.1038/s41467-018-06890-y>.
- (111) Ebbinghaus, C.; Ronca, R.; Kaspar M; Grabulovski, D.; Berndt, A.; Kosmehl, H.; Zardi, L.; Neri, D. Engineered Vascular-Targeting Antibody-Interferon- γ Fusion Protein for Cancer Therapy. *Int. J. Cancer* **2005**, *116*, 304–316. <https://doi.org/10.1002/ijc.20952>.
- (112) Metelitsa, L. S.; Gillies, S. D.; Super, M.; Shimada, H.; Reynolds, C. P.; Seeger, R. C. Antidisialoganglioside/Granulocyte Macrophage-Colony-Stimulating Factor Fusion Protein Facilitates Neutrophil Antibody-Dependent Cellular Cytotoxicity and Depends on FcRII (CD32) and Mac-1

- (CD11b/CD18) for Enhanced Effector Cell Adhesion and Azurophil Granule Exocytosis. *Blood* **2002**, 99 (11), 4166–4173. <https://doi.org/10.1182/blood.v99.11.4166>.
- (113) Dela Cruz, J. S.; Trinh, K. R.; Morrison, S. L.; Penichet, M. L. Recombinant Anti-Human HER2/ Neu IgG3- (GM-CSF) Fusion Protein Retains Antigen Specificity and Cytokine Function and Demonstrates Antitumor Activity. *The Journal of Immunology* **2000**, 165 (9), 5112–5121. <https://doi.org/10.4049/jimmunol.165.9.5112>.
- (114) Eckert, F.; Jelas, I.; Oehme, M.; Huber, S. M.; Sonntag, K.; Welker, C.; Gillies, S. D.; Strittmatter, W.; Zips, D.; Handgretinger, R.; Schilbach, K. Tumor-Targeted IL-12 Combined with Local Irradiation Leads to Systemic Tumor Control via Abscopal Effects in Vivo. *Oncoimmunology* **2017**, 6 (6). <https://doi.org/10.1080/2162402X.2017.1323161>.
- (115) Schliemann, C.; Palumbo, A.; Zuberbühler, K.; Villa, A.; Kaspar, M.; Trachsel, E.; Klapper, W.; Menssen, H. D.; Neri, D. Complete Eradication of Human B-Cell Lymphoma Xenografts Using Rituximab in Combination with the Immunocytokine L19-IL2. *Blood* **2009**, 113 (10), 2275–2283. <https://doi.org/10.1182/blood-2008-05-160747>.
- (116) Zheng, X.; Wu, Y.; Bi, J.; Huang, Y.; Cheng, Y.; Li, Y.; Wu, Y.; Cao, G.; Tian, Z. The Use of Supercytokines, Immunocytokines, Engager Cytokines, and Other Synthetic Cytokines in Immunotherapy. *Cell Mol Immunol* **2022**, 19 (2), 192–209. <https://doi.org/10.1038/s41423-021-00786-6>.
- (117) Klein, C.; Waldhauer, I.; Nicolini, V. G.; Freimoser-Grundschober, A.; Nayak, T.; Vugts, D. J.; Dunn, C.; Bolijn, M.; Benz, J.; Stihle, M.; Lang, S.; Roemmele, M.; Hofer, T.; van Puijenbroek, E.; Wittig, D.; Moser, S.; Ast, O.; Brünker, P.; Gorr, I. H.; Neumann, S.; de Vera Mudry, M. C.; Hinton, H.; Crameri, F.; Saro, J.; Evers, S.; Gerdes, C.; Bacac, M.; van Dongen, G.; Moessner, E.; Umaña, P. Cergutuzumab Amunaleukin (CEA-IL2v), a CEA-Targeted IL-2 Variant-Based Immunocytokine for Combination Cancer Immunotherapy: Overcoming Limitations of Aldesleukin and Conventional IL-2-Based Immunocytokines. *Oncoimmunology* **2017**, 6 (3). <https://doi.org/10.1080/2162402X.2016.1277306>.
- (118) Waldmann, T. A. The Biology of Interleukin-2 and Interleukin-15: Implications for Cancer Therapy and Vaccine Design. *Nat Rev Immunol* **2006**, 6 (8), 595–601. <https://doi.org/10.1038/nri1901>.
- (119) Gillies, S. D. A New Platform for Constructing Antibody-Cytokine Fusion Proteins (Immunocytokines) with Improved Biological Properties and Adaptable Cytokine Activity. *Protein Engineering, Design and Selection* **2013**, 26 (10), 561–569. <https://doi.org/10.1093/protein/gzt045>.
- (120) Hsu, E. J.; Cao, X.; Moon, B.; Bae, J.; Sun, Z.; Liu, Z.; Fu, Y. X. A Cytokine Receptor-Masked IL2 Prodrug Selectively Activates Tumor-Infiltrating Lymphocytes for Potent Antitumor Therapy. *Nat Commun* **2021**, 12 (1). <https://doi.org/10.1038/s41467-021-22980-w>.
- (121) Stauber, D. J.; Debler, E. W.; Horton, P. A.; Smith, K. A.; Wilson, I. A. Crystal Structure of the IL-2 Signaling Complex: Paradigm for a Heterotrimeric Cytokine Receptor. *Proceedings of the National Academy of Sciences* **2006**, 103 (8), 2788–2793. <https://doi.org/10.1073/pnas.0511161103>.
- (122) Morgunova, E.; Tuuttila, A.; Bergmann, U.; Isupov, M.; Lindqvist, Y.; Schneider, G.; Tryggvason, K. Structure of Human Pro-Matrix Metalloproteinase-2: Activation Mechanism Revealed. *Science (1979)* **1999**, 284 (5420), 1667–1670. <https://doi.org/10.1126/science.284.5420.1667>.
- (123) Gubler, U.; Ochua, A. A.; Schoenhaut, D. S.; Dwyer, C. M.; McComas, W.; Motyka, R.; Nabavi, N.; Wolitzky, A. G.; Quinn, P. M.; Familletti, P. C.; Gately, M. K. Coexpression of Two Distinct Genes Is Required to Generate Secreted Bioactive Cytotoxic Lymphocyte Maturation Factor. *Proc. Natl. Acad. Sci* **1991**, 88 (10), 4143–4147.
- (124) Wolf, S. F.; Temple, P. A.; Kobayashi, M.; Young, D.; Dicig, M.; Lowe, L.; Dzialo, R.; Fitz, L.; Ferenz, C.; Hewick, R. M. Cloning of cDNA for Natural Killer Cell Stimulatory Factor, a Heterodimeric Cytokine with Multiple Biologic Effects on T and Natural Killer Cells. *J Immunol* **1991**, 146 (9), 3074–3081.

2

**Chemical Inactivation and Reactivation of
an IL-1 β -Based Immunocytokine using
Click-to-Release Chemistry**

Introduction

Interleukin-1 β (IL-1 β) is a member of the IL-1 superfamily of cytokines.^{1,2} It is one of the 'master regulator' cytokines and has highly pleiotropic effects both locally and systemically. IL-1 β is secreted upon recognition of pathogen-associated molecular patterns (PAMPs) by pattern recognition receptors (PRRs) during inflammation³, particularly during inflammasome formation, and plays a role in various processes. These processes include sensing microbial invasion⁴ and tissue or cell damage⁵ during, for example, injuries or cancer. Besides this 'innate' function, it has also a role in lymphocyte differentiation and other adaptive responses.⁶

In the body, IL-1 β is produced as an inactive 31 kDa pro-protein by different cell types, such as monocytes and macrophages.³ It is activated by proteolytic processing of this species in specialized lysosomes resulting in active 17 kDa IL-1 β .⁷ IL-1 β is a very rigid protein, with the structure largely consisting of β -sheets which form a central barrel (Figure 1A human, Figure 1B mouse).⁸⁻¹⁰

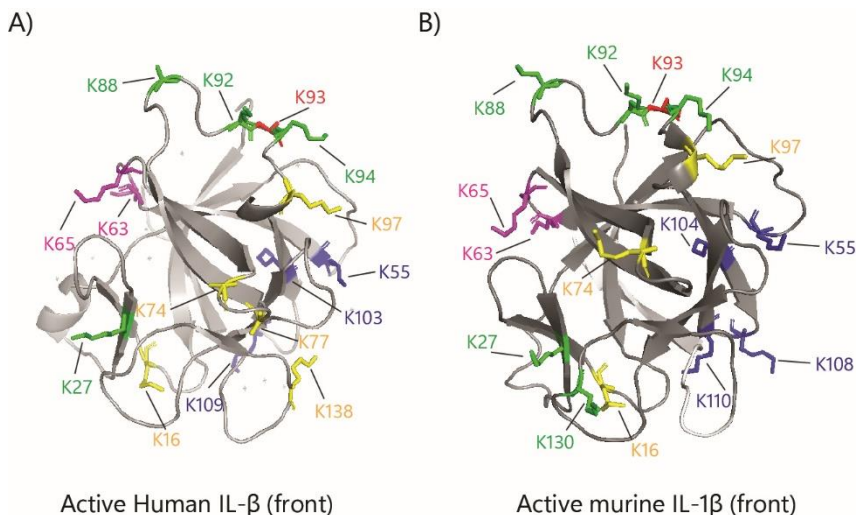


Figure 1 - Crystal structure of human and murine IL-1 β .

The structures of A) human and B) murine IL-1 β consist largely of β -sheets and strands forming barrels. The rest of the structure is mostly coiling and turns. Almost no α -helical structures can be observed. The lysine residues (15) are highlighted according to functionality: green for essential in receptor binding; red for receptor binding and hydrophilic interactions; magenta for IL-1RAcP interacting residues; blue for residues in close proximity of receptor interacting residues; yellow for the remaining residues. Crystal structures were modified based on A) Yu *et al.* (PDB: 9ILB)⁹ and B) Oostrum *et al.* (PDB: 2MIB).¹⁰

The active IL-1 β can bind two receptors in the body: Type I IL-1 receptor and type II IL-1 receptor (Figure 2).¹¹⁻¹³ Type I IL-1 receptor (IL1RI) is present on endothelial cells¹⁴, keratinocytes¹⁵, fibroblasts¹⁶, neurons¹⁷, smooth muscle cells¹⁴ and T-cells^{16,18} among others. Binding of IL-1 β to the IL1RI occurs by the three immunoglobulin-like domains of the receptor, wrapping around the IL-1 β molecule.¹⁹ Upon binding this receptor, IL-1 β initiates its pro-inflammatory function.¹⁹ It does so by 'activating' the cytosolic part of this bound receptor which consists of Toll-like-receptor-like (TLR-like) domains. Following activation, the TLR-like domain interacts with MyD88, leading to the activation

of NF- κ B. NF- κ B is a pro-inflammatory transcription factor, which provides the pro-inflammatory function of IL-1 β .^{20–22}

The type II IL-1 receptor (IL1RII) is found on B-cells¹⁴, keratinocytes¹⁵, monocytes¹⁴, neutrophils²³ and T-cells¹⁸, among others. As it lacks the intracellular TLR-domain, binding this receptor has a regulatory effect.² Binding to this receptor inhibits the function of IL-1 β .²⁴ These receptors thus serve a regulatory function instead of a signalling function performed by IL1RI (**Figure 2**). There is also a soluble form of the receptor, which is formed upon cleavage of the extracellular portion of the receptor when it is present on the cell surface. This too is believed to have anti-inflammatory or immune-modulating functions.^{25,26}

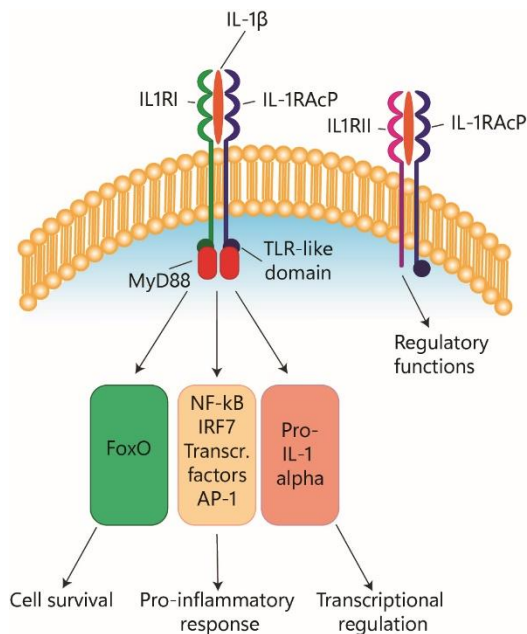


Figure 2 - Signalling of IL-1 β upon receptor binding.

IL-1 β can interact with either IL-1 receptor I (IL1RI) or IL-1 receptor II (IL1RII). Interaction with IL1RI and interleukin-1 receptor accessory protein (IL-1RAcP) leads to the activation of the Toll-like-receptor-like (TLR-like) domain and binding of MyD88. Activation of MyD88 can result in FoxO expression for cell survival, NF- κ B (among others) expression for a pro-inflammatory response or transcriptional regulation. Interaction with IL-1RII results in regulatory processes as no TLR-like domain is present. Figure was adjusted from R&D systems.^{11–13,27} NF- κ B: nuclear factor kappa B; AP-1: activator protein.

These diverse roles in the immune response have led to the pursuit of IL-1 β as both a therapeutic target, and as an immune therapy. Its inhibition (using a soluble IL-1 receptor called Anakinra) has been shown in the clinic to alleviate symptoms of auto-immune diseases, such as rheumatoid arthritis^{28,29}, cryopin-mediated auto-immune diseases³⁰, and diabetes.^{31,32} On the contrary, the use of recombinant IL-1 β has been explored as an immune therapy against cancer. However, the behaviour of IL-1 β in cancer may be rather controversial.

There are suggestions that IL-1 β can be a causative or disease-aggravating agent in cancer. This is largely caused by chronic non-resolved inflammation in which IL-1 β is one

of the cytokines involved. Here its presence can lead to the induction of immunosuppressive cells, tumour angiogenesis³⁰ and endothelial cell activation.^{31,32} A clear example of the cancer-promoting activities of IL-1 β , comes from multiple myeloma, a form of cancer in which monoclonal plasma cells, accumulate.³³ The production of IL-1 β by these cells causes the production of IL-6 which in turn causes the development of diseased plasma cells leading to disease aggravation.³⁴

For many other cancer types, it has been reported that IL-1 β can induce an anti-cancer immune response.³⁵ It was shown that IL-1 β can aid the clearance of different forms of cancer like breast, colon, lung cancers and melanomas.^{31,36} Allen *et al.* showed that decreased levels of IL-1 β were correlated with increased gastrointestinal tumour presence.³⁵ Yet, mice deficient in IL-1 β , were shown to be protected against chemically-induced carcinogenesis, suggesting a potential pro-tumorigenic effect of this cytokine too.³⁷

These highly diverse effects, both locally and systemically, have made the use of IL-1 β as an immune therapy difficult. Nevertheless, IL-1 β therapy has been explored by Neri *et al.* as an immunocytokine.³⁸ Here IL-1 β was coupled to an antibody targeting the tumour stroma to allow its delivery to the tumour micro-environment. The hypothesis was that this would minimize the systemic (toxic) effects and result in the local reactivation of the immune system in the tumour. Unfortunately, it was found that the on target-off tumour effects of the immunocytokine were too toxic for the host^{38,39} leading to its abandonment as an immune therapy.

A host-targeted IL-1 β -based immunocytokine was still developed. IL-1 β encoded with a mutation of Gln148 to a glycine resulted in a 168-fold reduction in receptor affinity.^{40,41} This modified IL-1 β was then coupled to an anti-CD8+ T-cell antibody, for targeted delivery of IL-1 β to the CD8+ T-cells where it was sufficiently active to improve T-cell activity.^{40,41} However, this immunocytokine was too weak to serve as a monotherapy and only showed activity in mice as an adjuvant to vaccination.

These results highlight the complexity of IL-1 β immunocytokines. On the one hand a highly active IL-1 β is needed to strongly activate the local immune response. Yet, at the same time the cytokine must be weak enough to not cause systemic toxicity on the way to the tumour. In this chapter, a new approach to unite these two properties in a single construct was explored. This approach is based on the 'click-to-release' chemistry outlined in *Chapter 0 of this thesis*. This technique is based on the bioorthogonal deprotection chemistry that allows the cleavage of allylic *trans*-cyclooctene carbamates (TCOs) by tetrazines, to allow their use as an *in vivo*-compatible protecting group.

Here, a similar approach is described in which IL-1 β is inactivated using TCO-modification in such a manner that it can be reactivated by the addition of tetrazines (**Figure 3**). This chemically inactivated cytokine was then linked to a targeting moiety using sortase-mediated ligation (**Figure 3**) to yield an immunocytokine in which the activity of the cytokine was blocked, but could be reactivated by the addition of tetrazine. It was envisaged that in this manner the systemic toxicity of the cytokine portion could be limited as the construct could first be allowed to accumulate in the tumour before

activation of the cytokine. This would allow the use of highly active IL-1 β to hopefully allow its use as a monotherapy.

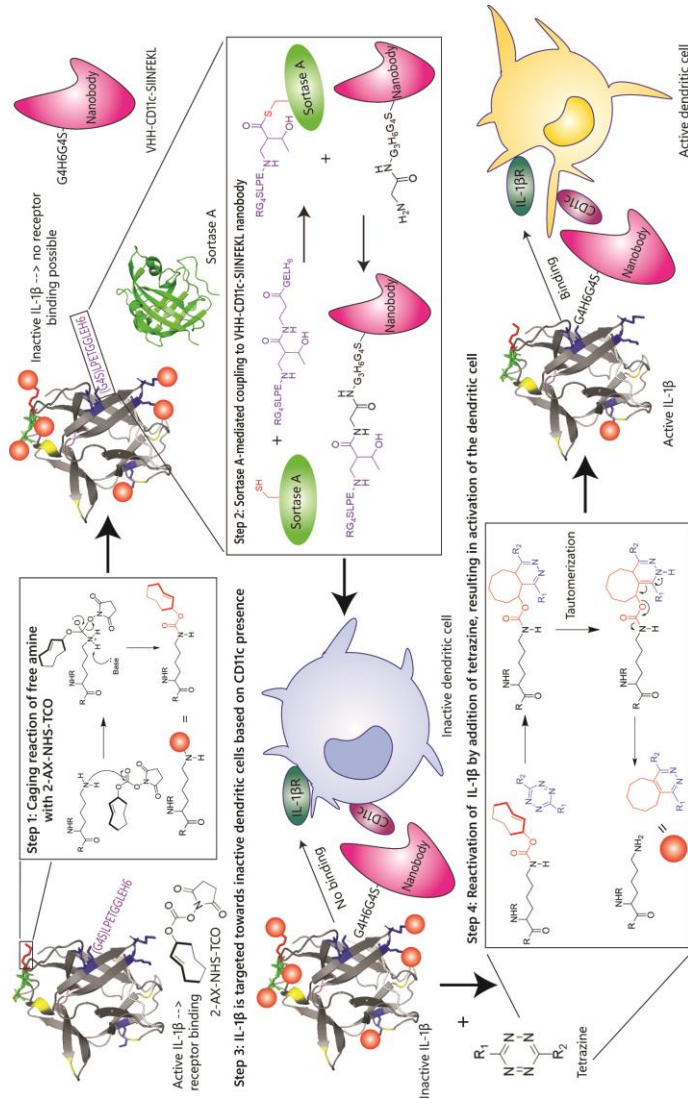


Figure 3 - Design of an IL-1 β -based immunocytokine using chemical inactivation and reactivation.

The first step in the generation of chemically controlled inactivation of immunocytokines. The cytokine (IL-1 β) has 15 lysine residues that can be caged using NHS-TCO. Upon caging, the cytokine becomes inactive due to its inability to bind its receptor. The second step is sortase A-mediated coupling the IL-1 β cytokine via its LPETGG-tag to a nanobody, VHH-CD11c-SINFEKL with a N-terminal tetraglycine tail. This allows for targeting of inactive dendritic cells. Inactive IL-1 β , unable to interact with its receptor present on the dendritic cell, is treated with a tetrazine, which can remove the TCO-group or 'cage' and thereby activate the IL-1 β moiety of the immunocytokine. This allows the IL-1 β to interact with its receptor (IL-1R) to activate the dendritic cell in the micro-environment of a tumour to clean up the tumour cells.

Results & Discussion

The aim of this chapter was to produce an IL-1 β immunocytokine in which the cytokine-portion was inactivated by TCO-masking and could be activated by the addition of tetrazines. The standard approach of producing an immunocytokine is genetic fusion. There are however complications with this approach when using (non-specific) lysine modifications. Using this modification method would lead to modifications in both the cytokine and the targeting part of the construct. Although this would result in the desired loss of cytokine activity, it would also result in undesired loss of antigen binding capacity. The targeting-reagent therefore had to be coupled to the cytokine only after it had been modified with TCO-carbamates. To achieve this, it was decided to use a sortase A-based approach in which a small single-chain fragment of a camelid antibody was genetically modified with an *N*-terminal tag and the cytokine with a C-terminal tag (LPETG). Sortase A from *Staphylococcus aureus* has been reported for ligating the motifs LPETG and the tetraglycine tail together in both peptide-protein⁴² and protein-protein ligations.^{43,44} Therefore, it was envisaged that these two fragments, LPETG and the tetraglycine tail could be ligated together after TCO-modification of the cytokine by this enzyme (**Figure 4**). The yields of the protein-protein ligation were reported to be on average 40-85%, which would be sufficient to produce caged immunocytokines for further evaluation.

Construct Design

In order to obtain an immunocytokine in which the cytokine was inactive, and the targeting moiety was not, it was decided to make a construct consisting of a nanobody targeting group, linked by a sortase reaction to the murine IL-1 β -gene construct. The choice was made to use a nanobody instead of an antibody as a targeting group. Until now immunocytokines were based on intact antibodies (IgGs)^{38,45,46} or single-chain variable fragments (scFv). However due to their small size, stability over broad temperature and pH ranges, and easy expression in *E. coli*, nanobodies provide beneficial properties compared to the aforementioned targeting moieties.⁴⁷ In addition, they are also monomeric, lack glycosylation, and lack hydrophobic domains, making them easy to work with compared to full length antibodies.⁴⁷

Coupling via sortase was chosen to allow the separate inactivation of the cytokine and its subsequent ligation to the active nanobody.^{45,46} As the cytokine was to be chemically modified with an amine-modifying agent, it was decided to install the C-terminal motif on the cytokine and the *N*-terminal ligation motif on the nanobody. Initially, a CD11c-targeting species was chosen, as this would allow for an easy *in vitro* assay of the construct's activity on dendritic cells. The gene for this construct, which also contained a SIINFEKL epitope used for CD8+ T-cell activation⁴⁸, was kindly provided by Dr. Martijn Verdoes. It consisted of an *N*-terminal thrombin cleavage site, which upon cleavage releases the G4-motif, needed for the nucleophilic attack on the sortase-coupled cytokine. The G4-motif is followed by a 6His-tag for purification and then the sequence of the nanobody (**Figure 4A**). The gene construct was provided in the pET22b plasmid that allowed bacterial expression.

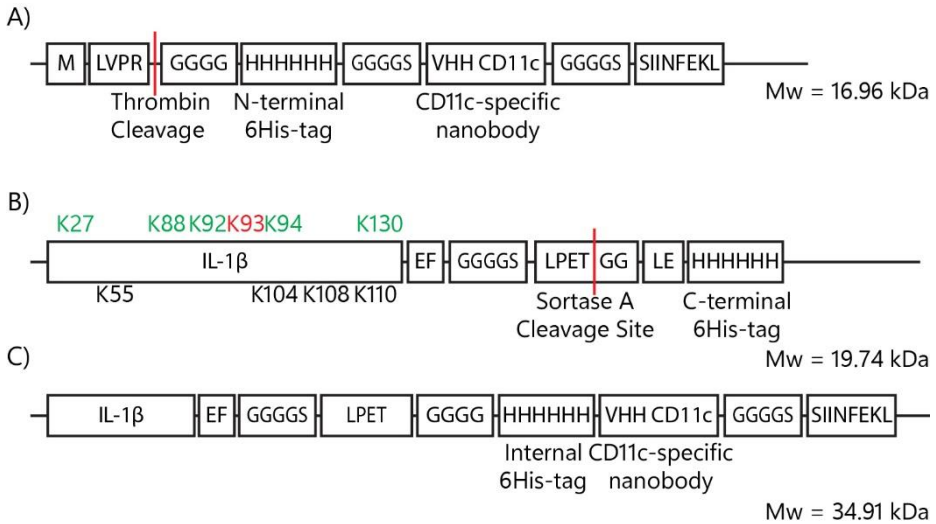


Figure 4 - Construct formation VHH-CD11c, IL-1 β -LPETGG-6His and the final product after sortase ligation.

A) The VHH-CD11c nanobody consists – from *N*- to *C*-terminus of thrombin-tag-protected tetraglycine *N*-terminus followed by a 6His-tag for purification purposes which is fused to the actual nanobody via a GGGGS-spacer. The *C*-terminus contains a SIINFEKL peptide for potential T-cell activation. B) Design of IL-1 β -LPETGG-6His. IL-1 β is *C*-terminally fused to LPETGG, the sortase A motif, via a GGGGS-spacer. For purification purposes, a *C*-terminal 6His-tag was introduced which is removed upon coupling to the VHH-CD11c-SIINFEKL nanobody. The green coloured lysines are involved in receptor interaction and the black lysine residues are adjacent to receptor interacting residues. The red coloured lysine has important hydrophilic interactions. C) Upon reaction with sortase A and the VHH-CD11c nanobody, the *C*-terminal 6His-tag is replaced by the CD11c-specific nanobody by a transpeptidation reaction.

IL-1 β was modified at its *C*-terminus for two reasons; the first was the aforementioned modification of the *N*-terminus with TCO, which would render the construct unligatable. The second was that it has been reported that *N*-terminal modification of IL-1 β can reduce the activity of this cytokine.⁴⁹ The IL-1 β protein was therefore designed in the following manner (**Figure 4B**): after the gene of murine IL-1 β (Gene ID 16176), the sortag (LPETGG) was introduced after a *C*-terminal GGGGS-spacer motif, as this has been shown to improve protein-protein ligation yields.^{50–53} Finally, *C*-terminal to the sortag-motif, a 6His-tag was introduced to facilitate purification of the protein after production and the removal of unreacted cytokine from the sortase ligation reaction mixture. Native IL-1 β was also made for optimisation purposes.

Protein expression and purification

For expression of the IL-1 β constructs, they were ligated into a pET28a(+)-vector using double digest and T4 ligase.⁵⁴ Expression was done using the *E. coli* ArcticExpress (DE3) RP system which can express proteins with rare codons^{55,56} with high yields of folded product (**Supplementary Figure S1A**). Expression of IL-1 β was under the control of the T7 promoter. The expression of T7 RNA polymerase, which drives the IL-1 β expression, is regulated by the *lacUV5* promoter, allowing the controlled induction of expression by the addition of IPTG.⁵⁷ After induction of expression with 0.5 mM IPTG, the cells were incubated at 10°C for 3 days, after which the bacteria were lysed using lysozyme in combination with sonication. The cytokines were then purified from the soluble fraction

using cation exchange in 20 mM MES pH 8 (for unmodified IL-1 β , **Figure 5A**), or using nickel affinity chromatography (for the 6His-containing sortagable IL-1 β ; **Supplementary Figure S1B**, **Figure 5A**).

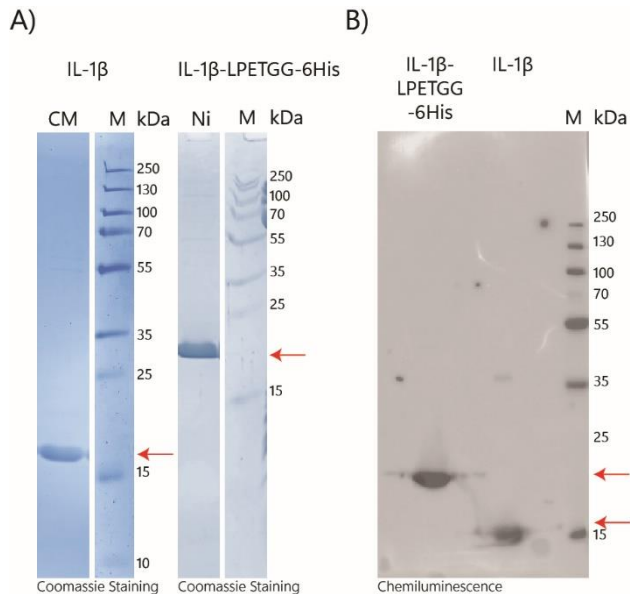


Figure 5 - Production of IL-1 β (-LPETGG-6His) in *E. coli* ArcticExpress (DE3) RP using IPTG-based expression. A) Purification of IL-1 β and IL-1 β -LPETGG-6His using cation exchange (CM) or nickel column purification (Ni), respectively, analysed by SDS-PAGE. B) Western blot analysis using IL-1 β -specific antibodies confirming cytokine presence.

Sortase A was kindly provided by Dr. Martijn Verdoes in the pET28aSrtA Δ 59-expression vector. Expression of this protein was performed as described previously.⁵⁸ Briefly, the construct was transformed into *E. coli* Rosetta-gami 2 (DE3), a strain capable of expressing proteins with rare codons usage as well.⁵⁹ The bacteria were grown to an OD₆₀₀ of 0.6, and incubated at 25°C for 20 hours after induction with 1 mM IPTG (**Supplementary Figure S1C**). Following, the bacteria were lysed using a combination of lysozyme and sonication and the soluble fraction of the lysate was loaded onto nickel resin to purify sortase A based on its 6His-tag (**Figure 6A**). Sortase A was eluted from the column using 250 mM imidazole in 50 mM Tris/150 mM NaCl.

The anti-CD11c nanobody or VHH-CD11c-SIINFEKL was provided in the pET22b-vector modified with a pelB signal sequence. Its expression in *E. coli* BL21 (DE3) pLysS has been reported.⁵⁸ After addition of 1 mM IPTG, expression took place for 20 hours at 25°C (**Supplementary Figure S1D**), whereafter lysis and purification based on the 6His-tag were similar compared to sortase A expression described above (**Figure 6B**).

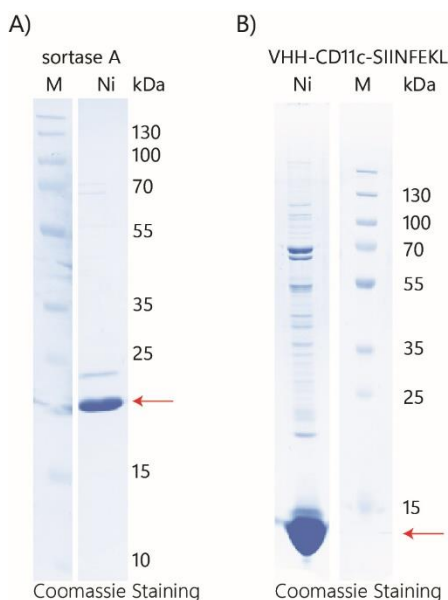


Figure 6 - Expression and purification of sortase A and VHH-CD11c-SIINFELK using IPTG.

A) Sortase A (~19 kDa) and B) anti-CD11c or VHH-CD11c-SIINFELK (~15 kDa) were purified by nickel (Ni) column. The respective proteins are highlighted with the red arrows.

Optimisation of NHS-TCO reaction with IL-1 β

Next, the inactivation of the cytokine with TCO was optimised. The native IL-1 β construct was first used to optimise the modification reaction with the NHS-carbonate of TCO (**1**, **Figure 7**) to obtain the modification level at which IL-1 β was no longer active, but could be reversed by addition of a tetrazine. Initial activity assays were done by ELISA (**Figure 8**), as this was a facile method to assess multiple modification conditions. ELISA, which is based on antibody binding, was also chosen because loss in antibody binding due to the introduction of TCO-groups, could also indicate loss in receptor binding when TCO-groups block essential residues for receptor interaction.

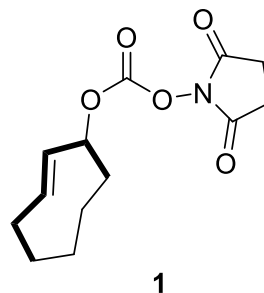


Figure 7 - Structure of (S,E)-cyclooct-2-en-1-yl(2,5-dioxopyrrolidin-1-yl) carbonate or 2-AX-NHS-TCO.

2-AX-NHS-TCO or NHS-TCO was kindly provided by Mark de Geus.

The modification reactions were performed at basic pH (pH 8) in 20 mM HEPES.⁶⁰ First, the effect of the concentration of **1** on the reactivity was assessed. For this IL-1 β (at 5.7 μ M) was modified with increasing concentrations of **1** for 1 hour. It was found that residual IL-1 β recognition after modification went down with increasing concentrations of TCO (**Figure 8A**). Next, the reaction time was optimised (**Figure 8B**). IL-1 β activity was assessed after 1 hour, 4 hours, or 18 hours of reaction with **1**. No significant reduction of recognition was observed after 1 hours of reaction. However, at the later timepoint, SDS-PAGE analysis showed loss of protein. This suggested that the IL-1 β had precipitated

from the reaction mixture. Finally, the effect of reaction temperature was investigated by performing the modification reaction for 1 hour with 8 mM **1** at 20°C, 25°C and 37°C (**Figure 8C**). The least residual IL-1 β binding was observed at 37°C, whilst minimising protein loss. As the mass difference per caged added to IL-1 β is rather low (152 Da/cage), mass differences could not clearly be observed. The only sign of caging which could be observed on the SDS-PAGEs is the diffuseness of the bands, indicating the presence of species with minimal differences in molecular weight. As optimal reaction conditions for the next steps, caging with 4.0-8.0 mM **1** for 1 hour at 37°C were chosen.

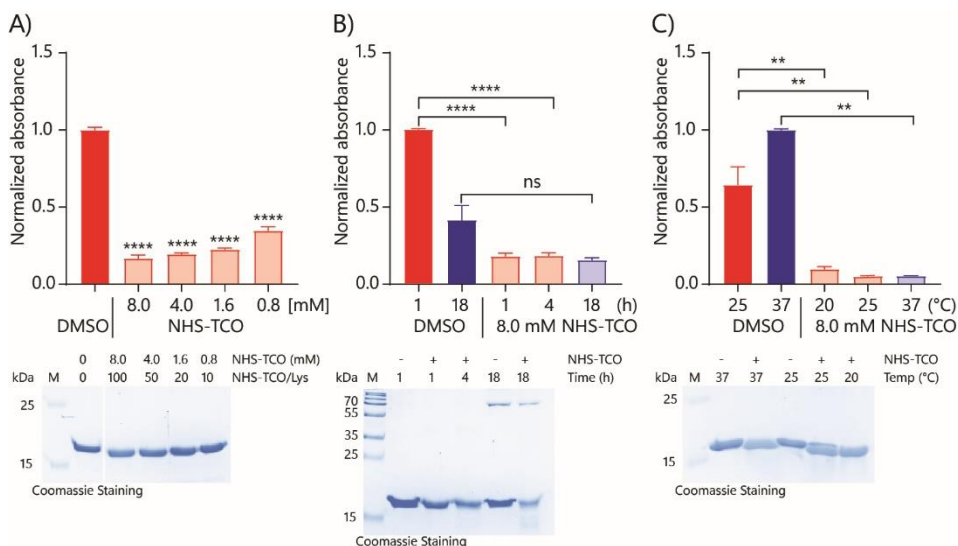


Figure 8 - Optimisation of caging reaction on IL-1 β analysed using ELISA.

An ELISA was performed to assess loss of interactions, with IL-1 β -specific antibodies in this case, due to NHS-TCO binding with lysines. The caging reaction using NHS-TCO (**1**) was optimised for A) concentration **1** (N=3); B) caging time (h) (N=5); and C) caging temperature (°C) (N=3) for IL-1 β . Reference conditions were set at caging with 8.0 mM NHS-TCO in 20 mM HEPES pH 8 at 37°C, 800 rpm for 1 hour. Bright colours indicate DMSO only samples and pastels the TCO-treated samples. Colour groups indicate different conditions with respective DMSO controls. Equal protein application was confirmed using SDS-PAGE coomassie staining (below each graph). Data were plotted as mean signal \pm SEM. Significances are indicated as follows: * $P < 0.05$; ** $P < 0.01$; *** $P < 0.001$; **** $P < 0.0001$; ns is non-significant.

To determine whether TCO-modification affected IL-1 β -receptor binding, HEK-Blue IL-1 β and RAW-Blue assays were performed.^{61,62} HEK-Blue IL-1 β is a reporter cell line specifically designed to detect IL-1 β via the NF- κ B pathway.⁶¹ Activation of this pathway results in the production of secreted embryonic alkaline phosphatase (SEAP), the activity of which can be measured by the addition of QUANTI-Blue, which converts from a pink substrate to a blue product (**Figure 9**).⁶³ RAW-Blue cells are murine macrophages that are also engineered to express SEAP upon NF- κ B activation.⁶² They are IL-1 β -receptor positive⁶⁴ and the binding of this receptor induces NF- κ B translocation to the nucleus. Colorimetric evaluation of SEAP activity⁵⁸ therefore allowed the quantitative assessment of IL-1 β -receptor activation by the TCO-modified IL-1 β construct.⁶⁵

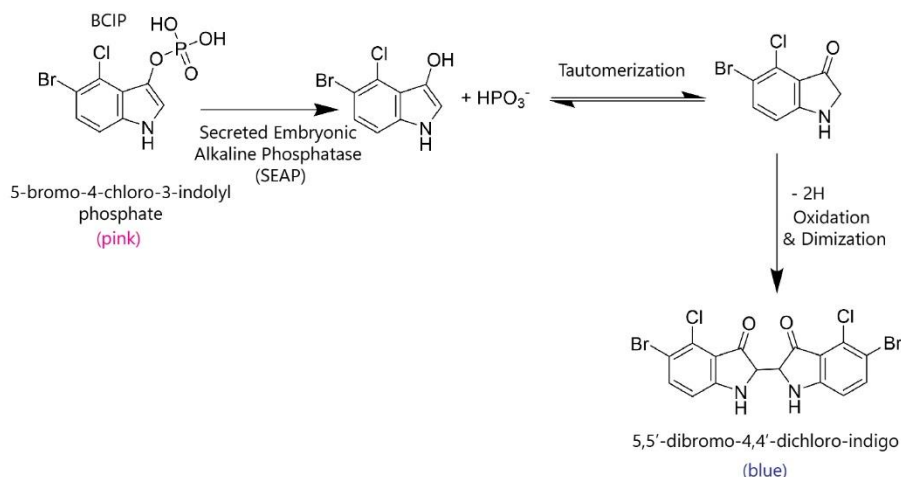


Figure 9 - Mechanism of secreted embryonic alkaline phosphatase in the QUANTI-Blue assay.

BCIP is colourless but is supplied in a pink coloured solution. BCIP is hydrolysed by secreted embryonic alkaline phosphatase (SEAP) which is expressed upon HEK-Blue or RAW-Blue cell activation by IL-1 β . Upon tautomerization it oxidizes and forms a dimer that is blue colored.⁶³

Both the HEK-Blue IL-1 β -assay (**Figure 10**) and the RAW-Blue assay (**Figure 11**) showed that increasing the NHS-TCO concentration during the modification reaction, resulted in a product that was less capable of activating these cells (**Figure 10A** and **Figure 11A**). The highest concentration of **1** (8 mM), reduced the activity to 10% of the original value. Longer reaction times also resulted in the loss of IL-1 β R binding (**Figure 10B** and **Figure 11B**) in the DMSO control, and – as seen for the ELISA - caging temperature did not affect caging efficiency (**Figure 10C** and **Figure 11C**).

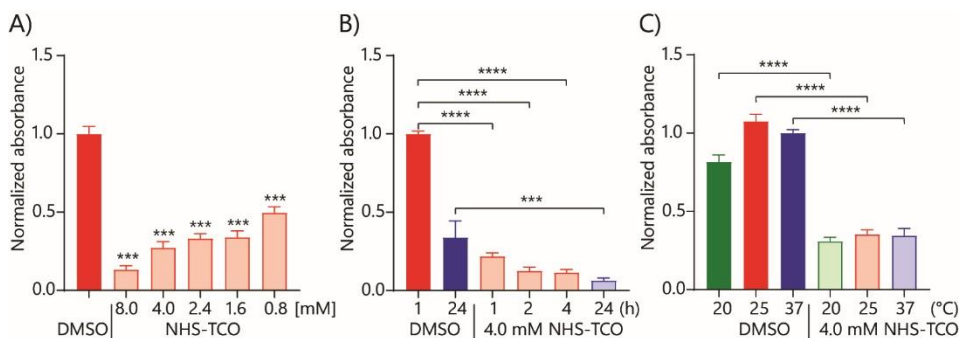


Figure 10 - Analysis of caging optimisation of IL-1 β on HEK-Blue IL-1 β cells using QUANTI-Blue colorimetric assay.

The caging reaction using NHS-TCO (**1**) was assessed using (caged) cytokine stimulated HEK-Blue IL-1 β . A) Analysis of caging with increasing concentration of **1** (N=4); B) analysis of caging time (h) (N=4); C) optimisation of the caging temperature (°C) (N=3). Reference conditions were set at caging with 4.0 mM NHS-TCO in 20 mM HEPES pH 8 at 37°C, 800 rpm for 1 hour. Bright colours indicate DMSO only samples and pastels the TCO-treated samples. Colour groups indicate different conditions with respective DMSO controls. Data were plotted as mean signal \pm SEM. Significances are indicated as follows: * $P < 0.05$; ** $P < 0.01$; *** $P < 0.001$; **** $P < 0.0001$; ns is non-significant.

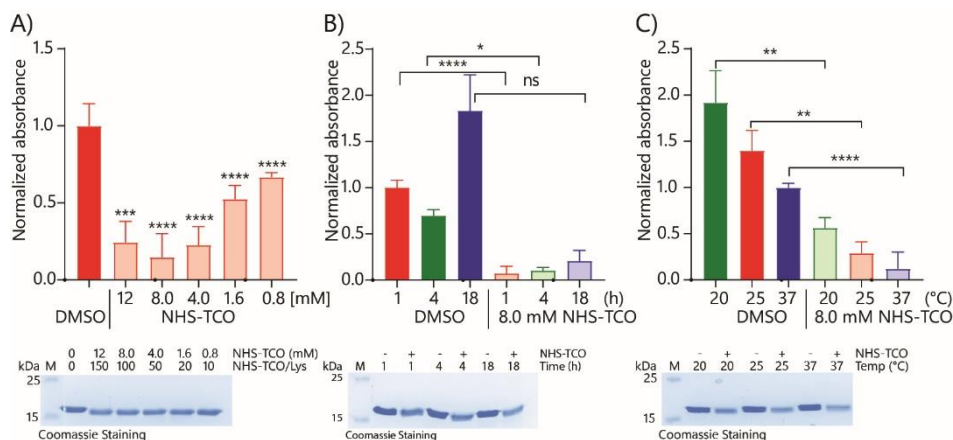


Figure 11 - Analysis of caging optimisation of IL-1 β on RAW-Blue cells using QUANTI-Blue colorimetric assay.

The caging reaction using NHS-TCO (**1**) was assessed using (caged) cytokine stimulated RAW-Blue. A) Analysis of caging with increasing concentration of **1** (N=3); B) analysis of caging time (h) (N=3); C) optimisation of the caging temperature (°C) (N=3). Reference conditions were set at caging with 8.0 mM NHS-TCO in 20 mM HEPES pH 8 at 37°C, 800 rpm for 1 hour. Bright colours indicate DMSO only samples and pastels the TCO-treated samples. Colour groups indicate different conditions with respective DMSO controls. Equal protein application was confirmed using SDS-PAGE coomassie staining (below each graph). Data were plotted as mean signal \pm SEM. Significances are indicated as follows: * $P < 0.05$; ** $P < 0.01$; *** $P < 0.001$; **** $P < 0.0001$; ns is non-significant.

In order to correlate the loss of activity of IL-1 β to the number of modified lysine residues, LC-MS was performed on the modified samples (**Figure 12**). To obtain sufficient material for LC-MS, the caging reactions with doubling the protein concentration were required to obtain signal (11 μ M). Murine IL-1 β has 15 lysines, which are all located on the outside of the protein and all, but Lys16, are possible targets for caging.¹⁰ These ESI LC-MS experiments showed that caging with 8.0 mM NHS-TCO resulted in IL-1 β with on average between 7 to 8 lysine residues modified (**Figure 12B**). Lowering the NHS-TCO concentration to 1.6 mM reduced this average to 4 (**Figure 12A**). Doubling the NHS-TCO concentration to 16 mM did not increase the average number of modified lysines, but did reduce the fraction of protein modified with <7 modifications (**Figure 12C**).

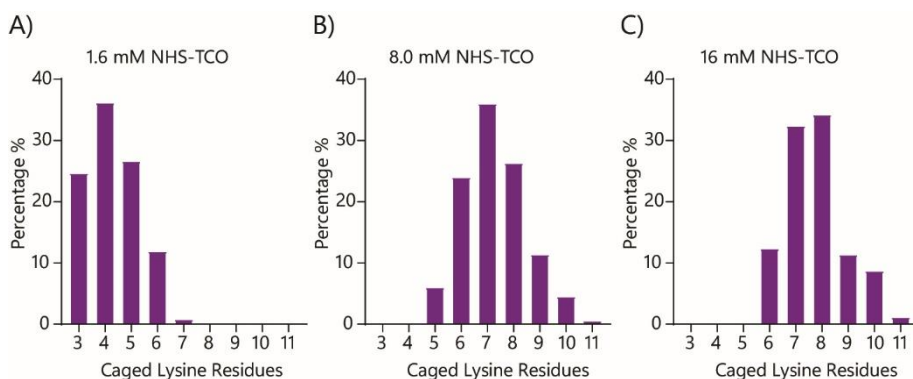


Figure 12 – Distribution amount of caged lysines in IL-1 β , caged with different amounts of NHS-TCO analysed by ESI LC-MS .

The amount of caged lysine residues of IL-1 β (11 μ M) treated with A) 1.6 mM, B) 8.0 mM and C) 16 mM NHS-TCO determined using ESI LC-MS. IL-1 β was caged in 20 mM HEPES for 1 hour at 37°C, following buffer exchange using Zeba™ Spin Desalting columns to 10 mM ammonium acetate pH 6. In general the more NHS-TCO was added, the more caged lysines were present. These are normalized data to the total amount of lysines present.

As caging of IL-1 β resulted in inactive IL-1 β , the same was assessed for the sortagable variant (IL-1 β -LPETGG) to confirm similar activity changes upon NHS-TCO treatment under various caging conditions (**Supplementary Figure S2**, **Figure S3** and **Figure S4**). These data supported a similar general behaviour of IL-1 β -LPETGG compared to IL-1 β . The optimised conditions for IL-1 β were therefore also applied for further reaction with IL-1 β -LPETGG.

With these optimised conditions in hand, initial decaging experiments were performed. (**Figure 15A-C**). **Figure 15B** did not even show a decrease in activation of RAW-Blue cells when IL-1 β was treated with NHS-TCO. This could be due to the passage number of RAW-Blue cells used, which was already quite high but within the range described by the manufacturer. Also the quality of IL-1 β could influence this read-out, as the presence or absence of endotoxins in various batches can slightly alter the background activation of these cells. Overall, these initial experiments indicated that the above caging approaches had yielded a product that could not be deprotected to a functional IL-1 β . It was postulated that the deprotection was insufficiently high yielding to remove enough TCO-groups to restore IL-1 β activity, or that the protection step led to permanent inactivation (e.g. due to unfolding) of the product. This was, however, not further pursued. Nevertheless, examining protein folding using circular dichroism or by determining the thermostability of IL-1 β could provide further insight in these results.

Examining the binding interaction of IL-1 β with its receptor indicated that multiple surface-exposed lysine residues could be the likely modification targets (**Figure 13**)¹⁰: a lysine residue at position 88 (K88) is involved in the binding of IL-1 β to the IL-1RI and changes its position upon binding.¹⁷ In addition, lysines at positions 27, 92, 93, 94 and 130 (mouse numbering)^{13,66} also lie within the ligand-receptor contact surface (**Figure 13**, green).¹³ Other lysines at positions 55, 104^{13,66}, 108 (mouse only) and 110 are in close proximity to the contact region (**Figure 13**, blue), with Lys55 even reported to be part of a T-cell activating peptide (VQGEESNDK (human) or VQGEPSNDK (mouse)).⁶⁷

In addition to the direct interaction between IL-1 β and IL-1RI, the *immune response interleukin (IL)-1 receptor accessory protein* (IL-1RAcP) also has to bind the complex of IL-1 β and IL1RI.^{68–71} This protein is not able to bind IL-1 β on its own but it does when there is an interaction with the IL-1RI. The binding mode of this protein has been researched extensively, with IL-1RAcP shown to make contact at the back of IL-1RI and wrapping around parts of IL-1 β .⁶⁸ Lysines at positions 63 and 65 (**Figure 13**, magenta) of IL-1 β are crucial for this binding as mutating them to serines diminishes the biological activity of IL-1 β .⁶⁸ The remaining lysine residues (**Figure 13**, yellow) are not involved in receptor interactions, but can however affect the folding of IL-1 β as the charge of the lysine is removed by its interaction with NHS-TCO.

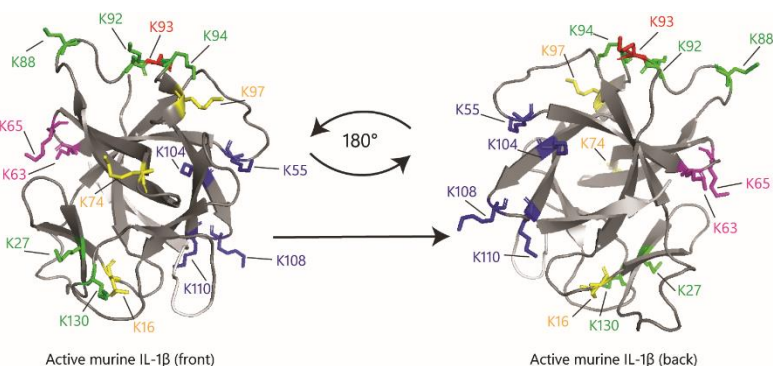


Figure 13 - Crystal structure of murine IL-1 β with highlighted lysine-residues.

Murine IL-1 β contains 15 lysine residues which are highlighted according to functionality: green for essential in receptor binding; red for receptor binding and hydrophilic interactions; magenta for IL-1RAcP interacting residues; blue for residues in close proximity of receptor interacting residues; yellow for the remaining residues. Crystal structure was modified based on Oostrum *et al.* (PDB: 2MIB).¹⁰

It was postulated that the ligation of buried lysine residues could result in a destabilisation of the protein fold, leading to protein precipitation. To circumvent this, it was assessed whether modifications at lower temperatures for longer time periods would yield more protein of which the activity could be rescued.⁶⁵

IL-1 β -LPETGG was therefore modified with 3.5 mM or 2.1 mM NHS-TCO for 1 hour at 37°C, as well as with 0.7 mM NHS-TCO for 24 hours at 10°C. The activity of the products was then analysed by ELISA and HEK-Blue assay (**Figure 14**). Both assays confirmed that caging with a lower NHS-TCO concentration (0.7 mM instead of 2.1 mM or 3.5 mM) for a longer period of time (24 hours instead of 1 hour) at this lower temperature resulted in similar reduction of IL-1 β -LPETGG activity. Preliminary deprotection experiments showed that this method of caging resulted in protected IL-1 β -LPETGG molecules that could be deprotected to the active species (**Supplementary Figure S3D**).

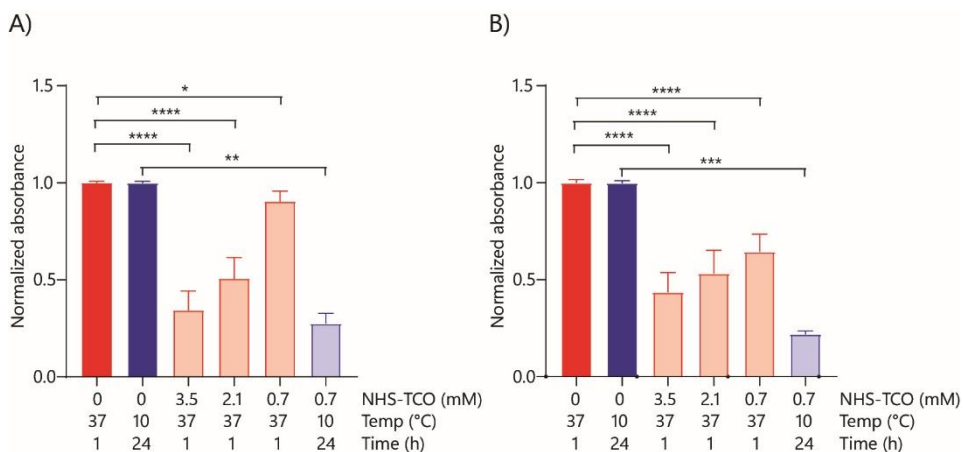


Figure 14 - Improving caging conditions of IL-1 β -LPETGG analysed by ELISA and on HEK-Blue IL-1 β cells.

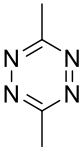
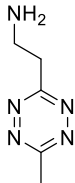
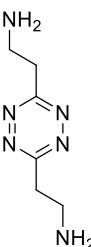
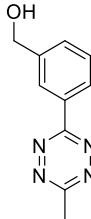
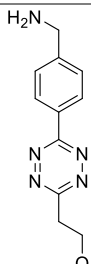
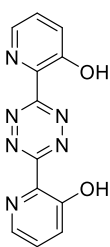
IL-1 β -LPETGG (5 μ M) was caged in 20 mM HEPES with either 3.5 mM, 2.1 mM or 0.7 mM NHS-TCO for 1 hour at 37°C or with 0.7 mM **1** for 24 hours at 10°C. The caged protein was assessed by A) ELISA (N=5) and B) HEK-Blue IL-1 β (N=5). Bright colours indicate DMSO only samples and pastels the TCO-treated samples. Colour groups indicate different conditions with respective DMSO control. Data were plotted as mean signal \pm SEM. Significances are indicated as follows: * P<0.05; ** P<0.01; **** P<0.0001; ns is non-significant.

Optimisation of deprotection reaction

Following the early success of TCO-removal outlined above, it was next assessed whether this could be optimised. First, a library of tetrazines (**2-6**) were tested for IL-1 β recovery (**Table 1, Figure 15D**). Some of these tetrazines (**2-4**) yielded significant recovery of IL-1 β activity by HEK-blue IL-1 β assay. In addition to the above reported compounds, a new unreported tetrazine, kindly provided by Prof. Dr Hannes Mikula, was also tested. This 2,2'-(1,2,4,5-tetrazine-3,6-diyl)bis(pyridin-3-ol) (2PyrH) $_2$ Tz, (**7**) out performed all other tetrazines and was used in all evaluations described below.

Table 1 - Overview tetrazines used for decaging optimisation.

All tetrazines were dissolved in DMSO. Compound **2** was kindly provided by Alexi Sarris, compounds **3-6** were kindly provided by Dr. Merel van der Plassche and compound **7** was kindly provided by Prof. Dr. Hannes Mikula.

	DMT	Tz1	Tz2	Tz3	Tz4	(2PyrH) ₂ Tz
Compound nr.	2	3	4	5	6	7
Full name	3,6-dimethyl-tetrazine	2-(6-methyl-1,2,4,5-tetrazin-3-yl)ethan-1-amine	2,2'-(1,2,4,5-tetrazine-3,6-diyl)bis(ethan-1-amine)	(3-(6-methyl-1,2,4,5-tetrazin-3-yl)phenyl)methanol	2-(6-(4-(aminomethyl)phenyl)-1,2,4,5-tetrazin-3-yl)ethan-1-ol	2,2'-(1,2,4,5-tetrazine-3,6-diyl)bis(pyridin-3-ol)
Structure						

The click-to-release efficiency of **7** was analysed by ELISA and HEK-Blue assay, as before. First, the effect of higher/lower modification levels of the protein was tested (**Figure 16A**) using ELISA. It was found that IL-1 β modified with 8 mM TCO failed to reactivate (**Figure 16A**). However, IL-1 β modified with 4.0 mM NHS-TCO yielded IL-1 β that was recognised in the ELISA to approximately 60% of the native IL-1 β signal after incubation with 2.5 mM (2PyrH)₂Tz (**Figure 16A**).

Next the above conditions were tested in the HEK-Blue IL-1 β assay, the cells were first treated with 250 ng/mL of the wildtype or caged IL-1 β proteins and then treated with various concentrations of **7**. After 18 hours at 37°C, activity was assessed (**Figure 16B**). It was found that here too, approximately 50-60% of IL-1 β activity could be recovered when 1-12.5 μ M tetrazine was added. Increasing the concentration of **7** did not result in higher recovery yields. A probable reason for this is the cytotoxicity of **7** when applied in these concentrations observed using the microscope.

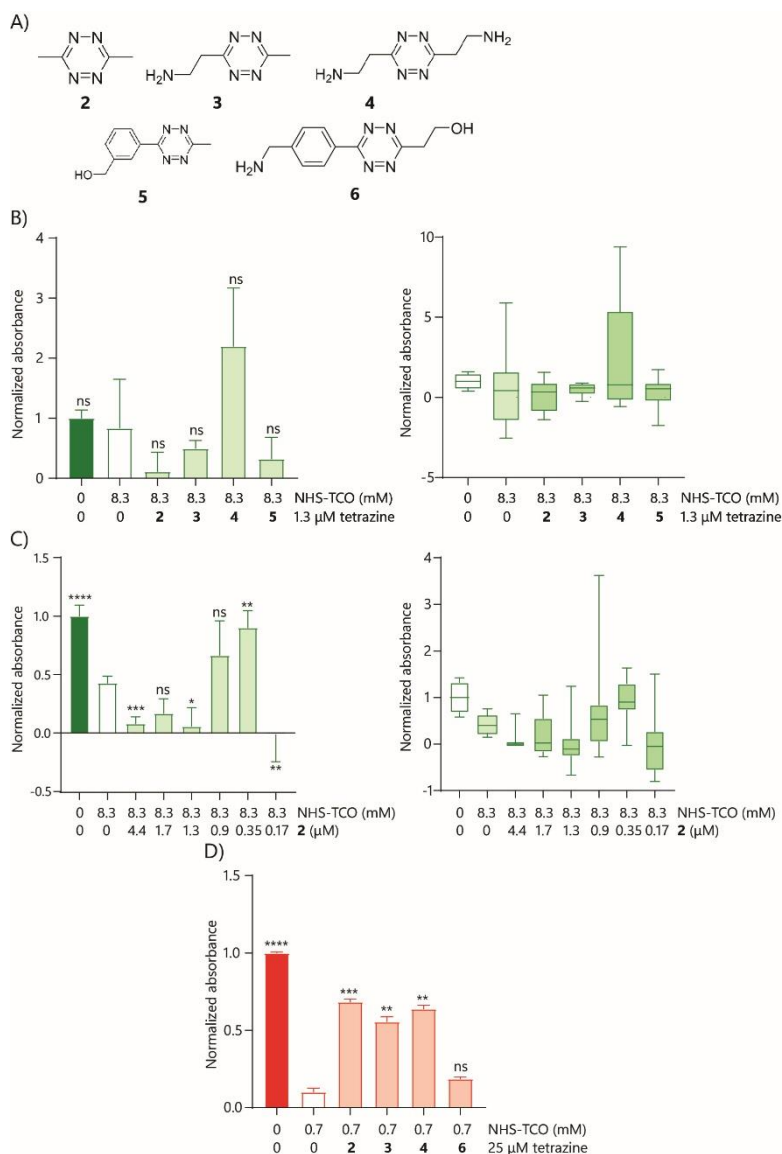


Figure 15 - Initial decaging optimisation of IL-1 β and IL-1 β -LPETGG using different tetrazines analysed by RAW-Blue cells and HEK-Blue IL-1 β cells, respectively.

A) Various tetrazines tested for decaging of IL-1 β (B,C) and IL-1 β -LPETGG (D). B,C) IL-1 β (11 μ M) was caged with 8.3 mM **1** for 1 hour at 37°C in 20 mM HEPES pH 8, dialysed in 20 mM HEPES pH 7 to remove unreacted NHS-TCO following addition to RAW-Blue cells in the applicable concentration. Decaging was performed with B) 1.3 μ M of different tetrazines **2-5** (N=6), or C) different concentrations of **2** (N=6), and took place for 18-20 hours at 37°C on the cells. D) IL-1 β -LPETGG (5 μ M) was caged with 0.7 mM **1** for 24 hours at 10°C in 20 mM HEPES pH 8, following addition to HEK-Blue IL-1 β cells in the applicable concentration. Decaging was performed with 25 μ M of different tetrazines and took place for 18-20 hours at 37°C on the cells (N=6). Bright colours indicate DMSO only samples and pastels the tetrazine treated samples. Data were plotted as mean signal \pm SEM. Significances are indicated as follows: * P < 0.05; ** P < 0.01; *** P < 0.001; **** P < 0.0001; ns is non-significant.

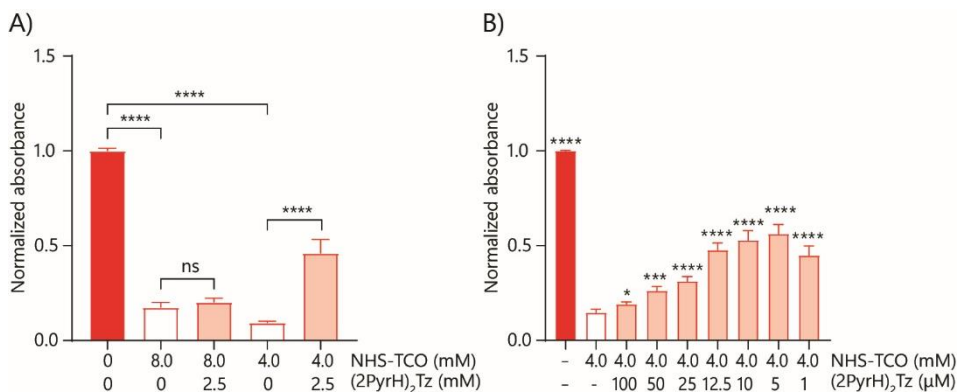


Figure 16 – Decaging of IL-1β assessed by ELISA and HEK-Blue IL-1β assay.

Decaging optimisation was assessed using (caged) IL-1β on A) ELISA (N=3) and on B) stimulated HEK-Blue IL-1β. A) Deprotection of high-TCO IL-1β (N=4); B) Deprotection of medium-TCO IL-1β. Decaging conditions were compared to caging control. Bright colours indicate DMSO only samples and pastels the tetrazine treated samples. Data were plotted as mean signal ± SEM. Significances are indicated as follows: * P<0.05; ** P<0.01; **** P<0.0001; ns is non-significant.

Having successfully blocked and recovered the activity of wild-type IL-1β, it was next determined whether IL-1β-LPETGG could be similarly controlled (**Figure 17**). IL-1β-LPETGG was therefore protected with either 3.5 mM (**Figure 17A**) or 2.1 mM NHS-TCO (**Figure 17B**) by incubation for 1 hour at 37°C, or by incubation with 0.7 mM NHS-TCO for 24 hours at 10°C (**Figure 17C**). For all three concentrations near complete loss of IL-1β-LPETGG activity was observed in a HEK-Blue assay. Differences in reactivation upon addition of **7** were observed, with the 0.7 mM-modified protein reactivating to >80%, the 2.1 mM reactivating to 30-50%, and the 3.5 mM protein only reaching 25% of the activity of the uncaged reagent. This last observation with 3.5 mM NHS-TCO was very different from the result in **Figure 16** as that experiment showed up to 60% recovery. A possible explanation for this could be that the form of IL-1β differs between the two assays although this should be confirmed using an assay with both proteins assessed under the same conditions. Similar to **Figure 16B**, increasing the concentration of **7** >25 μM does not improve the recovery of activity, most likely due to the cytotoxicity associated with **7** at these concentrations. It was therefore decided that for future experiments the proteins would be protected with 0.7 mM, and deprotection conditions would be using 25 μM **7** for 18 hours at 37°C. Caging and decaging of IL-1β-LPETGG at higher concentrations followed a similar pattern (**Figure 18**).

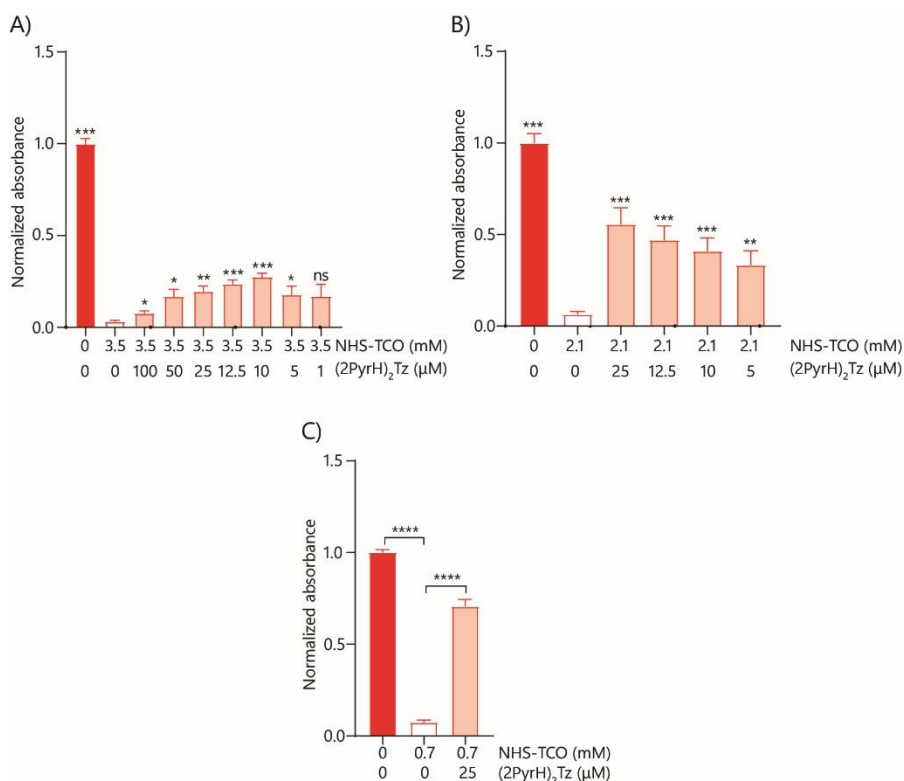


Figure 17 – Caging and decaging optimisation of IL-1 β -LPETGG analysed by HEK-Blue IL-1 β cells.

Figure 7 Caging and decaging optimisation of IL-1 β LPETGG analysed by HEK-Blue IL-1 β cells. The reactivation of IL-1 β -LPETGG, caged under various conditions, by **7** was analysed on HEK-Blue IL-1 β cells. A) protection with 3.5 mM **1** (for 1 hour at 37°C) (N=4); B) 2.1 mM **1** (for 1 hour at 37°C) (N=4); C) 0.7 mM **1** (for 24 hours at 10°C) (N=5). Bright colours indicate DMSO only samples and pastels the tetrazine treated samples. Data were plotted as mean signal \pm SEM. Significances are indicated as follows: * P<0.05; ** P<0.01; *** P<0.001; **** P<0.0001; ns is non-significant.

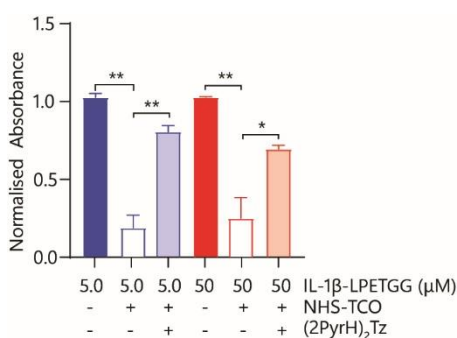


Figure 18 - Caging and decaging at various protein concentrations analysed using HEK-Blue IL-1 β cells.

IL-1 β -LPETGG was caged at either 0.1 mg/mL (5.0 μ M) or 1.0 mg/mL (50 μ M) with 0.7 mM or 70 mM **1**, respectively, for 24 hours at 10°C in 20 mM HEPES pH 8 following decaging on cells. Maximal signal was obtained by treating IL-1 β -LPETGG with 0 mM **1** (-). Significances were determined relative to the caged samples (+ NHTCO, - (2PrH)₂Tz) (N=3). Bright colours indicate DMSO only samples and pastels the tetrazine treated samples. Colour groups indicate different conditions with respective DMSO controls. Data were plotted as mean signal \pm SEM. Significances are indicated as follows: * P<0.05; ** P<0.01; *** P<0.001; **** P<0.0001; ns is non-significant.

Optimisation of coupling reaction between IL-1 β -LPETGG and VHH-CD11c-SIINFEKL by sortase A

Having shown that cytokine activity could be controlled using click-to-release chemistry, the sortase-mediated coupling reaction of the nanobody to the cytokine was optimised next. First, the coupling of unmodified IL-1 β -LPETGG was optimised, before moving to the coupling of the TCO-protected cytokine.

The initial reaction was performed in 50 mM Tris/150 mM NaCl/10% glycerol pH 7.5 for 1 hour at 37°C using equal equivalents of both IL-1 β -LPETGG (19.7 kDa) and VHH-CD11c-SIINFEKL (15 kDa 4 μ M each) and 0.75 equivalents of sortase A (3 μ M). If successful, the ligation reaction should form a 35 kDa product. A persistent intermediate, in which IL-1 β -LPETGG is coupled to sortase A via an ester linkage, could potentially also form and would be 38 kDa in size. An SDS-PAGE analysis of the reaction mixture (**Figure 19A**) confirmed the formation of this product with a new band at the height of the expected product (red arrow). To confirm this was indeed the case, a Western blot was performed using an IL-1 β -specific antibody (**Figure 19B**). This blot showed an additional band at about 38 kDa in which the nanobody was absent (green arrow), suggesting the formation of the intermediate product. None of this product was present in the actual reaction mixture. Both the coomassie staining and the Western blot showed additional bands at molecular weights lower than IL-1 β -LPETGG or sortase A, even in the absence of the nanobody. Further research into these proteins was not performed. The assumption was made that these bands originated from hydrolysis of the bond formed between sortase A and IL-1 β -LPETGG in the absence of the nanobody. This removes the C-terminal 6His-tag and the terminal glycines of IL-1 β -LPETGG, thereby reducing its molecular mass.

Despite this early promising result, the reaction was optimised to improve the yield. Various amounts and ratios of starting materials were assessed, as well as the reaction time and the reaction volume (**Supplementary Figure S5A-C and Figure S6**).

Increasing the amount of sortase relative to the IL-1 β -LPETGG and VHH-CD11c-SIINFEKL resulted in lower product yield (**Supplementary Figure S5A**), perhaps due to background hydrolysis by sortase A.⁷² Increasing the reaction time from 1 hour to 2 or 3 hours also reduced product formation. When the reaction time was shortened to 15 min or 1 min, the product yield improved (**Supplementary Figure S5B-C**). This was most likely due to the fact that sortase A can also hydrolyse the formed bonds between the nanobody and the IL-1 β -LPETGG. Similar to **Figure 19** these figures also show the presence of additional low-molecular weight proteins when both sortase A and IL-1 β are present, probably indicating the presence of hydrolysis products. These optimisations combined led to an optimised coupling protocol in which the cytokine was present in 4 μ M, the nanobody in 8 μ M, all with 3 μ M of sortase and left to react for 15 minutes (**Supplementary Figure S6**). This still did not lead to a complete reaction, but gave sufficient yields for further experiments.

These conditions were then used to ligate the caged cytokine to the anti-CD11c nanobody. Therefore, IL-1 β -LPETGG (5.0 μ M) was caged using 3.5 mM NHS-TCO and the caged product was coupled to VHH-CD11c-SIINFEKL by sortase A using the optimal conditions found in **Supplementary Figure S6**. The red arrow indicated the 35 kDa product formed between caged IL-1 β -LPETGG and VHH-CD11c-SIINFEKL, which was only

formed when both substrates and sortase A were present. The green arrow highlighted the intermediate (38 kDa) formed between sortase A and caged IL-1 β -LPETGG in the absence of VHH-CD11c-SIINFELK. Finally, the dark blue arrow indicates the presence of uncoupled caged IL-1 β -LPETGG. Product formation was assessed with IL-1 β -specific Western blot (**Figure 20C**) and, for the TCO-modified products, by reaction with the slow-eliminating tetrazine-BODIPY-TMR (unpublished data, thesis Alexi Sarris) (**Figure 20A, 8**). This latter experiment indeed confirmed the presence of TCO-modified compound in the 35 kDa and 38 kDa bands.

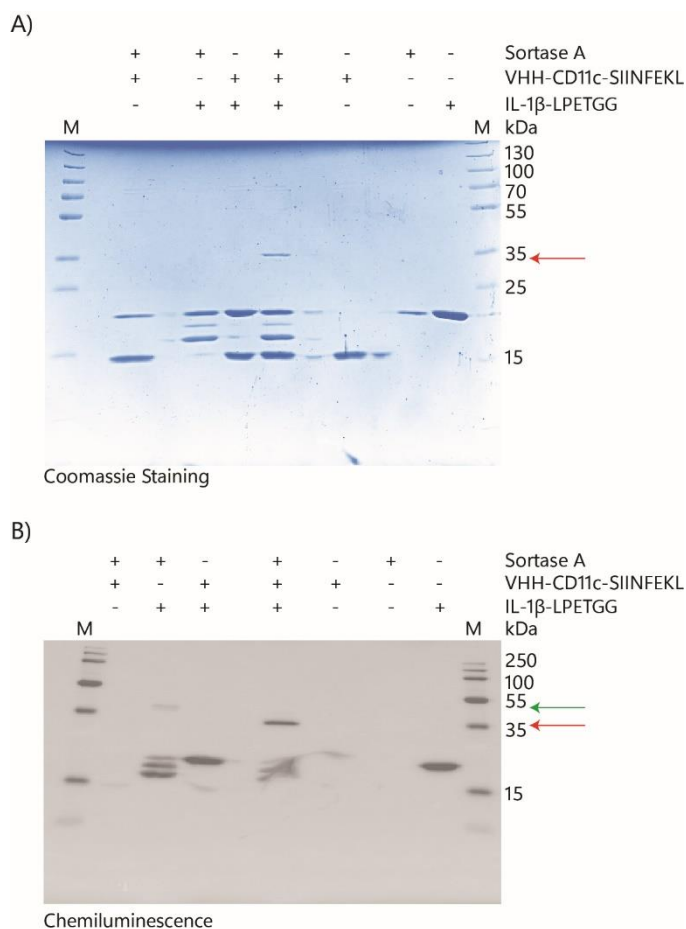


Figure 19 - Sortase reaction with IL-1 β -LPETGG and VHH-CD11c-SIINFELK analysed by SDS-PAGE and Western blot.

Sortase A recognizes the C-terminal LPETGG-sequence of IL-1 β , cleaves between the tyrosine and the glycine and couples it to the N-terminal polyglycine tail of the VHH-CD11c-SIINFELK nanobody. A) SDS-PAGE analysis with coomassie staining shows a product of 35 kDa (red arrow). B) Western blot with anti-IL-1 β of the same gel, showing the intermediate product at 38 kDa which is the coupling of sortase A to IL-1 β -LPETGG (green arrow) as well as the final product at 35 kDa (red arrow).

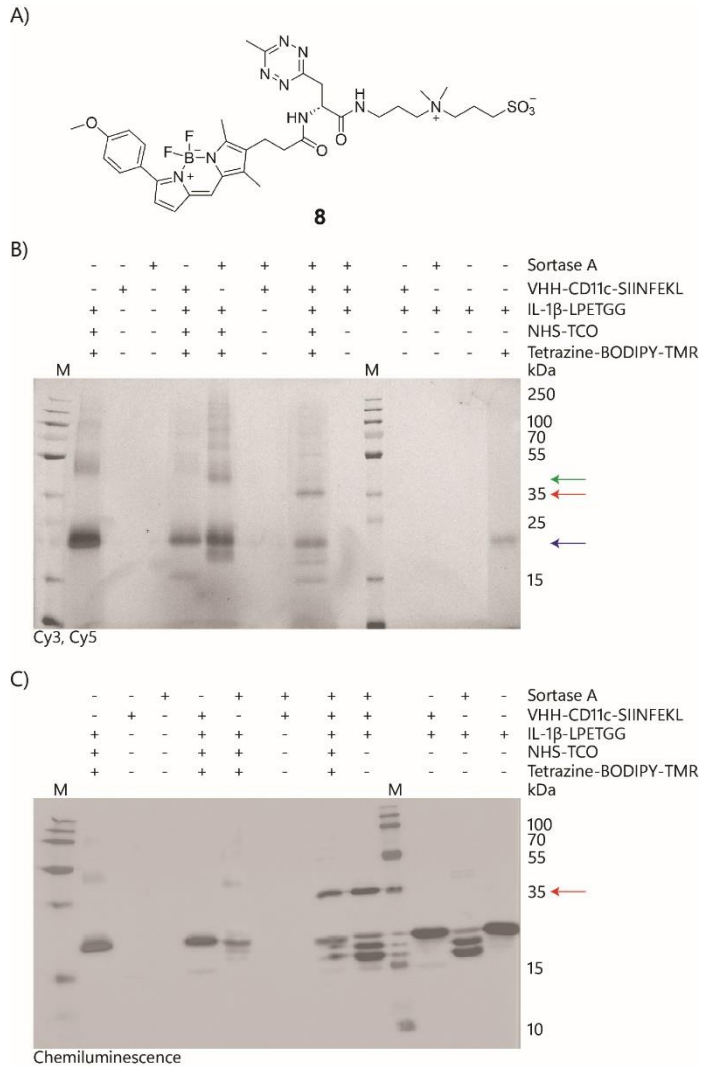


Figure 20 - Sortase reaction with caged IL-1 β -LPETGG and VHH-CD11c-SIINFEKL analysed using tetrazine-BODIPY-TMR and Western blot.

IL-1 β -LPETGG (5.0 μ M) was first caged using 3.5 mM NHS-TCO and then coupled to VHH-CD11c-SIINFEKL using sortase A. Tetrazine-BODIPY-TMR (A) was used for B) visualisation by fluorescence (settings: excitation 532 nm/emission 570 nm) of caged IL-1 β -LPETGG. Non-coupled IL-1 β -LPETGG was indicated with the blue arrow, sortase-coupled IL-1 β -LPETGG was indicated with a green arrow and product formation was indicated with the red arrow. C) Western blot using an IL-1 β -specific antibody shows that coupling between IL-1 β -LPETGG and VHH-CD11c-SIINFEKL took place (red arrows). Tetrazine-BODIPY-TMR was kindly provided by Alexi Sarris.

The initial optimisation of the deprotection reaction was performed with the crude product mixtures of the above reactions. For this the construct of IL-1 β -VHH-CD11c-SIINFEKL was formed by caging IL-1 β -LPETGG with either 3.5 mM, 2.1 mM, or 0.7 mM NHS-TCO following ligation to the nanobody. The crude reaction mixtures were then added to HEK-Blue IL-1 β cells and the activity measured. The three constructs showed residual IL-1R-binding activity of 2%, 5% and 16%, respectively (**Figure 21A-C**). As for the unligated product, major differences were observed in the deprotection of these constructs. The maximum recovery of the highly caged construct (**Figure 21A**) could not be increased over 20% of the activity of the parent molecule with (2PyrH)₂Tz. The constructs modified with 2.1 mM TCO and 0.7 mM TCO could be fully reactivated with this tetrazine (**Figure 21B-C**, respectively).

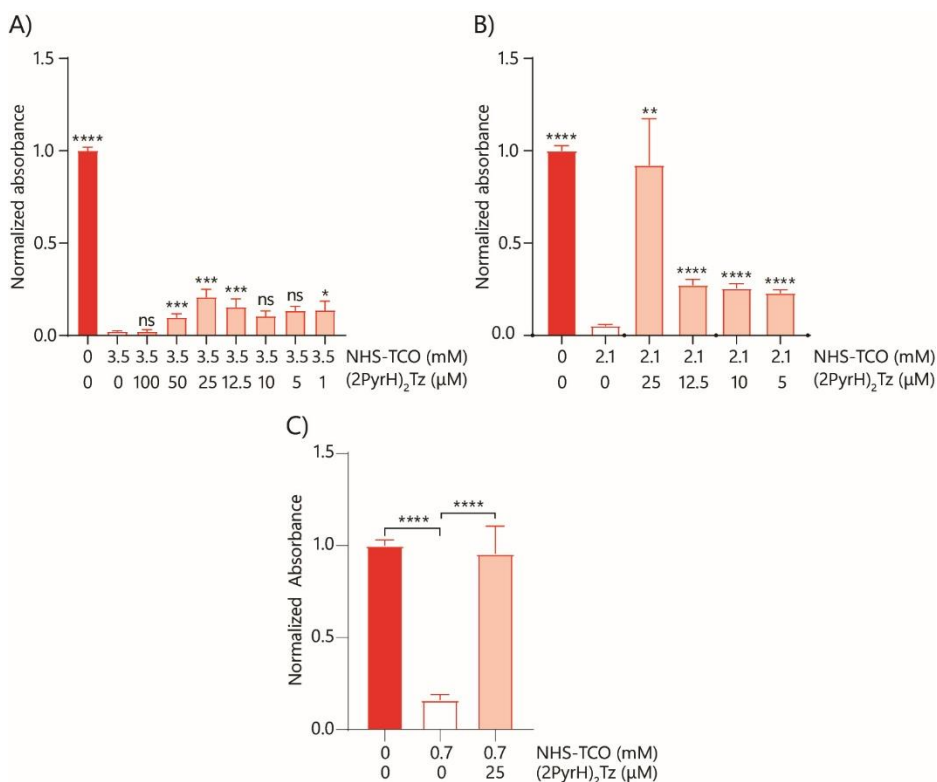


Figure 21 - Decaging optimisation of IL-1 β -VHH-CD11c-SIINFEKL using HEK-Blue IL-1 β cells.

The reactivation of IL-1 β -VHH-CD11c-SIINFEKL (5.0 μ M), caged under various conditions, by **7** was analysed on HEK-Blue IL-1 β cells. Caging was performed before coupling to VHH-CD11c-SIINFEKL, in 20 mM HEPES pH 8 for A) protection with 3.5 mM **1** (for 1 hour at 37°C) (N=3); B) 2.1 mM **1** (for 1 hour at 37°C) (N=5); C) 0.7 mM **1** (for 24 hours at 10°C) (N=5). Bright colours indicate DMSO only samples and pastels the tetrazine treated samples. Data were plotted as mean signal \pm SEM. Significances are indicated as follows: * $P < 0.05$; ** $P < 0.01$; *** $P < 0.001$; **** $P < 0.0001$; ns is non-significant.

The above experiments were performed on crude mixtures. Next the purification was attempted using size exclusion chromatography. Unfortunately, this method (**Supplementary Figure S7A-D**) resulted in low product yields and the co-elution of unreacted nanobody. This co-elution was most likely caused by the absence of salts. As a result, the immunocytokine seeks to interact with other molecules, like the excess of nanobody present, for stabilization, forming non-covalent interactions. Therefore, further purification of these constructs remains to be further investigated. Strategies that could be followed are the addition of (more) salt to minimize the non-covalent interactions of the caged immunocytokine with the unreacted nanobody and the increase of the reaction scale by increasing the immunocytokine concentration.

Conclusion

This chapter presented the initial results to demonstrate the applicability of click-to-release chemistry in reducing the toxicity of the cytokine IL-1 β . Upon treatment with NHS-TCO ester at a low temperature (10°C) for extend period of time (24 hours), IL-1 β and its sortagble variant IL-1 β -LPETGG lost their ability to bind IL-1R. Following treatment with (2PyrH)₂Tz at 37°C for 18 hours, activity of IL-1 β and IL-1 β -LPETGG was restored. This could be extended to large scale caging and decaging reactions. Coupling of caged IL-1 β -LPETGG to an anti-CD11c nanobody (VHH-CD11c-SIINFEKL) using sortase A proved to be possible. The purification of this conjugate was established in low yields and therefore demands for further optimisation.

Acknowledgements

First, I would like to thank Göktuğ Aba and Thierry Shema, who worked really hard with me on this project even though it was not always as promising as it eventually ended up. Second, I would like to thank Dr. Martijn Verdoes and Camille Le Gall, both from Radboud UMC, for providing me with the constructs for sortase A and VHH-CD11c-SIINFEKL and with the protocols how to use them. I would also like to thank Mark de Geus, Dr. Merel van der Plassche and Prof. Dr. Hannes Mikula for the supply of NHS-TCO, various tetrazines and the (2PyrH)₂Tz, respectively which all assisted in accomplishing this way of controlling cytokine activity. I would like to thank Dr. B. I. Florea for his assistance with the LC-MS experiments and finally, I would like to thank Dr. Diana Torres García for helping me with the statistical analyses of all the data, as this was a lot of work and my understanding of statistics was very minimal at that moment in time.

Materials & Methods

General reagents

All donor vectors (unless mentioned differently) were purchased from GenScript and primers were ordered at Sigma-Aldrich. All restriction enzymes, polymerases and ligases were purchased from Thermo Fisher Scientific. Benzonase was purchased from Santa Cruz Biotechnology. Sodium deoxycholate monohydrate (CAS:302-95-4) and phenylmethanesulfonyl fluoride (PMSF, CAS:329-98-6) were purchased from Sigma-Aldrich. Rabbit anti-6*His (Item No. 600-401-392) was purchased from Rockland and mouse anti-rabbit IgG-HRP (Catalog #sc-2357) was purchased from Santa Cruz Biotechnology. DMEM, L-glutamine, streptomycin and penicillin were purchased from Sigma-Aldrich. QUANTI-Blue (#rep-qbs) and zeocin were purchased from InvivoGen.

Construct formation

NheI restricted (1x Tango Buffer, 10U NheI) pcDNA3.1⁺/C-(K)DYK_IL1 β (Clone ID: OMu23150D, accession version: NM_008361.4) was used as template for IL-1 β amplification by PCR (GC Green Buffer, 0.2 mM dNTPs, 0.1 μ M of each primer, 50 ng restricted vector, 2U Phusion polymerase) using primers of **Table 2**. IL-1 β fragments were restricted in a two-step protocol with Esp3I/XhoI (IL-1 β) or Esp3I/EcoRI (IL-1 β -LPETGG), respectively and ligated into NcoI/XhoI (IL-1 β) or NcoI/EcoRI (IL-1 β -LPETGG) restricted pET28a vector behind the T7 promoter using T4 DNA Ligase (5U). Ligation products were transformed into *E. coli* XL10 via heat shock (42°C, 45 seconds) and SOC-medium recovery followed by growth on kanamycin (50 μ g/mL) containing LB-agar plates at 37°C.

Table 2 - Primer overview.

Primer Nr.	Construct	Sequence 5'→3'
1	IL-1 β	TATACCATGGTCCCATTAGACAACTG
2		AATGCTCGAGTTAGGAAGACACGGA
3	IL-1 β -LPETGG-6His	AAAACGTCCTCCCATGGTTCCCATTAGACAA
4		CCGGAATTCGGAAGACACGGATTC

Cytokine expression and isolation

Cytokine constructs isolated from *E. coli* XL10 using QIAprep Spin Miniprep Kit were used to transform calcium competent *E. coli* ArcticExpress (DE3) RP using heat shock (42°C, 45 seconds) and SOC-medium recovery. Colonies were used to inoculate LB-medium containing kanamycin (50 μ g/mL) for overnight growth at 37°C, 170 rpm. Overnight culture was diluted 100 times and grown at 37°C, 170 rpm until optical density at 600 nm (OD₆₀₀) of 0.6 was reached, after which protein expression was induced with addition of 0.5 mM IPTG. Expression took place for 48-72 hours at 10°C, 140 rpm whereafter the bacteria were harvested by centrifugation (30 minutes, 3400g at 4°C).

Per 500 mL bacterial culture, 10 mL lysis buffer (50 mM Tris Cl pH 8.0, 25% (w/v) sucrose, 1 mM EDTA, 1 mM PMSF, 2 mM DTT) was applied with 0.4 mg/mL lysozyme. Incubation while gently mixing for 30 minutes at 4°C was followed by adding 10 mM MgCl₂, 1 mM MnCl₂ and 10U benzonase and 30 minutes incubation at 4°C. The lysate was sonicated (Vibra-cell™ VCX130) for 30 seconds with 5 second pulses with 20% amplitude and 10 second intervals. The lysate was diluted three times with detergent buffer (0.2 M NaCl, 1% (w/v) sodium deoxycholate monohydrate, 1% octylphenoxypolyethoxyethanol (Igepal), 20 mM Tris Cl pH 7.5, 2 mM EDTA, 0.02 mM PMSF, 0.04 mM DTT), incubated for 30 minutes on ice and centrifuged for 20 minutes at 14000g, 4°C to collect the supernatant.

Cytokine purification

IL-1β containing lysate was diluted 10 times in 20 mM MES pH 6, incubated overnight at 4°C and centrifuged (10 minutes, 1000g, 4°C). The supernatant was loaded (1 mL/min) onto a HiTrap CM sepharose FF column (GE Healthcare Life Sciences) coupled to an ÄKTA Start System (GE Healthcare Life Sciences) and the protein was eluted using 0-500 mM NaCl in 20 mM MES pH 6. Protein containing fractions were combined, concentrated and buffer exchanged to 20 mM HEPES pH 8 using Amicon® Ultra-15 Centrifugal Filters 3K (MERCK #UFC900324). Yields were obtained between 0.5-1.5 mg/mL.

IL-1β-LPETGG containing lysate was first loaded (4 mL/min) onto a HisTrap™ (GE Healthcare Life Sciences) where after the protein was eluted using 0-250 mM imidazole in PBS. IL-1β-LPETGG containing fractions were combined, concentrated and buffer exchanged to 20 mM HEPES pH 8 using Amicon® Ultra-15 Centrifugal Filters 3K. Yields were obtained between 0.5-1.5 mg/mL.

Sortase A and VHH-CD11c-SIINFEKL expression and purification

Sortase A and VHH-CD11c-SIINFEKL were expressed and purified as has been described before.⁵⁸ Briefly, the vector pET28aSrtAΔ59 (kindly provided by Dr. Martijn Verdoes of Radboud UMC, #51138 AddGene) was transformed into *E. coli* Rosetta-gami 2 (DE3) via heat shock (42°C, 45 seconds) and SOC-medium recovery. Colonies were grown on kanamycin (50 µg/mL) containing LB-agar plates at 37°C. Colonies were used to inoculate LB-medium containing kanamycin (50 µg/mL) for overnight growth at 37°C, 170 rpm, which was then diluted 50 times in LB-medium and grown at 30°C, 140 rpm until OD₆₀₀~0.5-0.6. Expression was induced with 1 mM IPTG and took place at 25°C, 140 rpm for 20 hours whereafter the culture was centrifuged for 25 minutes at 3400g, 4°C. The resulting pellet was dissolved in 1/10 culture volume nickel binding buffer (50 mM Tris pH 7.5, 150 mM NaCl at room temperature) and centrifuged again. The resulting pellet was stored at -20°C overnight.

Per 500 mL bacterial culture 10 mL ice cold lysis buffer (50 mM Tris pH 7.4 (4°C), 150 mM NaCl, 5 mM MgCl₂, 10 mM imidazole, 10% (v/v) glycerol, 1 mg/mL lysozyme, 10U benzonase) was used to dissolve the cell pellet after which the suspension was sonicated on ice for 90 seconds with 30 seconds on/off pulses of 30% amplitude (vibra-cell™ VCX130 of Sonics). The culture was centrifuged (20 minutes, 10 000g at 4°C) and the supernatant was passed through a 0.2 µm filter and diluted once in wash buffer (50 mM Tris pH 7.5 (4°C), 150 mM NaCl, 5 mM MgCl₂, 10 mM imidazole, 10% (v/v) glycerol) which was then loaded onto 50% HisPur™ Ni-NTA Resin (Thermo Fischer Scientific #88222) and

incubated for 1 hour, gently mixing at 4°C. Proteins were eluted using 50-500 mM imidazole in storage buffer (50 mM Tris pH 7.5 (4°C), 150 mM NaCl, 10% (v/v) glycerol). Protein containing fractions were combined and buffer exchanged to storage buffer using Amicon® Ultra-15 Centrifugal Filters 10K (MERCK UFC901024) filters. Proteins were stored at -80°C.

The pET22b-vector encoding VHH-CD11c-SIINFEKL (kindly provided by Dr. Martijn Verdoes of Radboud UMC) was transformed into *E. coli* BL21 (DE3) pLysS similar as for sortase A described above. Instead of containing kanamycin, ampicillin (250 μ g/mL) and chloramphenicol (25 μ g/mL) were used to select for transformed bacteria. VHH-CD11c-SIINFEKL expression and purification were performed as for sortase A.

Western blot

Denaturing acrylamide gels (SDS-PAGEs) were blotted onto 0.2 μ m PVDF membranes (Trans-Blot Turbo Transfer Pack, midi format, single application of Bio-Rad) using the Turbo Trans Blot System (Bio-Rad). Blots were developed using luminol solution (25% (w/v) luminol in 0.1 M Tris pH 8.8), 100x diluted enhancer (1.1 mg/mL p-coumaric acid in DMSO) and H₂O₂.

6His-specific blot

Blots were washed 10 minutes and 3 times 5 minutes with TBS and TBST (1x TBS pH 7.5; 0.1% Tween-20), respectively before blocking with 5% milk in TBST overnight at 4°C. Washing with TBST was followed with rabbit anti-6*His incubation (1:1000) in blocking buffer for 3 hours at room temperature. Another three 5 minutes washes with TBST were followed by addition of mouse anti-rabbit IgG-HRP (1:4000) and incubation for 2 hours at room temperature. The blots were washed 3 times 5 minutes and 10 minutes with TBST and TBS, respectively before development with luminol.

Cytokine specific blot

Blots were washed with PBS and PBST (1x PBS pH 7.4, 0.5% Tween-80). Blocking was performed with 0.2% BSA in PBST. The primary antibody used was biotin-conjugate anti-mouse IL-1 beta (1:1000, #88-7013-88, Thermo Fisher Scientific). Strep-Tactin® HRP conjugate (1:100000, #2-1502-001, IBA solutions) was used as a secondary antibody.

Blots were imaged with the ChemiDoc™ MP Imaging System of Bio-Rad with setting chemiluminescence, Cy3 and Cy5 and analysed using ImageLab Software version 4.1.

Caging and decaging procedure

Caging

Caging was performed in 20 mM HEPES pH 8 at 10°C, 800 rpm for 24 hours. An excess of 10 molar equivalents 2-AX-NHS-TCO (kindly provided by Mark de Geus) was used per lysine in IL-1 β or IL-1 β -LPETGG-6His. Protein concentrations were determined using the Qubit™ Protein assay kit on the Qubit® 2.0 Fluorometer of Invitrogen (Life Technologies). Caging was visualised by using 0.6 μ M Tetrazine Bodipy-TMR Sol2 (kindly provided by Alexi Sarris) incubating for 30 minutes at 25°C, 800 rpm. Gels were analysed using ChemiDoc™ MP Imaging System of Bio-Rad and ImageLab Software version 4.1.

Decaging – ELISA

Decaging was performed in 20 mM HEPES pH 8 with 2.5 mM (2PyrH)₂Tz and 5.7 μ M IL-1 β caged with various amounts of NHS-TCO. Decaging was performed at 37°C, 300 rpm for 1 hour.

Decaging – HEK-Blue IL-1 β

Decaging was performed in complete medium in well with 5-25 μ M (2PyrH)₂Tz (kindly provided by Prof. Dr. Hannes Mikula) on cells at 37°C overnight.

Sortase A reaction

VHH-CD11c-SIINFEKL coupling

VHH-CD11c-SIINFEKL was produced with a *N*-terminal thrombin cleavage site protecting the polyglycine *N*-terminus. Using the 25x diluted thrombin (Merck #69671-3) with 10 μ g protein in 50 μ L total volume released the *N*-terminal polyglycine tail. Caging took place prior to the reaction with sortase and nanobody. Sortase reaction was performed with 4 μ M IL-1 β -LPETGG-6His, 3 μ M sortase A, 8-10 μ M VHH-CD11c-SIINFEKL in sortase buffer (50 mM Tris pH 7.5, 150 mM NaCl, 10% (v/v) glycerol, 4°C) supplemented with 1 mM CaCl₂. Incubation took place for 15 minutes at 37°C, 300 rpm.

Purification IL-1 β -VHH-FR-SIINFEKL

Coupled protein was concentrated to a final volume of maximal 500 μ L before loading onto a Superdex™ 75 increase 10/300 GL column connected to ÄKTA start system, equilibrated with 20 mM HEPES pH 8. Fractions of 500 μ L IL-1 β -VHH-CD11c-SIINFEKL were separated from the starting materials. Fraction analysis was performed using SDS-PAGE with coomassie staining. Pure fractions were combined and stored at -80°C.

ESI LC-MS experiments

Liquid chromatography-mass spectrometry analysis (LC-MS) was performed to study the caged lysine residues. Instruments Nanoacquity UPLC system (Waters) and Synapt G2Si mass spectrometer (Waters) were used and operated with Masslynx for acquisition and Ent3 software for polymer envelope signal deconvolution. Acquity UPLC M-class 300 μ m x 50 mm column (Waters), packed with BEH C4 material of 1.7 μ m diameter and 300 Å pore size particles was used as stationary phase. All materials used for mobile phase were of ULC-MS grade quality and were purchased from Biosolve or Sigma-Aldrich. Mobile phase A was 0.1% formic acid (FA) in ultrapure water and mobile phase B was 0.1% formic acid in acetonitrile (ACN). Caged samples (described above) were filtered using Zeba™ Spin Desalting columns, 7K MWCO, 0.5 mL (Thermo Fischer Scientific) equilibrated first three times with 10 mM ammonium acetate pH 6 (1 minute at 1500g) before loading the caged sample (2 minutes at 1500g). Approximately 5 μ L of the sample was injected on the column followed by elution with a 10-90% mobile phase B gradient within 20 minutes ending with 10 minutes equilibration to 10% B at a flow of 2 μ L/min. Ionization was executed with electro-spray ionization (ESI) via Nano-spray source with ESI emitters (New Objectives) fused silica tubing 360 μ m OD x 25 μ m ID tapered to 5 \pm 0.5 μ m (5 nL/cm void volume). Source temperature of 80°C, capillary voltage of 4.5 kV, nano flow gas of 0.25 bar, purge gas of 250 L/h, trap gas flow of 2.0 mL/min, cone gas of 100 L/h, sampling cone of 25 V, source offset of 25, trap CE of 32 V, scan time of 3.0 sec,

mass range of 400-2400 m/z settings were using in positive mode. Lock mass acquiring was done with a mixture of Leu Enk (556.2771) and Glu Fib (785.84265), lockspray voltage of 3.5 kV, Glufib fragmentation was used as calibrant. Charge state envelopes were analysed and deconvoluted with the MaxEnt 1 software. LC-MS analysis was performed with help of Dr. B. I. Florea. Only the amount of cages present could be determined, the exact location of each cage remained unknown.

ELISA assay

Uncoated ELISA kit for IL-1 β (#88-7013-88) was from Invitrogen. The assays were performed using 96-wells microplate half area high binding (#675061, Greiner Bio-one). Assay was performed according to the manufactures protocol with the following adaptations. Both antibodies and streptavidin-HRP were applied in 25 μ L per well and blocking was performed with 100 μ L per well. Samples were applied in 30 μ L (80-1000 pg/mL for IL-1 β or IL-1 β -LPETGG per well. Final substrate was supplied in 25 μ L per well and the enzymatic reaction was stopped with 12.5 μ L per well. Absorbance at 450 nm was measured with the Bio-Rad iMark™ Microplate Reader.

Cell culture

RAW-Blue

RAW-Blue™ (cat. raw-sp, InvivoGen) were maintained in Dulbecco's Modified Eagle's Medium – high glucose (DMEM-high glucose, #D6546-500ML) supplemented with 2 mM L-glutamine, 10% (v/v) heat-inactivated fetal calf serum, 100 IU/mL penicillin and 50 μ g/mL streptomycin at 37°C, 5% CO₂. Every other passage (300 000 cells/mL in T75) 200 μ g/mL zeocin was added for selection.

HEK-Blue IL-1 β

HEK-BLUE™ IL-1 β (cat. Hkb-il1bv2, InvivoGen) were maintained in Dulbecco's Modified Eagle's Medium – high glucose (DMEM-high glucose, #D6546-500ML) supplemented with 2 mM L-glutamine, 10% (v/v) heat-inactivated fetal calf serum, 100 IU/mL penicillin and 50 μ g/mL streptomycin at 37°C, 5% CO₂. Every other passage (130 000 cells/mL in T75) 200 μ g/mL zeocin was added for selection.

RAW-Blue assay

RAW-Blue cells were seeded at 50 000 cells/well in a 96-wells flat bottom plate, in growth medium without zeocin and incubated for 18-24 hours at 37°C, 5% CO₂. Samples were prepared 10 times concentrated in a separate 96-wells plate. The medium of the cells was replaced with 90 μ L fresh medium and 10 μ L sample reaching a final cytokine concentration of 15-1000 ng/mL. Cells were incubated for 18-20 hours at 37°C, 5% CO₂, centrifuged (2 minutes, 1000g at room temperature) and the 20 μ L supernatant was incubated with 180 μ L QUANTI-Blue in a new 96-wells plate at 37°C for 30 minutes to 6 hours. Absorbance at 655 nm was measured using the Bio-Rad iMARK Microplate reader.

HEK-BLUE IL-1 β assay

Protein samples were prepared 4 times concentrated in a separate 96-wells plate of which 50 μ L per well was transferred to the assay plate. HEK-BLUE IL-1 β cells were seeded at 45 000 cells/well in 150 μ L medium. The final protein concentration ranged 15.6 – 1000 ng/mL. Cells were incubated for 18-20 hours at 37°C, 5% CO₂ whereafter 20 μ L supernatant was added to 180 μ L QUANTI-Blue in a new 96-wells plate and incubated at 37°C for 30 minutes – 3 hours. Absorbance at 655 nm was measured using the Bio-Rad iMARK Microplate reader.

Statistical analysis

All data were normalized using Microsoft Excel. All data are reported as mean \pm SD of n=3-7 independent experiments. Statistical analysis were carried out using R 4.1.0 (R Core Team, 2021), the base, graphics, methods, stats, utils, and ggplot2 packages. Parametric tests, one-way ANOVA, or Brown-Forsythe ANOVA tests were used for data with normal distribution, based on the homoscedasticity of the data, verified with Bartlett's test. If the omnibus test had a $p < 0.05$, unpaired t-test with or without Welch's correction (Welch's correction applied to different SD pairs) post hoc tests were performed based on the F-test. For data not normally distributed, non-parametrical Kruskal-Wallis comparisons were carried out with Mann-Whitney post hoc comparisons test. Results were considered significant when $p < 0.05$. Graphs were made using GraphPad Prism 8.4.3. Statistical analyses were performed with assistance of Dr. Diana Torres García.

References

- (1) Krumm, B.; Xiang, Y.; Deng, J. Structural Biology of the IL-1 Superfamily: Key Cytokines in the Regulation of Immune and Inflammatory Responses. *Protein Science* **2014**, *23* (5), 526–538. <https://doi.org/10.1002/pro.2441>.
- (2) Essayan, D. M.; Fox, C. C.; Levi-Schaffer, F.; Alam, R.; Rosenwasser, L. J. Biologic Activities of IL-1 and Its Role in Human Disease. *Journal of Allergy and Clinical Immunology* **1998**, *102* (3), 344–350. [https://doi.org/10.1016/S0091-6749\(98\)70118-6](https://doi.org/10.1016/S0091-6749(98)70118-6).
- (3) Lopez-Castejon, G.; Brough, D. Understanding the Mechanism of IL-1 β Secretion. *Cytokine Growth Factor Rev* **2011**, *22* (4), 189–195. <https://doi.org/10.1016/j.cytogfr.2011.10.001>.
- (4) LaRock, C. N.; Todd, J.; LaRock, D. L.; Olson, J.; O'Donoghue, A. J.; Robertson, A. A. B.; Cooper, M. A.; Hoffman, H. M.; Nizet, V. IL-1 β Is an Innate Immune Sensor of Microbial Proteolysis. *Sci Immunol* **2016**, *1* (2). <https://doi.org/10.1126/sciimmunol.aah3539>.
- (5) Martin, S. J.; Frezza, V.; Davidovich, P.; Najda, Z.; Clancy, D. M. IL-1 Family Cytokines Serve as “activity Recognition Receptors” for Aberrant Protease Activity Indicative of Danger. *Cytokine* **2022**, *157*, 155935. <https://doi.org/10.1016/j.cyt.2022.155935>.
- (6) Garlanda, C.; Dinarello, C. A.; Mantovani, A. The Interleukin-1 Family: Back to the Future. *Immunity* **2013**, *39* (6), 1003–1018. <https://doi.org/10.1016/j.immuni.2013.11.010>.THE.
- (7) Andrei, C.; Dazzi, C.; Lotti, L.; Torrisi, M. R.; Chimini, G.; Rubartelli, A. The Secretory Route of the Leaderless Protein Interleukin 1 β Involves Exocytosis of Endolysosome-Related Vesicles. *Mol Biol Cell* **1999**, *10* (5), 1463–1475. <https://doi.org/10.1091/mbc.10.5.1463>.
- (8) Priestle, J. P.; Schär, H. P.; Grütter, M. G. Crystal Structure of the Cytokine Interleukin-1 Beta. *EMBO J* **1988**, *7* (2), 339–343. <https://doi.org/10.1002/j.1460-2075.1988.tb02818.x>.
- (9) Yu, B.; Blaber, M.; Gronenborn, A. M.; Clore, G. M.; Caspar, D. L. D. Disordered Water within a Hydrophobic Protein Cavity Visualized by X-Ray Crystallography. *Proc Natl Acad Sci U S A* **1999**, *96* (1), 103–108. <https://doi.org/10.1073/pnas.96.1.103>.
- (10) Oostrum, J. Van; Priestle, J. P.; Grutter, M. G.; Schmitz, A. The Structure of Murine Interleukin-1 β at 2.8 Å Resolution. *J Struct Biol* **1991**, *107* (2), 189–195. [https://doi.org/10.1016/1047-8477\(91\)90021-N](https://doi.org/10.1016/1047-8477(91)90021-N).
- (11) Sims, J. E.; Gayle, M. A.; Slack, J. L.; Alderson, M. R.; Bird, T. A.; Giri, J. G.; Colotta, F.; Re, F.; Mantovani, A.; Shanebeck, K.; Grabstein, K. H.; Dower, S. K. Interleukin 1 Signaling Occurs Exclusively via the Type I Receptor. *Proc Natl Acad Sci U S A* **1993**, *90* (13), 6155–6159. <https://doi.org/10.1073/pnas.90.13.6155>.
- (12) Joshi, B. H.; Puri, R. K. Optimization of Expression and Purification of Two Biologically Active Chimeric Fusion Proteins That Consist of Human Interleukin-13 and Pseudomonas Exotoxin in Escherichia Coli. *Protein Expr Purif* **2005**, *39* (2), 189–198. <https://doi.org/10.1016/j.pep.2004.10.012>.
- (13) Sims, J. E. IL-1 and IL-18 Receptors, and Their Extended Family. *Curr Opin Immunol* **2002**, *14* (1), 117–122. [https://doi.org/10.1016/S0952-7915\(01\)00306-5](https://doi.org/10.1016/S0952-7915(01)00306-5).
- (14) Colotta, F.; Dower, S. K.; Sims, J. E.; Mantovani, A. The Type II “decoy” Receptor: A Novel Regulatory Pathway for Interleukin 1. *Immunol Today* **1994**, *15* (12), 562–566. [https://doi.org/10.1016/0167-5699\(94\)90217-8](https://doi.org/10.1016/0167-5699(94)90217-8).
- (15) Groves, R. W.; Giri, J.; Sims, J.; Dower, S. K.; Kupper, T. S. Inducible Expression of Type 2 IL-1 Receptors by Cultured Human Keratinocytes. Implications for IL-1-Mediated Processes in Epidermis. *J Immunol* **1995**, *154* (8), 4065–4072.
- (16) Sims, J. E.; Acres, R. B.; Grubin, C. E.; McMahan, C. J.; Wignall, J. M.; March, C. J.; Dower, S. K. Cloning the Interleukin 1 Receptor from Human T Cells. *Proc Natl Acad Sci U S A* **1989**, *86* (22), 8946–8950. <https://doi.org/10.1073/pnas.86.22.8946>.
- (17) Yabuuchi, K.; Minami, M.; Katsumata, S.; Satoh, M. Localization of Type I Interleukin-1 Receptor mRNA in the Rat Brain. *Molecular Brain Research* **1994**, *27* (1), 27–36. [https://doi.org/10.1016/0169-328X\(94\)90180-5](https://doi.org/10.1016/0169-328X(94)90180-5).
- (18) McKean, D. J.; Podzorski, R. P.; Bell, M. P.; Nilson, A. E.; Huntoon, C. J.; Slack, J.; Dower, S. K.; Sims, J. Murine T Helper Cell-2 Lymphocytes Express Type I and Type II IL-1 Receptors, but Only the Type I Receptor Mediates Costimulatory Activity. *Journal of Immunology* **1993**, *151* (7), 3500–3510.
- (19) Vigers, G. P. A.; Anderson, L. J.; Caffes, P.; Brandhuber, B. J. Crystal Structure of the Type-I Interleuking-1 Receptor Complexed with Interleukin-1beta. *Nature* **1997**, *386*, 190–194. <https://doi.org/https://doi.org/10.1038/386190a0>.
- (20) Wesche, H.; Henzel, W. J.; Shillinglaw, W.; Li, S.; Cao, Z. MyD88: An Adapter That Recruits IRAK to the IL-1 Receptor Complex. *Immunity* **1997**, *7* (6), 837–847. [https://doi.org/10.1016/S1074-7613\(00\)80402-1](https://doi.org/10.1016/S1074-7613(00)80402-1).
- (21) Cao, Z.; Henzel, W. J.; Gao, X. IRAK: A Kinase Associated with the Interleukin-1 Receptor. *Science* (1979) **1996**, *271* (5252), 1128–1131. <https://doi.org/10.1126/science.271.5252.1128>.

- (22) Croston, G. E.; Cao, Z.; Goeddel, D. V. NF-KB Activation by Interleukin-1 (IL-1) Requires an IL-1 Receptor-Associated Protein Kinase Activity. *Journal of Biological Chemistry* **1995**, *270* (28), 16514–16517. <https://doi.org/10.1074/jbc.270.28.16514>.
- (23) Colotta, F.; Orlando, S.; Fadlon, E. J.; Sozzani, S.; Matteucci, C.; Mantovani, A. Chemoattractants Induce Rapid Release of the Interleukin 1 Type II Decoy Receptor in Human Polymorphonuclear Cells. *Journal of Experimental Medicine* **1995**, *181* (6), 2181–2186.
- (24) Neumann, D.; Kollewe, C.; Martin, M. U.; Boraschi, D. The Membrane Form of the Type II IL-1 Receptor Accounts for Inhibitory Function. *The Journal of Immunology* **2000**, *165* (6), 3350–3357. <https://doi.org/10.4049/jimmunol.165.6.3350>.
- (25) Bossù, P.; Visconti, U.; Ruggiero, P.; Macchia, G.; Muda, M.; Bertini, R.; Bizzarri, C.; Colagrande, A.; Sabbatini, V.; Maurizi, G. Transfected Type II Interleukin-1 Receptor Impairs Responsiveness of Human Keratinocytes to Interleukin-1. *Am J Pathol* **1995**, *147* (6), 1852–1861.
- (26) Van der Laken, C. J.; Boerman, O. C.; Oyen, W. J.; Van de Ven, M. T.; Chizzonite, R.; Corstens, F. H.; Van der Meer, J. W. Preferential Localization of Systemically Administered Radiolabeled Interleukin 1 Alpha in Experimental Inflammation in Mice by Binding to the Type II Receptor. *Journal of Clinical Investigation* **1997**, *100* (12), 2970–2976.
- (27) R&D Systems Inc. *IL-1 Family Signaling Pathways*. Biotechnie R&D systems. <https://www.rndsystems.com/pathways/il-1-family-signaling-pathways> (accessed 2023-04-04).
- (28) Joosten, L. A. B.; Helsen, M. M. A.; Saxne, T.; Van de Loo, F. A. J.; Heinegard, D.; Van den Berg, W. B. IL-1ab Blockade Prevents Cartilage Aan Bone Bestruction in Murine Type II Collagen-Induced Arthritis, Whereas TNFa Blockade Only Ameliorates Joint Inflammation. *Journal of Immunology* **1999**. <https://doi.org/10.4049/jimmunol.167.1.98>.
- (29) Dinarello, C. A. Blocking Interleukin-1b in Acute and Chronic Autoinflammatory Diseases. *Journal of intern Med* **2011**, *23* (1), 1–7. <https://doi.org/10.1038/jid.2014.371>.
- (30) Carmi, Y.; Dotan, S.; Rider, P.; Kaplanov, I.; White, M. R.; Baron, R.; Abutbul, S.; Huszar, M.; Dinarello, C. A.; Apte, R. N.; Voronov, E. The Role of IL-1 β in the Early Tumor Cell-Induced Angiogenic Response. *The Journal of Immunology* **2013**, *190* (7), 3500–3509. <https://doi.org/10.4049/jimmunol.1202769>.
- (31) Mantovani, A.; Barajon, I.; Garlanda, C. IL-1 and IL-1 Regulatory Pathways in Cancer Progression and Therapy. *Immunol Rev* **2018**, *281* (1), 57–61. <https://doi.org/10.1111/imr.12614>.
- (32) Bent, R.; Moll, L.; Grabbe, S.; Bros, M. Interleukin-1 Beta—A Friend or Foe in Malignancies? *Int J Mol Sci* **2018**, *19* (8). <https://doi.org/10.3390/ijms19082155>.
- (33) Liegel, J.; Avigan, D.; Rosenblatt, J. Cellular Immunotherapy as a Therapeutic Approach in Multiple Myeloma. *Expert Rev Hematol* **2018**, *11* (7), 525–536. <https://doi.org/10.1080/17474086.2018.1483718>.
- (34) Costes, V.; Portier, M.; Lu, Z. Y.; Rossi, J. F.; Bataille, R.; Klein, B. Interleukin-1 in Multiple Myeloma: Producer Cells and Their Role in the Control of IL-6 Production. *Br J Haematol* **1998**, *103* (4), 1152–1160. <https://doi.org/10.1046/j.1365-2141.1998.01101.x>.
- (35) Allen, I. C.; Tekippe, E. M.; Woodford, R.-M. T.; Uronis, J. M.; Holl, E. K.; Rogers, A. B.; Herfarth, H. H.; Jobin, C.; Ting, J. P. Y. The NLRP3 Inflammasome Functions as a Negative Regulator of Tumorigenesis during Colitis-Associated Cancer. *Journal of Experimental Medicine* **2010**, *207* (5), 1045–1056. <https://doi.org/10.1084/jem.20100050>.
- (36) Baker, K. J.; Houston, A.; Brint, E. IL-1 Family Members in Cancer; Two Sides to Every Story. *Front Immunol* **2019**, *10* (JUN). <https://doi.org/10.3389/fimmu.2019.01197>.
- (37) Krelm, Y.; Voronov, E.; Dotan, S.; Elkabets, M.; Reich, E.; Fogel, M.; Huszar, M.; Iwakura, Y.; Segal, S.; Dinarello, C. A.; Apte, R. N. Interleukin-1 β -Driven Inflammation Promotes the Development and Invasiveness of Chemical Carcinogen-Induced Tumors. *Cancer Res* **2007**, *67* (3), 1062–1071. <https://doi.org/10.1158/0008-5472.CAN-06-2956>.
- (38) Hess, C.; Neri, D. Tumor-Targeting Properties of Novel Immunocytokines Based on Murine IL1 β and IL6. *Protein Engineering, Design and Selection* **2014**, *27* (6), 207–213. <https://doi.org/10.1093/protein/gzu013>.
- (39) Veltri, S.; Smith, J. W. Interleukin 1 Trials in Cancer Patients: A Review of the Toxicity, Antitumor and Hematopoietic Effects. *Stem Cells* **1996**, *14* (2), 164–176. <https://doi.org/10.1002/stem.140164>.
- (40) Van Den Eeckhout, B.; Tavernier, J.; Gerlo, S. Interleukin-1 as Innate Mediator of T Cell Immunity. *Front Immunol* **2020**, *11*, 621931. <https://doi.org/10.3389/fimmu.2020.621931>.
- (41) Van Den Eeckhout, B.; Van Hoecke, L.; Burg, E.; Van Lint, S.; Peelman, F.; Kley, N.; Uzé, G.; Saelens, X.; Tavernier, J.; Gerlo, S. Specific Targeting of IL-1 β Activity to CD8+ T Cells Allows for Safe Use as a Vaccine Adjuvant. *NPJ Vaccines* **2020**, *5* (1). <https://doi.org/10.1038/s41541-020-00211-5>.
- (42) Policarpo, R. L.; Kang, H.; Liao, X.; Rabideau, A. E.; Simon, M. D.; Pentelute, B. L. Flow-Based Enzymatic Ligation by Sortase A. *Angewandte Chemie - International Edition* **2014**, *53* (35), 9203–9208. <https://doi.org/10.1002/anie.201403582>.
- (43) Levary, D. A.; Parthasarathy, R.; Boder, E. T.; Ackerman, M. E. Protein-Protein Fusion Catalyzed by Sortase A. *PLoS One* **2011**, *6* (4). <https://doi.org/10.1371/journal.pone.0018342>.

- (44) Li, J.; Zhang, Y.; Soubias, O.; Khago, D.; Chao, F. A.; Li, Y.; Shaw, K.; Byrd, R. A. Optimization of Sortase A Ligation for Flexible Engineering of Complex Protein Systems. *Journal of Biological Chemistry* **2020**, *295* (9), 2664–2675. <https://doi.org/10.1074/jbc.RA119.012039>.
- (45) Carnemolla, B.; Borsi, L.; Balza, E.; Castellani, P.; Meazza, R.; Berndt, A.; Ferrini, S.; Kosmehl, H.; Neri, D.; Zardi, L. Enhancement of the Antitumor Properties of Interleukin-2 by Its Targeted Delivery to the Tumor Blood Vessel Extracellular Matrix. *Blood* **2002**, *99* (5), 1659–1665. <https://doi.org/10.1182/blood.V99.5.1659>.
- (46) Borsi, L.; Balza, E.; Carnemolla, B.; Sassi, F.; Castellani, P.; Berndt, A.; Kosmehl, H.; Birò, A.; Siri, A.; Orecchia, P.; Grassi, J.; Neri, D.; Zardi, L. Selective Targeted Delivery of TNF α to Tumor Blood Vessels. *Blood* **2003**, *102* (13), 4384–4392. <https://doi.org/10.1182/blood-2003-04-1039>.
- (47) Muyldermans, S. Nanobodies: Natural Single-Domain Antibodies. *Annu Rev Biochem* **2013**, *82*, 775–797. <https://doi.org/10.1146/annurev-biochem-063011-092449>.
- (48) Hulseberg, P. D.; Zozulya, A.; Chu, H. H.; Triccas, J. A.; Fabry, Z.; Sandor, M. The Same Well-Characterized T Cell Epitope SIINFEKL Expressed in the Context of a Cytoplasmic or Secreted Protein in BCG Induces Different CD8 $^{+}$ T Cell Responses. *Immunol Lett* **2010**, *130* (1–2), 36–42. <https://doi.org/10.1016/j.imlet.2009.12.004>.
- (49) Mosley, B.; Urdal, D. L.; Prickett, K. S.; Larsen, A.; Cosman, D.; Conlon, P. J.; Gillis, S.; Dower, S. K.; Macdonald, H. R. The Interleukin-1 Receptor Binds the Human Interleukin-1 α Precursor but Not the Interleukin-1 β Precursor. *J Biol Chem* **1987**, *262* (7), 2941–2944.
- (50) Van Rosmalen, M.; Krom, M.; Merks, M. Tuning the Flexibility of Glycine-Serine Linkers to Allow Rational Design of Multidomain Proteins. *Biochemistry* **2017**, *56* (50), 6565–6574. <https://doi.org/10.1021/acs.biochem.7b00902>.
- (51) Heck, T.; Pham, P. H.; Yerlikaya, A.; Thöny-Meyer, L.; Richter, M. Sortase A Catalyzed Reaction Pathways: A Comparative Study with Six SrtA Variants. *Catal Sci Technol* **2014**, *4* (9), 2946–2956. <https://doi.org/10.1039/c4cy00347k>.
- (52) Beerli, R. R.; Hell, T.; Merkel, A. S.; Grawunder, U. Sortase Enzyme-Mediated Generation of Site-Specifically Conjugated Antibody Drug Conjugates with High In Vitro and In Vivo Potency. *PLoS One* **2015**, *10* (7). <https://doi.org/10.1371/journal.pone.0131177>.
- (53) Popp, M. W. L.; Antos, J. M.; Ploegh, H. L. Site-Specific Protein Labeling via Sortase-Mediated Transpeptidation. *Curr Protoc Protein Sci* **2009**. <https://doi.org/10.1002/0471140864.ps1503s56>.
- (54) ThermoFisher Scientific. *T4 DNA Ligase*; 2014. www.thermoscientific.com/onebio.
- (55) Aligent Technologies. *ArcticExpress RIL Competent Cells and ArcticExpress RP Competent Cells Instruction Manual*; 2015. www.genomics.agilent.com.
- (56) Ferrer, M.; Chernikova, T. M.; Yakimov, M. M.; Golyshin, P. N.; Timmis, K. N. Chaperonins Govern Growth of *Escherichia Coli* at Low Temperatures. *Nat Biotechnology* **2003**, *21* (11), 1266–1267. <https://doi.org/10.1038/nbt1103-1266>.
- (57) McGrath, J.; Waskeu, J. J.; Dunn, L.; Studier, F. W.; Chambedin, M.; Ring, J.; Golomb, M.; Chamberlin, M.; Chen, W.; Tabor, S.; Struhl, K. Use of T7 RNA Polymerase to Direct Expression of Cloned Genes. *Methods Enzymol* **1970**, *228* (2), 259. [https://doi.org/10.1016/0076-6879\(90\)85008-c](https://doi.org/10.1016/0076-6879(90)85008-c).
- (58) Le Gall, Camille. M. Dendritic Cell-Targeted Vaccines for Cancer Immunotherapy, Radboud Universiteit Nijmegen, Nijmegen, 2022.
- (59) Sahdev, S.; Khattar, S. K.; Saini, K. S. Production of Active Eukaryotic Proteins through Bacterial Expression Systems: A Review of the Existing Biotechnology Strategies. *Mol Cell Biochem* **2008**, *307* (1–2), 249–264. <https://doi.org/10.1007/s11010-007-9603-6>.
- (60) Uptima. *TCO (Trans-CycloOctyne) Reagents for “Click Chemistry”-Amine Reactive Products Information*. <https://www.interchim.fr/ft/M/MRU990.pdf> (accessed 2023-03-16).
- (61) InvivoGen. *HEK-Blue™ IL-1 β Cells*. <https://www.invivogen.com/hek-blue-il1b>.
- (62) InvivoGen. *RAW-Blue™ Cells*; InvivoGen. <https://www.invivogen.com/raw-blue> (accessed 2023-03-17).
- (63) Merck. *Colorimetric Alkaline Phosphatase and Peroxidase Substrate Detection Systems*. <https://www.sigmaaldrich.com/NL/en/technical-documents/technical-article/protein-biology/immunohistochemistry/colorimetric-alkaline> (accessed 2023-03-16).
- (64) Liu, T.; Zhang, L.; Joo, D.; Sun, S.-C. NF-KB Signaling in Inflammation. *Signal Transduct Target Ther* **2017**, *2* (1), 17023. <https://doi.org/10.1038/sigtrans.2017.23>.
- (65) InvivoGen. *QUANTI-Blue™ Solution*; 2020. <https://www.invivogen.com/quanti-blue> (accessed 2023-03-17).
- (66) Labriola-Tompkins, E.; Chandran, C.; Kaffka, K. L.; Biondi, D.; Graves, B. J.; Hatada, M.; Madison, V. S.; Karas, J.; Kilian, P. L.; Ju, G. Identification of the Discontinuous Binding Site in Human Interleukin 1 β for the Type I Interleukin 1 Receptor. *Proc Natl Acad Sci U S A* **1991**, *88* (24), 11182–11186. <https://doi.org/10.1073/pnas.88.24.11182>.

Chapter 2

- (67) Antoni, G.; Presentini, R.; Perin, F.; Tagliabue, A.; Ghiara, P. A Short Synthetic Peptide Fragment of Human Interleukin 1 with Immunostimulatory but Not Inflammatory Activity . *Jouranal of Immunology* **1986**, *137* (10), 3201–3204.
- (68) Casadio, R.; Frigimelica, E.; Bossù, P.; Neumann, D.; Martin, M. U.; Tagliabue, A.; Boraschi, D. Model of Interaction of the IL-1 Receptor Accessory Protein IL-1RAcP with the IL-1 β /IL-1RI Complex. *FEBS Lett* **2001**, *499* (1–2), 65–68. [https://doi.org/10.1016/S0014-5793\(01\)02515-7](https://doi.org/10.1016/S0014-5793(01)02515-7).
- (69) Greenfeder, S. A.; Nunes, P.; Kwee, L.; Labow, M.; Chizzonite, R. A.; Ju, G. Molecular Cloning and Characterization of a Second Subunit of the Interleukin 1 Receptor Complex. *Journal of Biological Chemistry* **1995**, *270* (23), 13757–13765. <https://doi.org/10.1074/jbc.270.23.13757>.
- (70) Wesche, H.; Korherr, C.; Kracht, M.; Falk, W.; Resch, K.; Martin, M. U. The Interleukin-1 Receptor Accessory Protein (IL-1RAcP) Is Essential for IL-1-Induced Activation of Interleukin-1 Receptor-Associated Kinase (IRAK) and Stress-Activated Protein Kinases (SAP Kinases). *Journal of Biological Chemistry* **1997**, *272* (12), 7727–7731. <https://doi.org/10.1074/jbc.272.12.7727>.
- (71) Cullinan, E. B.; Kwee, L.; Nunes, P.; Shuster, D. J.; Ju, G.; McIntyre, K. W.; Chizzonite, R. A.; Labow, M. A. IL-1 Receptor Accessory Protein Is an Essential Component of the IL-1 Receptor. *J Immunol* **1998**, *161* (10), 5614–5620.
- (72) Huang, X.; Aulabaugh, A.; Ding, W.; Kapoor, B.; Alksne, L.; Tabei, K.; Ellestad, G. Kinetic Mechanism of Staphylococcus Aureus Sortase SrtA. *Biochemistry* **2003**, *42* (38), 11307–11315. <https://doi.org/10.1021/bi034391g>.

Supplementary figures

Expression IL-1 β , IL-1 β -LPETGG, sortase A and VHH-CD11c-SIINFEKL

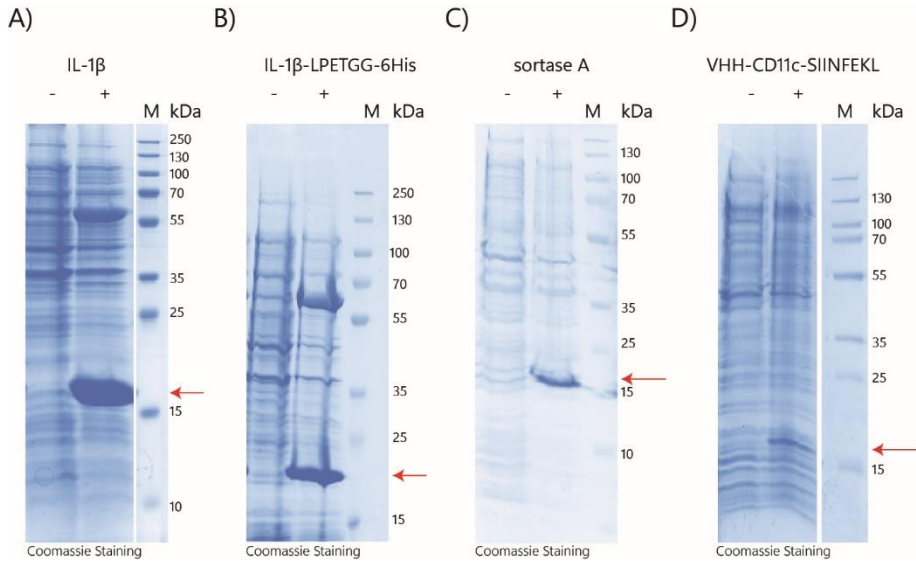


Figure S1 - Bacterial expression of IL-1 β , IL-1 β -LPETGG, sortase A and VHH-CD11c-SIINFEKL upon IPTG induction.

SDS-PAGE analysis of IPTG induced expression of A) IL-1 β (~17 kDa), B) IL-1 β -LPETGG-6His (~19 kDa) by *E. coli* ArcticExpress (DE3) RP, C) Sortase A (~19 kDa) and D) anti-CD11c or VHH-CD11c-SIINFEKL (~15 kDa), by *E. coli* Rosetta-gami 2 (DE3) and *E. coli* BL21 (DE3) pLysS, respectively. The expressed proteins are highlighted by the red arrows at the respective gels.

Optimisation caging condition IL-1 β -LPETGG

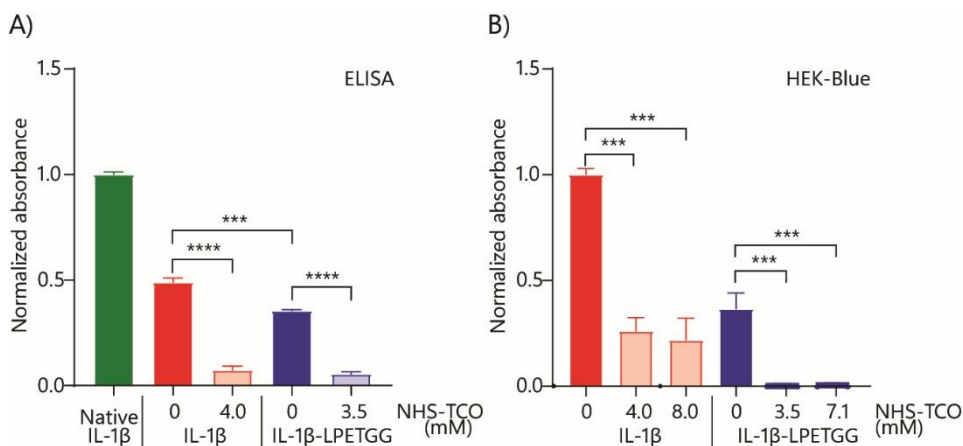


Figure S2 - Analysis of IL-1 β -LPETGG activity relative to IL-1 β activity using ELISA and HEK-Blue IL-1 β assays.—The activity and folding of IL-1 β and IL-1 β -LPETGG were compared by A) ELISA (N=3) and B) HEK-Blue IL-1 β cells (N=4). Caging was performed at 5.7 μ M IL-1 β or 5.0 μ M IL-1 β -LPETGG with 4.0 mM or 8.0 mM **1** and 3.5 mM or 7.1 mM **1**, respectively, in 20 mM HEPES pH 8 for 1 hour at 37°C. Bright colours indicate DMSO only samples and pastels the TCO-treated samples. Colour groups indicate different conditions with respective DMSO controls. For (B) the maximal signal was obtained by adding DMSO. Caging conditions were compared to DMSO control (0 mM **1**). In general, IL-1 β and IL-1 β -LPETGG behave similarly in the ELISA format also under caging conditions and caging improved when the NHS-TCO concentration increased. Receptor binding differed between the two IL-1 β variants. Data were plotted as mean signal \pm SEM. Significances are indicated as follows: * P<0.05; ** P<0.01; *** P<0.001; **** P<0.0001; ns is non-significant.

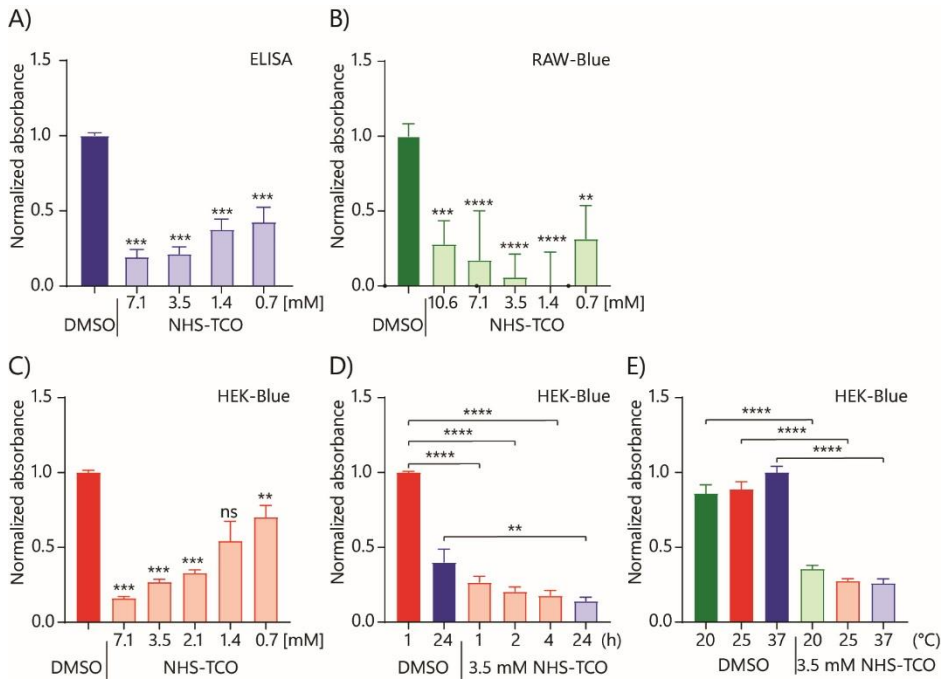


Figure S3 - Caging optimisation of IL-1 β -LPETGG analysed using various assays.

Various concentrations of **1** for IL-1 β -LPETGG were analysed by A) ELISA (N=3), B) RAW-Blue cells (N=9) and C) HEK-Blue IL-1 β cells (N=3). Caging was performed at 5.0 μ M IL-1 β -LPETGG with various concentrations of **1** in 20 mM HEPES pH 8 for 1 hour at 37°C (A,B,C). The maximal signal was obtained by addition of DMSO. The activity of IL-1 β -LPETGG incubated with 3.5 mM **1** for D) various periods of time (h) (N=5) or at E) different temperatures (°C) (N=3) was assessed on stimulated HEK-Blue IL-1 β . Bright colours indicate DMSO only samples and pastels the TCO-treated samples. Colour groups indicate different conditions with respective DMSO controls. In general, IL-1 β -LPETGG became inactive with higher concentrations of NHS-TCO at various temperatures when incubated for 1 hour. Data were plotted as mean signal \pm SEM. Significances are indicated as follows: * $P < 0.05$; ** $P < 0.01$; *** $P < 0.001$; **** $P < 0.0001$; ns is non-significant.

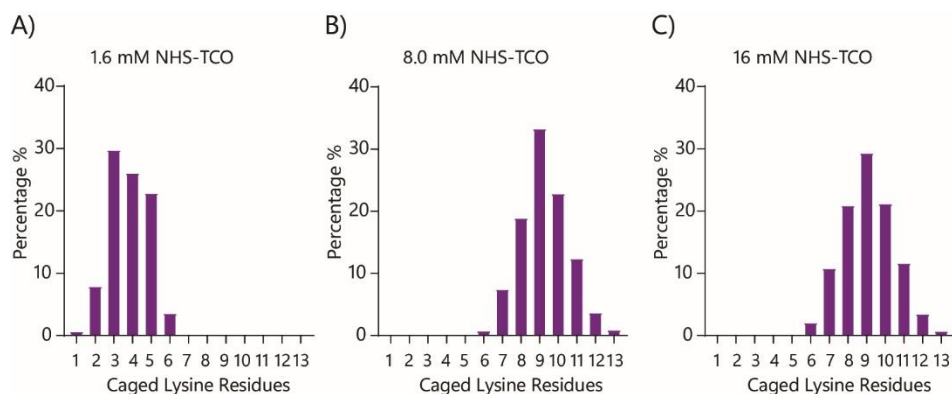
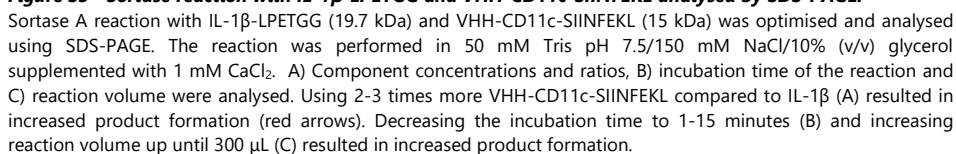


Figure S4 - Distribution amount of caged lysines in IL-1 β -LPETGG, caged with different amounts of NHS-TCO analysed by ESI LC-MS.

The amount of caged lysine residues of IL-1 β -LPETGG (10 μ M) treated with A) 1.6 mM, B) 8.0 mM and C) 16 mM NHS-TCO determined using ESI LC-MS. IL-1 β -LPETGG was caged in 20 mM HEPES pH 8 for 1 hour at 37°C, following buffer exchange using Zeba™ Spin Desalting columns to 10 mM ammonium acetate pH 6. In general the more NHS-TCO was added, the more caged lysines were present. These are normalized data to the total amount of lysines present.



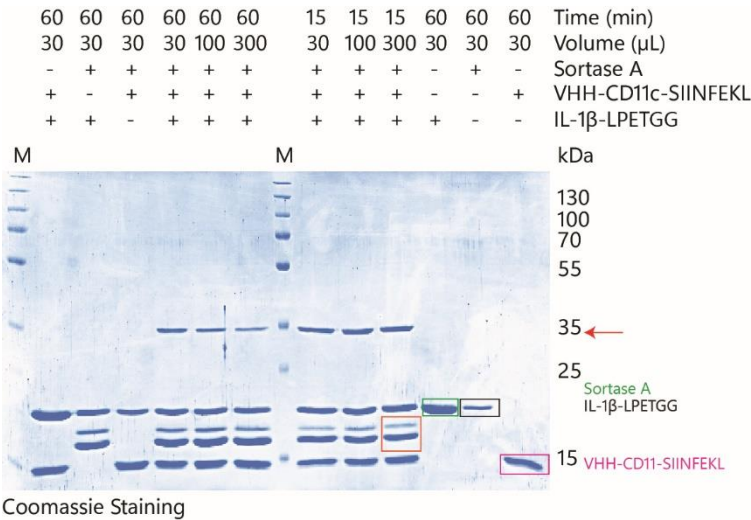


Figure S6 - Sortase A reaction optimisation of reaction volume and time.
Sortase A (3 μM) reaction with IL-1β-LPETGG (19.7 kDa, 4 μM) and VHH-CD11c-SIINFEKL (15 kDa, 8 μM) was optimised and analysed using SDS-PAGE. The reaction was performed in 50 mM Tris pH 7.5/150 mM NaCl/10% (v/v) glycerol supplemented with 1 mM CaCl₂. Both reaction time and reaction volume were optimised. Maximal product formation was realized with 15 minutes reaction time in 100-300 μL reaction volume.

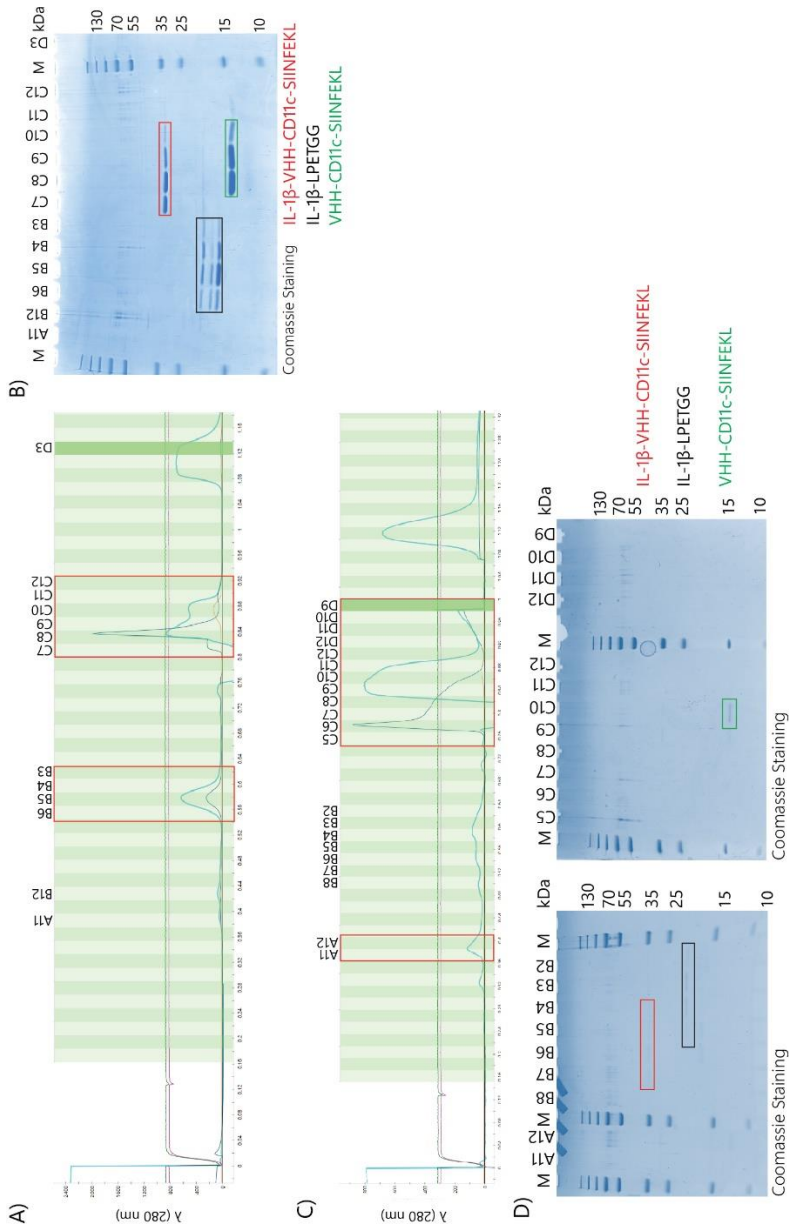


Figure S7 - Initial purification non-caged and caged IL-1 β -LPETGG coupled to VHH-CD11c-SIINFEKL.

A, B) Non-caged and C, D) caged IL-1 β -LPETGG was coupled to VHH-CD11c-SIINFEKL and purified on a SuperdexTM 75 10/300 column equilibrated with 20 mM HEPES pH 8. A) Fractions of purification of non-caged IL-1 β -VHH-CD11c-SIINFEKL were analysed on SDS-PAGE (B). C) Fractions of purification of caged IL-1 β -VHH-CD11c-SIINFEKL (3.5 mM NHS-TCC) were analysed on SDS-PAGE (D). In the SDS-PAGES, the red boxes indicate formed product, the green boxes indicate unreacted VHH-CD11c-SIINFEKL and the black boxes indicate unreacted IL-1 β -LPETGG. In general, non-caged protein is more easily purified at an high concentration (>0.5 mg/mL), and the purification of the caged coupled IL-1 β -VHH resulted in 41 μ g/mL in 500 μ L volume, which is barely visible on the SDS-PAGE.

3

TNF- α : Chemical Inactivation and Reactivation of a Master Regulator Cytokine

Introduction

In 1893 Coley observed the striking phenomenon that tumours in cancer patients could shrink, and even disappear, when they suffered bacterial infections.¹ This brought him to develop Coley's toxin, a mixture of bacterial extracts that he successfully used for the treatment of sarcoma.¹ This was initially dismissed as quackery, but over the following century his results were increasingly vindicated. The observation that it was actually the immune system, activated by these bacteria, that caused the tumour shrinkage, was one of the key discoveries.^{2,3} The key immunological mediator of this phenomenon turned out to be *tumour necrosis factor-alpha* (TNF- α), a key pro-inflammatory cytokine released during the early phase of the immune response.^{4,5} Later studies showed that TNF- α has complex functionality, having both pro-survival and cell death inducing functionalities (Figure 1).⁶

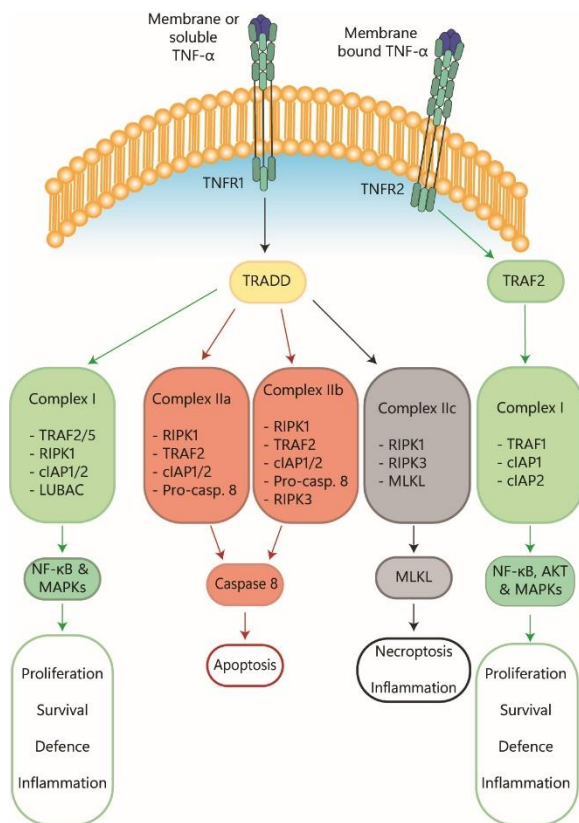


Figure 1 - Signalling pathways activated upon TNF- α binding to either TNFR1 or TNFR2.

Upon binding of TNF- α to either TNFR1 or TNFR2, different processes are initiated: cell death by either apoptosis or necrosis, survival, inflammation, cell differentiation or proliferation. Cascades involving ubiquitination and phosphorylation among others, communicate to get a certain response. Figure was adapted from Jang *et al.*⁶ TNFR: tumour necrosis factor receptor; TRADD: TNF receptor-associated death domain; TRAF: TNFR-associated factor; RIPK: receptor-interacting serine/threonine protein kinase; cIAP: cellular inhibitor of apoptosis protein; LUBAC: linear ubiquitin chain assembly complex; NF-κB: nuclear factor kinase B; MAPKs: mitogen-activated protein kinases; MLKL: mixed lineage kinase domain-like protein; AKT: protein kinase B.

TNF- α itself displayed a potent anti-tumour effect. Its infusion into a tumour led to visible tumour shrinkage in animal models.⁷⁻⁹ This striking observation led to its extensive pursuit as an anti-cancer therapy.¹⁰⁻¹⁴ The first studies using it as a treatment modality, employed a systemic administration strategy of 1×10^5 units/m² to 16×10^5 units/m². This resulted in such severe side-effects that the trial had to be abandoned.^{10,11} Later studies used direct intra-tumoral administration¹² or isolated limb perfusion^{13,14} to circumvent these systemic adverse effects. Some clinical efficacy was observed in late stage melanoma or soft tissue sarcoma, but results remained inconsistent¹⁵⁻¹⁷, due to the therapeutic window being too small.^{11,18,19} The main reason is its severe side-effect profile. Within minutes of administration, side-effects such as fever, hypertension, eosinophilia, and monocytosis can be observed.¹⁹ In addition, renal impairment and abnormal liver enzyme activities are also observed.²⁰ Harnessing the power of TNF to broaden its therapeutic window would therefore be of great clinical benefit.

Much effort has gone into increasing the therapeutic window of TNF- α . This has been done, for example, by adding targeting motifs, such as the integrin-binding peptide Asn-Gly-Arg (NGR), which targets TNF- α to the tumour micro-environment (TME).²¹ Alternatively, radiation was used to a protected form of TNF- α .^{21,22} This method is based on tumour targeting by an adenovirus encoded TNF- α . The cDNA of TNF- α was fused to the early growth response protein 1 (Egr-1) promoter.²² This promoter is activated upon ionizing radiation²³, inducing the transcription of whatever gene that is controlling. Therefore, TNF- α encoded on this adenovirus, which targets the tumour micro-environment, is only transcribed and therefore active, when the tumour is radiated. Unfortunately, none of these approaches improved survival rates while adverse side-effects remained.

The most promising avenue for targeting TNF has been its incorporation into immunocytokine (IC).²⁴⁻²⁷ Here, TNF- α is coupled to an antibody reagent targeting a feature of the tumour. These have been extensively explored over the last two decades^{24,28,29}, leading to the development of a clinical candidate, L19-TNF- α .²⁴ L19-TNF- α is TNF- α coupled to the an antibody (L19) which targets the extra-domain B of fibronectin which is present on newly formed blood vessels of the tumour's neovasculature.³⁰ Pre-clinical data evaluation of this compound in glioma showed that mice treated with L19-TNF α gave a 50% decrease in tumour volume and a 20% survival rate after 60 days compared to the L19-only treated control group where tumour regression was not observed and all mice died within 21 days. The cured animals were also shown to be protected from recurring tumours.³¹ This immunocytokine was also tested in a phase I trial of six patients with treatment-refractive glioblastoma. This small trial resulted in stabilisation of disease for three patients after the third infusion of L19-TNF α , probably as a result of increased invasion of CD4+ and CD8+ T-cells in the tumour, together with increasing tumour necrosis, suggesting its therapeutic potential for this very hard-to-treat cancer. Combination therapy of L19-TNF α with L19-IL2 has yielded an even more spectacular result: a complete response in 1 of 20 patients (5%), a partial response in 10 of 20 patients (50%), and stable disease in 5 of 20 patients (20%) suffering from refractive sarcoma. Additionally, 7 of 13 untreated lesions present on these patients showed a complete response as a bystander effect.³² Despite these promising results, the therapeutic window of TNF, even in an immunocytokine, remains too small. On-target off-tumour

toxicity remained a problem and further opening the therapeutic window would likely yield improved clinical benefits.

As in *Chapter 2* of this work, the aim in this chapter was to develop a new chemical approach to inactivate TNF- α to allow its reactivation at a tumour site. Again, the choice was made to use *click-to-release* chemistry for this, in which lysines of the cytokine are modified with an NHS-ester of *trans*-cyclooctene (TCO) to deactivate it. This TCO can then be removed with a tetrazine trigger^{33–35} (**Figure 2**). Compared to IL-1 β this is more complex, as no lysines are involved in receptor binding or trimer formation, adding to the challenge of caging this cytokine.

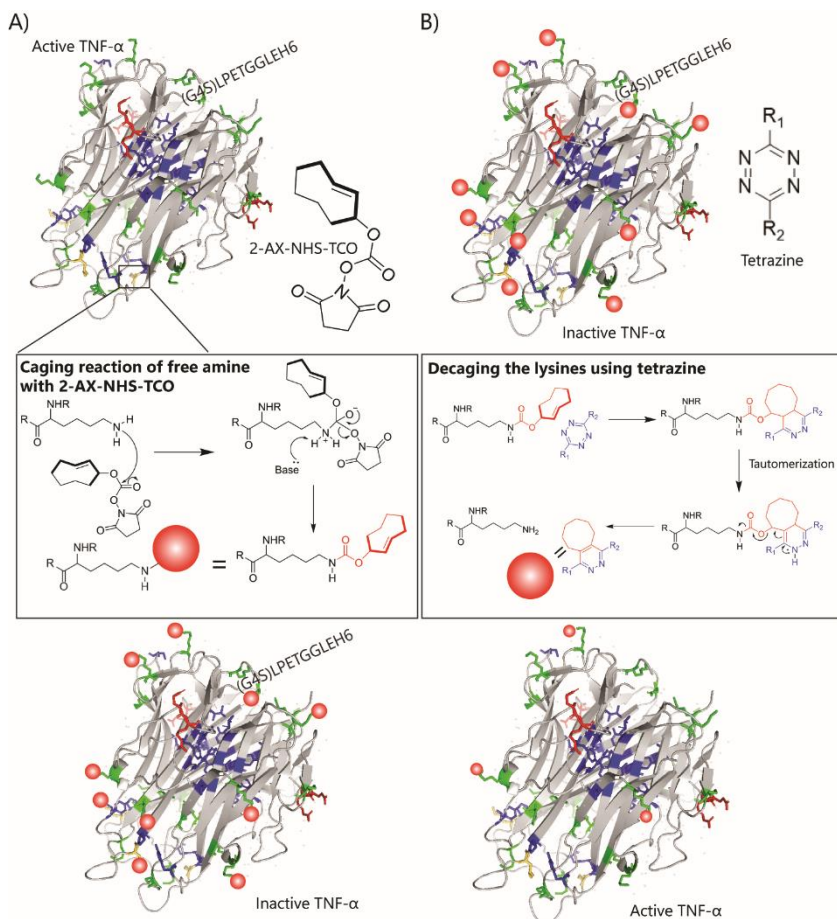


Figure 2 - Overview scheme of inactivating (caging) and reactivating (decaging) trimeric mTNF- α using click-to-release chemistry.

A) The free amines in trimeric mTNF- α react with NHS-TCO ester, binding the cyclooctene, which results in inactivated or caged mTNF- α . B) Reactivation or decaging is performed using tetrazine which reacts with the strained cyclooctene, releasing N₂ together with cyclooctene, which results to active mTNF- α . The essential receptor interacting residues are indicated in red (Gln31 and Arg32). The residues essential for trimer formation are indicated in blue. The lysines (9) are given in green. The lysine (K112) next to proline 113, which is essential for trimer formation, is indicated in yellow. Crystal structures were obtained and modified from Baeyens *et al.* (PDB: 2tnf).

Results & Discussion

To establish whether a click-to-release approach could work for TNF- α , its 'cagability' was assessed. TNF- α is expressed as a membrane-bound pro-protein having an *N*-terminal cytosolic domain linked to a transmembrane and stem-domain, linked to a C-terminal, extracellular TNF- α domain (**Figure 3**).³⁶ It requires cleavage by TNF- α -converting enzyme (TACE) to release the C-terminal domain. Trimerization of TNF- α takes place after this release to get active TNF- α . This mature soluble human TNF- α is 157 amino acids (156 amino acids in murine TNF- α) in size (~17 kDa).

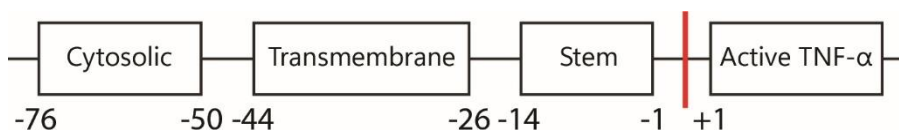


Figure 3 - Schematic overview of pro-TNF- α .

Pro-TNF- α consists of an *N*-terminal cytosolic domain followed by a transmembrane domain and a stem domain. Cleavage by TACE after the stem domain results in active extracellular TNF- α . The numbers below indicate amino acid positions of murine pro-TNF- α .³⁶

Human (hTNF- α) and murine TNF- α (mTNF- α) are closely related, allowing for murine TNF- α to cross-react with both human TNF-receptors.³⁷ On the contrary, hTNF- α can only interact with murine TNF-receptor 1.³⁷ Each TNF- α monomer consists of β -sheets composed of antiparallel β -strands coupled via flexible loops (**Figure 4**). Ordering of the hydrophilic and hydrophobic residues results in the formation of a cone-shaped homotrimer.³⁸ Some of the hydrophilic residues that form hydrogen bonds essential for trimer formation and stability are conserved between human and murine TNF- α ; Tyr59-Val123, Tyr72-Pro113, Ser95-Gly148, Tyr119-Gly121 and Gly121-Tyr151 (blue in **Figure 4**).³⁹ Interference with these interactions abolishes trimerization and thereby TNF- α function. Residues directly involved in receptor recognition are arginine 31 and 32 in hTNF- α and glutamine and arginine at positions 31 and 32, respectively in mTNF- α (red in **Figure 4**).⁴⁰ There are no lysines involved in the trimer formation, precluding trimer disruption as a feasible *click-to-release* strategy. However there is a lysine at position 112, next to proline 113 which is essential for trimer formation, suggesting that the introduction of steric bulk could achieve this disruption.

TNF- α can bind to two receptors: TNF-receptor 1 (TNFR1) and TNF-receptor 2 (TNFR2) (**Figure 1**). These are present on, amongst others, immune cells, epithelial cells and fibroblasts.^{41,42} The general perception is that soluble TNF- α binds TNFR1, while the membrane bound monomeric TNF- α can interact with both TNFR1 and TNFR2.⁶ The interaction with these two receptors also does not directly involve critical lysine residues, therefore the disruption of correct trimer formation was opted.

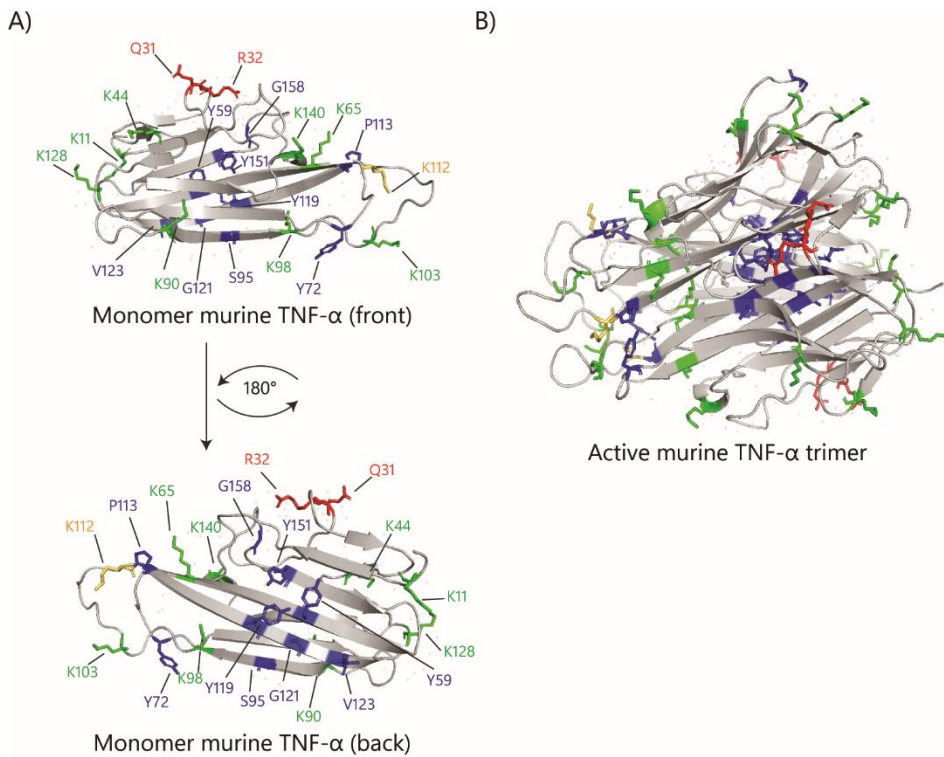


Figure 4 - Crystal structures of monomeric and trimeric murine TNF- α .

A) Monomeric murine TNF- α visualised from the front and the back with annotated residues. B) Murine TNF- α forms functional trimers which interact with both TNF-receptor 1 and 2. The essential receptor interacting residues are indicated in red (Gln31 and Arg32). The residues essential for trimer formation are indicated in blue. The lysines (9) are given in green. The lysine (K112) next to proline 113, which is essential for trimer formation, is indicated in yellow. Crystal structures were obtained and modified from Baeyens *et al.* (PDB: 2tnf).

Construct Design

To test the caging approach, three TNF- α constructs were designed. It is known that (*N*-terminal) tags can influence the function of TNF- α , precluding their use.⁴³ TNF- α was therefore cloned without any tags (**Figure 5A**), with a C-terminal 6His-tag (**Figure 5B**) and with a C-terminal sortag recognition site (LP(X)TGG) followed by a C-terminal 6His-tag (**Figure 5C**). A G4S spacer was introduced between the cytokine's C-terminus and the LPETGG-recognition sequence. These three sequences would allow the assessment of the general caging strategy of the wildtype protein, study the feasibility of a purification tag on the construct, and eventually – with the third construct – allow introduction into an immunocytokine with the same strategy as used in *Chapter 2*.

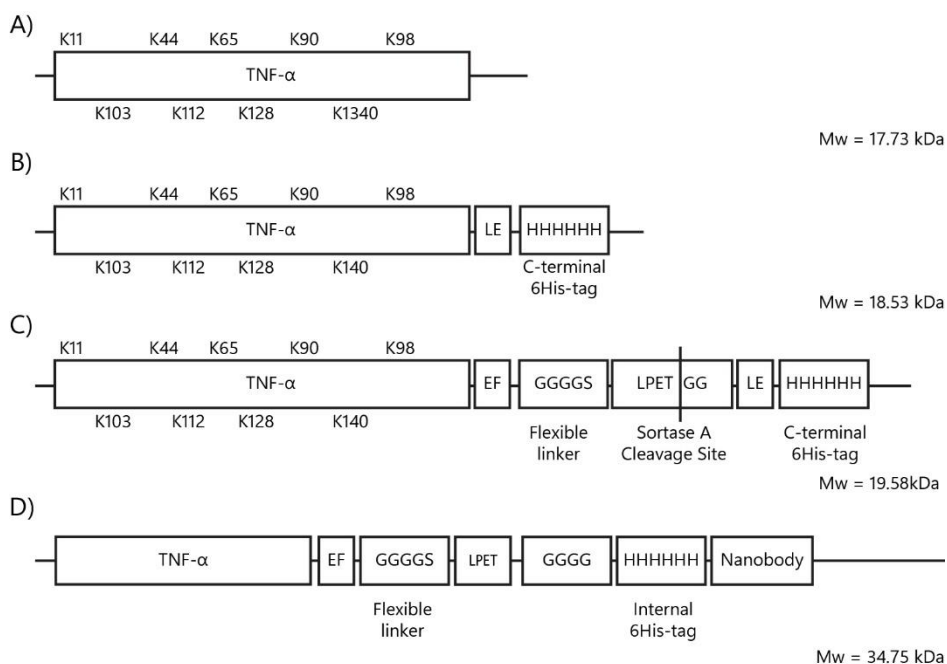


Figure 5 - Construct formation of various forms of TNF- α and the final product upon sortase A reaction.

A pET28a(+)-vector was used for expression of A) TNF- α , B) TNF- α -6His and C) TNF- α -LPETGG-6His. All tags were placed C-terminally of TNF- α . The LPETGG sequence is recognized by sortase A and the 6His-tag was introduced for purification purposes. The location of the lysines is given as K followed by an amino acid position in the mature protein. D) Upon reaction with sortase A, the C-terminal 6His-tag is removed for the TNF- α -LPETGG-6His and replaced with a nanobody with N-terminal 6His-tag.

Protein expression and purification

The expression of the TNF- α -constructs was attempted in two different bacterial strains, namely *E. coli* Rosetta-gami 2 (DE3), which has additional tRNAs encoding rare codons⁴⁴, and *E. coli* ArcticExpress (DE3) RP. The latter has these additional tRNA molecules as well⁴⁵, but is also able to produce soluble proteins at low temperatures (4°C-10°C) in the correctly folded state, due to the presence of chaperonins Cpn10 and Cpn60 which function at these low temperatures.⁴⁶

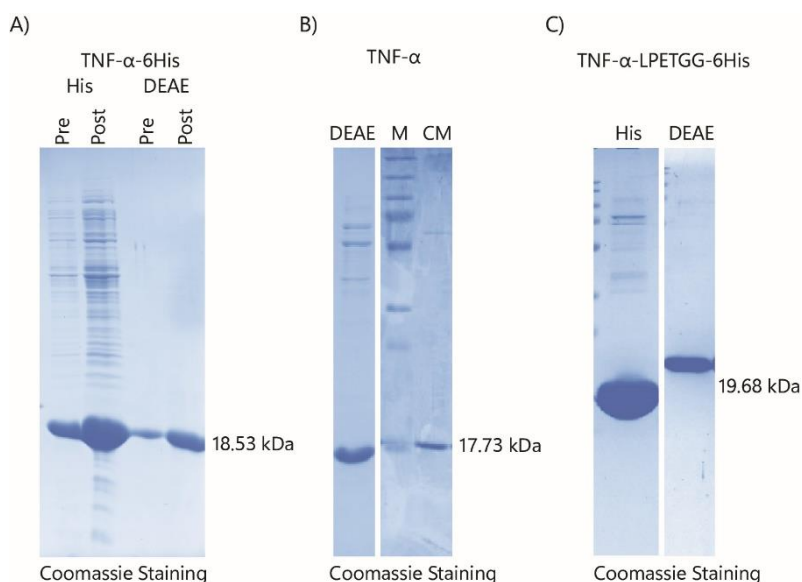
Expression in *E. coli* ArcticExpress (DE3) RP took place for 4 days at 10°C, while expression in *E. coli* Rosetta-gami 2 (DE3) took place for 3 days at 30°C. Samples taken before and after IPTG induction showed the expression of TNF- α /TNF- α -6His by the appearance of a prominent protein band around 18-19 kDa (**Figure 6A-B**). As no significant difference in protein expression was observed between the two strains and the pre-induction protein expression in *E. coli* Rosetta-gami 2 (DE3) was more prominent, the choice was made to continue protein expression for the all constructs in *E. coli* ArcticExpress (DE3) RP. All three TNF- α variants expressed equally well (**Figure 6A-D**).

Table 1 - Overview purification steps per TNF- α protein.

Each variant was purified using different columns based on both the presence of purification tags or the intrinsic charge of the protein.

Protein	TNF- α -6His	TNF- α	TNF- α -LPETGG-6His
Purification Methods	1: Nickel column (imidazole in PBS)	1: DEAE anion column (NaCl in 20 mM Tris/1 mM EDTA pH8)	1: Nickel column (imidazole in PBS)
	2: DEAE anion column (NaCl in 20 mM HEPES pH 8)	2: CM cation column (NaCl in 20 mM MES in pH 6)	2: DEAE anion column (NaCl in 20 mM HEPES pH 8)

Unmodified TNF- α was purified based on the protocols described by Zhang *et al.*⁴⁸ Sequentially DEAE anion and carboxymethyl (CM) cation purification were used (**Supplementary Figure S2 - Figure S3**) as DEAE anion purification alone did not yield sufficiently pure TNF- α . DEAE anion purification in 20 mM Tris/1 mM EDTA pH 8 followed by CM cation purification in 20 mM MES pH 6, both using 0-500 mM NaCl for elution of TNF- α resulted in >90% pure TNF- α (**Figure 7B**).

**Figure 7 - Overview purification of TNF- α , TNF- α -6His and TNF- α -LPETGG-6His.**

All TNF- α variants expressed in *E. coli* ArcticExpress (DE3) RP were purified using either tag-based purification and/or ion exchange based purification. A) TNF- α -6His was purified using nickel column purification with imidazole in PBS followed by DEAE anion purification with NaCl in 20 mM HEPES pH 8. B) TNF- α was purified using DEAE anion purification with NaCl in 20 mM Tris/1 mM EDTA pH 8 followed by CM cation purification with NaCl in 20 mM MES pH 6. C) TNF- α -LPETGG-6His was purified using nickel column purification with imidazole in PBS followed by DEAE anion purification with NaCl in 20 mM HEPES pH 8.

TNF- α -LPETGG-6His was purified based on its C-terminal 6His-tag (**Supplementary Figure S4A**) following DEAE anion exchange (**Supplementary Figure S4B**) similar to TNF- α -6His purification to yield the protein in >95% purity (**Figure 7C**).

Caging optimisation of TNF- α -6His using NHS-TCO

Initial optimisation of the inactivation of TNF with TCO-NHS **1** were performed next (**Figure 8**). TNF- α -6His was chosen for this optimisation as it could readily be produced and purified, and visualised by anti-6His Western blot. The success of the caging reaction was first assessed using an enzyme-linked immunosorbent assay (ELISA, **Figure 9**). ELISA is based on interaction between antibodies and (epitopes of) a particular protein (TNF- α , in this case). This format was chosen because when blocking lysines in/near the epitope prevents the antibodies from binding, this could indicate that receptor interactions could be blocked as well by blocking lysines in/near the receptor interacting domain.

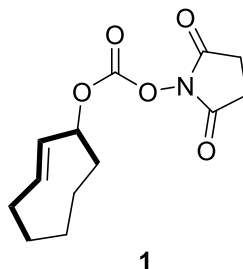


Figure 8 - Structure of (S,E)-cyclooct-2-en-1-yl(2,5-dioxopyrrolidin-1-yl) carbonate or 2-AX-NHS-TCO.

2-AX-NHS-TCO or NHS-TCO was kindly provided by Mark de Geus.

The first attempts at caging were done in 20 mM HEPES pH 8 for 1 hour at 37°C with varying concentrations of **1** and 5.4 μ M of TNF- α -6His (**Figure 9A**). The largest signal reduction – to 60% of the value of the unmodified cytokine – was obtained using 2.4 mM **1** for caging of 5.4 μ M TNF- α -6His. Surprisingly, neither increasing or decreasing this concentration **1** resulted in a reduction in TNF-binding. Changing the reaction time (1-18 hours) did not improve this either (**Figure 9B**). It did, however, result in an increased loss of protein from the DMSO-control. Reducing the temperature of the modification reaction had no effect on caging either (**Figure 9C**).

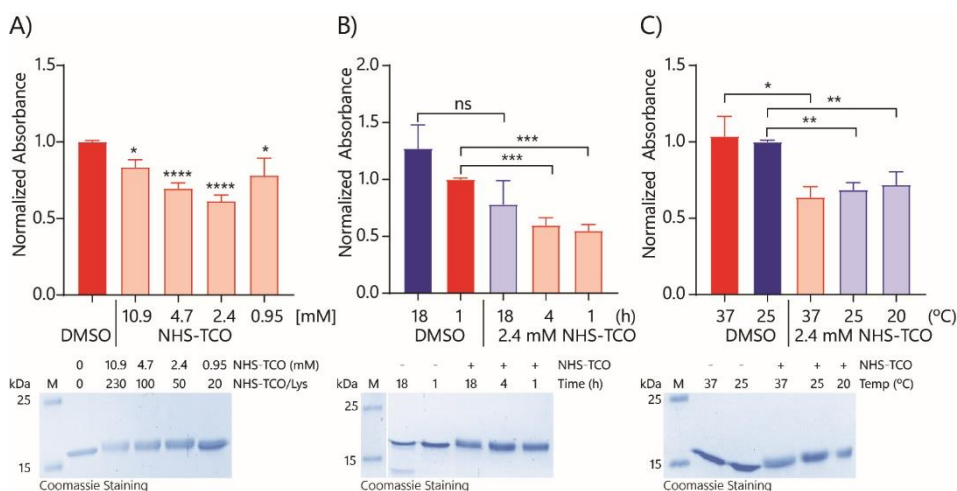


Figure 9 - Caging optimisation of TNF- α -6His analysed using ELISA.

ELISA was performed to assess whether NHS-TCO bound by lysines in/near the recognized epitope could prevent antibody interactions. Caging of TNF- α -6His (0.1 mg/mL or 5.4 μ M in 20 mM HEPES pH 8) was assessed using A) different concentrations of **1** (N=3), B) for various periods of time (h) (N=3) and C) at various temperatures ($^{\circ}$ C) (N=4). The initial standard caging conditions were set at caging with 2.4 mM **1** (B,C) for 1 hour (A,C) at 37 $^{\circ}$ C (A,B). Caging was compared with the DMSO control which gave the maximum signal. Bright colours indicate DMSO only samples and pastels the TCO-treated samples. Colour groups indicate different conditions with respective DMSO controls. In general, caging reduced the signal compared to the DMSO control. Coomassie staining below each graph indicated equal protein application. Data were plotted as mean signal \pm SEM. Significances are indicated as follows: * $P < 0.05$; ** $P < 0.01$; *** $P < 0.001$; **** $P < 0.0001$; ns is non-significant.

It was postulated that the ELISA was not able to fully distinguish between the caged and free TNF- α . It was therefore deemed more relevant to look at the effect of receptor binding. This was done in two ways: using HEK-Blue TNF- α cells and L929 cells.^{49,50} HEK-Blue TNF- α cells are HEK293 cells which express TNFR1, that binds both human and murine TNF- α . Upon binding TNF- α , NF- κ B gets activated which leads to the expression of a secreted embryonic alkaline phosphatase (SEAP). This alkaline phosphatase converts QUANTI-Blue reagent from a pink coloured compound to a blue product, which could be measured using 655 nm absorbance.^{49,51}

The L929 assay, on the other hand looks at TNFR-binding in a more functional manner. These murine fibroblasts are sensitive to TNF- α induced cell death (apoptosis and necrosis) in combination with other toxic compounds like actinomycin D.^{50,52} TNF- α binds to the TNFR1 which can normally cause proliferation via NF- κ B pathways. However, when the protein synthesis is blocked, this becomes a signal for apoptosis. Actinomycin D, a DNA binding compound, blocks DNA transcription and thereby protein synthesis.^{52,53} The combination of TNF- α and actinomycin D causes L929 cell death, allowing the assessment of TNF-function by a simple live-dead assay. For this the MTT-assay was used. This colorimetric assay, by the formation of purple crystals, indicated cell viability by the activity of the mitochondria.⁵⁴

The HEK-Blue assay

This assay indeed showed a different trend to the ELISA: higher concentrations of **1** reduced TNF- α -6His' capability to interact with the TNFR1 to <10% of the native binding affinity, thereby preventing NF- κ B activation and SEAP expression (**Figure 10A**). Lower concentrations, < 1.4 mM of **1**, reduced the binding to 40% of its native capacity. Changes in caging time (**Figure 10B**) had no significant effect on TNF- α -6His activity in general although increasing this time does not seem to improve caging. Changes in temperature (**Figure 10C**) only had a minor effect although incubation at 25°C appeared to result in the largest signal reduction to about 30%. **Figure 10B** and **Figure 10C** in general show less inactivation compared to **Figure 10A**. Possibly, this is due to the passage number of the HEK-Blue TNF- α cells. Even though this was within the manufacturer's description, a higher passage number affects the cell's behaviour. Also the batch quality of TNF- α -6His used could affect activation.

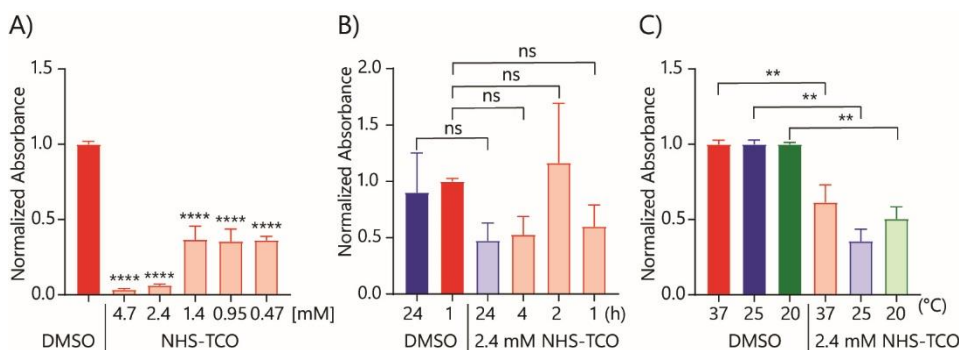


Figure 10 - Caging optimisation of TNF- α -6His using HEK-Blue TNF- α cells via a colorimetric assay.

Optimization of TNF- α -6His (0.1 mg/mL or 5.4 μ M) caging in 20 mM HEPES pH 8 was assessed with stimulated HEK-Blue TNF- α cells. A) Analyses of different concentrations of **1** (N=5), B) for various periods of time (h) (N=3) and C) at various temperatures ($^{\circ}$ C) (N=3) were performed. The initial standard caging conditions were set at caging with 2.4 mM **1** (B,C) for 1 hour (A,C) at 37 $^{\circ}$ C (A,B). Caging was compared with the DMSO control which gave the maximum signal. Bright colours indicate DMSO only samples and pastels the TCO-treated samples. Colour groups indicate different conditions with respective DMSO controls. In general, caging reduced the signal compared to the DMSO control. Data were plotted as mean signal \pm SEM. Significances are indicated as follows: * P<0.05; ** P<0.01; *** P<0.001; **** P<0.0001; ns is non-significant.

L929 assay

L929 cells were used to assess whether the change in TNFR1 affinity due to caging (**Figure 11**, **Supplementary Figure S5A-C**) also resulted in a loss of function of TNF- α . Caging experiments with different concentrations **1**, for different periods of time and at different temperatures were performed as has been described for the HEK-Blue assays mentioned above (**Supplementary Figure S5A-C**). These experiments showed comparable results regarding the optimal caging conditions; caging with 2.4 mM **1** for 1 hour at 25 $^{\circ}$ C. Due to the ease of this assay, it was also used to optimise the reaction buffer by testing a range of pH-values in PBS, Tris, and HEPES-buffers. The reaction of **1** with free amines is known to proceed better under slightly basic conditions.⁵⁵ Therefore PBS, 20 mM Tris and 20 mM HEPES at various pH-values were assessed using 2.4 mM **1** at 25 $^{\circ}$ C for 1 hour (**Figure 11A**). These experiments showed that PBS can be used at neutral or slightly basic pH but also showed that Tris and HEPES are more applicable, also in a wider pH-range (**Figure 11B** and **Figure 11C**). At pH 6, the functionality of TNF- α -6His changes which could be due its

pI (5.64, ExPasy) which is very close to the buffer pH, causing TNF- α -6His to behave differently. As TCO-reagent **1** can potentially be sequestered by reacting with the free amine in Tris, HEPES pH 8 was used for all further experiments.⁵⁶ Overall, it could be concluded that caging with TCO-reagent **1** worked in a broader range of slightly basic/neutral pH-values in various buffers.

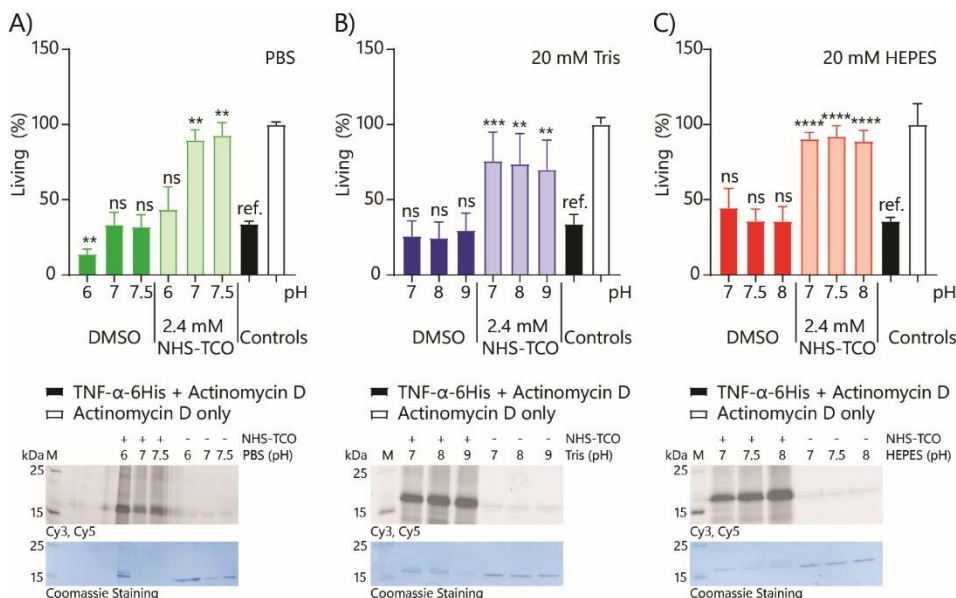


Figure 11 - Caging optimisation of TNF- α -6His analysed using L929 cells in a MTT-viability assay.

TNF- α -6His (0.1 mg/mL or 5.4 μ M) was caged in buffers with various pH-values: A) PBS (N=3), B) 20 mM Tris (N=3) and C) 20 mM HEPES (N=3) with 2.4 mM **1** for 1 hour at 25°C. Caging was compared with the TNF- α -6His + actinomycin D annotated as **ref.** (black, negative control). Actinomycin D served as a positive control (white). Bright colours indicate DMSO only samples and pastels the TCO-treated samples. In general, caging increased the signal compared to the DMSO control and negative control. Fluorescence at 570 nm of a slow-eliminating BODIPY-TMR tetrazine was used to visualise caging on SDS-PAGE. Coomassie staining below each graph indicated equal protein usage. Data were plotted as mean signal \pm SEM. Significances are indicated as follows: * P<0.05; ** P<0.01; *** P<0.001; **** P<0.0001; ns is non-significant.

When applied to the sortagable TNF- α variant, TNF- α -LPETGG-6His, the same reduced activity was observed in all assays performed (**Supplementary Figure S6 - Figure S8**).

Although the determined caging conditions seemed optimal, at this point in the proceedings the discovery was made that cold caging led to improved caging (see *Chapter 2*). Therefore, caging was also performed at lower temperatures (25°C to 10°C) with lower concentrations of **1** (2.2 mM to 0.45 mM **1**) and longer caging time (1 hour to 24 hours; **Figure 12**).

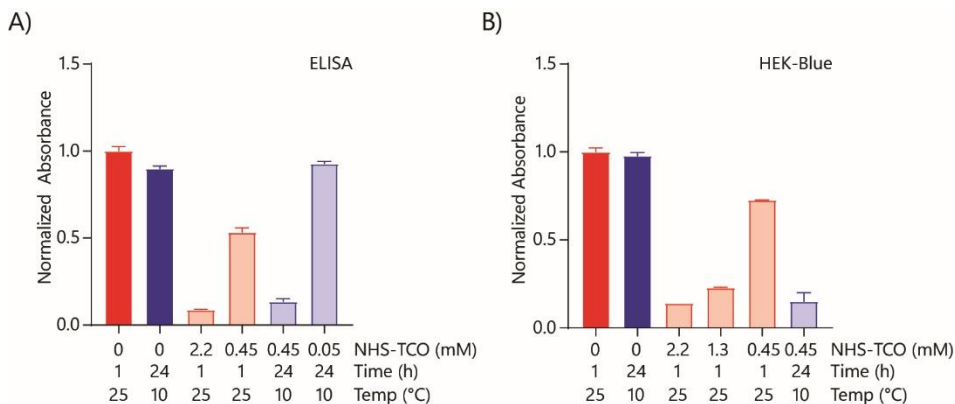


Figure 12 - Preliminary data of caging at lower temperatures of TNF- α -LPETGG-6His analysed by ELISA and HEK-Blue TNF- α cells.

TNF- α -LPETGG-6His (0.1 mg/mL or 5.1 μ M) in 20 mM HEPES pH 8 was caged either at 25°C for 1 hour with 0.45-2.2 mM **1** or at 10°C for 24 hours with 0.05-0.45 mM **1**. The caging was analysed by A) ELISA (N=1) and B) HEK-Blue TNF- α cells (N=1). Caging was compared with the DMSO control which gave the maximum signal. Bright colours indicate DMSO only samples and pastels the TCO-treated samples. Colour groups indicate different conditions with respective DMSO controls. These preliminary results suggested that caging with 0.45 mM **1** for 24 hours at 10°C resulted in similar TNF- α -LPETGG-6His inactivation compared to caging at 25°C for 1 hour with 2.2 mM **1**. Data were plotted as mean signal \pm SEM. Due to the limited number of datapoints no significances could be determined.

Due to the limited number of datapoints no significances could be determined. However, the preliminary data suggested that caging with 0.45 mM **1** for 24 hours at 10°C, resulted in similar TNF- α -LPETGG-6His inactivation as the optimal caging conditions determined before: caging with 2.2 mM **1** for 1 hour at 25°C. This was shown in both the ELISA (**Figure 12A**) and the HEK-Blue TNF- α assay (**Figure 12B**). As these caging conditions had a similar result as has been described for IL-1 β in *Chapter 2* of this work, no further optimisation was performed.

Optimisation of reactivation of TNF- α -6His and TNF- α -LPETGG-6His using tetrazine

Next, the reactivation of caged TNF using tetrazine **2** (**Table 2**) was optimised. Decaging was first performed in a test tube. This allowed the use of high tetrazine concentrations, which would be toxic to the target cells. Deprotection was assessed using the 3,6-dimethyltetrazine (**2**, DMT, **Table 2**; kindly provided by Alexi Sarris) as this tetrazine **2** has a fast elimination rate and has been extensively used in previous studies^{33,34,57} (**Figure 13**).

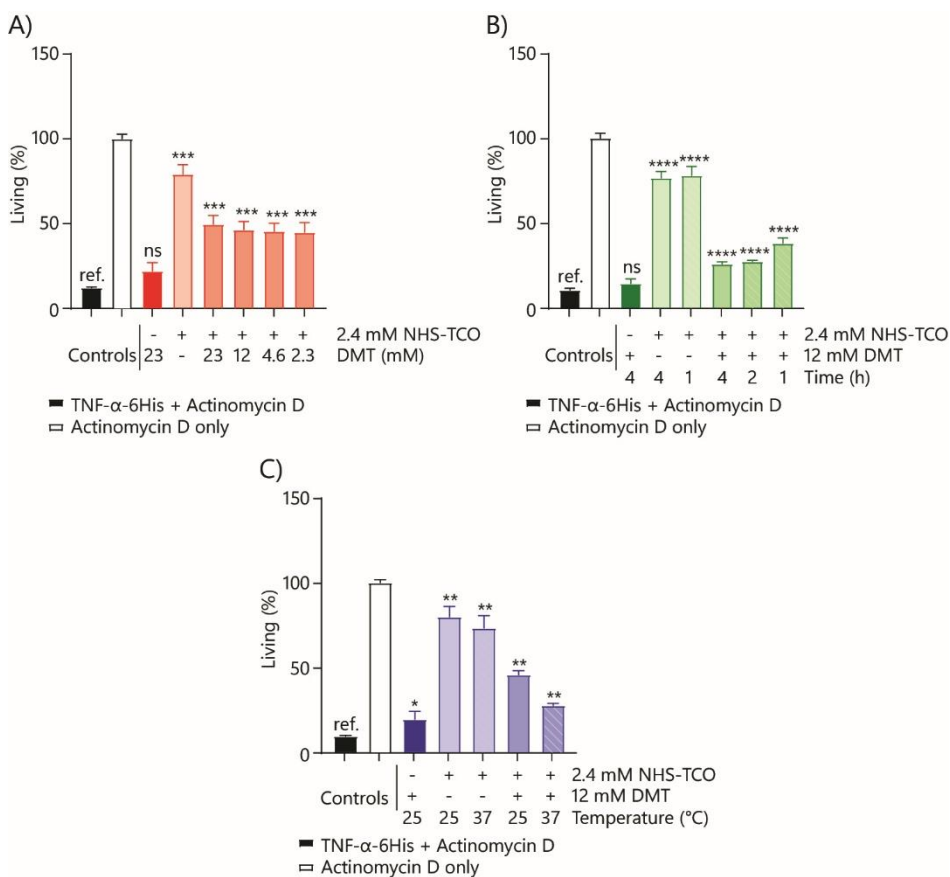


Figure 13 - Decaging optimisation of TNF- α -6His in vitro assessed via L929 viability assays.

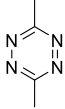
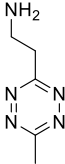
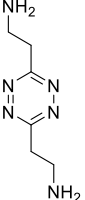
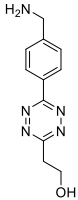
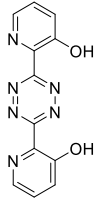
TNF- α -6His (0.1 mg/mL or 5.4 μ M) caged with 2.4 mM **1** in 20 mM HEPES pH 8 was decaged under A) various conditions to determine the optimal concentration of **2** (DMT) (N=4), B) the optimal decaging time (h) (N=4) and C) temperature ($^{\circ}$ C) (N=3). After caging, the reaction mixture was filtered to remove excess of TCO following a decaging reaction in 20 mM HEPES pH 7. Standard reaction conditions were decaging at 37 $^{\circ}$ C for 1 hour. L929 viability was determined using an MTT assay. The signals were compared to the TNF- α -6His + actinomycin D control annotated as **ref.** (black). Bright colours indicate DMSO only samples, the light pastels the TCO-treated samples and the dark pastels the DMT-treated samples. In general, upon treatment with **2**, the viability of L929 decreased. Data were plotted as mean signal \pm SEM. Significances are indicated as follows: * $P < 0.05$; ** $P < 0.01$; *** $P < 0.001$; **** $P < 0.0001$; ns is non-significant.

Various aspects of the deprotection reaction were explored initially, such as tetrazine concentration (**Figure 13A**), deprotection time (**Figure 13B**), and deprotection temperature (**Figure 13C**). The optimal conditions were found to be 37 $^{\circ}$ C for 1 hour in 20 mM HEPES pH 7. Applying 2.3-23 mM of **2** showed decreasing L929 viability, as a result of TNF- α -6His regaining significant activity (50%). Increasing the decaging time from 1 to 2-4 hours resulted in further reactivation to about 80% (**Figure 13B**). Finally, decreasing decaging temperature to 25 $^{\circ}$ C did not improve decaging compared to decaging at 37 $^{\circ}$ C (**Figure 13C**).

Until now all deprotection reactions took place in Eppendorf tubes with 0.1 mg/mL TNF- α -6His without the removal of unreacted NHS-TCO. This demanded and also allowed for the use of higher concentrations of tetrazine. Next, the on-cell deprotection reaction was assessed using the HEK-Blue TNF- α cell line. Briefly, without the removal of unreacted NHS-TCO caged TNF- α -6His was diluted to 625 pg/mL and provided to HEK-Blue TNF- α cells whereafter 25 μ M of various tetrazines was applied in 0.5 μ L DMSO. Four additional tetrazines were evaluated (**Table 2**) in these reactions to increase the chance of a successful reactivation.

Table 2 - Overview tetrazine used for decaging optimisation.

All tetrazines were dissolved in DMSO. DMT was kindly provided by Alexi Sarris, Tz1-2 and Tz4 were kindly provided by Dr. Merel van der Plassche and (2PyrH)₂Tz was kindly provided by Prof. Dr. Hannes Mikula.

	DMT	Tz1	Tz2	Tz4	(2PyrH) ₂ Tz
Compound nr.	2	3	4	6	7
Full name	3,6-dimethyl-tetrazine	2-(6-methyl-1,2,4,5-tetrazin-3-yl)ethan-1-amine	2,2'-(1,2,4,5-tetrazine-3,6-diyl)bis(ethan-1-amine)	2-(6-(4-(aminomethyl)phenyl)-1,2,4,5-tetrazin-3-yl)ethan-1-ol	2,2'-(1,2,4,5-tetrazine-3,6-diyl)bis(pyridin-3-ol)
Structure					

Decaging was done using 25 μ M final concentration tetrazine at 37°C for 20-24 hours (**Figure 14**, see *Chapter 2*). Sadly, no significant deprotection was observed for both TNF- α -6His (**Figure 14A**) and TNF- α -LPETGG-6His (**Figure 14B**) for any of the tetrazines tested.

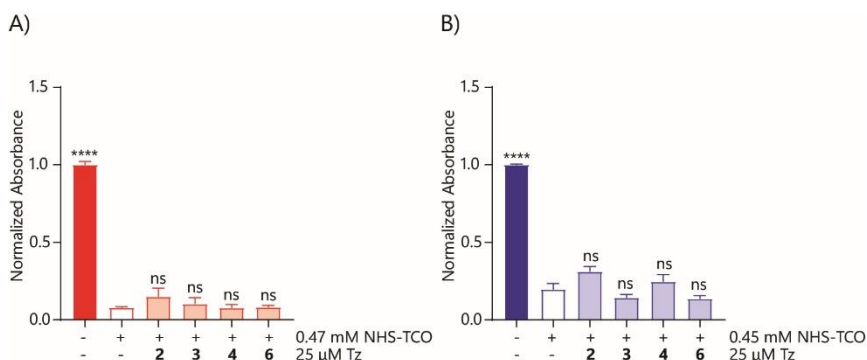


Figure 14 - Decaging of TNF- α -6His and TNF- α -LPETGG-6His using different tetrazines analysed by HEK-Blue TNF- α cells via a colorimetric assay.

A) TNF- α -6His (0.1 mg/mL or 5.4 μ M) (N=7) and B) TNF- α -LPETGG-6His (0.1 mg/mL or 5.1 μ M) (N=5) caged at 10°C for 24 hours with 0.47 mM and 0.45 mM **1**, respectively, in 20 mM HEPES pH 8 were decaged using 25 μ M of various tetrazines for 20-24 hours at 37°C on HEK-Blue TNF- α cells. Tetrazine was supplied in 0.5 μ L DMSO. Bright colours indicate DMSO only samples and pastels the tetrazine treated samples. In general, decaging did not increase the signal significantly compared to the caged control. Data were plotted as mean signal \pm SEM. Significances are indicated as follows: * P<0.05; ** P<0.01; *** P<0.001; **** P<0.0001; ns is non-significant.

Of all the tetrazines tested, **2** showed the most promising decaging results, particularly when TNF- α -LPETGG-6His caged with 0.45 mM **1** for 24 hours at 10°C was decaged on HEK-Blue TNF- α cells with increasing concentrations of **2** (Figure 15A). At the same time, a different tetrazine (2PyrH)₂Tz (**7**), kindly provided by Prof. Dr. Hannes Mikula, was tested at different concentrations as it proved to work well for IL-1 β decaging described in Chapter 2 of this work (Figure 15B).

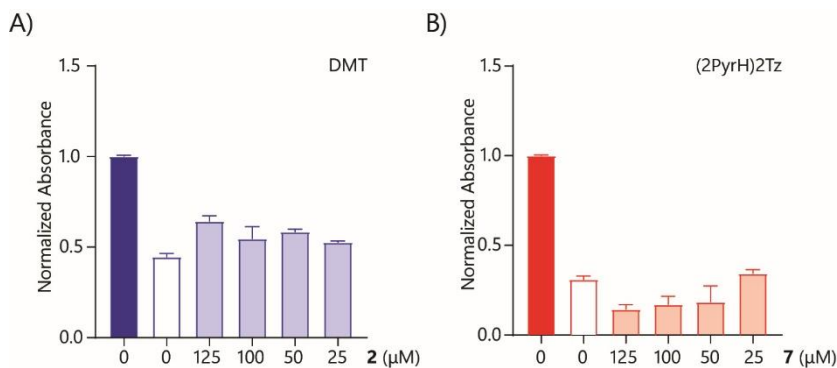


Figure 15 - Decaging optimisation of TNF- α -LPETGG-6His analysed by HEK-Blue TNF- α .

TNF- α -LPETGG-6His (0.1 mg/mL or 5.1 μ M) in 20 mM HEPES, caged with 0.45 mM **1** for 24 hours at 10°C, was decaged with A) increasing concentrations of **2** (N=2) or B) increasing concentrations of **7** (N=2) on HEK-Blue TNF- α cells. Decaging took place for 20-24 hours at 37°C. Tetrazine was supplied in 0.5 μ L DMSO. Bright colours indicate DMSO only samples and pastels the tetrazine treated samples. In general, these preliminary data showed that increasing concentration **2** caused more decaging, while decaging with **7** did not result in decaging. Data were plotted as mean signal \pm SEM. Due to the limited number of datapoints no significances could be determined.

Due to the limited number of datapoints no significances could be determined. Increasing the concentration of **2** showed increased decaging (**Figure 15A**). Using 125 μM **2** caused about 50% increase in TNF- α -LPETGG-6His activity compared to the caged sample. The cells did not show signs of toxicity. Decaging with **7**, unlike with IL-1 β in *Chapter 2*, did not result in decaging for unknown reasons (**Figure 15B**). Increasing concentrations of **7** also seemed to be toxic for these cells (data not shown).

Although some decaging could be observed, the regained activity with 125 μM **2** was minimal. Therefore, unfortunately no further steps were taken regarding the formation of the actual immunocytokine by coupling it to a targeting moiety.

Conclusion

TNF- α is one of the master regulator cytokines in the immune system and has been the target in various forms of cancer treatment. Its intrinsic toxicity posed a significant problem in these treatments and therefore it has been included in immunocytokines which target the cytokine to the tumour micro-environment. Nevertheless, toxicities remained and this work presented a method involving *click-to-release* chemistry based on NHS-TCO and tetrazines to create spatiotemporal control over TNF- α activity. Using NHS-TCO to block the lysines caused the inactivation of TNF- α , unable to interact with its TNFR1. Reactivation of TNF- α proved to be difficult as decaging conditions in Eppendorf tubes were not translated to decaging on cells. The reasons for that could be that TNF- α functions as trimer rather than a monomer which is the case for IL-1 β . This means that decaging has to be more 'complete' in the sense that more lysines have to be restored to get the active trimer back, while for a monomer potentially some caged lysines could remain. Even though it was not proven yet, it is speculated that the trimer can fall apart after caging and is hard to restore after decaging. Because of this further optimisation has to be performed regarding the decaging of TNF- α , potentially using a covalent trimer or using even different tetrazines.

Acknowledgements

First, I would like to thank Shimrit David, who helped me starting up this project and with whom I prepared the basis for this technique and this chapter. Second, I would like to thank Rick Hofman and Joris Veger, for their hard work and assistance on expressing and purifying the various variants of TNF- α as well as performing the various functionality assays after the caging procedure. It was a hard project which did not always go as we wished for but it provided a basis from which I could and still can continue. Then I would like to thank Mark de Geus, Alexi Sarris, Dr. Merel van der Plassche and Prof. Dr. Hannes Mikula for the supply of NHS-TCO, BODIPY-TMR-Sol2 tetrazine, various decaging tetrazines and (2PyrH)₂Tz, respectively. These compounds allowed to me to examine this strategy in the first place. Finally I would like to thank Dr. Diana Torres García as she helped me with all the statistics performed in this chapter. Besides assisting me in getting the statistics right, she also helped improving my knowledge about this subject.

Materials & Methods

General reagents and equipment

All donor vectors were purchased from *cript* and primers were ordered at Sigma-Aldrich. All restriction enzymes, polymerases and ligases were purchased from Thermo Fisher Scientific. Benzonase was purchased from Santa Cruz Biotechnology. Sodium deoxycholate monohydrate (CAS:302-95-4) and phenylmethanesulfonyl fluoride (PMSF,CAS:329-98-6) were purchased from Sigma-Aldrich. Amicon® Ultra-15 Centrifugal Filters 3K (UFC900324) and Amicon® Ultra-15 Centrifugal Filters 10K (UFC901024) filters were purchased from Merck Millipore. Zeba™ Spin Desalting columns, 7K MWCO (cat. nr. 89883) and HisPur™ Ni-NTA Resin (cat. nr. 88222) were purchased from Thermo Fischer Scientific and the automated columns (HisTrap™ FF, HiTrap™ DEAE FF, HiTrap™ CM Sepharose FF) were purchased from GE Healthcare Life Science. Rabbit anti-6*His (Item No. 600-401-392) was purchased from Rockland and mouse anti-rabbit IgG-HRP (Catalog # sc-2357) was purchased from Santa Cruz Biotechnology. DMEM-medium, L-glutamine, streptomycin and penicillin were purchased from Sigma-Aldrich. QUANTI-Blue (#rep-qbs) and zeocin were purchased from InvivoGen.

Construct formation

NheI restricted (1x Tango Buffer, 10U NheI) pcDNA3.1⁺/C-(K)DYK_TNF α (Clone ID: OMu20592, assession version: NM_013693.3) was used as template for TNF- α amplification by PCR (GC Green Buffer, 0.2 mM dNTPs, 0.1 μ M of each primer, 50 ng restricted vector, 2U Phusion polymerase) using primers of **Table 3**. TNF- α fragments were restricted with XhoI/NcoI (10U; TNF- α /TNF- α -6His) and NcoI/EcoRI (10U; TNF- α -LPETGG-6His) respectively and ligated into XhoI/NcoI (10U) restricted pET28a(+) and NcoI/EcoRI (10U) restricted pET28a(+)-GGGGG-LPETGG-6His vectors behind the T7 promoter using T4 DNA Ligase (5U) at room temperature for 2 hours. Restrictions were performed for 20-24 hours at 37°C, 300 rpm. Ligation products were transformed into *E. coli* XL10 via heat shock (42°C, 45 seconds) and SOC-medium recovery followed by growth at glucose (1%) and kanamycin (50 μ g/mL) containing LB-agar plates at 37°C overnight. Transformation was checked by colony PCR using the primers of **Table 3**.

Table 3 - Primer overview.

Primer Nr.	Construct	Sequence 5'→ 3'
1	TNF- α	TATACCATGGCACTCAGATCATCTTCT
2		GGTGCTCGAGTCACAGAGCAATGAC
3	TNF- α -6His	TATACCATGGCACTCAGATCATCTTCT
4		AATGCTCGAGCAGAGCAATGACTCC
5	TNF- α -LPETGG-6His	TATACCATGGCACTCAGATCATCTTCTCAA
6		CGCCGAATTCCAGAGCAATGACTCCAAA

Cytokine expression and isolation

Cytokine constructs isolated from *E. coli* XL10 using QIAprep Spin Miniprep Kit were used to transform calcium competent *E. coli* ArcticExpress (DE3) RP using heat shock (42°C, 45 seconds) and SOC-medium recovery. Colonies were used to inoculate LB-medium containing kanamycin (50 µg/mL) and gentamycin (7 µg/mL) for overnight growth at 37°C, 170 rpm. Overnight culture was diluted 100 times and grown at 37°C, 170 rpm until optical density at 600 nm (OD₆₀₀) of 0.6 was reached after which protein expression was induced with addition of 0.5 mM IPTG. Expression took place for 48-72 hours at 10°C, 140 rpm where after the bacteria were harvested by centrifugation (30 minutes, 3400g at 4°C).

Per 500 mL bacterial culture, 10 mL lysis buffer (50 mM Tris Cl pH 8.0, 25% (w/v) sucrose, 1 mM EDTA, 1 mM PMSF, 2 mM DTT) was applied with 0.4 mg/mL lysozyme. Incubation while gently mixing for 30 minutes at 4°C was followed by adding 10 mM MgCl₂, 1 mM MnCl₂ and 10U benzonase and 30 minutes incubation at 4°C. The lysate was sonicated (Vibra-cell™ VCX130) for 30 seconds with 5 second pulses with 20% amplitude and 10 second intervals. The lysate was diluted three times with detergent buffer (0.2 M NaCl, 1% (w/v) sodium deoxycholate monohydrate, 1% octylphenoxypolyethoxyethanol (Igepal), 20 mM Tris Cl pH 7.5, 2 mM EDTA, 0.02 mM PMSF, 0.04 mM DTT), incubated for 30 minutes on ice and centrifuged for 20 minutes at 14000g, 4°C to collect the supernatant.

Cytokine purification

TNF-α-6His and TNF-α-LPETGG-6His

6His-tag based Purification - Manual

Supernatant obtained after lysis was applied to the appropriate amount of equilibrated HisPur™ Ni-NTA Resin. Overnight incubation under constant stirring (4°C) was followed by applying the resin on a reaction syringe and flushing by gravity flow. Washing and elution were performed with a number of fractions (two column volumes) of 50 mM, 70 mM and 250 mM imidazole in PBS. Protein presence was assessed using SDS-PAGE and Coomassie R250 staining. TNF-α containing samples were combined and concentrated using an Amicon® Ultra-15 Centrifugal Filter 3K (30 minutes, 4°C, 3428g) equilibrated with 20 mM HEPES pH 8.

6His-tag based Purification – Automatically

Supernatant obtained after lysis was loaded (4 mL/minute) on a properly washed HisTrap™ FF (5 mL) connected to an ÄKTA Start System (GE Healthcare, Life Sciences). The column was washed (at least 2 column volumes) with different concentrations imidazole in PBS. Collected washes were analysed by gel electrophoresis using SDS-PAGE and Coomassie R250 staining. Protein containing samples were combined and concentrated using an Amicon® Ultra-15 Centrifugal Filter 3K equilibrated with 20 mM HEPES pH 8. The concentrated protein was washed three times with 20 mM HEPES pH 8 (30 minutes, 4°C, 3428g).

Ion Exchange Purification

Concentrated protein solution was desalted using Zeba™ Spin Desalting columns, 7K MWCO with 20 mM HEPES pH 8 as stacking and washing solution. Protein concentration was determined using Bradford assay. The desalted, concentrated protein solution was loaded over an HiTrap™ DEAE FF column which was equilibrated with 20 mM HEPES pH 8. The column was washed twice with four column volumes 20 mM HEPES pH 8/0.05 M NaCl. The protein was eluted with four column volumes 20 mM HEPES pH 8/0.25 M NaCl. Purity was checked with SDS-PAGE analysis and Coomassie R250 staining.

TNF- α

The soluble protein fraction was diluted at least 5 times in 20 mM Tris/1 mM EDTA pH 8 and loaded (4 mL/minute) on a properly washed HiTrap™ DEAE Sepharose FF column connected to an ÄKTA Start System (GE Healthcare, Life Sciences). Protein was washed and eluted (at least two column volumes) with different NaCl concentrations in 20 mM Tris/1 mM EDTA pH 8. Collected washes/elutions were analysed by SDS-PAGE and Coomassie R250 staining. TNF- α containing samples were combined, concentrated using an Amicon® Ultra-15 Centrifugal Filter 3K and washed twice with 20 mM MES pH 6. Concentrated TNF- α was desalted using Zeba™ Spin Desalting columns, 7K MWCO with 20 mM MES pH 6 as stacking and washing solution.

TNF- α in 20 mM MES pH 6 was loaded on properly washed HiTrap™ CM Sepharose FF column connected to an ÄKTA Start System (GE Healthcare, Life Sciences). TNF- α was washed and eluted (at least two column volumes) with different NaCl concentrations in 20 mM MES pH 6. Collected washes/elutions were analysed by SDS-PAGE and Coomassie R250 staining. Pure TNF- α fractions were concentrated using Amicon® Ultra-15 Centrifugal Filters 3K and washed twice with 20 mM HEPES pH 8. Aliquots were stored at -80°C.

Western blot

Denaturing acrylamide gels (SDS-PAGEs) were blotted onto 0.2 μ m PVDF membrane (midi format, single application of Bio-Rad) using the Turbo Trans Blot System (Bio-Rad). Blots were developed using luminol solution (25% (w/v) luminol in 0.1 M Tris pH 8.8), 100x diluted enhancer (1.1 mg/mL p-coumaric acid in DMSO) and H₂O₂. Blots were imaged with the ChemiDoc™ MP Imaging System of Bio-Rad with settings chemiluminescence, Cy3 and Cy5 and analysed using ImageLab Software version 4.1.

6His-specific blot

Blots were washed with TBS (10 minutes) and TBST (3x 5 minutes) (1x TBS pH 7.5; 0.1% Tween-20), respectively before blocking with 5% milk in TBST overnight at 4°C. Washing with TBST (3x 5 minutes) was followed with rabbit anti-6*His incubation (1:1000) in blocking buffer for 3 hours at room temperature. Another wash (3x 5 minutes) with TBST was followed by addition of mouse anti-rabbit IgG-HRP (1:4000) and incubation for 2 hours at room temperature. The blots were washed with TBST (3x 5 minutes) and TBS (10 minutes) respectively, before development with luminol.

TNF- α specific blot

Blots were washed with PBS and PBST (1x PBS pH 7.4, 0.5% Tween-80) instead of TBS and TBST, respectively. Blocking was performed with 0.2% BSA in PBST. The primary antibody used was biotin-conjugate anti-mouse TNF- α (1:1000, #88-7324-88, Thermo Fisher Scientific). Streptactin-HRP (1:100000, #2-1502-001, IBA solutions) was used as a secondary antibody.

Caging and decaging procedure

Caging

Caging was performed in 20 mM HEPES pH 8 at 10°C, 800 rpm for 24 hour. An excess of 10 molar equivalents 2-AX-NHS-TCO (NHS-TCO; kindly provided by Mark de Geus) was used per lysine in TNF- α -6His or TNF- α -LPETGG-6His. Protein concentrations were determined using the Qubit™ Protein assay kit on the Qubit® 2.0 Fluorometer of Invitrogen (Life Technologies). Caging was visualised by using 0.6 μ M Tetrazine Bodipy-TMR Sol2 (kindly provided by Alexi Sarris) incubating for 30 minutes at 25°C, 800 rpm. Gels were analysed using ChemiDoc™ MP Imaging System of Bio-Rad and ImageLab Software version 4.1.

Decaging – in vitro

Decaging was first performed in Eppendorf tubes under various conditions i.e. 3,6-dimethyl-tetrazine (DMT; kindly provided by Alexi Sarris) concentration, decaging time and decaging temperature. Caging was performed under the conditions determined to be optimal described above except for starting with 0.2-0.3 mg/mL protein. The caging samples were filtered using Zeba™ Spin Desalting columns, 7K MWCO, 0.5 mL using 20 mM HEPES pH 7 as equilibration buffer. The protein concentration was determined afterwards using Qubit® 2.0 Fluorometer of Invitrogen (Life Technologies) and adjusted to 0.1 mg/mL using 20 mM HEPES pH 7. Optimal *in vitro* decaging was obtained using 2.5 mM DMT and incubation for 1 hour at 37°C, 300 rpm for 4 hours.

Decaging – HEK-Blue TNF- α

Decaging was performed in medium with 25 μ M DMT, Tz1-2, Tz4 and (2PyrH)₂Tz (kindly provided by Prof. Dr. Hannes Mikula) on cells at 37°C overnight. Tz1-2 and Tz4 were kindly provided by Dr. Merel van der Plassche. All used tetrazines used are visualised in **Table 2**.

ELISA assay

Uncoated ELISA kit for mouse TNF- α (#88-7324-88) was used from Invitrogen. The assays were performed using 96-wells microplate half area high binding (#675061, Greiner Bio-one). Assay was performed according to the manufactures protocol with the following adaptations. Both antibodies and streptavidin-HRP were applied in 25 μ L per well and blocking was performed with 100 μ L per well. Samples were applied in 30 μ L (80-10000 pg/mL for TNF- α) per well. Final substrate was supplied in 25 μ L per well and the enzymatic reaction was stopped with 12.5 μ L per well. The absorbance at 450 was measured with the Bio-Rad iMark™ Microplate Reader.

Cell culture**L929**

Cells were maintained in 10 cm dishes in Dulbecco's Modified Eagle's Medium – high glucose (DMEM-high glucose, #D6546-500ML) supplemented with 10% Newborn Calf Serum (NCS), 2 mM glutamine, 100 IU/mL penicillin and 50 μ g/mL streptomycin at 37°C, 7% CO₂. For each passage 50.000-100.000 cells/mL were used, which took place every 4-5 days using 0.25% trypsin in PBS/EDTA. Incubation of about 3-5 minutes was followed by neutralization of the trypsin by adding complete medium in 1:1 ratio.

HEK-Blue TNF- α

HEK-BLUE™ TNF- α (cat. Hkb-tnfdmyd, InvivoGen) were maintained in Dulbecco's Modified Eagle's Medium – high glucose (DMEM-high glucose, #D6546-500ML) supplemented with 2 mM L-glutamine, 10% (v/v) heat-inactivated fetal calf serum, 100 IU/mL penicillin and 50 μ g/mL streptomycin at 37°C, 5% CO₂. Every other passage (130 000 cells/mL in T75), 200 μ g/mL zeocin was added for selection.

L929 assay

Cells were seeded in 96-wells flat bottom plates at 200.000 – 250.000 cells per well in 100 μ L and incubated for at least 6 hours at 37°C, 7% CO₂. Samples were prepared 5 times concentrated in growth medium containing 6 μ g/mL actinomycin D (Merck cas nr. 50-76-0; dissolved in 5% DMSO in PBS forming 1 mg/mL stocks) in a separate 96-wells plate. 20 μ L protein sample was added to the cells in duplicates reaching final cytokine concentrations of 6.4 pg/mL-100 ng/mL. Various controls with and without actinomycin D or TNF- α -6His/TNF- α -LPETGG-6His were placed on the same plate. Incubation for 19-20 hours at 37°C, 7% CO₂ was followed by 20 seconds centrifugation of the cells at room temperature at 1000g. The medium was removed using suction and replaced with 90 μ L medium and 10 μ L MTT (3-[4,5-dimethylthiazole-2-yl]-2,5-diphenyltetrazolium bromide, MP Biomedicals cat. 102227) in PBS (5 mg/mL). Cells were incubated for 3 hours at 37°C, 7% CO₂ before centrifugation (2 minutes, 500g at room temperature). Medium was removed by suction and the purple crystals were dissolved in 100 μ L DMSO per well. The absorbance at 570 nm was measured after 2 minutes incubation at 37°C, 500 rpm using the CLARIOstar of BMG Labtech.

HEK-Blue TNF- α assay

Protein samples were prepared 10 times concentrated in a separate 96-wells plate of which 20 μ L per well was transferred to the assay plate. HEK-BLUE TNF- α cells were seeded at 50 000 cells/well in 180 μ L medium. The final protein concentration ranged 78 – 5000 pg/mL. Cells were incubated for 18-20 hours at 37°C, 5% CO₂ whereafter 20 μ L medium was added to 180 μ L QUANTI-Blue in a new 96-wells plate and incubated at 37°C for 30 minutes – 3 hours. Absorbance at 655 nm was measured using the Bio-Rad iMARK Microplate reader.

Statistical analysis

All data were normalized using Microsoft Excel. All data are reported as mean \pm SD of n=3-7 independent experiments. Statistical analysis were carried out using R 4.1.0 (R Core Team, 2021), the base, graphics, methods, stats, utils, and ggplot2 packages. Parametric tests, one-way ANOVA, or Brown-Forsythe ANOVA tests were used for data with normal distribution, based on the homoscedasticity of the data, verified with Bartlett's test. If the omnibus test had a $p < 0.05$, unpaired t-test with or without Welch's correction (Welch's correction applied to different SD pairs) post hoc tests were performed based on the F-test. For data not normally distributed, non-parametrical Kruskal–Wallis comparisons were carried out with Mann-Whitney post hoc comparisons test. Results were considered significant when $p < 0.05$. Graphs were made using GraphPad Prism 8.4.3. Statistical analyses were performed with assistance of Dr. Diana Torres García.

References

- (1) Coley, W. B. The Treatment of Malignant Tumors by Repeated Inoculations of Erysipelas. With a Report of Ten Original Cases. *Am J Med Sci* **1893**, 105 (487).
- (2) Ehrlich, P. Über Den Jetzigen Stand Der Karzinomforschung. *Nederlandsch Tijdschrift voor Geneeskunde* **1909**, 5, 273–290.
- (3) Thomas, L. On Immunosurveillance in Human Cancer. *Yale J Biol Med* **1982**, 55 (3–4), 329–333.
- (4) Lacy, P.; Stow, J. L. Cytokine Release from Innate Immune Cells: Association with Diverse Membrane Trafficking Pathways. *Blood* **2011**, 118 (1), 9–18. <https://doi.org/10.1182/blood-2010-08-265892>.
- (5) Sethi, J. K.; Hotamisligil, G. S. Metabolic Messengers: Tumour Necrosis Factor. *Nat Metab* **2021**, 3 (10), 1302–1312. <https://doi.org/10.1038/s42255-021-00470-z>.
- (6) Jang, D. I.; Lee, A. H.; Shin, H. Y.; Song, H. R.; Park, J. H.; Kang, T. B.; Lee, S. R.; Yang, S. H. The Role of Tumor Necrosis Factor Alpha (TNF- α) in Autoimmune Disease and Current TNF- α Inhibitors in Therapeutics. *Int J Mol Sci* **2021**, 22 (5), 1–16. <https://doi.org/10.3390/ijms22052719>.
- (7) Montfort, A.; Colacios, C.; Levade, T.; Andrieu-Abadie, N.; Meyer, N.; Ségui, B. The TNF Paradox in Cancer Progression and Immunotherapy. *Front Immunol* **2019**, 10 (7). <https://doi.org/10.3389/fimmu.2019.01818>.
- (8) Carswell, E. A.; Old, L. J.; Kassel, R. L.; Green, S.; Fiore, N.; Williamson, B. An Endotoxin-Induced Serum Factor That Causes Necrosis of Tumors. *Proceedings of the National Academy of Sciences* **1975**, 72 (9), 3666–3670. <https://doi.org/10.1073/pnas.72.9.3666>.
- (9) Pennica, D.; Nedwin, G. E.; Hayflick, J. S.; Seeburg, P. H.; Derynck, R.; Palladino, M. A.; Kohr, W. J.; Aggarwal, B. B.; Goeddel, D. V. Human Tumour Necrosis Factor: Precursor Structure, Expression and Homology to Lymphotoxin. *Nature* **1984**, 312 (5996), 724–729. <https://doi.org/10.1038/312724a0>.
- (10) Budd, G. T.; Green, S.; Baker, L. H.; Hersh, E. P.; Weick, J. K.; Kent Osborne, C. A Southwest Oncology Group Phase II Trial of Recombinant Tumor Necrosis Factor in Metastatic Breast Cancer. *Cancer* **1991**, 68 (8), 1694–1695. [https://doi.org/10.1002/1097-0142\(19911015\)68:8<1694::AID-CNCR2820680806>3.0.CO;2-K](https://doi.org/10.1002/1097-0142(19911015)68:8<1694::AID-CNCR2820680806>3.0.CO;2-K).
- (11) Kimura, K.; Taguchi, T.; Urushizaki, I.; Ohno, R.; Abe, O.; Furue, H.; Hattori, T.; Ichihashi, H.; Inoguchi, K.; Majima, H.; Niitani, H.; Ota, K.; Saito, T.; Suga, S.; Suzuoki, Y.; Wakui, A.; Yamada, K. Phase I Study of Recombinant Human Tumor Necrosis Factor. *Cancer Chemother Pharmacol* **1987**, 20, 223–229. <https://doi.org/10.1007/bf00570490>.
- (12) Kahn, J. O.; Kaplan, L. D.; Volberding, P. A.; Ziegler, J. L.; Crowe, S.; Saks, S. R.; Abrams, D. I. IntraleSIONal Recombinant Tumor Necrosis Factor-Alpha for AIDS-Associated Kaposi's Sarcoma: A Randomized, Double-Blind Trial. *Journal of Acquired Immune Deficient Syndrome* **1989**, 2, 217–223.
- (13) Creagh, O.; Krementz, E. T.; Ryan, R. F.; Winblad, J. N. Chemotherapy of Cancer: Regional Perfusion Utilizing an Extracorporeal Circuit. *Annals of surgery* **1958**, 148 (4), 616–632. <https://doi.org/10.1097/00000658-195810000-00009>.
- (14) van Horssen, R.; ten Hagen, T. L. M.; Eggermont, A. M. M. TNF- α in Cancer Treatment: Molecular Insights, Antitumor Effects, and Clinical Utility. *Oncologist* **2006**, 11 (4), 397–408. <https://doi.org/10.1634/theoncologist.11-4-397>.
- (15) Lienard, D.; Ewalenko, P.; Delmotte, J. J.; Renard, N.; Lejeune, F. J. High-Dose Recombinant Tumor Necrosis Factor Alpha in Combination with Interferon Gamma and Melphalan in Isolation Perfusion of the Limbs for Melanoma and Sarcoma. *Journal of Clinical Oncology* **1992**, 10 (1), 52–60. <https://doi.org/10.1200/jco.1992.10.1.52>.
- (16) M Eggermont, A. M.; Schraffordt Koops, H.; Klausner, J. M.; R Kroon, B. B.; Schlag, P. M.; Danielle Li, I.; van Geel, A. J.; Hoekstra, H. J.; Meller, I.; Nieweg, O. E.; Kettelhack, C.; Ben-Ari, G.; Pector, J.-C.; Lejeune, F. J. Isolated Limb Perfusion with Tumor Necrosis Factor and Melphalan for Limb Salvage in 186 Patients with Locally Advanced Soft Tissue Extremity Sarcomas The Cumulative Multicenter European Experience. *Ann Surg* **1996**, 224 (6), 756–765. <https://doi.org/10.1097/00000658-199612000-00011>.
- (17) Grunhagen, D. J.; de Wilt, J. H. W.; Graveland, W. J.; van Geel, A. N.; Eggermont, A. M. M. The Palliative Value of Tumor Necrosis Factor α -Based Isolated Limb Perfusion in Patients with Metastatic Sarcoma and Melanoma. *Cancer* **2006**, 106 (1), 156–162. <https://doi.org/10.1002/cncr.21547>.
- (18) Lejeune, F. J.; Rliegg, C.; Lienard, D. Clinical Applications of TNF-Alpha in Cancer. *Curr Opin Immunol* **1998**, 10, 573–580. [https://doi.org/10.1016/s0952-7915\(98\)80226-4](https://doi.org/10.1016/s0952-7915(98)80226-4).
- (19) Creaven, P. J.; Plager, J. E.; Dupere, S.; Huben, R. P.; Takita, H.; Mittelman, A.; Proefrock, A. Phase I Clinical Trial of Recombinant Human Tumor Necrosis Factor. *Cancer Chemother Pharmacol* **1987**, 20, 137–144. <https://doi.org/10.1007/bf00253968>.
- (20) Selby, P.; Hobbs, S.; Viner, C.; Jackson, E.; Jones, A.; Newell, D.; Calvert, A. H.; Mcelwain, T.; Fearon, K.; Humphreys, J.; Shiga, T. Tumor Necrosis Factor in Man: Clinical and Biological Observations. *Br J Cancer* **1987**, 803, 808. <https://doi.org/10.1038/bjc.1987.294>.

- (21) Curnis, F.; Sacchi, A.; Borgna, L.; Magni, F.; Gasparri, A.; Corti, A. Enhancement of Tumor Necrosis Factor Alpha Antitumor Immunotherapeutic Properties by Targeted Delivery to Aminopeptidase N (CD13). *Nat Biotechnol* **2000**, *18*, 1185–1190. <https://doi.org/10.1038/81183>.
- (22) Herman, J. M.; Wild, A. T.; Wang, H.; Tran, P. T.; Chang, K. J.; Taylor, G. E.; Donehower, R. C.; Pawlik, T. M.; Ziegler, M. A.; Cai, H.; Savage, D. T.; Canto, M. I.; Klapman, J.; Reid, T.; Shah, R. J.; Hoffs, S. E.; Rosemurgy, A.; Wolfgang, C. L.; Laheru, D. A. Randomized Phase III Multi-Institutional Study of Tumor Necrosis Factor with Fluorouracil and Radiotherapy for Locally Advanced Pancreatic Cancer: Final Results. *Journal of Clinical Oncology* **2013**, *31* (7), 886–894. <https://doi.org/10.1200/JCO.2012.44.7516>.
- (23) Datta, R.; Rubin, E.; Sukhatme, V.; Qureshi, S.; Hallahan, D.; Weichselbaum, R. R.; Kufe, D. W. Ionizing Radiation Activates Transcription of the EGR1 Gene via CAR Elements. *Proceedings of the National Academy of Sciences* **1992**, *89* (21), 10149–10153. <https://doi.org/10.1073/pnas.89.21.10149>.
- (24) Borsi, L.; Balza, E.; Carnemolla, B.; Sassi, F.; Castellani, P.; Berndt, A.; Kosmehl, H.; Birò, A.; Siri, A.; Orecchia, P.; Grassi, J.; Neri, D.; Zardi, L. Selective Targeted Delivery of TNF α to Tumor Blood Vessels. *Blood* **2003**, *102* (13), 4384–4392. <https://doi.org/10.1182/blood-2003-04-1039>.
- (25) Liu, Y.; Cheung, L. H.; Marks, J. W.; Rosenblum, M. G. Recombinant Single-Chain Antibody Fusion Construct Targeting Human Melanoma Cells and Containing Tumor Necrosis Factor. *Int J Cancer* **2004**, *108* (4), 549–557. <https://doi.org/10.1002/ijc.11524>.
- (26) Lyu, M. A.; Kurzrock, R.; Rosenblum, M. G. The Immunocytokine ScFv23/TNF Targeting HER-2/Neu Induces Synergistic Cytotoxic Effects with 5-Fluorouracil in TNF-Resistant Pancreatic Cancer Cell Lines. *Biochem Pharmacol* **2008**, *75* (4), 836–846. <https://doi.org/10.1016/j.bcp.2007.10.013>.
- (27) De Luca, R.; Neri, D. Potentiation of PD-L1 Blockade with a Potency-Matched Dual Cytokine–Antibody Fusion Protein Leads to Cancer Eradication in BALB/c-Derived Tumors but Not in Other Mouse Strains. *Cancer Immunology, Immunotherapy* **2018**, *67* (9), 1381–1391. <https://doi.org/10.1007/s00262-018-2194-0>.
- (28) Hoogenboom, H. R.; Volckaert, G.; Raus, J. C. M. Construction and Expression of Antibody–Tumor Necrosis Factor Fusion Proteins. *Mol Immunol* **1991**, *28* (9), 1027–1037. [https://doi.org/10.1016/0161-5890\(91\)90189-Q](https://doi.org/10.1016/0161-5890(91)90189-Q).
- (29) Dakhel, S.; Lizak, C.; Matasci, M.; Mock, J.; Villa, A.; Neri, D.; Cazzamalli, S. An Attenuated Targeted-TNF Localizes to Tumors In Vivo and Regains Activity at the Site of Disease. *Int J Mol Sci* **2021**, *22* (18), 10020. <https://doi.org/10.3390/ijms221810020>.
- (30) Kaspar, M.; Zardi, L.; Neri, D. Fibronectin as Target for Tumor Therapy. *Int J Cancer* **2006**, *118* (6), 1331–1339. <https://doi.org/10.1002/ijc.21677>.
- (31) Weiss, T.; Puca, E.; Silginer, M.; Hemmerle, T.; Pazahr, S.; Bink, A.; Weller, M.; Neri, D.; Roth, P. Immunocytokines Are a Promising Immunotherapeutic Approach against Glioblastoma. *Sci Transl Med* **2020**, *12* (564), 2311. <https://doi.org/10.1126/scitranslmed.abb2311>.
- (32) Danielli, R.; Patuzzo, R.; Di Giacomo, A. M.; Gallino, G.; Maurichi, A.; Cutaia, O.; Lazzeri, A.; Fazio, C.; Miracco, C.; Giovannoni, L.; Elia, G.; Neri, D.; Maio, M.; Santinami, M. Intralesional Administration of L19-IL2/L19-TNF in Stage III or Stage IV M1a Melanoma Patients: Results of a Phase II Study. *Cancer Immunology, Immunotherapy* **2015**, *64* (8), 999–1009. <https://doi.org/10.1007/s00262-015-1704-6>.
- (33) Versteegen, R. M.; Rossin, R.; Ten Hoeve, W.; Janssen, H. M.; Robillard, M. S. Click to Release: Instantaneous Doxorubicin Elimination upon Tetrazine Ligation. *Angewandte Chemie - International Edition* **2013**, *52* (52), 14112–14116. <https://doi.org/10.1002/anie.201305969>.
- (34) Rossin, R.; van Duijnhoven, S. M. J.; ten Hoeve, W.; Janssen, H. M.; Kleijn, L. H. J.; Hoebe, F. J. M.; Versteegen, R. M.; Robillard, M. S. Triggered Drug Release from an Antibody–Drug Conjugate Using Fast “Click-to-Release” Chemistry in Mice. *Bioconjug Chem* **2016**, *27* (7), 1697–1706. <https://doi.org/10.1021/acs.bioconjchem.6b00231>.
- (35) Rossin, R.; Versteegen, R. M.; Wu, J.; Khasanov, A.; Wessels, H. J.; Steenbergen, E. J.; Ten Hoeve, W.; Janssen, H. M.; Van Onzen, A. H. A. M.; Hudson, P. J.; Robillard, M. S. Chemically Triggered Drug Release from an Antibody–Drug Conjugate Leads to Potent Antitumor Activity in Mice. *Nat Commun* **2018**, *9* (1), 1. <https://doi.org/10.1038/s41467-018-03880-y>.
- (36) Vilcek, J.; Lee, T. H. Tumor Necrosis Factor: New Insights into the Molecular Mechanisms of Its Multiple Actions. *J Biol Chem* **1991**, *266* (12), 7313–7316.
- (37) Garcia-Beltran, W. F.; Claiborne, D. T.; Maldini, C. R.; Phelps, M.; Vrbanc, V.; Karpel, M. E.; Krupp, K. L.; Power, K. A.; Boutwell, C. L.; Balazs, A. B.; Tager, A. M.; Altfeld, M.; Allen, T. M. Innate Immune Reconstitution in Humanized Bone Marrow–Liver–Thymus (HuBLT) Mice Governs Adaptive Cellular Immune Function and Responses to HIV-1 Infection. *Front Immunol* **2021**, *12*. <https://doi.org/10.3389/fimmu.2021.667393>.
- (38) Eck, M. J.; Sprang, S. R. The Structure of Tumor Necrosis Factor- α at 2.6 Å Resolution. *Journal of Biological Chemistry* **1989**, *264* (29), 17595–17605. [https://doi.org/10.1016/s0021-9258\(81\)71533-0](https://doi.org/10.1016/s0021-9258(81)71533-0).

- (39) Baeyens, K. J.; de Bondt, H. L.; Raeymaekers, A.; Fiers, W.; de Ranter, C. J. The Structure of Mouse Tumour-Necrosis Factor at 1.4 Å Resolution: Towards Modulation of Its Selectivity and Trimerization. *Acta Crystallogr D Biol Crystallogr* **1999**, *55* (4), 772–778. <https://doi.org/10.1107/S0907444998018435>.
- (40) Mukai, Y.; Shibata, H.; Nakamura, T.; Yoshioka, Y.; Abe, Y.; Nomura, T.; Taniai, M.; Ohta, T.; Ikemizu, S.; Nakagawa, S.; Tsunoda, S. ichi; Kamada, H.; Yamagata, Y.; Tsutsumi, Y. Structure-Function Relationship of Tumor Necrosis Factor (TNF) and Its Receptor Interaction Based on 3D Structural Analysis of a Fully Active TNFR1-Selective TNF Mutant. *J Mol Biol* **2009**, *385* (4), 1221–1229. <https://doi.org/10.1016/j.jmb.2008.11.053>.
- (41) Idriss, H. T.; Naismith, J. H. TNF and the TNF Receptor Superfamily: Structure-Function Relationship(s). *Microsc. Res. Tech* **2000**, *50*, 184–195. [https://doi.org/10.1002/1097-0029\(20000801\)50:3<184::AID-JEMT2>3.0.CO;2-H](https://doi.org/10.1002/1097-0029(20000801)50:3<184::AID-JEMT2>3.0.CO;2-H).
- (42) Armitage, R. J. Tumor Necrosis Factor Receptor Superfamily Members and Their Ligands. *Curr Opin Immunol* **1994**, *6* (3), 407–413. [https://doi.org/10.1016/0952-7915\(94\)90119-8](https://doi.org/10.1016/0952-7915(94)90119-8).
- (43) Fonda, I.; Kenig, M.; Gaberc-Porekar, V.; Pristovaek, P.; Menart, V. Attachment of Histidine Tags to Recombinant Tumor Necrosis Factor-Alpha Drastically Changes Its Properties. *The Scientific World Journal* **2002**, *2*, 1312–1325. <https://doi.org/10.1100/tsw.2002.215>.
- (44) Novy, R.; Drott, D.; Yaeger, K.; Mierendorf, R. Overcoming the Codon Bias of E. coli for Enhanced Expression. *Innovations* **2001**, No. 12, 4–6.
- (45) Aligent Technologies. *ArcticExpress RIL Competent Cells and ArcticExpress RP Competent Cells Instruction Manual*; 2015. www.genomics.agilent.com.
- (46) Ferrer, M.; Chernikova, T. M.; Yakimov, M. M.; Golyshin, P. N.; Timmis, K. N. Chaperonins Govern Growth of Escherichia Coli at Low Temperatures. *Nat Biotechnology* **2003**, *21* (11), 1266–1267. <https://doi.org/10.1038/nbt1103-1266>.
- (47) Spriestersbach, A.; Kubicek, J.; Schäfer, F.; Block, H.; Maertens, B. Purification of His-Tagged Proteins. In *Methods in Enzymology*; Academic Press Inc., 2015; Vol. 559, pp 1–15. <https://doi.org/10.1016/bs.mie.2014.11.003>.
- (48) Zhang, C.; Liu, Y.; Zhao, D.; Li, X.; Yu, R.; Su, Z. Facile Purification of Escherichia Coli Expressed Tag-Free Recombinant Human Tumor Necrosis Factor Alpha from Supernatant. *Protein Expr Purif* **2014**, *95*, 195–203. <https://doi.org/10.1016/j.pep.2013.12.012>.
- (49) InvivoGen. HEK-Blue™ TNF- α Cells. <https://www.invivogen.com/hek-blue-tnfa>.
- (50) Humphreys, D. T.; Wilson, M. R. Modes of L929 Cell Death Induced by TNF-Alpha and Other Cytotoxic Agents. *Cytokine* **1999**, *11* (10), 773–782. <https://doi.org/10.1006/cyto.1998.0492>.
- (51) InvivoGen. *QUANTI-Blue™ Solution*; 2020. <https://www.invivogen.com/quant-blue> (accessed 2023-03-17).
- (52) Vanlangenakker, N.; Bertrand, M. J. M.; Bogaert, P.; Vandenabeele, P.; vanden Berghe, T. TNF-Induced Necroptosis in L929 Cells Is Tightly Regulated by Multiple TNFR1 Complex I and II Members. *Cell Death Dis* **2011**, *2* (11), e230–e230. <https://doi.org/10.1038/cddis.2011.111>.
- (53) Sobell, H. M. Actinomycin and DNA Transcription. *Proceedings of the National Academy of Sciences* **1985**, *82* (16), 5328–5331. <https://doi.org/10.1073/pnas.82.16.5328>.
- (54) Mosmann, T. Rapid Colorimetric Assay for Cellular Growth and Survival: Application to Proliferation and Cytotoxicity Assays. *Journal of Immunological Methods* **1983**, *65* (1–2), 55–63. [https://doi.org/10.1016/0022-1759\(83\)90303-4](https://doi.org/10.1016/0022-1759(83)90303-4).
- (55) Mattson, G.; Conklin, E.; Desai, S.; Nielander, G.; Savage, M. D.; Morgensen, S. A Practical Approach to Crosslinking. *Mol Biol Rep* **1993**, *17*, 167–183. <https://doi.org/10.1007/BF00986726>.
- (56) Microbiologie-clinique. *HEPES buffer*. <https://microbiologie-clinique.com/hepes-buffer.html> (accessed 2023-03-16).
- (57) Lahav-van der Gracht, A. M. F. Bioorthogonal Deprotection Strategy to Study T-Cell Activation and Cross-Presentation, Leiden University, Leiden, 2020.

Supplementary Figures

Optimisation of purification of TNF- α , TNF- α -6His and TNF- α -LPETGG-6His *TNF- α -6His*

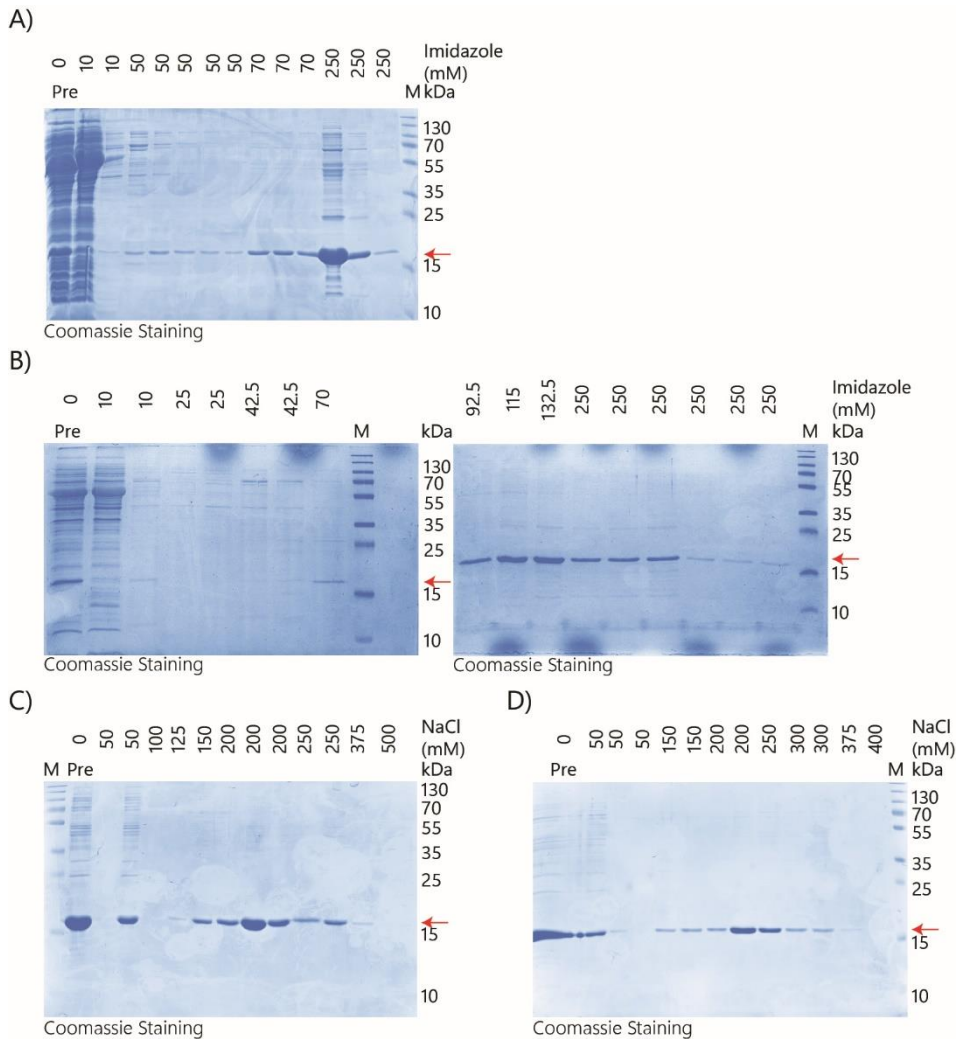


Figure S1 – Optimisation of TNF- α -6His purification

TNF- α -6His was isolated from the lysate using nickel beads following A) manual purification or B) automated purification. Washing and elution were performed with 0-250 mM imidazole in PBS. Following, TNF- α -6His was isolated using DEAE anion exchange based on TNF- α -6His negative charge in either C) 20 mM HEPES pH 7 or D) 20 mM HEPES pH 8. TNF- α -6His has a calculated pI ~5.64 causing it to be negatively charged. Therefore it would stick to the positively charged diethylaminoethyl (DEAE) resin. Washing and elution were performed with 0-500 mM NaCl. The red arrow indicate TNF- α -6His (~18 kDa).

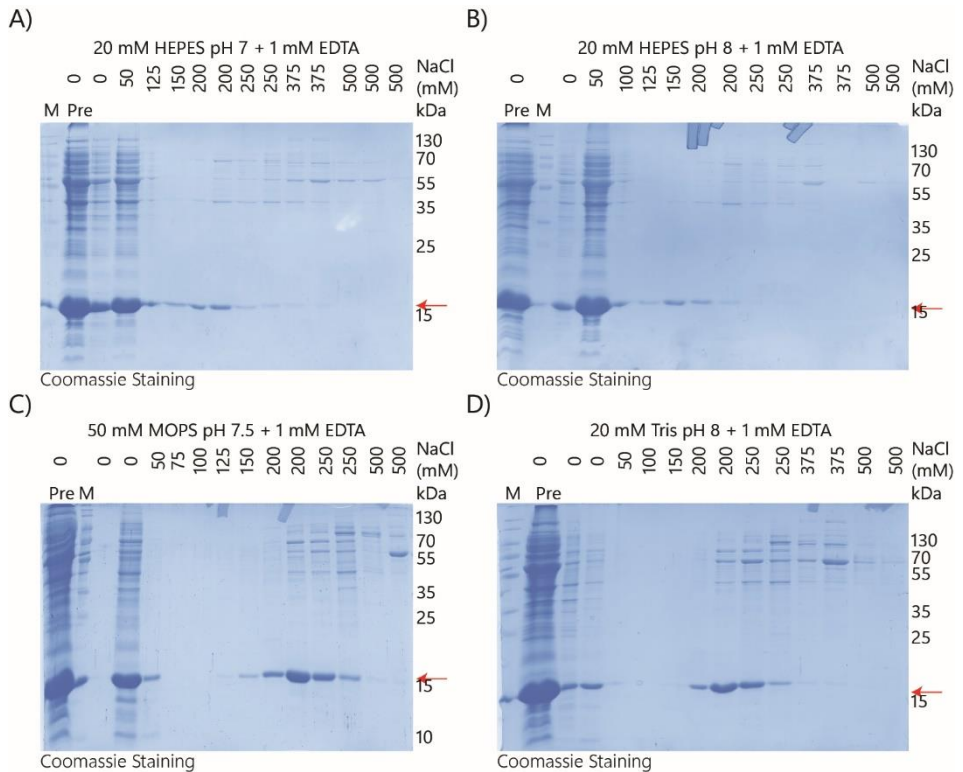
TNF- α 

Figure S2 - Optimisation of TNF- α purification using DEAE anion exchange.

TNF- α , produced in *E. coli* ArcticExpress (DE3) RP without purification tags, was purified using DEAE anion exchange. TNF- α was dissolved, together with 1 mM EDTA, in A) 20 mM HEPES pH 7, B) 20 mM HEPES pH 8, C) 50 mM MOPS pH 7.5 or D) 20 mM Tris pH 8. Under these conditions TNF- α is negatively charged ($pI \sim 4.96$) and therefore interacted with the positively charged column material. The red arrows indicate TNF- α (~ 17 kDa). Both HEPES buffer were not suitable for this purification while both MOPS- and Tris-based buffers were applicable.

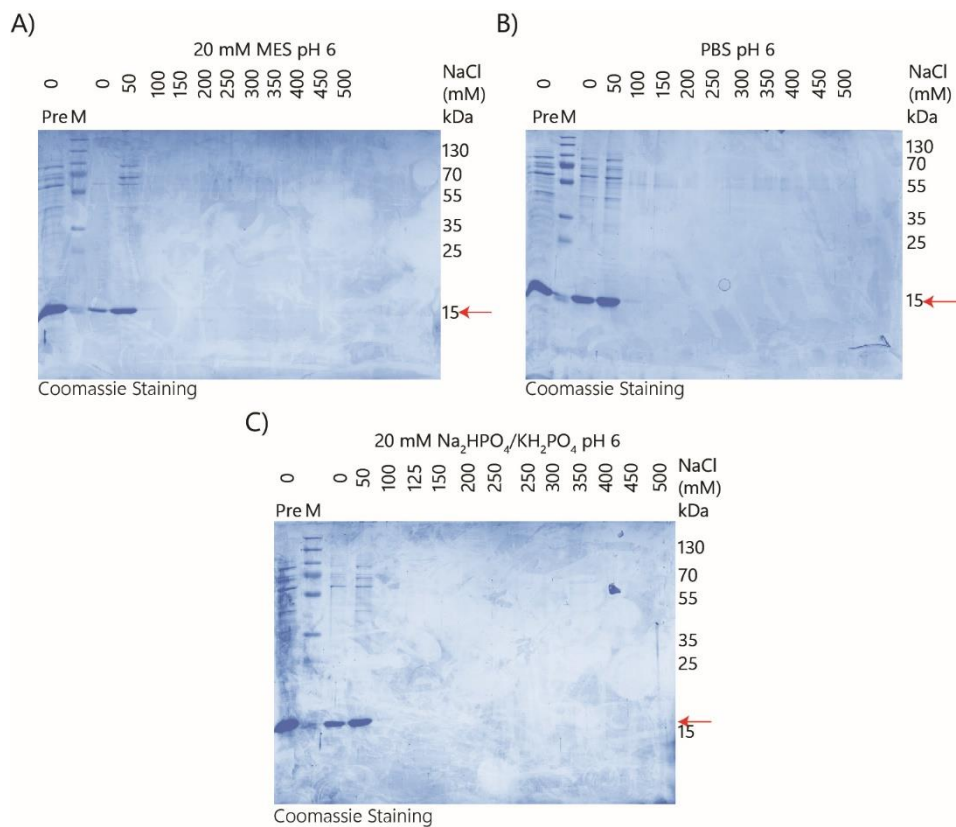
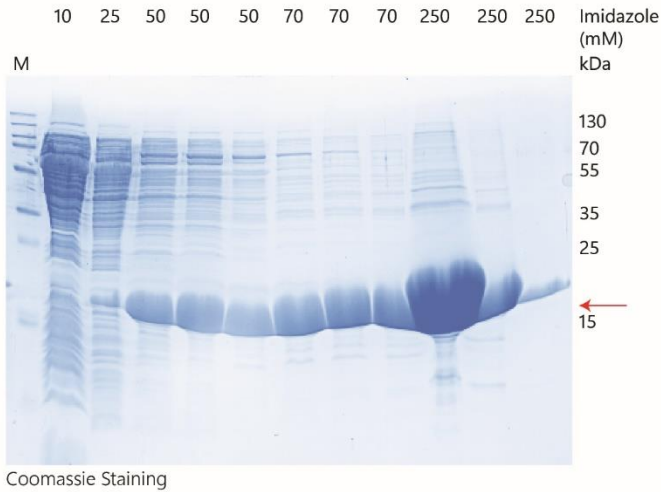


Figure S3 - Optimisation TNF- α purification using CM cation exchange.

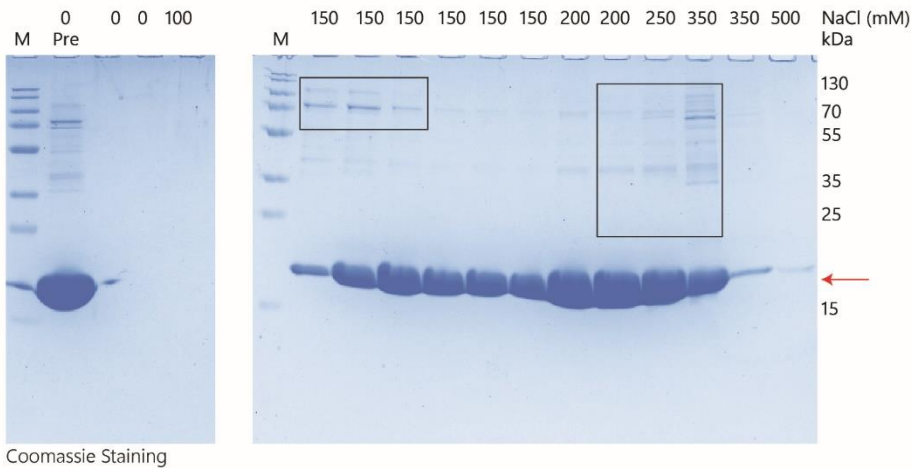
Anion exchange purified TNF- α was further purified using CM cation exchange. TNF- α was buffer exchanged to A) 20 mM MES pH 6, B) PBS pH 6 or C) 20 mM $\text{Na}_2\text{HPO}_4/\text{KH}_2\text{PO}_4$ pH 6. Under these conditions TNF- α is slightly positively charged ($pI \sim 4.96$) and therefore interacted with the negatively charged column material. The red arrows indicate TNF- α (~ 17 kDa).

TNF- α -LPETGG-6His

A)



B)

**Figure S4 - Purification of TNF- α -LPETGG-6His by nickel beads and DEAE anion exchange.**

TNF- α -LPETGG-6His was purified similar to TNF- α -6His purification by A) 6His-tag based purification using nickel beads and elution with 0-250 mM imidazole in PBS followed by B) anion exchange using a DEAE column in 20 mM HEPES pH 8 and 0-500 mM NaCl for elution. The red arrows indicate the molecular weight of TNF- α -LPETGG-6His (~19 kDa). The black boxes indicate some minor impurities after anion exchange.

Caging optimisation of TNF-α-6His

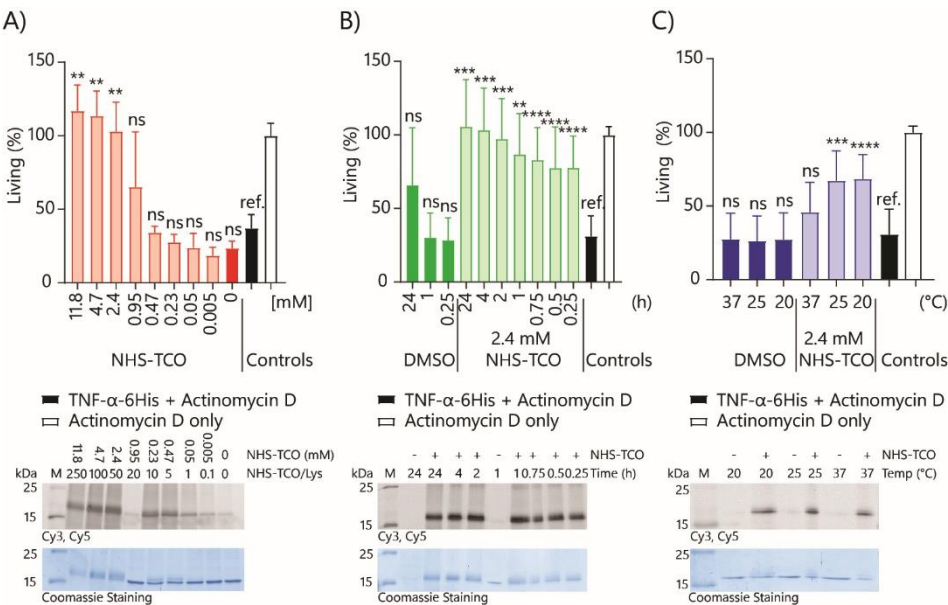


Figure S5 - Optimisation of TNF-α-6His caging analysed on L929 cells using a MTT-assay. TNF-α-6His (0.1 mg/mL or 5.4 μM) in 20 mM HEPES pH 8 was caged using A) various concentrations of **1** (N=4), B) for various periods of time (h) (N=4) and C) at various temperatures (°C) (N=5). Caging was compared with the TNF-α-6His + actinomycin D annotated as **ref.** (black, negative control). Actinomycin D served as a positive control (white). Bright colours indicate DMSO only samples and pastels the TCO-treated samples. In general, increased concentrations of **1** caused blocked TNF-α-6His activity. Increasing the caging time did not change the caging effect, but altered TNF-α-6His behaviour after 4 hours incubation. Lower caging temperature improved the caging. Overall caging increased cell viability compared to the negative control and the DMSO treated samples. Fluorescence at 570 nm of a slow-eliminating BODIPY-TMR tetrazine was used to visualise caging on SDS-PAGE. Coomassie staining below each graph indicated equal protein usage. Data were plotted as mean signal ± SEM. Significances are indicated as follows: * P<0.05; ** P<0.01; *** P<0.001; **** P<0.0001; ns is non-significant.

Caging optimisation of TNF- α -LPETGG-6His

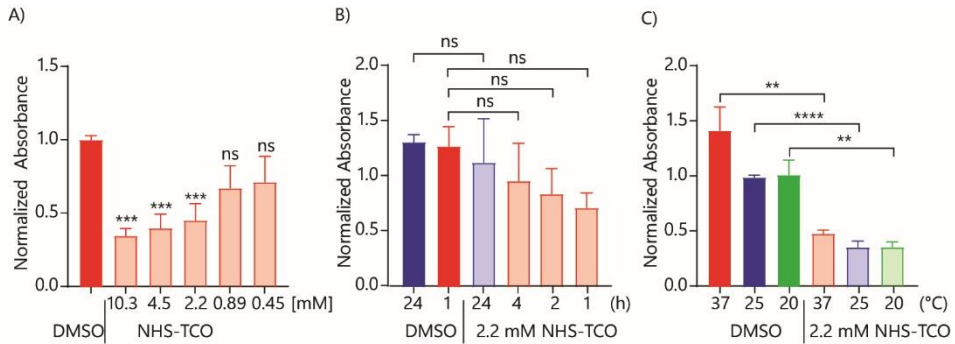


Figure S6 - Caging optimisation of TNF- α -LPETGG-6His analysed by ELISA.

TNF- α -LPETGG-6His (0.1 mg/mL or 5.1 μ M in 20 mM HEPES pH 8) was caged using A) various concentrations of **1** (N=4), B) for various periods of time (h) (N=3) and C) at various temperatures (°C) (N=3). The initial standard caging conditions were set at caging with 2.2 mM **1** (B,C) for 1 hour (A,C) at 37°C (A,B). Bright colours indicate DMSO only samples and pastels the TCO-treated samples. Caging was compared with the DMSO control which gave the highest signal. Colour groups indicate different conditions with respective DMSO controls. In general, the data showed a decreased signal upon caging, except when incubation time was varied. Data were plotted as mean signal \pm SEM. Significances are indicated as follows: * $P < 0.05$; ** $P < 0.01$; *** $P < 0.001$; **** $P < 0.0001$; ns is non-significant.

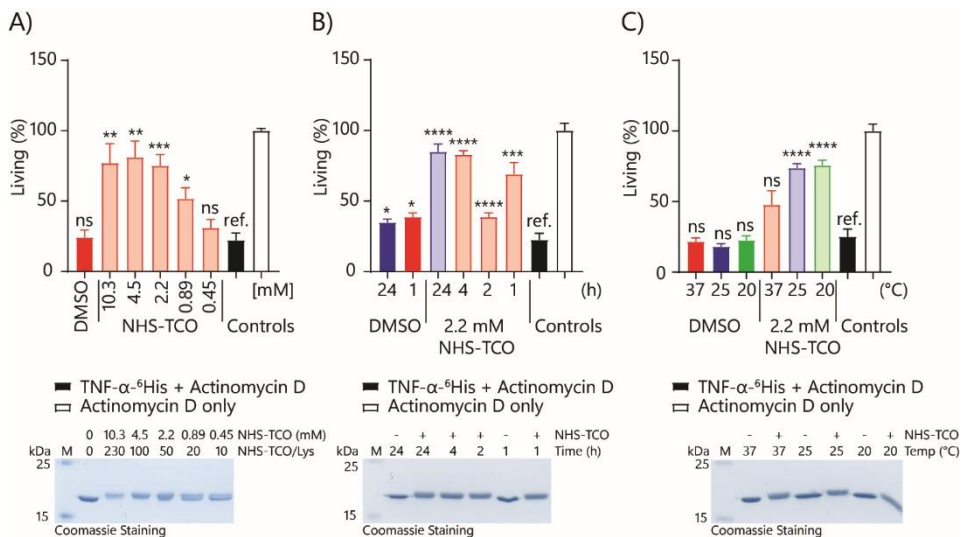


Figure S7 - Caging optimisation of TNF- α -LPETGG-6His analysed using L929 viability in MTT assays.

TNF- α -LPETGG-6His (0.1 mg/mL or 5.1 μ M in 20 mM HEPES pH 8) was caged using A) various concentrations of **1** (N=4), B) for various periods of time (h) (N=3) and C) at various temperatures (°C) (N=3). The initial standard caging conditions were set at caging with 2.2 mM **1** (B,C) for 1 hour (A,C) at 37°C (A,B). Caging was compared with the TNF- α -6His + actinomycin D annotated as **ref.** (black, negative control). Bright colours indicate DMSO only samples and pastels the TCO-treated samples. Colour groups indicate different conditions with respective DMSO controls. In general, the signal increased upon caging as expected. Coomassie staining below each graph indicates equal protein application. Data were plotted as mean signal \pm SEM. Significances are indicated as follows: * $P < 0.05$; ** $P < 0.01$; *** $P < 0.001$; **** $P < 0.0001$; ns is non-significant.

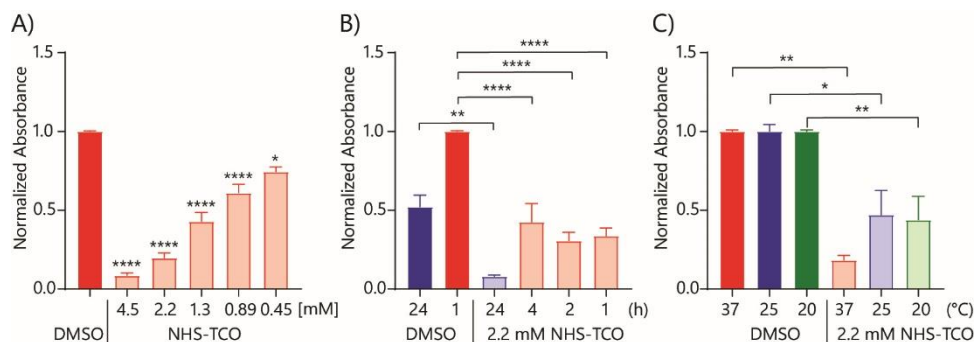


Figure S8 - Caging optimisation of TNF- α -LPETGG-6His assessed using HEK-Blue TNF- α cells.

TNF- α -LPETGG-6His (0.1 mg/mL or 5.1 μ M) was caged in 20 mM HEPES pH 8 using A) various concentrations of **1** (N=5), B) for various periods of time (h) (N=3) and C) at various temperatures ($^{\circ}$ C) (N=3). Bright colours indicate DMSO only samples and pastels the TCO-treated samples. Caging was compared with the DMSO control which gave the maximum signal. Colour groups indicate different conditions with respective DMSO controls. In general, caging reduced the signal compared to the DMSO control. An increased concentration of **1** caused TNF- α signalling inhibition. Longer incubation time altered TNF- α intrinsic activity. Incubation at higher temperatures prevented TNF- α from binding better than by caging at lower temperatures. Data were plotted as mean signal \pm SEM. Significances are indicated as follows: * $P < 0.05$; ** $P < 0.01$; *** $P < 0.001$; **** $P < 0.0001$; ns is non-significant.

4

Towards Crystallization of Recombinant HLA-DR1

Introduction

HLA-DR is a two-subunit class II MHC protein present on antigen-presenting cells.¹ It is used by these cells to present peptides derived from material they have taken up (9-25 amino acids in length²) to CD4+ T-helper cells.³ The recognition of such a peptide by a specific T-cell is one of the key moments in the initiation of the adaptive T-cell response that the body uses to clear pathogens in a highly specific manner, leading to the clearance of pathogens. This activation of T-cells by specific peptide-MHC complexes also underpins the memory response that forms the basis of both prophylactic and therapeutic vaccination strategies.⁴

The HLA-DR genetic locus is also very interesting, as it is the most widely divergent locus in the human genome. For example, for HLA-DR >1000 different allelic combinations exist^{5,6}, which can have a drastic effect on the susceptibility to given diseases of an individual. Diseases as rheumatoid arthritis^{7,8}, Crohn's disease⁹ and psoriasis¹⁰ have all been associated with specific HLA-DR1 haplotypes (DRB1*01:02¹¹, DRB1*01:03¹² and DRB1*01:02:DQB1*05:01¹³, respectively). It is believed that this high heterogeneity has evolved to allow the binding of a wide variety of peptide constructs, minimising the risk of 'escape mutants' during an infection. This hypothesis is based on the fact that the most heterogeneous area of the protein is in the peptide binding region, with many of the different allelic combinations able to bind different peptide sequence families.

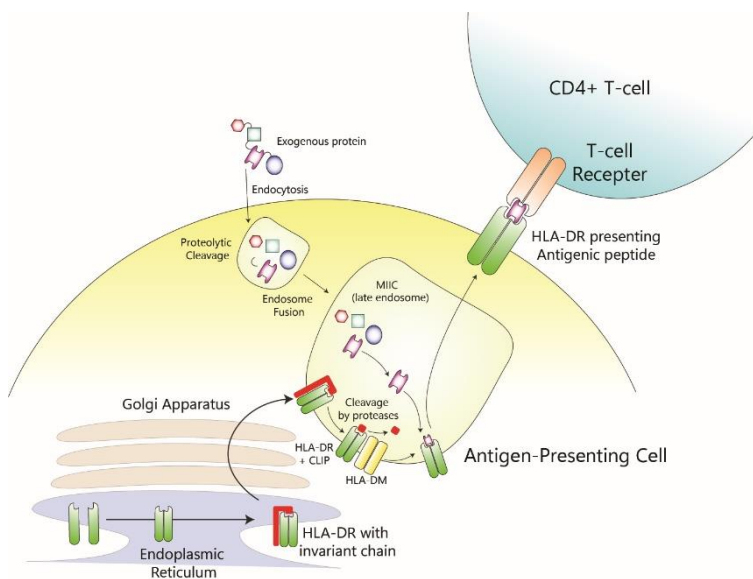


Figure 1 - Overview HLA-DR assembly and antigen presentation.

HLA-DR is assembled in the endoplasmic reticulum of an antigen-presenting cell where it then interacts with the invariant chain for stability. It is then translocated via the Golgi to a late endosome forming the MHC class II compartment (MIIC). The late endosome fuses with an endosome containing proteolytic products of an exogenous protein. After proteolytic cleavage of the invariant chain and with HLA-DM assistance, the CLIP peptide is replaced for an exogenous antigenic peptide. The loaded HLA-DR then travels to the cell surface where it presents the peptide to CD4+ T-cells.¹⁴

HLA-DR loads by and large peptides from endocytosed exogenous sources (**Figure 1**). The complex is first assembled in the endoplasmic reticulum (ER), where the peptide binding groove is occupied with the invariant chain (Ii). This is believed to have evolved to prevent the 'accidental' loading of endogenous ER-resident peptides. After assembly, the complex of MHC-II and the invariant chain is transferred through the Golgi apparatus to the late endosomal compartment called the "MHC class II compartment" (MIIC).¹⁴ Here, the endolysosomal proteases will cleave the Ii-chain down to a small set of peptides called the CLIP-fragments, which serves as a metastable 'placeholder peptide'. Upon encountering peptide fragments from exogenous sources through the fusion of vesicles with the MIIC, HLA-DM will replace the CLIP peptides with a high affinity exogenous peptide. This will lead to dissociation from HLA-DM followed by translocation to the cell surface where it can be sampled by CD4+ T-cells.¹⁴

The precise way in which such a MHC-II complexed with a foreign peptide binds to its cognate T-cell receptor, and how this subsequently leads to T-cell activation is not fully understood. No direct correlation between the binding constants of the receptor and the activation strength is apparent, furthermore, the kinetic binding parameters that allow the prediction of T-cell activation are unknown.¹⁵⁻¹⁸ This is particularly true for MHC-II restricted T-cell activation, where the number of tools to study the biology of this interaction at the molecular level is severely limited. This is due to the relative difficulty of its recombinant expression compared to that of the class-I HLAs.

One aspect that has been a research interest in the van Kasteren-group has been the question of whether the length of the antigenic pulse to which a specific T-cell is exposed affects the strength and nature of downstream T-cell activation. For this, methods were developed based on click-to-release chemistry (see also *Chapter 2-3*). This is a chemical reaction which can be used as a tool in the immunology to research processes taking place in the immune system. Earlier papers from the group have shown that for MHC-I restricted T-cell activation, this approach could be used to control the point in time at which a T-cell becomes activated, thereby controlling the interaction time between the T-cell receptor and the antigen. This was achieved by modifying the presented peptides with bioorthogonal protecting groups, such as organic azides^{19,20} and *trans*-cyclooctenyl carbamates (TCO, **Figure 2**).^{21,22}

Similar research was attempted for MHC-II or human leukocyte antigen class II (HLA-DR)²¹, but uncovering peptides that could be modified with TCO-groups to block their activity proved complicated, as the chemically modified peptides in some cases could still activate T-cells that were normally selective for the unmodified peptide.

A)

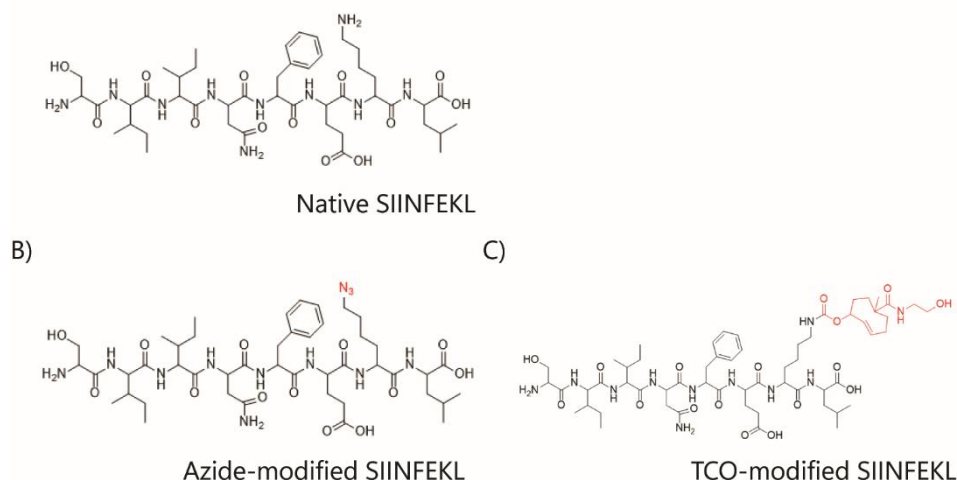


Figure 2 - Various forms of protected MHC-I epitope SIINFEKL.

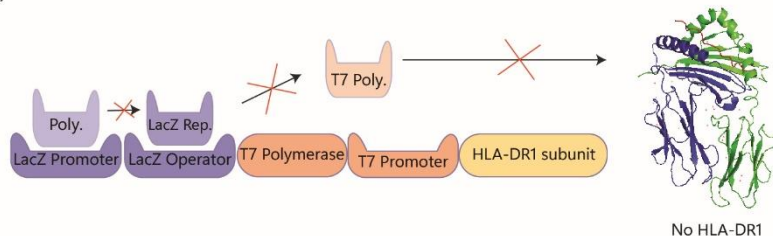
A) MHC-I cross-presented epitope SIINFEKL. B) Azide-modified SIINFEKL. The lysine is modified to having an azide group instead of a free amine. This abolished T-cell recognition.^{19,20} C) mbTCO-modified SIINFEKL. The lysine is modified with a TCO-ester, thereby abolishing T-cell recognition.²² The red groups indicate the protecting groups.

It was therefore decided that – to gain more insight in why TCO/azide blockade resulted in abolition of T-cell recognition for MHC-I and not MHC-II and to better assess the mechanisms by which this blockade could be achieved in future – crystallographic information would be insightful. If crystals of both MHC-classes could be obtained with various TCO/azide protected peptides and their wildtype cognate counterparts in the peptide binding groove, this could lead to new insights into any conformational factors in this difference in ‘cageability’. The attempted crystallisation of MHC-I was previously reported by A. van der Gracht²² This chapter described the expression and attempted crystallisation of MHC-II with MHC-II restricted peptides. It was chosen to use the human ortholog HLA-DR1 – a highly prevalent human MHC-II haplotype – with the view to begin the translation of the caging work to human systems.

HLA-DR1 has been recombinantly expressed before in bacteria^{23,24}, insect cells^{25–28} and mammalian cells²⁹, with each expression system having its own advantages, disadvantages and challenges. The individual subunits can be readily expressed in bacteria using the T7-lac system²³ present in the *E. coli* BL21 (DE3) pLysS strain used. The T7-lac system minimizes toxicity of the target protein by coordinated expression in the presence of lactose or a structural analogue (**Figure 3**).³⁰ For functional HLA-DR1, however, a heterodimer has to be formed which cannot be done by the bacteria and therefore has to be done afterwards via refolding. Frayser *et al.* and Günther *et al.* used a glutathione redox couple to gradually assist in HLA-DR1 refolding.^{23,24} Günther *et al.* managed to obtain milligrams yield, which proved enough to make crystal structures.²⁴ A major downside of the bacterial approach is that this variant will yield a non-glycosylated variant of HLA-DR1. It has been shown, however, that glycosylation of the complex can imbue critical properties on the complex by virtue of interacting with lectins on T-cells leading to their altered regulation.³¹

In addition, it has also been posed that glycosylation affects complex stability as well as localization and clustering at the cell surface.³²

A) - Lactose or IPTG



B) + Lactose or IPTG

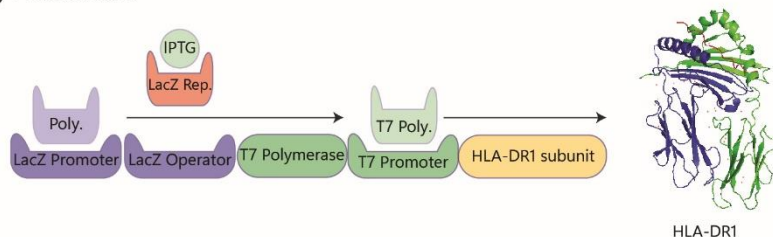


Figure 3 - Control on protein expression by the Lac operon.

A) In the absence of lactose or IPTG, the LacZ repressor binds the LacZ operator which prevents the expression of T7 polymerase and by that the expression of the protein of interest. B) In the presence of lactose or IPTG, the LacZ repressor is bound and unable to bind to the LacZ operator allowing T7 polymerase to be transcribed and translated. As a consequence, the gene of interest can be transcribed leading to the production of the protein of interest. Crystal structure was obtained from Murthy and Stern (PDB: 1AQD).

As an alternative production strategy – one that does yield glycosylated HLA-DR1 – is through expression in insect cells. These eukaryotic cells have the potential to correctly fold the individual subunits due to the presence, although different from human, post-translational modifications.³³ Pos *et al.* used *Sf9* cells and were able to yield pure HLA-DR1 for crystallization purposes.²⁶ This method of recombinant production was based on the Baculovirus Expression Vector System (BEVS), in which a donor vector encoding the gene of interest recombines with bacmid DNA.³⁴ This recombined bacmid DNA encodes the gene of interest and upon transfection of the insect cells is translated to a baculovirus, which can infect other insect cells and cause the production of the gene of interest³⁵ (**Figure 4**). Busch *et al.* were able to express HLA-DR1 in *Drosophila melanogaster* cells by normal transfection for a structural study regarding HLA-DM interactions.²⁸

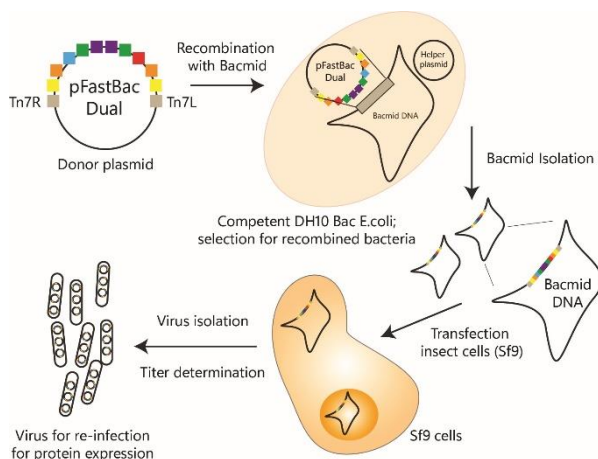


Figure 4 - Overview of Baculovirus Expression Vector System.

A donor vector (pFastBac dual) encoding the gene(s) of interest recombines via its transposon (Tn7) sequences with bacmid DNA in competent DH10Bac *E. coli*. Correctly recombined bacmid is isolated and used for transfection of insect cells (*Sf9*). In these cells the bacmid DNA is translated to virus DNA and secreted in virus particles. These particles can be used to transfect a (different) insect cell line for protein expression.

Finally, mammalian expression systems have also been used to express HLA-DR1. These expression systems yield correctly folded, glycosylated receptors. Szeto *et al.* showed that a HEK293s GnTI⁻ strain was ideal for this. Due to its mammalian origin, codon usage is the same and due to its simplified post-translational modifications, the probability of correct folding increases.³⁶ However, the disadvantage of this system is that it is more complex to get high-yielding expression, especially in the absence of serum (which is beneficial for later purification).³⁷ Also, even though post-translational modifications such as glycosylation are essential for folding, they can be troublesome for crystallization purposes, as the glycans introduced are highly heterogeneous and very flexible, making crystallization more difficult.³⁸ The use of strains with minimal glycosylation patterns such as HEK293s GnTI⁻³⁹, which lack N-acetyl-glucosaminyltransferase I only to produce predominantly Man5GlcNAc(2)N-glycans, is beneficial but not essential. Alternatively, treatment with glycan-cleaving enzymes such as protein N-glycanase F and endoglycosidases⁴⁰ post-expression can be used to simplify the carbohydrate diversity.

In this chapter, the expression of HLA-DR1 and the exchange of peptides using HLA-DM was explored with the aim of producing caged epitope-containing receptors. Three different expression systems were explored, bacterial-refolding, followed by an insect cell-baculovirus system, before finally producing the first crystals in a HEK293 expression system.

Results & Discussion

Bacterial expression

Construct design

First the expression of HLA-DR1 in *E. coli* was attempted. The two subunits of HLA-DR1 are both membrane anchored proteins. Gene constructs were therefore designed that omitted the *N*-terminal signal sequence, as this cannot be recognized in a bacterial system as such, and the C-terminal transmembrane and cytosolic region (**Supplementary Figure S1**). All constructs were cloned using restriction/ligation into a pET28(+)-vector under the control of the T7 promoter. This vector also has a C-terminal 6His-tag encoded in its backbone which could be used for purification purposes. Each subunit was designed with and without the presence of this tag (**Figure 5**).

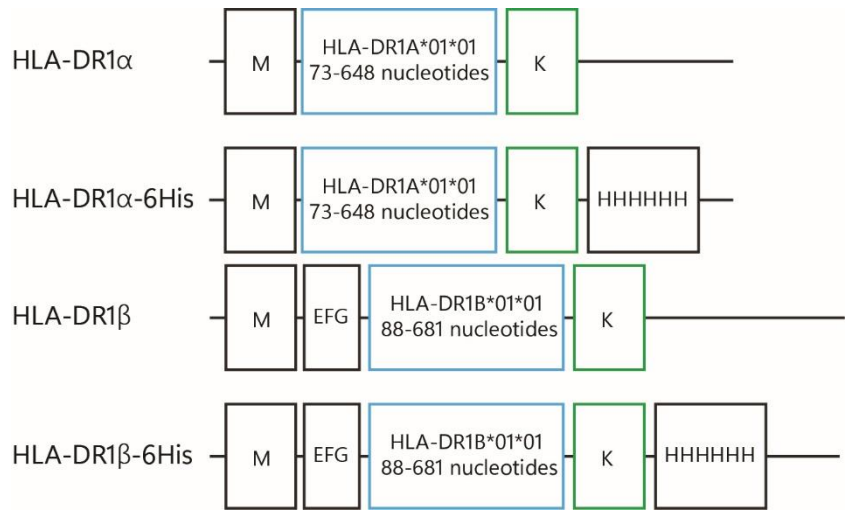


Figure 5 - Construct overview for bacterial expression.

Both HLA-DR1A*01*01 and HLA-DR1B*01*01 were expressed with or without C-terminal 6His-tag. The *N*-terminal secretion signal sequence was removed and replaced a methionine and the amino acids EFG for HLA-DR1β, respectively. The C-terminal transmembrane and cytosolic domain were removed as well for both subunits and replaced with one lysine (K).

Protein expression and purification

Even with the membrane bound part genetically removed, the HLA-DR1 subunits are still expressed in inclusion bodies.⁴¹ Commonly used bacterial strains for expressing (mammalian) proteins such as *Escherichia coli* (*E. coli*) BL21 (DE3), *E. coli* Rosetta-gami 2 (DE3) and *E. coli* ArcticExpress (DE3) RP were assessed. All make use of the T7-Lac system (**Figure 3**) to minimize the possible toxicity of the expressed protein.^{30,42} By addition of IPTG, subunit expression was initiated and assessed (**Figure 6**).

Expression in *E. coli* BL21 (DE3) (**BL**) did not result in significant amounts of either subunit (dark blue boxes, **Figure 6**), which was most likely due to the presence of some rare codons in the construct. The presence of the respective tRNAs in both *E. coli* Rosetta-gami 2 (DE3) (**RG**) and *E. coli* ArcticExpress (DE3) RP (**AE**) solved this problem as significant subunit presence (red boxes for HLA-DR1 α (-6His), yellow boxes for HLA-DR1 β (-6His)) was observed after induction of these strains. Western blot analysis using 6His-specific detection confirmed the presence of the 6His-tagged subunits in the samples after IPTG induction (**Figure 6E**). In particular in **Figure 6B** and **Figure 6C**, the same protein runs at different heights in the same gel. This could be due to not-fully denaturing conditions under which the gels were performed; the samples were cooked at 95°C for 5 minutes in Laemmli buffer containing β -mercaptoethanol, but in the absence of dithiothreitol (DTT). Therefore, some minor changes in protein migration distance could be observed. Another aspect could be that the current going through the gel was not equally distributed due to flaws in the running systems. The above mentioned rationale could also explain why in **Figure 6E** HLA-DR1 α -6His is running higher than HLA-DR1 β -6His, even though it is a bit larger in size.

Next, the individual subunits were purified. The bacteria were lysed using lysozyme and sonication to release their content.⁴³ The remaining inclusion bodies were washed to remove coprecipitated impurities, before dissolving them in PBS and loading them on nickel resin for His-tag based purification. After incubation the resin was washed with increasing concentrations of imidazole in PBS (10 mM to 250 mM) to elute the subunits individually (**Figure 7**). **Figure 7A** shows that HLA-DR1 α -6His was isolated, although the fractions containing the subunit were not completely pure. In contrast, HLA-DR1 β -6His (**Figure 7B**) was isolated with high purity.

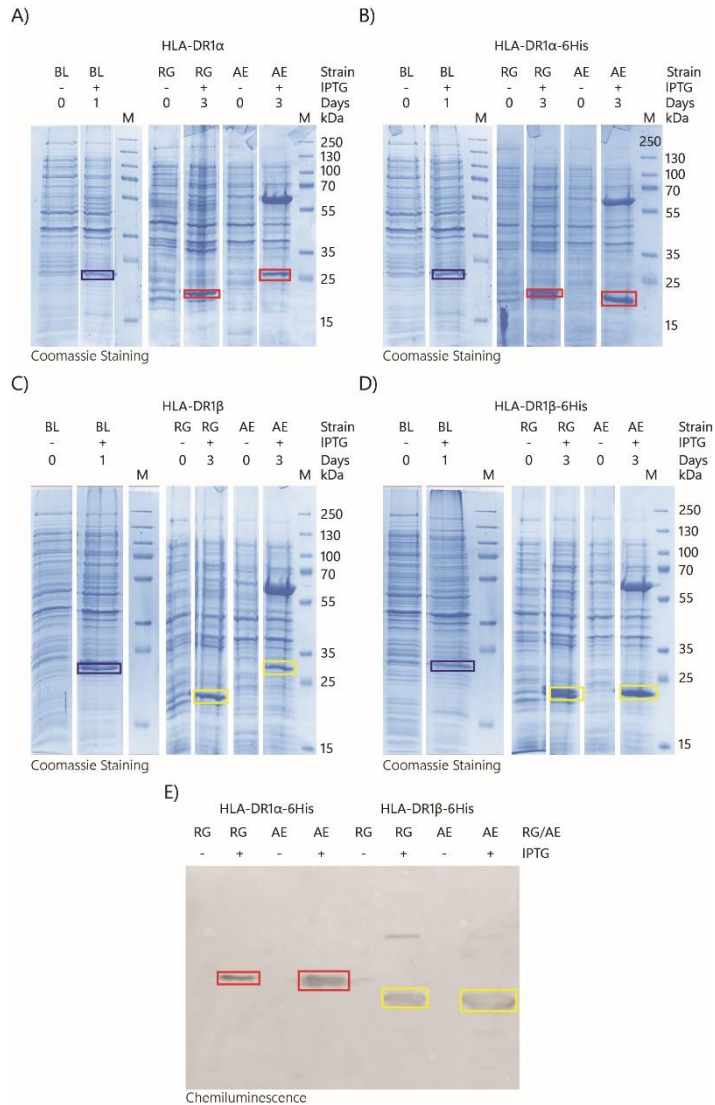


Figure 6 - Expression of HLA-DR1(-6His) subunits by *E. coli* BL21 (DE3), Rosetta-gami 2 (DE3) and *E. coli* ArcticExpress (DE3) RP.

HLA-DR1α and HLA-DR1β were cloned into a pET28a(+)-vector with or without a C-terminal 6His-tag encoded in frame. The vector was transformed in *E. coli* BL21 (DE3) (BL), *E. coli* Rosetta-gami 2 (DE3) (RG) and *E. coli* ArcticExpress (DE3) RP (AE) for regulated expression of the subunits by the addition of IPTG. Samples were taken before and after addition of IPTG. Samples were analysed on SDS-PAGE; A) HLA-DR1α, B) HLA-DR1α-6His, C) HLA-DR1β and D) HLA-DR1β-6His. Each subunit is 20-25 kDa. The dark blue boxes indicate the absence or minimal presence of the protein of interest. The red boxes indicate HLA-DR1α(-6His) and the yellow boxes indicate HLA-DR1β(-6His). E) 6His-tag based Western blot to confirm the expression of both HLA-DR1α-6His and HLA-DR1β-6His by both *E. coli* Rosetta-gami 2 (DE3) and *E. coli* ArcticExpress (DE3) RP by IPTG induction. The boxes indicate HLA-DR1α-6His (red) and HLA-DR1β-6His (yellow).

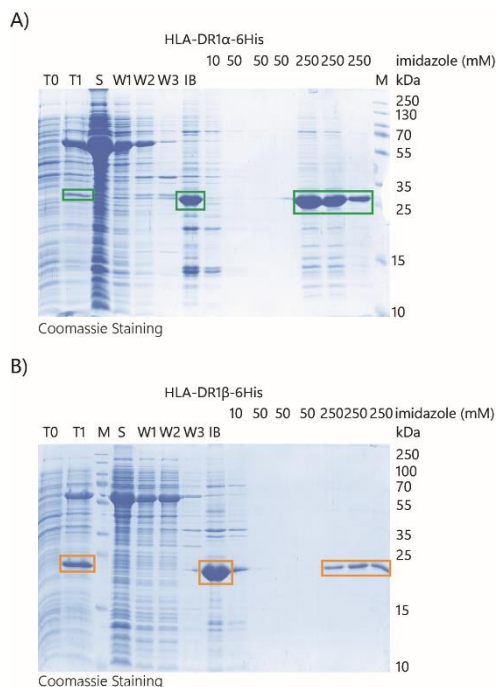


Figure 7 - 6His-tag-based purification of HLA-DR1 subunits expressed by *E. coli* ArcticExpress (DE3) RP.

A) HLA-DR1 α -6His and B) HLA-DR1 β -6His were expressed in *E. coli* ArcticExpress (DE3) RP and purified using nickel resin and imidazole in PBS. The various fractions were analysed by SDS-PAGE. The boxes indicate HLA-DR1 α -6His (green, A) and HLA-DR1 β -6His (orange, B) of about 20-25 kDa. T0: pre-induction; T1: post-induction; S: soluble fraction after lysis; W1-W3: washes of the inclusion bodies; IB: inclusion bodies.

The non-histagged subunits were also expressed and purified to get the native HLA-DR1 complex. Lysis was followed by separation of the soluble fraction from the membrane fraction including the inclusion bodies (IB).^{41,44} To minimize the impurities present in the IB several washes were performed using Triton X-100 containing buffer.^{44,45} After lysis, the IBs were dissolved in 8 M urea in 20 mM Tris with pH 8 or pH 9 for HLA-DR1 α and HLA-DR1 β , respectively. Further purification was done based on the intrinsic charge of each subunit at a certain pH. The calculated pI-values of unfolded HLA-DR1 α and HLA-DR1 β were determined to be 4.7 and 6.3, respectively. As each subunit was dissolved and unfolded completely after bacterial lysis in a urea/Tris buffer with pH 8 and pH 9 for HLA-DR1 α and HLA-DR1 β , respectively, the overall charge of each subunit was negative. Therefore, a strong anion exchange was applied to purify each of these subunits separately (**Figure 8**).

The solubilized IBs were loaded onto a Q-column, which is modified with positively charged quaternary amino groups. Various concentrations of NaCl were used to elute the subunits (red and yellow boxes). After this, the HLA-DR1 α purity was significantly improved as the ratio impurities/subunit was rather low (**Figure 8A**). For HLA-DR1 β , this ratio was rather higher (**Figure 8B**), suggesting that some additional purifications may be necessary.

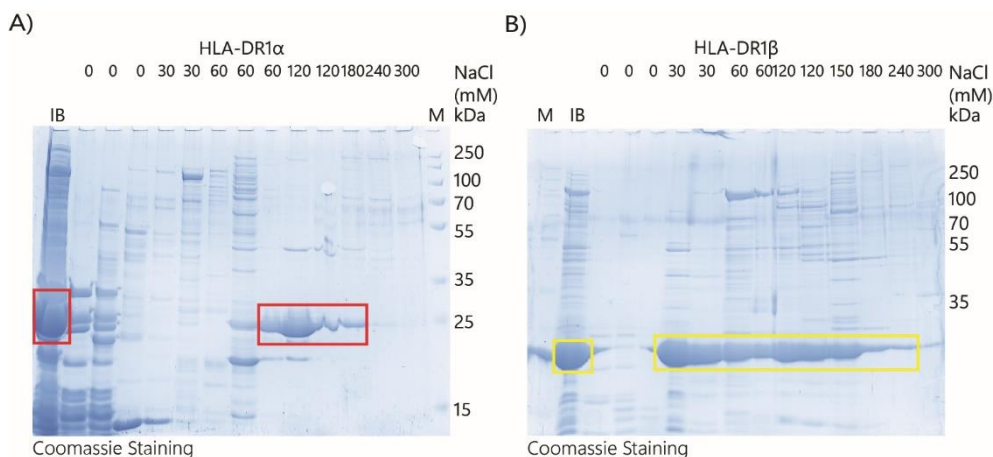


Figure 8 - HLA-DR1 purification by strong anion exchange.

HLA-DR1 α (A) and HLA-DR1 β (B) were purified from *E. coli* ArcticExpress (DE3) RP by lysis via lysozyme and sonication. Following, the subunits were dissolved in an 8 M urea solution in 20 mM Tris pH 8 or pH 9 for HLA-DR1 α (A) and HLA-DR1 β (B), respectively. The boxes indicated HLA-DR1 α (red) and HLA-DR1 β (yellow) which are 20-25 kDa.

HLA-DR1 refolding

Two methods of refolding were attempted, both using the glutathione redox couple to assist in the process.^{23,46} The reported methods differed in the ratio between this redox couple and the amount of HLA-DR1 subunits. Refolding was assessed using native PAGE, 6His-specific Western blot and SDS-PAGE (**Supplementary Figure S2**). The latter was possible due to the SDS-resistance of HLA-DR1 at SDS concentrations applied in SDS-PAGEs (0.2-0.5%).⁴⁷ Both reduced (by boiling and β -mercaptoethanol presence) and non-reduced samples were analysed and the folded HLA-DR1 could be identified as a band that disappeared upon reduction. Some bands (red arrows in **Figure S2A-B**) seemed to show this behaviour. However, assessment via native PAGE and 6His-specific Western blot (**Figure S2C**) did not confirm this to be HLA-DR1 complex. Optimising the refolding conditions (**Table 1**) did not result in better complex formation (data not shown).

Even though both refolding methods showed minor band formation upon refolding, the actual presence of correctly folded HLA-DR1 could not be confirmed. Therefore, alternative methods involving insect cell expression or mammalian expression described in literature were pursued next.

Table 1 - Overview refolding optimisation protocols.

Refolding was performed based on research done by Büchner *et al.*⁴⁶ and Frayer *et al.*²³. The protocol based on work of Lahav-van der Gracht was an optimisation in itself.

Origin Method	Buffer and conditions	Adaptations for optimisation
Büchner <i>et al.</i> ⁴⁶	100 mM Tris pH 8, 400 mM L-arginine, 2 mM EDTA, 5 mM reduced glutathione, 0.5 mM oxidized glutathione, 1.0 μ M per subunit in urea + 10 μ M peptide ISQ 24 hours at 4°C	Change subunit concentration; 1.0 μ M – 5.0 μ M
		Increase incubation time to 40 hours
Frayer <i>et al.</i> ²³	20 mM Tris, 25% (w/v) glycerol, 0.5 mM EDTA, 3 mM reduced glutathione, 0.3 mM oxidized glutathione pH 8.5 80 nM per subunit in urea + 0.5 μ M peptide ISQ 3 days at 4°C	Increase peptide concentration to 10 μ M
		Reduce subunit concentration to 13 nM
Lahav-van der Gracht ²²	100 mM Tris, 0.07 g/L L-arginine, 5 mM reduced glutathione, 0.5 mM oxidized glutathione, 2 mM EDTA, 1 mM PMSF 1:2 ratio between subunits in urea + 60 μ M peptide ISQ Sequential addition of subunits over 3 days, 1 day additional incubation at 4°C	Not further pursued

Insect cell expression

Insect cell expression has also been reported for HLA-DR expression.⁴⁸ Here, an attempt was made to use *Sf9* insect cells to produce a baculovirus which encodes both subunits of HLA-DR1 under two separate promoters. Two separate promoters were used to allow for transfection with one bacmid construct instead of two to introduce both subunits. The use of two promoters also prevents competition for het polymerase used by these promoters, resulting in (almost) equal protein expression of each subunit from one construct. This virus was then used to infect *High Five* insect cells which are commonly used for the actual protein expression.^{49,50}

Construct formation and virus production

The expression and dimerization of two subunits simultaneously has been reported in insect cells.⁵¹ To recapitulate this, the pFastBac dual vector was used⁵², which encodes for two antiparallel promoters (P10 and polyhedrin (PH)) that are initiated by different polymerases (**Figure 9**). The promoter is followed by a secretion signal sequence (gp67) which causes the protein of interest to be exported from the insect cell to the medium. The gp67 sequence was then followed by the gene of interest – HLA-DR1A*01:01 or HLA-DR1B*01:01. For detection and purification purposes, each gene of interest was provided with a C-terminal tag, a dual-Strep-tag for the P10 promoter and a 6His-tag for the PH promoter. To remove these tags after purification a tobacco etch virus protease (TEV) recognition site was placed between the gene of interest and this tag (**Figure 9**). The promoters, secretion sequences, cleavage sites, tags and the genes of interest, were flanked by transposon sequences (Tn7L and Tn7R) which allowed for recombination with bacmid DNA via het BEVS system described in the introduction (**Figure 4**, **Figure 10A**).

Besides the HLA-DR1 subunits, the gene for YFP was also present on the bacmid, which was used to determine whether transfection and later on infection were accomplished (**Figure 10B**). The presence of the genes for the individual HLA-DR1 subunits without transmembrane and cytosolic parts was confirmed by PCR (**Figure 10C**).

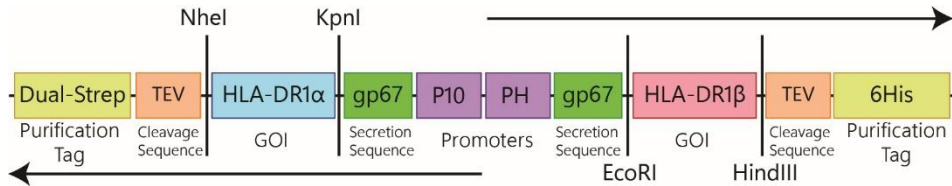


Figure 9 - Construct design between the transposons for HLA-DR1 expression by insect cells.

Vector pFastBac Dual (pFastBac_CSCH) was designed as follows: two anti-parallel promoters, P10 and polyhedrin (PH) were followed each with a secretion sequence (gp67), followed by the gene of interest (GOI), a cleavage sequence (TEV) and a purification tag, dual-Strep-tag and 6His-tag, respectively. The restriction sites and the respective enzymes are indicated as well. The construct could be designed with one GOI (HLA-DR1α or HLA-DR1β) or two. After expression and purification, the subunits or complex could be purified based on the tags, which could afterwards be removed by using tobacco etch virus (TEV) protease. Vector pFastBac Dual encodes gentamycin and ampicillin resistance genes for transfection into bacteria.

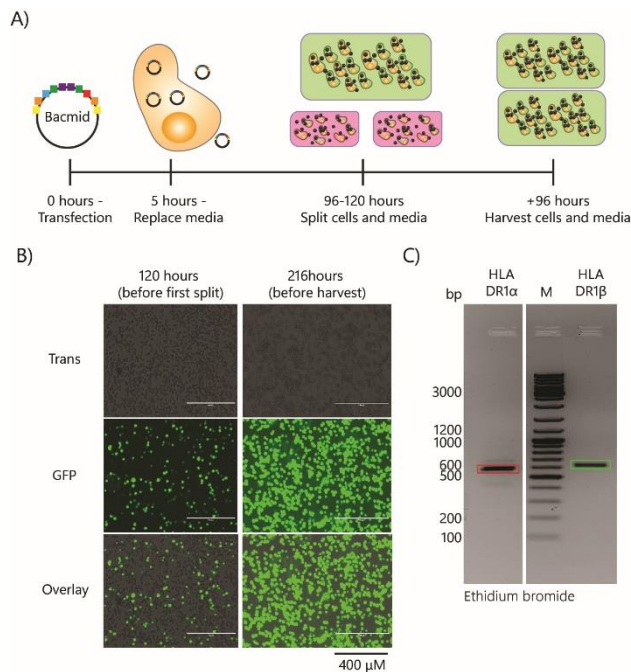


Figure 10 - Baculovirus generation encoding both subunits of HLA-DR1.

A) Schematic overview of baculovirus generation encoding both subunits of HLA-DR1; pFastBac dual vector recombines using transposon regions with bacmid DNA to transfer the genes of both subunits. The bacmid was used for transfection of adherent *Sf9* cells at low confluence. Splitting the transfected *Sf9* cells resulted in higher virus titers. B) Microscopic overview of protein expression (YFP) during virus co-incubation (10 times magnification). C) Presence of genetic code for each HLA-DR1 subunit was confirmed using PCR. The red box indicate HLA-DR1α and the green box indicates HLA-DR1β.

After virus titer determination, the baculovirus was used to infect both *Sf9* adherent and suspension cells and *High Five* cells. Although, *Sf9* cells are not optimised for recombinant protein expression, some HLA-DR1 expression was observed. Western blot analysis of expression in *Sf9* cells following harvest, virus isolation and lysis suggested the presence of the individual subunits (red and blue boxes at 30-35 kDa) of HLA-DR1 and some signs of the formed complex (yellow box at 70 kDa) were also observed (**Supplementary Figure S3** and **Figure S4**). However, these subunits and the complex remained in the membrane fraction after various lysis methods (data not shown), making it extremely hard to isolate them in a correctly folded state.

Expression in *High Five* cells (**Figure 11**) showed no clear overexpression of the individual HLA-DR1 subunits, or of the complex. The Western blot analysis based on the dual-Strep tag and 6His-tag (**Figure 11**) confirmed signs of HLA-DR1 subunits expression, although most of the signal was observed in the membrane fraction. Due to these difficulties with the expression, the insect cell system was abandoned and alternative ways of expression were pursued.

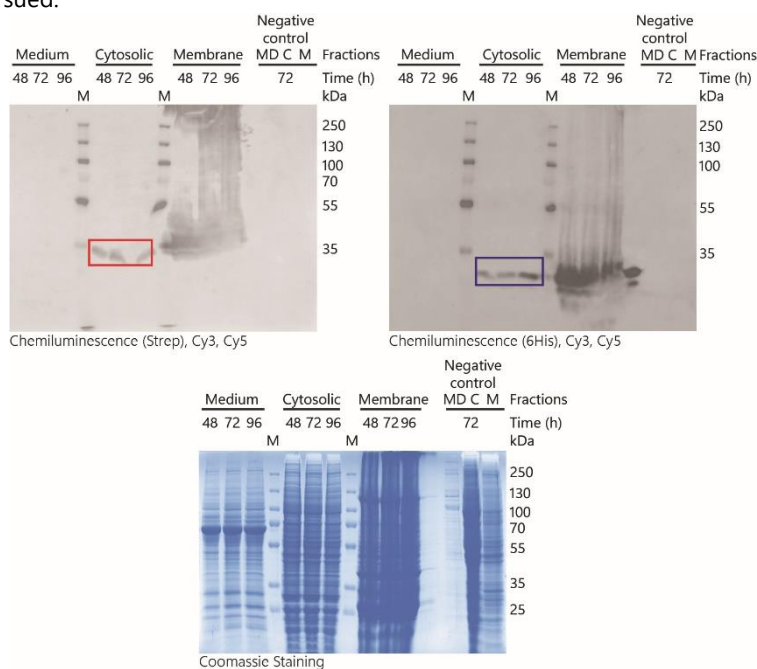


Figure 11 - HLA-DR1 expression by *High Five* insect cells analysed by Western blot and coomassie staining. *High Five* insect cells were infected with HLA-DR1 encoding baculovirus and incubated for 2-4 days after which the cells were separated from the medium (MD), followed by lysis of the cell pellet resulting in a cytosolic (C) and membrane (M) fraction. Samples of each day were analysed using dual-Strep and 6His-specific antibodies for Western blot visualisation of HLA-DR1 α (30.97 kDa) and HLA-DR1 β (25.75 kDa), respectively. The red and blue box indicated monomeric HLA-DR1 α and HLA-DR1 β , respectively. No clear sign of (correctly) folded HLA-DR1 could be observed.

Mammalian expression

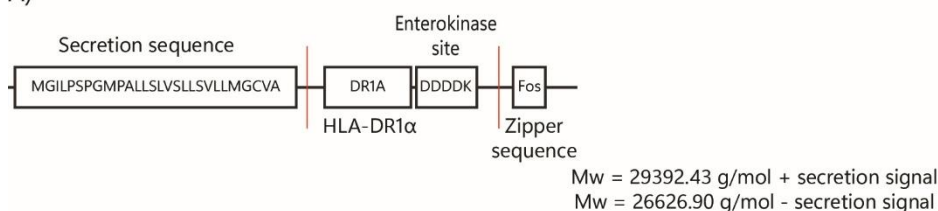
Expression system

As expression by bacteria and insect cells did not result in (significant yields of) correctly folded HLA-DR1, a mammalian expression system was explored. There are various mammalian cell lines that are used for protein expression of which CHO cells^{53,54} and the HEK293⁵⁵ expression system are the most commonly used. Szeto *et al.*⁵⁵ have described the expression of HLA-DR1.⁵⁶ They used HEK293s GnT1⁻ cells, which lack *N*-acetylglucosaminyltransferase I (GnT1).⁵⁷ The resulting proteins are therefore produced with predominantly Man5GlcNAc(2)N-glycans.³⁹

Construct design

The two plasmids encoding HLA-DR1 α *01:01 or HLA-DR1 β *01:01 were kindly provided by Prof. Dr. Stephanie Gras (**Figure 12, Supplementary Figure S5**), as were the protocol for expressing in and purifying the protein from HEK293s GnT1⁻ cells. The genes and tags were inserted in the pHL-SEC vector which encodes an *N*-terminal secretion signal sequence to allow for transport out of the cell. At the C-terminus of both genes an enterokinase site (DDDDK)⁵⁸ was encoded to remove the elements of the Fos/Jun leucine zipper and the purification tag before crystallization. The two subunits were designed to recombine and fold assisted by a Fos/Jun leucine zipper.⁵⁹ HLA-DR1 α encodes the Fos part C-terminally of the enterokinase sequence (**Figure 12A**). HLA-DR1 β was expressed together with the CLIP-peptide, which was encoded *N*-terminally from HLA-DR1 β followed by a linker sequence and a factor Xa site. Factor Xa can cleave off the peptide to allow for other peptides to be incorporated.⁶⁰ The CLIP-peptide was *N*-terminally connected to a Strep-tag for isolation purposes. Furthermore, the HLA-DR1 β constructs encodes the Jun part followed by a BirA biotinylation site and a 7His-tag for purification purposes. This is all upstream from the enterokinase site (**Figure 12B**).

A)



B)

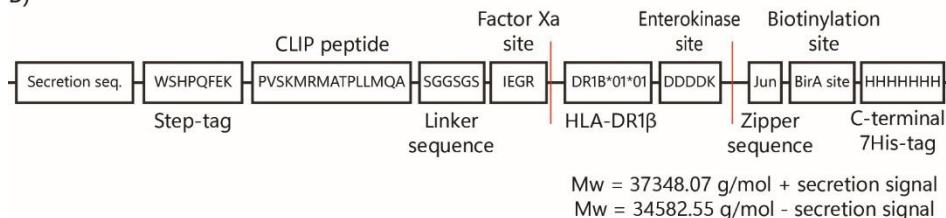


Figure 12 - Overview constructs HLA-DR1.

A) HLA-DR1A*01*01 was designed with a *N*-terminal secretion sequence and a C-terminal enterokinase sequence followed by the Fos protein sequence for the leucine zipper. B) HLA-DR1B*01*01 was designed with the same *N*-terminal secretion sequence as HLA-DR1 α followed by a Strep-tag and the CLIP peptide. A flexible linker and a factor Xa site separates this peptide from HLA-DR1 β . A C-terminal enterokinase site allows for the cleavage of the Jun protein, as part of the leucine zipper, the BirA biotinylation site and a 7His-tag.

HLA-DR1 was isolated from the medium using its C-terminal 6His-tag (**Figure 13E**). HLA-DR1 containing medium was loaded onto nickel resin, incubated for 2 hours at 4°C and eluted with various concentrations of imidazole on ice. Analysis by SDS-PAGE indicated the fractions containing both subunits of HLA-DR1 and these fractions were combined and concentrated for further purification.

For crystallography the concentrated fractions were further purified using size exclusion chromatography (SEC). Fractions were collected and based on absorbance detection at 280 nm and protein-containing fractions were analysed by SDS-PAGE (**Figure 14**). Pure fractions containing only both subunits were combined and concentrated for further experiments (red box).

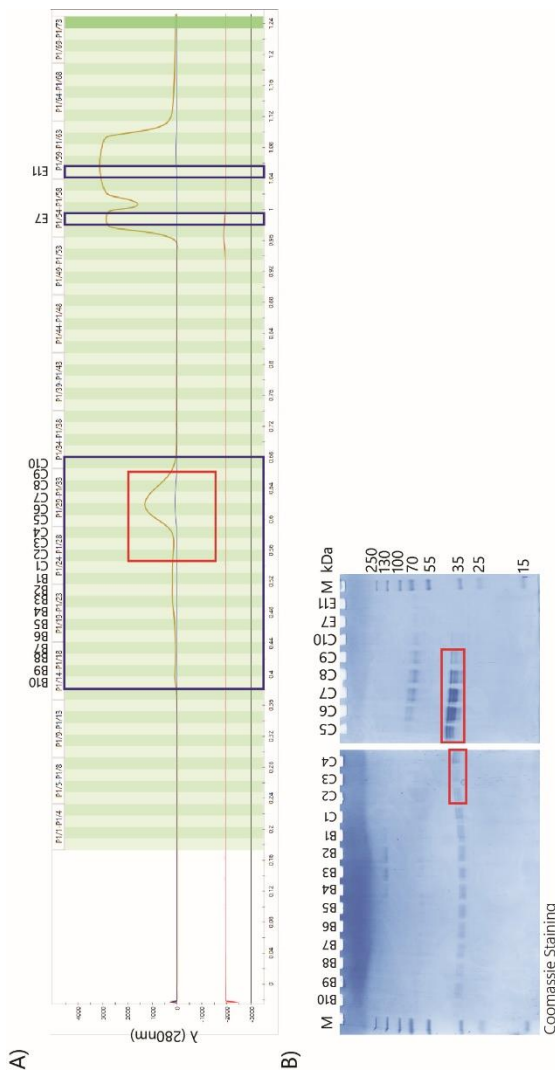


Figure 14 – HLA-DR1 purified using size exclusion chromatography (SEC).

A) HLA-DR1 was purified using an HiLoad Superdex 16/600 200 µg column equilibrated with 10 mM Tris/150 mM NaCl pH 8. The fractions indicated in the blue boxes were analysed on SDS-PAGE (B). The red boxes indicate the fractions containing HLA-DR1 and correspond to the fractions depicted by the red boxes in (A). The individual subunits are about 35-40 kDa.

Within cells HLA-DM is essential for the removal of the CLIP peptide (which stabilizes HLA-DR1 in the endoplasmic reticulum) and the replacement thereof with a higher affinity peptide.¹⁴ Therefore, to allow for *in vitro* exchange of peptides in HLA-DR1, HLA-DM was expressed in a similar fashion as HLA-DR1. pHL-SEC-vectors encoding either the HLA-DM α or HLA-DM β chain – both provided by Prof. Dr. Stephanie Gras – were used to transfect HEK293s GnTI⁻ cells (**Supplementary Figure S6**). Following, similar 6His-tag based and SEC purification were performed as with HLA-DR1. The results thereof are given in **Supplementary Figure S6**. Similar results regarding purity were obtained.

Protein analysis and initial crystallization

After concentrating the fractions of both proteins, samples were loaded onto a native page to check for purity (**Figure 15A**). Both protein complexes were pure and present in the same folded state, indicated by the presence of only one band on the native page. The thermostability of HLA-DR1 was also determined by measuring tryptophan emission both at 330 nm (unfolded state) and 350 nm (folded state) while steadily heating the sample (**Figure 15B**).⁶¹ According to the resulting spectrum, unfolding took place in two steps; the first step around 60°C, and the second step at 90°C. This is comparable with data published by Szeto *et al.*²⁹

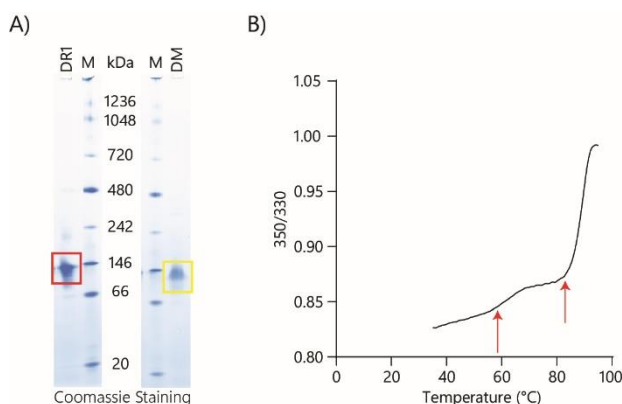


Figure 15 - Native page analysis of HLA-DR1 and HLA-DM and thermostability analysis of HLA-DR1.

A) HLA-DR1 (red box) and HLA-DM (yellow box) purity analysed by native page. Both protein complexes were pure indicated by the presence of one band. B) Thermostability analysis of HLA-DR1 using the 350/330 ratio. The red arrows indicate two points at which (partial) unfolding took place.

As sufficient HLA-DR1 could be expressed, some initial crystallization experiments were performed. HLA-DR1 was co-expressed with the CLIP peptide.^{62,63} Conditions under which HLA-DR1-CLIP crystallized, also in previous research, provided a starting point for other (clickable) peptides. Crystallization started based on research published by Günther *et al.* in which HLA-DR1 was crystallized with various CLIP-peptides.²⁴ A screen was designed based on these conditions; HLA-DR1 (~12 mg/mL) in 20 mM MES/50 mM NaCl pH 6.4 was used for this and after 5 days some circular crystals formed (**Figure 16**). These crystals could not be used for diffraction but could be used as seeding material in future experiments. A more general screen could be set-up to find alternative crystallization conditions. This should be performed for both the native and the clickable peptide-containing HLA-DR1.

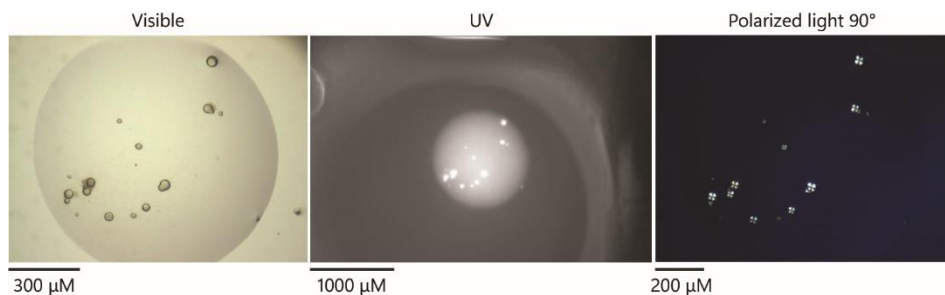


Figure 16 - Initial crystal formation of HLA-DR1.

After 5 days circular HLA-DR1 crystals were formed. After 60 days crystals were visualised using UV and polarized light 90°. Crystallization took place with 12 mg/mL HLA-DR1 in 20 mM MES/50 mM NaCl pH 6.4; drop size was 200 nL with 70% protein and 30% buffer. The crystallization condition contained 0.15 M magnesium formate, 12.857% (w/v) PEG 3350.

Conclusion

As it was possible to bind clickable peptides in the MHC-I binding groove and that this would allow for research in peptide processing and T-cell activation, an attempt was made to do this for MHC-II or the human HLA-DR1. However, performing click-to-release chemistry on this complex proved to be difficult and therefore more structural insight of the peptide binding could be of essence. Here the first steps were taken to express, purify and crystallize HLA-DR1. This proved to be rather difficult as bacterial expression made refolding necessary which was a very inefficient and low-yielding process. Expression by insect cells resulted in the individual subunits and some signs of complex formation were observed as well. However, the complex resided in the membrane fraction of the lysate, making it hard to purify the correctly folded complex from it. Eventually, expression by HEK293s GnT1⁻ cells resulted in significant amounts of complex HLA-DR1 which was relatively easy to purify. Some initial crystallization experiments with HLA-DR1 bearing the CLIP peptide resulted in phase separation but also in circular crystal formation. Although, these could not be used for diffraction, this can function as a starting point for further crystallisation efforts.

Acknowledgements

For this chapter I would like to thank Prof. Dr. Stephanie Gras of La Trobe University, Australia. She provided me with the plasmids encoding both HLA-DR1 subunits for expression in HEK293s cells. This proved to be the method that was most applicable for our purpose and there really started the project. Next, I would like to thank Anouk Lahav-van der Gracht for teaching me the technique how to work with MHC-molecules, how to express and how to refold proteins.

Materials & Methods

General reagents

All restriction enzymes, polymerases and ligases were purchased from Thermo Fisher Scientific. Non-essential amino acids (100x, Gibco #11140050) and HisPur™ Ni-NTA (Catalog #88222) were purchased from Thermo Fisher Scientific. Amicon® Ultra-4 Centrifugal Filters (#UFC801008) and Amicon® Ultra-15 Centrifugal Filters (#UFC901008) 10K were purchased from Merck. HiTrap™ 5 mL Q HP columns and the ÄKTA start system were purchased from GE Life Sciences. Rabbit anti-6*His (Item No. 600-401-392) was purchased from Rockland and mouse anti-rabbit IgG-HRP (Catalog #sc-2357) was purchased from Santa Cruz Biotechnology. L243 (#11-690-C025) was purchased from Exbio and mem-267 (#SAB700664) was purchased from Merck. *Strep-tactin*® (#2-1502-001) was purchased from IBA. Goat anti-mouse IgG-HRP (#113-035-003) was purchased from Jackson. DMEM-medium, L-glutamine, streptomycin and penicillin were all purchased from Sigma-Aldrich (MERCK). SF-900™ II Serum Free medium (Catalog #10902088) from Gibco was purchased from Thermo Fisher Scientific. QIAprep® Spin Miniprep kit (Cat No. 27104) and QIAGEN Plasmid Maxi Kit (ref. 12163) were purchased from Qiagen.

Construct formation

Expression in bacteria

HindIII restricted (1x R Buffer, 10U HindIII) donor vectors pcDNA3.2-HLADR1α and pcDNA3.2-HLADR1β (subtype DRB1*01:01) were used as template for HLA-DR1α(-6His) and HLA-DR1β(-6His) amplification respectively, by PCR (GC Green Buffer, 0.2 mM dNTPs, 0.1 μM of each primer, 50 ng restricted vector, 2U Phusion polymerase) using primers of **Table 2**. The PCR products and pET28a(+)-vector were restricted (24 hours at 37°C, 300 rpm) with NcoI/XhoI (10U) and ligated (2 hours at room temperature) using T4 DNA Ligase (5U). Ligation products were transformed into *E. coli* XL10 via heat shock (42°C, 45 seconds), recovery on ice for 2 minutes and SOC-medium recovery followed by overnight growth at kanamycin (50 μg/mL) containing LB-agar plates.

Table 2 – Primers for construct design for expression insect cells and bacteria.

Primer Nr.	Expression System	Construct	Sequence 5'→ 3'
1	Bacteria	HLA-DR1α	GGTACCATGGCTATCAAAGAAGAACAT
2			GGTGCTCGAGTTACTTCTCTGTAGTCTC
3		HLA-DR1α-6His	GGTACCATGGCTATCAAAGAAGAACAT
4			GGTGCTCGAGCTTCTCTGTAGTCTC
5		HLA-DR1β	TATACCATGGCTGGGGACACCCGACCA
6			AAAACCTCGAGTTACTTGCTCTGTGCAGA
7		HLA-DR1β-6His	TATACCATGGCTGGGGACACCCGACCA
8			AAAACCTCGAGCTTGCTCTGTGCAGA
9	Insect cells	HLA-DR1α	AAAGCTAGCAATCAAAGAAGAACAT
10			TTTGGTACCTTCTCTGTAGTCTCTG
11		HLA-DR1β	AAAGAATTCGGGGACACCCGAC
12			GGGAAGCTTTTCTTGCTCTGTG

Expression in insect cells

HindIII restricted (1x R Buffer, 10U HindIII) donor vectors pcDNA3.2-HLADR1 α and pcDNA3.2-HLADR1 β were used as template for HLA-DR1 α and HLA-DR1 β amplification respectively, by PCR (GC Green Buffer, 0.2 mM dNTPs, 0.1 μ M of each primer, 50 ng restricted vector, 2U Phusion polymerase) using primers of **Table 2**. The PCR products were cloned in the pFastBac Dual (pFastBac_CSCHE, **Figure 9**) which was modified with *N*-terminal secretion sequences (gp67) for the genes of interest followed by a C-terminal TEV-sequence followed by either a dual Strep-tag (P10 promoter) or a 6His-tag (polyhedrin promoter) (**Figure 9**). HLA-DR1 α was placed behind the P10 promoter by restriction with KpnI/NheI (10U) and HLA-DR1 β was placed behind the polyhedrin promoter by restriction with EcoRI/HindIII (10U, 24 hours at 37°C, 300 rpm). The restricted fragment and vector were ligated with T4 DNA ligase (5U, 20 hours at 16°C). Ligation products were transformed into *E. coli* XL10 via heat shock (42°C, 45 seconds), recovery on ice for 2 minutes and SOC-medium recovery followed by overnight growth on ampicillin (250 μ g/mL) and gentamycin (7 μ g/mL) containing LB-agar plates at 37°C.

Colonies containing properly ligation pFastBac, encoding either HLA-DR1 α , HLA-DR1 β or both, were selected and DNA was isolated using the QIAprep® Spin Miniprep kit according the manufacture's manual. Following, 1-5 ng DNA was used for transfection of competent DH10Bac® *E. coli* by first incubating for 30 minutes on ice, following a heat shock (42°C, 45 seconds) and recovery on ice. Recovery in SOC-medium for at least 4 hours at 37°C was followed by overnight growth on X-gal-containing LB-agar (50 μ g/mL kanamycin, 7 μ g/mL gentamycin, 100 μ g/mL tetracycline, 40 μ g/mL IPTG and 100 μ g/mL X-gal) plates at 37°C for 48 hours. White colonies were selected and a re-streak was performed to obtain a pure culture which was then grown overnight in glucose-medium (LB-medium supplemented with kanamycin (100 μ g/mL), gentamycin (7 μ g/mL), tetracycline (100 μ g/mL), glucose (1% v/v)) at 30°C. Overnight culture was diluted 10 times in glucose-medium and grown until OD₆₀₀ ~ 0.8 whereafter bacmid DNA was isolated using the QIAGEN® Plasmid Maxi Kit. Manufacture's manual was followed with some adaptations mentioned below; before applying the soluble fraction of the bacteria on the QIAGEN column, it was filtered using cheese cloth. After iso-propanol precipitation, the resulting pellets were dissolved in TNE-buffer (10 mM Tris pH 8, 150 mM NaCl, 1 mM EDTA), following precipitation with two volumes 96% ethanol and centrifugation (10 minutes at 15000 *rcf*, room temperature). The resulting pellet was air-dried and dissolved in TE-buffer (10 mM Tris pH 8, 1 mM EDTA) overnight.

Expression in HEK293s GnTI⁻

Constructs encoding the truncated, codon optimised version of each subunit of HLA-DR1 (pHLSEC-HLADR1A*0101 (Uniprot: P01903), pHLSEC-HLADR1B*01*01 (Uniprot: A9JJF6)) and HLA-DM (pHLSEC-HLADM α , pHLSEC-HLADM β)²⁹ were kindly provided by Prof. Dr. Stephanie Gras of La Trobe University, Melbourne, Australia. The sequences used are given in **Supplementary Figure S5**.

Cell culture

Insect cells

Adherent Sf9 cells

Sf9 cells (#CRL-1711TM, ATCC) were maintained in TNM-FH insect medium (Grace's medium provided with lactalbumin hydrolysate and yeast extract)⁶⁴ supplemented with 5% (v/v) heat-inactivated fetal calf serum, penicillin (100 IU/mL) and streptomycin (0.1 mg/mL) at 27°C, 0% CO₂. For passage, cells were treated with 0.25% trypsin in PBS/EDTA for 15 minutes at 27°C, 0% CO₂. Cells were seeded twice a week at 2.5E5-3.0E5 cells/mL.

Suspension Sf9 cells

Sf9 cells for suspension growth were maintained in SF-900™ II Serum Free medium containing penicillin (100 IU/mL) and streptomycin (0.1 mg/mL) at 27°C, 130 rpm. Cells were split at a density of 1-2E6 cells/mL and diluted to 2.5E5 cells/mL. Infection took place at a cell density of 3-4E6 cells/mL.

Suspension High Five cells

High Five™ Cells (BTI-TN-5B1-4, Thermo Fisher Scientific) were maintained in Gibco express Five® SFM medium supplemented with 2 mM glutamine at 27°C, 0% CO₂, 130 rpm. Cells were split before the density reached 4E6 cells/mL and seeded at 3E5 cells/mL.

HEK293s GnTI⁻ cells

HEK293s GnTI⁻ cells (#CRL-3022, ATCC) were maintained in Dulbecco's Modified Eagle's Medium – high glucose (DMEM – high glucose, #D6546-500ML) supplemented with 10% Newborn Calf Serum (NCS), 2 mM glutamine, 100 IU/mL penicillin and 50 µg/mL streptomycin at 37°C, 7% CO₂. For each passage, twice a week, the cells were diluted 20 times.

Bacterial expression and purification

HLA-DR1 constructs isolated from *E. coli* XL10 using QIAprep Spin Miniprep Kit were used to transform calcium competent *E. coli* ArcticExpress (DE3) RP using heat shock (42°C, 45 seconds) and SOC-medium recovery. Colonies were used to inoculate LB-medium containing kanamycin (50 µg/mL) and gentamycin (7 µg/mL) for overnight growth at 37°C, 170 rpm. Overnight culture was diluted 100 times and grown at 37°C, 180 rpm until optical density at 600 nm (OD₆₀₀) of 0.6 was reached after which protein expression was induced with addition of 0.5 mM IPTG. Expression took place for 48-72 hours at 10°C, 140 rpm where after the bacteria were harvested by centrifugation (30 minutes, 3400g at 4°C).

Lysis

Per 500 mL culture, 10 mL lysis buffer (50 mM Tris Cl pH 8.0, 25% (w/v) sucrose, 1 mM EDTA, 1 mM PMSF, 2 mM DTT) was applied with 0.4 mg/mL lysozyme. Incubation while gently mixing for 30 minutes at 4°C was followed by adding 10 mM MgCl₂, 1 mM MnCl₂ and 10U benzonase and 30 minutes incubation at 4°C. The lysate was sonicated (Vibra-cell™ VCX130) for 30 seconds with 5 second pulses with 20% amplitude and 10 second intervals. The lysate was diluted three times with detergent buffer (0.2 M NaCl, 1% (w/v) sodium deoxycholate monohydrate, 1% Igepal, 20 mM Tris Cl pH 7.5, 2 mM EDTA, 0.02 mM PMSF, 0.04 mM DTT), incubated for 30 minutes on ice and centrifuged for 20 minutes at 14000g, 4°C to collect the supernatant.

Nickel column purification

Inclusion bodies dissolved in equilibration buffer (8 M urea, 100 mM Tris, 10 mM imidazole pH 8) and loaded onto HisPur Ni-NTA resin and incubated overnight at 4°C, constant rolling. The resin was loaded on a reaction syringe and washed with two column volumes of different concentrations imidazole in equilibration buffer. Samples of each fraction were analysed using SDS-PAGE and subunit containing fractions were concentrated using Amicon® Ultra-15 Centrifugal Filters 10K (30 minutes at 3200 *rcf*, 4°C).

Anion exchange purification

Inclusion bodies dissolved equilibration buffer (8 M urea, 20 mM Tris, 1 mM DTT) at pH 8 and pH 9 for HLA-DR1 α and HLA-DR1 β , respectively and loaded onto a HiTrap™ 5 mL Q HP column. The subunits were eluted with various concentrations (0-300 mM) NaCl in equilibration buffer. Fractions were analysed by SDS-PAGE and subunit containing fractions were concentrated using Amicon® Ultra-4 Centrifugal Filters 10K (30 minutes at 3200 *rcf*, 4°C) equilibrated with equilibration buffer. Concentrated protein solutions were supplied with 0.5 mM EDTA and adjusted to pH 8.

*Refolding**Method 1*

The protocol was based work from Frayser *et al.* Each HLA-DR1 subunit was diluted to 80 nM in 100 mL Frayser refolding buffer (20 mM Tris, 25% (w/v) glycerol, 500 μ M EDTA, 3 mM reduced glutathione, 300 μ M oxidized glutathione, pH 8.5). Refolding was performed in both presence and absence of ISQAVHAAHAEINAEGR (ISQ) peptide for 72 hours at 6°C, while constant mixing. The refolding mixture was then co-incubated with 2.5 mL 100% DEAE Sepharose™ beads overnight at 4°C, while constant mixing. After washing with 20 mM Tris pH 8, elution was performed with 500 mM NaCl in 20 mM Tris pH 8 and the eluent was concentrated using an Amicon® Ultra-15 Centrifugal Filter 30K (30 minutes at 4°C, 3220 *rcf*).

Method 2

The protocol was based on research published by Buchner *et al.* Each HLA-DR1 subunit was diluted dropwise to 1 μ M in 100 mL Buchner refolding buffer (100 mM Tris, 400 mM L-arginine, 2 mM EDTA, 5 mM reduced glutathione, 500 μ M oxidized glutathione, 500 PMSF). Refolding was performed in both the presence and absence of 10 μ M ISQ peptide. Refolding was performed for 48 hours at 6°C while constant mixing. Refolded complex was concentrated using Amicon® Ultra-15 Centrifugal Filters 30K (30 minutes at 4°C, 3220 *rcf* per run) in PBS.⁴⁶

Insect cell expression

The transfection, expression and purification was based on work described in previous work of Barendrecht.⁶⁵ Transfection was based on a protocol described by Philipps *et al.*⁶⁶ Adherent *Sf9* insect cells at 40% confluence were transfected with bacmid DNA. Transfection was performed with 12 µg DNA, using polyethylenimine (PEI) as transport vehicle in a DNA/PEI (w/w)-ratio of 1:2. Following 30 minutes room temperature incubation, the DNA/mixture was diluted until a final DNA concentration of 1.2 µg/mL on the cells in *Sf9*-medium. The transfection mixture was incubated for 5 hours at 27°C, 0% CO₂, following replacement with fresh *Sf9*-medium and another incubation for 96-120 hours at 27°C, 0% CO₂. Both medium and cells, using 0.25% trypsin in PBS/EDTA, were harvested and equally divided over two T175 flasks together with new *Sf9*-medium until a total volume of 37 mL. After incubation for 96 hours at 27°C, 0% CO₂, cells and medium were harvested and separated by centrifugation for 5 minutes at 500 *rcf*, room temperature.

Virus titer determination and amplification

The resulting supernatant was centrifuged for 30 minutes at 100 000 *rcf*, 20°C whereafter the virus-containing pellet was dissolved in PBS resulting in virus stocks ranging from 10² – 10⁹ dilutions. Insect cells were seeded as 12 500 cells/well and infected with 10 µL/well of these dilution with 12 replicates, following incubation for 48 hours at 27°C, 0% CO₂. The optimal virus dilution was set to be the dilution at which 50% of the cells was infected. Infection was determined by YFP expression. PCR as described above proved the presence of the genes for each HLA-DR1 subunit. Cells were analysed using the EVOS FL Auto 2 of Invitrogen by Thermo Fisher Scientific. Virus was amplified by adding twice the amount of virus as determined to infect 50% of the cells in a 80% confluent flask. Incubation took place for 48 hours at 27°C, 5% CO₂.⁶⁵

Protein expression Sf9

Cells were infected with a 10⁻³ P₀ virus stock using 1 µL virus/mL culture. Both adherent and suspension *Sf9* were incubated for 96 hours at 27°C, 0% CO₂ at 130 rpm (suspension cells only). Cells and medium were harvested and separated by centrifugation for 5 minutes at 500 *rcf*, room temperature.⁶⁵

Lysis Sf9 cells

60E6 cells were dissolved in 1 mL lysis buffer 1 (20 mM HEPES, 2 mM DTT, 250 mM sucrose, 1 mM MgCl₂, 2.5 U/mL benzonase) following 30 minutes incubation on ice before 1 hour centrifugation at 30 000 *rcf*, 4°C. The resulting pellet was dissolved in 20 mM HEPES/20 mM DTT.⁶⁵ The fraction content was analysed by SDS-PAGE.

Protein expression High Five

Cells at 2E6 cells/mL were infected with baculovirus obtained from *Sf9* cells as described above. Incubation took place for 96 hours at 27°C, 0% CO₂, 130 rpm. Medium and cells were separated by centrifugation for 20 minutes at 3220 *rcf*, 4°C.

Lysis High Five cells

The cell pellet was lysed using 1/100 culture volume lysis buffer (50 mM Tris pH 8, 25% (w/v) sucrose, 1 mM EDTA, 1 mM PMSF, 2 mM DTT) followed by 30 minutes incubation on ice. Centrifugation for 10 minutes at 3220 *rcf*, 4°C resulted in the soluble (cytosolic) and membrane fraction. The fraction content was analysed by SDS-PAGE.

HEK293s GnTI⁻ expression and purification*Expression*

This protocol was based on the protocol provided by Prof. Dr. Stephanie Gras of La Trobe University, Melbourne, Australia. HEK293s GnTI⁻ cells were grown until 80% confluence in a T175 flask. Transfection was performed with 60 µg DNA, 1:1 ratio DNA encoding HLA-DR1α:HLA-DR1β or HLA-DMα:HLA-DMβ, using PEI as transport vehicle in a DNA/PEI w/w-ratio of 1:3. Following 30 minutes room temperature incubation, the DNA/mixture was added to the cells with transfection medium (DMEM-high glucose, 2 mM glutamine, 1% NCS) and 6.7x concentrated master mix (DMEM-high glucose, 40 mM glutamine, 20 mM pyruvate, 200 mM HEPES pH 7.4, 20x non-essential amino acids and 4 µM β-mercaptoethanol) until a total volume of 40 mL. Cells were incubated for 7 days at 37°C, 7% CO₂ before medium and cells were harvested. This suspension was supplied with 50 mM Tris pH 8, 1 mM NiCl₂ and 5 mM CaCl₂, final concentrations. After 30 minutes incubation at 4°C, constant rolling, the suspension was centrifuged for 20 minutes at 3200 *rcf*, 4°C and the resulting supernatant was filtered using a 0.2 µm filter. The filtrate was supplied with 20 mM imidazole.

Purification

HisPur Ni-NTA was equilibrated as has been described in the manufacture's manual. The HLA-DR1- or HLA-DM-containing medium was incubated with the resin for 2 hours at 4°C, constant rolling. Following, the proteins were washed and eluted on ice with various concentrations of imidazole in 10 mM Tris pH 8/150 mM NaCl. The protein containing fractions were combined and concentrated using Amicon® Ultra-15 Centrifugal Filters 10K equilibrated with 10 mM Tris pH 8/150 mM NaCl (20 minutes at 3200 *rcf*, 4°C). This was then applied onto a HiLoad® 16/600 Superdex® 200 pg column equilibrated with 10 mM Tris/150 mM NaCl (maximum volume per run: 2.5 mL). The chromatogram depicted in **Figure 14A** shows the absorbance of 280 nm over the elution period. The fractions within the blue box (**Figure 14A**) were analysed by SDS-PAGE (**Figure 14B**). These fractions correspond to the fractions in the red box in **Figure 14A**. The HLA-DR1/HLA-DM containing fractions were combined and concentrated using 10 mM Tris pH 8/150 mM NaCl equilibrated Amicon® Ultra-4 Centrifugal Filters 10K.

Western blot

Denaturing acrylamide gels (SDS-PAGEs) were blotted onto 0.2 µm PVDF, midi format (Trans-Blot Turbo Transfer Pack, single application of Bio-Rad) using the Turbo Trans Blot System (Bio-Rad). Blots were developed using luminol solution (25% (w/v) luminol in 0.1 M Tris pH 8.8), 100x diluted enhancer (1.1 mg/mL p-coumaric acid in DMSO) and H₂O₂. Blots were imaged with the ChemiDoc™ MP Imaging System of Bio-Rad with setting chemiluminescence, Cy3 and Cy5 and analysed using ImageLab Software version 4.1.

6His-specific blot

Blot was washed with TBS (10 minutes) and TBST (1x TBS pH 7.5; 0.05% Tween-20; 3x 5 minutes) before blocking with 5% milk in TBST overnight at 4°C. Washing 3 times for 5 minutes with TBST was followed with rabbit anti-6*His incubation (1:1000) in blocking buffer for 3 hours at room temperature. Another 3 times 5 minutes washing with TBST was followed by addition of mouse anti-rabbit IgG-HRP (1:4000) and incubation for 2 hours at room temperature. The blots were washed 3 times for 5 minutes with TBST and 10 minutes with TBS before development with luminol.

Strep-specific blot

For dual-Strep-tag detection, the blot was washed with PBS and PBS-T (1x PBS with 0.1% (v/v) Tween-20) instead of TBS and TBST, respectively. Blocking was performed with 3% (w/v) BSA in PBS with 0.5% (v/v) Tween-20. The detection agent used was *Strep-Tactin*®, diluted stepwise first 100 times in PBS buffer containing 0.2% (w/v) BSA and 0.1% (v/v) Tween-20, following 1000 times dilution in PBS-T. No secondary antibody was used. Visualisation was performed with luminol.

DR1 α - and DR1 β -specific blots

For HLA-DR1 α -specific detection, the blot was washed with PBS and PBS-T (1x PBS pH 7.4 with 0.5% Tween-20) instead of TBS and TBST, respectively. Blocking buffer consisted of 5% BSA in PBS-T. The primary antibody, L243, was diluted 500 times in blocking buffer. The secondary antibody, goat anti-mouse IgG-HRP conjugate was diluted 2500 times in blocking buffer.

For HLA-DR1 β -specific detection, the blot was washed and blocked in the same was as for 6His-specific detection. The primary antibody mem-267 was diluted 1000 times in blocking buffer and the secondary antibody goat anti-mouse IgG-HRP was diluted 2500 times in blocking buffer.

Thermostability

The thermostability of HLA-DR1 was assessed using the NanoTemper Tychno NT.6. Emission was measured at 330 nm and 350 nm. The ratio 330/350 was used as a measure for protein unfolding.

Crystallography

Crystallization was based on work of Günther *et al.* using a sitting-drop vapor diffusion method. The drop size of 200 nL contained either 50/50 or 70/30 protein and buffer. HLA-DR1 was applied at 12 mg/mL in 20 mM MES/50 mM NaCl pH 6.4. Circular crystals were obtained in 0.15 M magnesium formate with 12.857% (w/v) PEG 3350.

References

- (1) ten Broeke, T.; Wubbolts, R.; Stoorvogel, W. MHC Class II Antigen Presentation by Dendritic Cells Regulated through Endosomal Sorting. *Cold Spring Harb Perspect Biol* **2013**, *5* (12), 1–21. <https://doi.org/10.1101/cshperspect.a016873>.
- (2) Hunt, D. F.; Michel, H.; Dickinson, T. A.; Shabanowitz, J.; Cox, A. L.; Sakaguchi, K.; Appella, E.; Grey, H. M.; Sette, A. Peptides Presented to the Immune System by the Murine Class II Major Histocompatibility Complex Molecule I-Ad. *Science* (1979) **1992**, *256* (5065), 1817–1820. <https://doi.org/10.1126/science.1319610>.
- (3) Holling, T. M.; Schooten, E.; Van Den Elsen, P. J. Function and Regulation of MHC Class II Molecules in T-Lymphocytes: Of Mice and Men. *Hum Immunol* **2004**, *65* (4), 282–290. <https://doi.org/10.1016/j.humimm.2004.01.005>.
- (4) Malonis, R. J.; Lai, J. R.; Vergnolle, O. Peptide-Based Vaccines: Current Progress and Future Challenges. *Chem Rev* **2020**, *120* (6), 3210–3229. <https://doi.org/10.1021/acs.chemrev.9b00472>.
- (5) Marsh, S. G. E.; Albert, E. D.; Bodmer, W. F.; Bontrop, R. E.; Dupont, B.; Erlich, H. A.; Fernández-Viña, M.; Geraghty, D. E.; Holdsworth, R.; Hurley, C. K.; Lau, M.; Lee, K. W.; Mach, B.; Maiers, M.; Mayr, W. R.; Müller, C. R.; Parham, P.; Petersdorf, E. W.; Sasazuki, T.; Strominger, J. L.; Svejgaard, A.; Terasaki, P. I.; Tiercy, J. M.; Trowsdale, J. Nomenclature for Factors of the HLA System, 2010. *Tissue Antigens* **2010**, *75* (4), 291–455. <https://doi.org/10.1111/j.1399-0039.2010.01466.x>.
- (6) Robinson, J. IMGT/HLA and IMGT/MHC: Sequence Databases for the Study of the Major Histocompatibility Complex. *Nucleic Acids Res* **2003**, *31* (1), 311–314. <https://doi.org/10.1093/nar/gkg070>.
- (7) Kerlan-Candon, S.; Combe, B.; Vincent, R.; Clot, J.; Eliaou, J. F. HLA-DRB1 Gene Transcripts in Rheumatoid Arthritis. *Clin Exp Immunol* **2001**, *124* (1), 142–149. <https://doi.org/10.1046/j.1365-2249.2001.01498.x>.
- (8) Roudier, J. HLA-DRB1 Genes and Extraarticular Rheumatoid Arthritis. *Arthritis Res Ther* **2006**, *8* (1), 103. <https://doi.org/10.1186/ar1886>.
- (9) Mahdi, B. M. Role of HLA Typing on Crohn's Disease Pathogenesis. *Annals of Medicine & Surgery* **2015**, *4* (3), 248–253. <https://doi.org/10.1016/j.amsu.2015.07.020>.
- (10) Marcusson, J. A.; Johannesson, A.; Möller, E. HLA-A,B,C and DR Antigens in Psoriasis. *Tissue Antigens* **2008**, *17* (5), 525–529. <https://doi.org/10.1111/j.1399-0039.1981.tb00740.x>.
- (11) Kapitány, A.; Zilahi, E.; Szántó, S.; Szűcs, G.; Szabó, Z.; Végvári, A.; Rass, P.; Sipka, S.; Szegedi, G.; Szekancz, Z. Association of Rheumatoid Arthritis with HLA-DR1 and HLA-DR4 in Hungary. *Ann N Y Acad Sci* **2005**, *1051* (1), 263–270. <https://doi.org/10.1196/annals.1361.067>.
- (12) Fernandez, L.; Mendoza, J. L.; Martinez, A.; Urcelay, E.; Fernandez-Arquero, M.; Garcia-Paredes, J.; Peña, A. S.; Diaz-Rubio, M.; de la Concha, E. G. IBD1 and IBD3 Determine Location of Crohn's Disease in the Spanish Population. *Inflamm Bowel Dis* **2004**, *10* (6), 715–722. <https://doi.org/10.1097/00054725-200411000-00004>.
- (13) Cardoso, C. B.; Uthida-Tanaka, A. M.; Magalhães, R. F.; Magna, L. A.; Kraemer, M. H. S. Association between Psoriasis Vulgaris and MHC-DRB, -DQB Genes as a Contribution to Disease Diagnosis. *Eur J Dermatol* **2005**, *15* (3), 159–163.
- (14) Neefjes, J.; Jongsma, M. L. M.; Paul, P.; Bakke, O. Towards a Systems Understanding of MHC Class I and MHC Class II Antigen Presentation. *Nat Rev Immunol* **2011**, *11* (12), 823–836. <https://doi.org/10.1038/nri3084>.
- (15) Aleksic, M.; Liddy, N.; Molloy, P. E.; Pumphrey, N.; Vuidepot, A.; Chang, K.-M.; Jakobsen, B. K. Different Affinity Windows for Virus and Cancer-Specific T-Cell Receptors: Implications for Therapeutic Strategies. *Eur J Immunol* **2012**, *42* (12), 3174–3179. <https://doi.org/10.1002/eji.201242606>.
- (16) Irving, M.; Zoete, V.; Hebeisen, M.; Schmid, D.; Baumgartner, P.; Guillaume, P.; Romero, P.; Speiser, D.; Luescher, I.; Rufer, N.; Michielin, O. Interplay between T Cell Receptor Binding Kinetics and the Level of Cognate Peptide Presented by Major Histocompatibility Complexes Governs CD8+ T Cell Responsiveness. *Journal of Biological Chemistry* **2012**, *287* (27), 23068–23078. <https://doi.org/10.1074/jbc.M112.357673>.
- (17) McKeithan, T. W. Kinetic Proofreading in T-Cell Receptor Signal Transduction. *Proceedings of the National Academy of Sciences* **1995**, *92* (11), 5042–5046. <https://doi.org/10.1073/pnas.92.11.5042>.
- (18) Swamy, M. ZAP70 Holds the Key to Kinetic Proofreading for TCR Ligand Discrimination. *Nat Immunol* **2022**, *23* (9), 1293–1294. <https://doi.org/10.1038/s41590-022-01297-w>.
- (19) Pawlak, J. B.; Gentil, G. P. P.; Ruckwardt, T. J.; Bremmers, J. S.; Meeuwenoord, N. J.; Ossendorp, F. A.; Overkleef, H. S.; Filippov, D. V.; van Kasteren, S. I. Bioorthogonal Deprotection on the Dendritic Cell Surface for Chemical Control of Antigen Cross-Presentation. *Angewandte Chemie International Edition* **2015**, *54* (19), 5628–5631. <https://doi.org/10.1002/anie.201500301>.

- (20) Pawlak, J. B.; Hos, B. J.; van de Graaff, M. J.; Megantari, O. A.; Meeuwenoord, N.; Overkleef, H. S.; Filippov, D. V.; Ossendorp, F.; van Kasteren, S. I. The Optimization of Bioorthogonal Epitope Ligation within MHC-I Complexes. *ACS Chem Biol* **2016**, *11* (11), 3172–3178. <https://doi.org/10.1021/acscchembio.6b00498>.
- (21) Groenewold, G. J. M. The Advantages and Disadvantages of Bioorthogonal Proteins, Universiteit Leiden, Leiden, 2021.
- (22) Lahav-van der Gracht, A. M. F. Bioorthogonal Deprotection Strategy to Study T-Cell Activation and Cross-Presentation, Universiteit Leiden, Leiden, 2020.
- (23) Frayser, M.; Sato, A. K.; Xu, L.; Stern, L. J. Empty and Peptide-Loaded Class II Major Histocompatibility Complex Proteins Produced by Expression in Escherichia Coli and Folding in Vitro. *Protein Expr Purif* **1999**, *15* (1), 105–114. <https://doi.org/10.1006/prep.1998.0987>.
- (24) Gunther, S.; Schlundt, A.; Sticht, J.; Roske, Y.; Heinemann, U.; Wiesmuller, K.-H.; Jung, G.; Falk, K.; Rotzschke, O.; Freund, C. Bidirectional Binding of Invariant Chain Peptides to an MHC Class II Molecule. *Proceedings of the National Academy of Sciences* **2010**, *107* (51), 22219–22224. <https://doi.org/10.1073/pnas.1014708107>.
- (25) Anders, A.-K.; Call, M. J.; Schulze, M.-S. E. D.; Fowler, K. D.; Schubert, D. A.; Seth, N. P.; Sundberg, E. J.; Wucherpfennig, K. W. HLA-DM Captures Partially Empty HLA-DR Molecules for Catalyzed Removal of Peptide. *Nat Immunol* **2011**, *12* (1), 54–61. <https://doi.org/10.1038/ni.1967>.
- (26) Pos, W.; Sethi, D. K.; Call, M. J.; Schulze, M.-S. E. D.; Anders, A.-K.; Pyrdol, J.; Wucherpfennig, K. W. Crystal Structure of the HLA-DM–HLA-DR1 Complex Defines Mechanisms for Rapid Peptide Selection. *Cell* **2012**, *151* (7), 1557–1568. <https://doi.org/10.1016/j.cell.2012.11.025>.
- (27) Stern, L. J.; Wiley, D. C. Antigenic Peptide Binding by Class I and Class II Histocompatibility Proteins. *Structure* **1994**, *2* (4), 245–251. [https://doi.org/10.1016/S0969-2126\(00\)00026-5](https://doi.org/10.1016/S0969-2126(00)00026-5).
- (28) Busch, R.; Pashine, A.; Garcia, K. C.; Mellins, E. D. Stabilization of Soluble, Low-Affinity HLA-DM/HLA-DR1 Complexes by Leucine Zippers. *J Immunol Methods* **2002**, *263* (1–2), 111–121. [https://doi.org/10.1016/S0022-1759\(02\)00034-0](https://doi.org/10.1016/S0022-1759(02)00034-0).
- (29) Szeto, C.; Bloom, J. I.; Sloane, H.; Lobos, C. A.; Fodor, J.; Jayasinghe, D.; Chatzileontiadou, D. S. M.; Grant, E. J.; Buckle, A. M.; Gras, S. Impact of HLA-DR Antigen Binding Cleft Rigidity on T Cell Recognition. *Int J Mol Sci* **2020**, *21* (19), 1–20. <https://doi.org/10.3390/ijms21197081>.
- (30) Alberts, B.; Johnson, A.; Lewis, J.; Raff, M.; Roberts, K.; Walter, P. *Molecular Biology of the Cell*, 4th ed.; Garland Science: New York, 2002.
- (31) Lester, D. K.; Burton, C.; Gardner, A.; Innamarato, P.; Kodumudi, K.; Liu, Q.; Adhikari, E.; Ming, Q.; Williamson, D. B.; Frederick, D. T.; Sharova, T.; White, M. G.; Markowitz, J.; Cao, B.; Nguyen, J.; Johnson, J.; Beatty, M.; Mockabee-Macias, A.; Mercurio, M.; Watson, G.; Chen, P.-L.; McCarthy, S.; MoranSegura, C.; Messina, J.; Thomas, K. L.; Darville, L.; Izumi, V.; Koomen, J. M.; Pilon-Thomas, S. A.; Ruffell, B.; Luca, V. C.; Haltiwanger, R. S.; Wang, X.; Wargo, J. A.; Boland, G. M.; Lau, E. K. Fucosylation of HLA-DRB1 Regulates CD4+ T Cell-Mediated Anti-Melanoma Immunity and Enhances Immunotherapy Efficacy. *Nat Cancer* **2023**, *4* (2), 222–239. <https://doi.org/10.1038/s43018-022-00506-7>.
- (32) Rudd, P. M.; Wormald, M. R.; Stanfield, R. L.; Huang, M.; Mattsson, N.; Speir, J. A.; DiGennaro, J. A.; Fetrow, J. S.; Dwek, R. A.; Wilson, I. A. Roles for Glycosylation of Cell Surface Receptors Involved in Cellular Immune Recognition. *J Mol Biol* **1999**, *293* (2), 351–366. <https://doi.org/10.1006/jmbi.1999.3104>.
- (33) Altmann, F.; Staudacher, E.; Wilson, I. B. H.; März, L. Insect Cells as Hosts for the Expression of Recombinant Glycoproteins. *Glycoconj J* **1999**, *16* (2), 109–123. <https://doi.org/10.1023/A:1026488408951>.
- (34) Invitrogen. Bac-to-Bac® Baculovirus Expression System. *User Guide* **2015**, No. August, 1–78. https://doi.org/10.1007/SpringerReference_28001.
- (35) Felberbaum, R. S. The Baculovirus Expression Vector System: A Commercial Manufacturing Platform for Viral Vaccines and Gene Therapy Vectors. *Biotechnol J* **2015**, *10* (5), 702–714. <https://doi.org/10.1002/biot.201400438>.
- (36) Walsh, G. Post-Translational Modifications of Protein Biopharmaceuticals. *Drug Discov Today* **2010**, *15* (17–18), 773–780. <https://doi.org/10.1016/j.drudis.2010.06.009>.
- (37) Tripathi, N. K.; Shrivastava, A. Recent Developments in Bioprocessing of Recombinant Proteins: Expression Hosts and Process Development. *Front Bioeng Biotechnol* **2019**, *7*. <https://doi.org/10.3389/fbioe.2019.00420>.
- (38) Chang, V. T.; Crispin, M.; Aricescu, A. R.; Harvey, D. J.; Nettleship, J. E.; Fennelly, J. A.; Yu, C.; Boles, K. S.; Evans, E. J.; Stuart, D. I.; Dwek, R. A.; Jones, E. Y.; Owens, R. J.; Davis, S. J. Glycoprotein Structural Genomics: Solving the Glycosylation Problem. *Structure* **2007**, *15* (3), 267–273. <https://doi.org/10.1016/j.str.2007.01.011>.
- (39) Reeves, P. J.; Callewaert, N.; Contreras, R.; Khorana, H. G. Structure and Function in Rhodopsin: High-Level Expression of Rhodopsin with Restricted and Homogeneous N-Glycosylation by a Tetracycline-Inducible N -Acetylglucosaminyltransferase I-Negative HEK293S Stable Mammalian Cell Line. *Proceedings of the National Academy of Sciences* **2002**, *99* (21), 13419–13424. <https://doi.org/10.1073/pnas.212519299>.

- (40) Stura, E. A.; Nemerow, G. R.; Wilson, I. A. Strategies in the Crystallization of Glycoproteins and Protein Complexes. *J Cryst Growth* **1992**, *122* (1–4), 273–285. [https://doi.org/10.1016/0022-0248\(92\)90256-l](https://doi.org/10.1016/0022-0248(92)90256-l).
- (41) Tsumoto, K.; Ejima, D.; Kumagai, I.; Arakawa, T. Practical Considerations in Refolding Proteins from Inclusion Bodies. *Protein Expr Purif* **2003**, *28* (1), 1–8. [https://doi.org/10.1016/S1046-5928\(02\)00641-1](https://doi.org/10.1016/S1046-5928(02)00641-1).
- (42) Studier, F. W.; Moffatt, B. A. Use of Bacteriophage T7 RNA Polymerase to Direct Selective High-Level Expression of Cloned Genes. *J Mol Biol* **1986**, *189* (1), 113–130. [https://doi.org/10.1016/0022-2836\(86\)90385-2](https://doi.org/10.1016/0022-2836(86)90385-2).
- (43) Falgenhauer, E.; Schönberg, S.; Meng, C.; Mückl, A.; Vogele, K.; Emslander, Q.; Ludwig, C.; Simmel, F. C. Evaluation of an E. Coli Cell Extract Prepared by Lysozyme-Assisted Sonication via Gene Expression, Phage Assembly and Proteomics. *ChemBioChem* **2021**, *22* (18), 2805–2813. <https://doi.org/10.1002/cbic.202100257>.
- (44) Singh, A.; Upadhyay, V.; Upadhyay, A. K.; Singh, S. M.; Panda, A. K. Protein Recovery from Inclusion Bodies of Escherichia Coli Using Mild Solubilization Process. *Microb Cell Fact* **2015**, *14* (1), 1–10. <https://doi.org/10.1186/s12934-015-0222-8>.
- (45) Patra, A. K.; Mukhopadhyay, R.; Mukhija, R.; Krishnan, A.; Garg, L. C.; Panda, A. K. Optimization of Inclusion Body Solubilization and Renaturation of Recombinant Human Growth Hormone from Escherichia Coli. *Protein Expr Purif* **2000**, *18* (2), 182–192. <https://doi.org/10.1006/prep.1999.1179>.
- (46) Buchner, J.; Rudolph, R. Renaturation, Purification and Characterization of Recombinant Fab-Fragments Produced in Escherichia Coli. *Nat Biotechnol* **1991**, *9* (2), 157–162. <https://doi.org/10.1038/nbt0291-157>.
- (47) Natarajan, S. K.; Stern, L. J.; Sadegh-Nasseri, S. Sodium Dodecyl Sulfate Stability of HLA-DR1 Complexes Correlates with Burial of Hydrophobic Residues in Pocket 1. **1999**.
- (48) Kollewe, C.; Vilcinskas, A. Production of Recombinant Proteins in Insect Cells. *Am J Biochem Biotechnol* **2013**, *9* (3), 255–271. <https://doi.org/10.3844/ajbbsp.2013.255.271>.
- (49) Krammer, F.; Schinko, T.; Palmberger, D.; Tauer, C.; Messner, P.; Grabherr, R. Trichoplusia Ni Cells (High FiveTM) Are Highly Efficient for the Production of Influenza A Virus-like Particles: A Comparison of Two Insect Cell Lines as Production Platforms for Influenza Vaccines. *Mol Biotechnol* **2010**, *45* (3), 226–234. <https://doi.org/10.1007/s12033-010-9268-3>.
- (50) Wilde, M.; Klausberger, M.; Palmberger, D.; Ernst, W.; Grabherr, R. Tnao38, High Five and Sf9-Evaluation of Host-Virus Interactions in Three Different Insect Cell Lines: Baculovirus Production and Recombinant Protein Expression. *Biotechnol Lett* **2014**, *36* (4), 743–749. <https://doi.org/10.1007/s10529-013-1429-6>.
- (51) Gauthier, L.; Smith, K. J.; Pyrdol, J.; Kalandadze, A.; Strominger, J. L.; Wiley, D. C.; Wucherpfennig, K. W. Expression and Crystallization of the Complex of HLA-DR2 (DRA, DRB1*1501) and an Immunodominant Peptide of Human Myelin Basic Protein. *Proceedings of the National Academy of Sciences* **1998**, *95* (20), 11828–11833. <https://doi.org/10.1073/pnas.95.20.11828>.
- (52) Trometer, C.; Falson, P. Mammalian Membrane Protein Expression in Baculovirus-Infected Insect Cells; 2010; pp 105–117. https://doi.org/10.1007/978-1-60761-344-2_7.
- (53) Page, D. B.; Postow, M. A.; Callahan, M. K.; Allison, J. P.; Wolchok, J. D. Immune Modulation in Cancer with Antibodies. *Annu Rev Med* **2014**, *65* (1), 185–202. <https://doi.org/10.1146/annurev-med-092012-112807>.
- (54) Gray, D. Overview of Protein Expression by Mammalian Cells. *Curr Protoc Protein Sci* **1997**, *10* (1). <https://doi.org/10.1002/0471140864.ps0509s10>.
- (55) Tan, E.; Chin, C. S. H.; Lim, Z. F. S.; Ng, S. K. HEK293 Cell Line as a Platform to Produce Recombinant Proteins and Viral Vectors. *Front Bioeng Biotechnol* **2021**, *9*. <https://doi.org/10.3389/fbioe.2021.796991>.
- (56) Szeto, C.; Bloom, J. I.; Sloane, H.; Lobos, C. A.; Fodor, J.; Jayasinghe, D.; Chatzileontiadou, D. S. M.; Grant, E. J.; Buckle, A. M.; Gras, S. Impact of HLA-DR Antigen Binding Cleft Rigidity on T Cell Recognition. *Int J Mol Sci* **2020**, *21* (19), 1–20. <https://doi.org/10.3390/ijms21197081>.
- (57) Chaudhary, S.; Pak, J. E.; Gruswitz, F.; Sharma, V.; Stroud, R. M. Overexpressing Human Membrane Proteins in Stably Transfected and Clonal Human Embryonic Kidney 293S Cells. *Nat Protoc* **2012**, *7* (3), 453–466. <https://doi.org/10.1038/nprot.2011.453>.
- (58) Kitamoto, Y.; Yuan, X.; Wu, Q.; McCourt, D. W.; Sadler, J. E. Enterokinase, the Initiator of Intestinal Digestion, Is a Mosaic Protease Composed of a Distinctive Assortment of Domains. *Proceedings of the National Academy of Sciences* **1994**, *91* (16), 7588–7592. <https://doi.org/10.1073/pnas.91.16.7588>.
- (59) Kouzarides, T.; Ziff, E. The Role of the Leucine Zipper in the Fos–Jun Interaction. *Nature* **1988**, *336* (6200), 646–651. <https://doi.org/10.1038/336646a0>.
- (60) Brown, M. A.; Stenberg, L. M.; Stenflo, J. Coagulation Factor Xa. In *Handbook of Proteolytic Enzymes*; Elsevier, 2013; pp 2908–2915. <https://doi.org/10.1016/B978-0-12-382219-2.00642-6>.
- (61) Ghisaidoobe, A.; Chung, S. Intrinsic Tryptophan Fluorescence in the Detection and Analysis of Proteins: A Focus on Förster Resonance Energy Transfer Techniques. *Int J Mol Sci* **2014**, *15* (12), 22518–22538. <https://doi.org/10.3390/ijms151222518>.

Chapter 4

- (62) Hedley, M. L.; Urban, R. G.; Strominger, J. L. Assembly and Peptide Binding of Major Histocompatibility Complex Class II Heterodimers in an in Vitro Translation System. *Proceedings of the National Academy of Sciences* **1994**, 91 (22), 10479–10483. <https://doi.org/10.1073/pnas.91.22.10479>.
- (63) Jasanoff, A.; Park, S. J.; Wiley, D. C. Direct Observation of Disordered Regions in the Major Histocompatibility Complex Class II-Associated Invariant Chain. *Proceedings of the National Academy of Sciences* **1995**, 92 (21), 9900–9904. <https://doi.org/10.1073/pnas.92.21.9900>.
- (64) Hit media. TNM-FH Insect Medium. *CellCulture Enabling Breakthroughs* **2016**, 4–5.
- (65) Barendrecht, A. *HLA-DR1 Production in Insect Cells Using Baculovirus Expression Vector System*; Leiden, 2018.
- (66) Philipps, B.; Rotmann, D.; Wicki, M.; Mayr, L. M.; Forstner, M. Time Reduction and Process Optimization of the Baculovirus Expression System for More Efficient Recombinant Protein Production in Insect Cells. *Protein Expr Purif* **2005**, 42 (1), 211–218. <https://doi.org/10.1016/j.pep.2005.03.020>.

Supplementary figures

HLA-DR1 sequences for bacterial expression

A)

HLA-DR1A*01*01 or HLA-DR1 α **DNA Sequence**

72 nucleotides -

CAATCAAAGAAGAACATGTGATCATCCAGGCCGAGTTCTATCTGAATCCTGACCAATCAGGCGAGTTT
 ATGTTTGACTTTGATGGTGATGAGATTTTCCATGTGGATATGGCAAAGAAGGAGACGGTCTGGCGGC
 TTGAAGAATTTGGACGATTTGCCAGCTTTGAGGCTCAAGGTGATTGGCCAACATAGCTGGACA
 AAGCCAACCTGGAATCATGACAAAGCGCTCCAATACTCCGATCACAATGTACCTCCAGAGGT
 AACTGTGCTACGAACAGCCCTGTGGAAGTGAAGAGAGCCCAACGTCCTCATCTGTTTCATCGACAAG
 TTCACCCACCAAGTGGTCAATGTCACGTGGCTTCGAAATGAAAACTGTCAACACAGGAGTGTGAG
 AGACAGTCTTCTGCCAGGGAAGACCACCTTTCCGCAAGTCCACTATCTCCCCTTCTGCCCTCA
 ACTGAGGACGTTACGACTGCAGGTGGAGCACTGGGCTTGGATGAGCTCTTCTCAAGCACTGG
 GAGTTTGATGCTCAAGCCCTCTCCAGAGACTACAGAGAAAG - 114 nucleotides

Protein Translation

MAISGVPVLGFFIIAVLMSAQESW

AIKEEHVIIQAEFYNPDQSGEFMFDFDGEIFHVDMAKKET
 VWRLEEFGRFASFEAQGALANIAVDKANLEIMTKRSNYTPIT
 NVPPEVTVLTNSPVELREPNVLCIDKFTPPVNVNVTWLRNG
 KPVTTVGVSETVFLPREDFHFRKFHYLPFLPSTEDVYDCRVEH
 WGLDEPLKHWFEFDAPSPLPETTEK
 NVVCALGLTVGLVGIIGTIFIIGLRLKSNAEERRGPL

B)

HLA-DR1B*01*01 or HLA-DR1 β **DNA Sequence**

87 Nucleotides -

CGGGGACACCCGACCACGTTTCTGTGGCAGCTTAAGTTGAATGTCATTCTTCAATGGGACGGAGC
 GGGTGCGGTTGCTGGAAGATGCATCTATAACCAAGAGGAGTCCGTGCGCTTCGACAGCGACGTGGG
 GGAGTACCGGGCGGTGACGAGCTGGGGCGCCTGATGCCGAGTACTGGAACAGCCAGAAGGACC
 TCCTGGAGCAGAGCGGGCGCGGTGGACACCTACTGCAGACACAACACGGGGTTGGTGAGAGC
 TTCACAGTGACGCGCGAGTTGAGCCTAAGGTGACTGTGTATCCTTCAAAGACCCAGCCCTGCAGCA
 CCACAACCTCCTGGTCTGCTGTGAGTGGTTTCTATCCAGGCAGCATTGAAGTCAGGTGGTTCGGAA
 CGGCCAGGAAGAGAAGGCTGGGGTGGTGTCCACAGGCCTGATCCAGAATGGAGATTGGACCTTCCA
 GACCTGGTGATGCTGGAACAGTTCTCGGAGTGGAGAGGTTACACCTGCCAAGTGGAGCACCCA
 AGTGTGACGAGCCCTCTACAGTGAATGGAGAGCACGGTCTGAATCTGCACAGAGCAAGAAA

- 93 nucleotides

Protein Translation

MVCLKLPGGSCMTALTVTLMVLSSPLALA

GDTRPRFLWQLKFECHFFNGTERVRLLERCIYNQEEVSFRFDS
 VGEYRAVTELGRPD AEYWN SQKDLLEQRRAAVD TYCRHNYG
 VGESFTVQRRVEPKVTVP SKTQPLQHNNLLVCSVSGFYPGSI
 EVRWFRNGQEEKAGVSTGLIQNGDWTFTQLVMLETVPVRS
 EVYTCQVEHPSVTSPLTVEWRARSESAQSKK
 MLSGVGGFVLGLLFLGAGLFYFRNQKGLS

Figure S1 - Sequences of the HLA-DR1 subunits for bacterial expression.

A) cDNA and amino acid (**Uniprot: p01903**) sequence of HLA-DR1A*01*01. The first 72 nucleotides encoding the signal sequence were removed. At the C-terminus the nucleotides encoding lysine (AAG) were added and 114 nucleotides (718-762 nucleotides) were removed to remove the transmembrane and cytosolic domains. B) cDNA and amino acid (**Uniprot: A9JJF6**) sequence of HLA-DR1B*01*01. The first 87 nucleotides encoding the signal sequence were removed. At the C-terminus the nucleotides encoding lysine (AAA) were added and 93 nucleotides (682-774) were removed to remove the transmembrane and cytosolic domains.

Refolding HLA-DR1 subunits expressed by bacteria

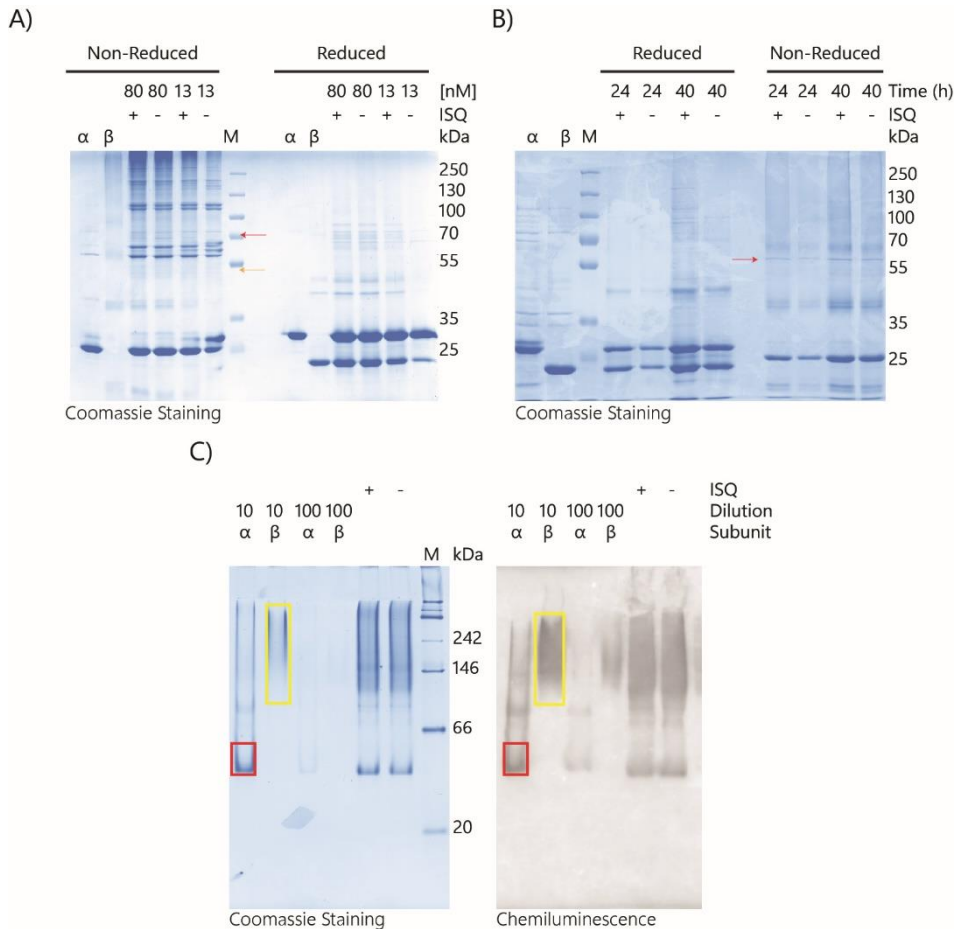


Figure S2- Refolding optimisation of HLA-DR1 expressed by bacteria.

The subunits of HLA-DR1 were expressed individually by *E. coli* ArcticExpress (DE3) RP and purified. Refolding was performed based on work of A) Frayser *et al.*²³ and B,C) Buchner *et al.*⁴⁶ Both the individual subunits, HLA-DR1α and HLA-DR1β, as the optimised refolding conditions after concentration, were analysed on A,B) SDS-PAGE, C) Native PAGE and 6His-specific Western blot. Reduced samples were boiled at 100°C and dissolved in Laemmli buffer with β-mercaptoethanol, while non-reduced samples were not boiled and dissolved without β-mercaptoethanol presence. The red arrows in A and B indicate a band appearing under non-reducing conditions under all refolding conditions. The orange arrow in A could indicate a homodimer of either subunit. The red and yellow boxes in C indicate HLA-DR1α and HLA-DR1β, respectively. C) The native PAGE and Western blot did not provide for clear formation of HLA-DR1 complex.

HLA-DR1 expression by adherent and suspension *Sf9* cells

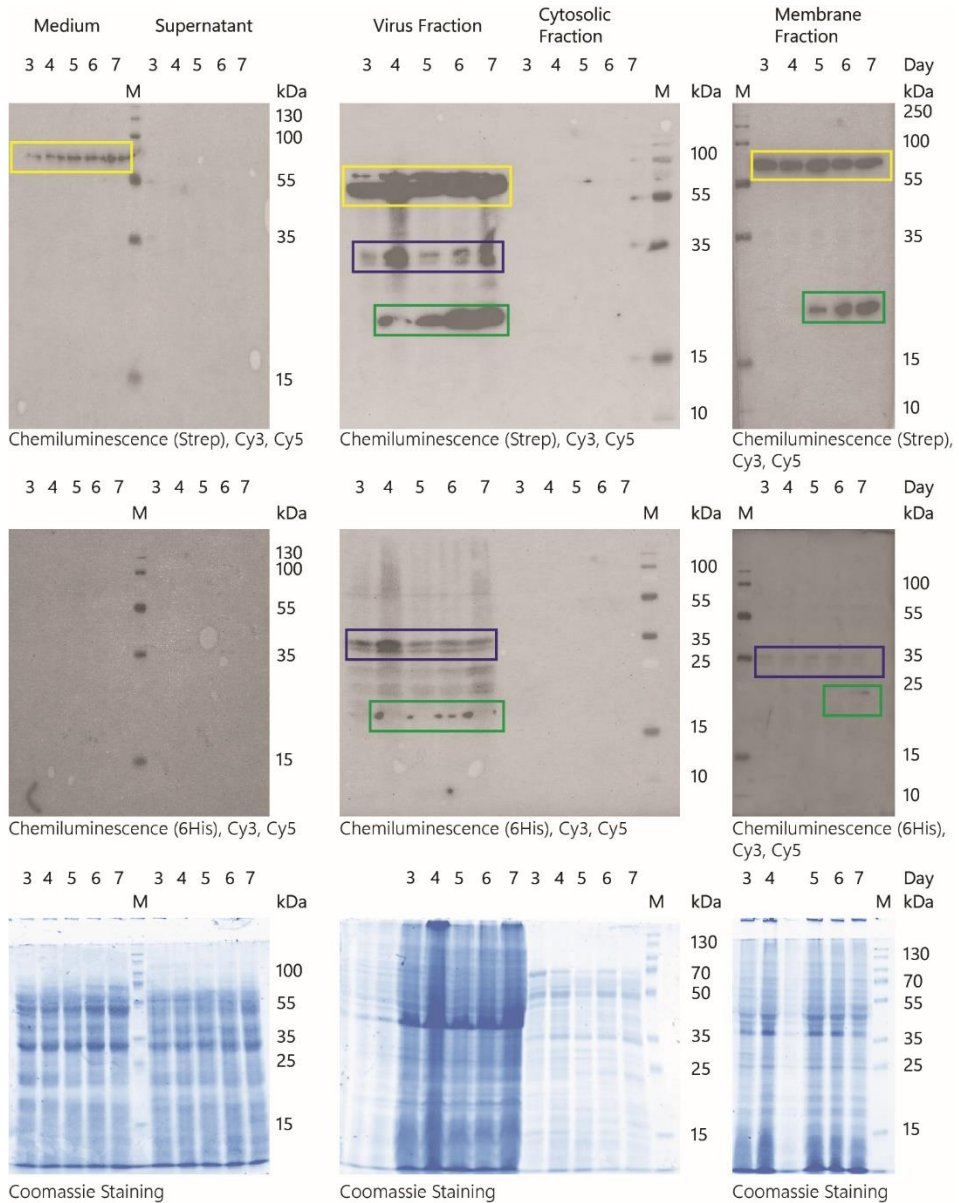


Figure S3 - HLA-DR1 expression by adherent *Sf9* cells analysed by Western blot and coomassie staining.

Adherent *Sf9* insect cells were infected with HLA-DR1 encoding baculovirus and incubated for 3-7 days after which the cells were separated from the medium, followed by isolation of the baculovirus from the medium and lysis of the cell pellet resulting in a cytosolic and membrane fraction. Samples of each day were analysed using dual-Strep (top) and 6His-specific (middle) antibodies for Western blot visualisation of HLA-DR1 α (30.97 kDa) and HLA-DR1 β (25.75 kDa), respectively. The yellow boxes indicated biotinylated protein, possibly HLA-DR1 α , the blue boxes indicated monomeric HLA-DR1 β , while the green boxes indicate possible degradation products. No clear sign of (correctly) folded HLA-DR1 could be observed.

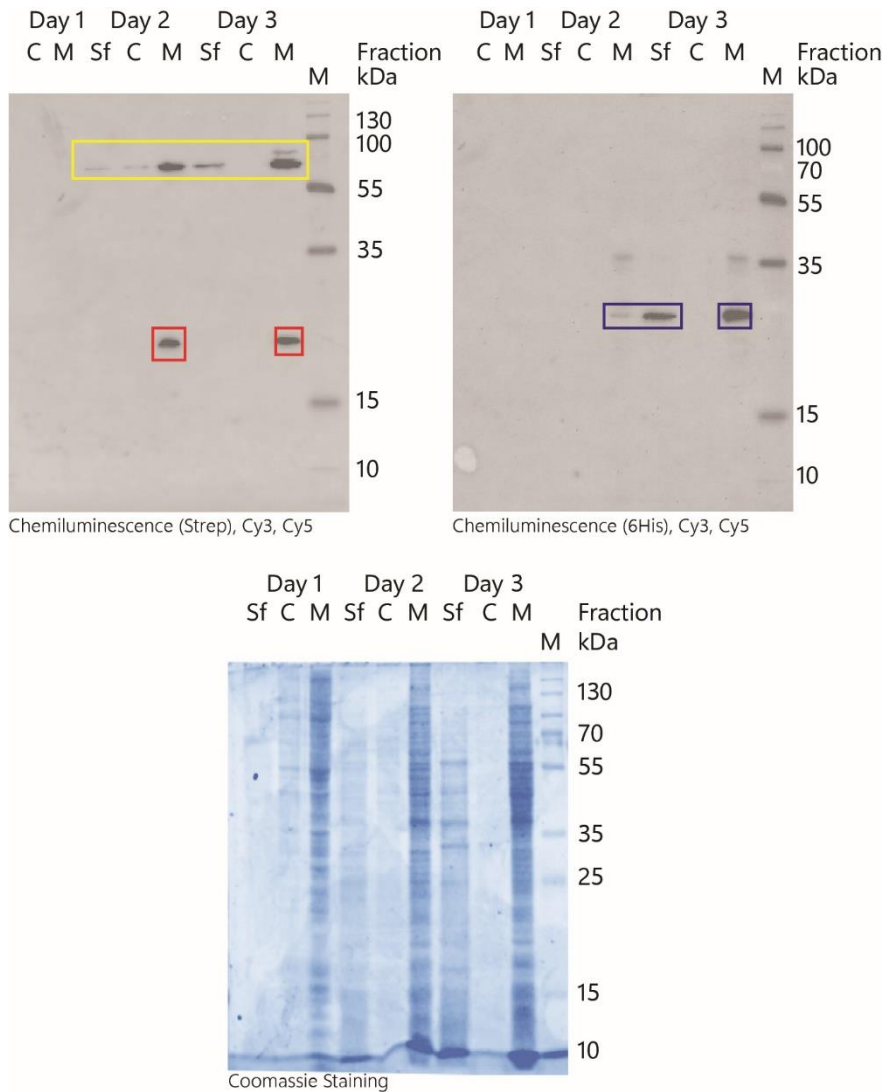


Figure S4 - HLA-DR1 expression by suspension Sf9 cells analysed by Western blot and coomassie staining. Suspension Sf9 insect cells were infected with HLA-DR1 encoding baculovirus and incubated for 1-3 days after which the cells were separated from the medium (Sf), followed lysis of the cell pellet resulting in a cytosolic (C) and membrane fraction (M). Samples of each day were analysed using dual-Strep and 6His-specific antibodies for Western blot visualisation of HLA-DR1α (30.97 kDa) and HLA-DR1β (25.75 kDa), respectively. The yellow box indicated biotinylated protein, possibly HLA-DR1α, the red boxes indicated monomeric HLA-DR1α and the blue boxes indicated monomeric HLA-DR1β. No clear sign of (correctly) folded HLA-DR1 could be observed.

HLA-DR1 sequences for mammalian expression

A)

HLA-DR1A*01*01 or HLA-DR1 α

DNA Sequence

GAATTC AAGC TTGCCGCCAC CATGGGAATC CTGCCTTCAC CCGGAATGCC TCGCCTTCTG TCACTGGTGT
 CGTTGCTTTC GGACTCTCTG ATGGGATGCG TGGCCATTAA GGAGGAACAC GTCATCATTC AGGCGGAGTT
 CTATCTGAAC CCGGATCAAT CGGGCGAGTT TATGTTTCGAC TTCGACGGTG ATGAGATCTT CCATGTGGAT
 ATGGCAAAGA AAGAGACAGT CTGGCGCCTT GAAGAATTG GGAGGTTTCG CAGCTTTGAG GCCCAAAGGTG
 CCCTCGCGAA TATCGCTGTA GACAAAGCGA ACCTTGAAT CATGACGAAG AGATCTAACT ATACTCCGAT
 TACGAACGTG CCACCGGAGG TCACGGTGCT CACCAACTCC CCGGTGGAGC TGAGGGAGCC AAATGTGTTG
 ATCTGTTTCA TCGATAAGTT TACCCTCCC GTCGTAACG TAACATGGTT GCGAAATGTT AAACCGGTGA
 CAACAGCGGT TAGCGAAACT GTATTCCTTC CACGTGAGGA TCACCTCTTT CGGAAATTCC ATTACCTCCC
 TTTTTCGCC TCCACGGAGG ACGGTGACGA CTGTCGAGTT GAACACTGGG GACTTGACGA ACCCTTGTG
 AAGCATTGGG AGTTTGATAC TAGTGGGGGAC GATGATGATA AGGGAAGTGG GAGCGGGCTC ACAGACACCC
 TCCAAGCCGA AACGGACCAG CTGGAAGATG AAAAGTCAGC ACTTCAGACG GAGATTGCGA ATCTGTTGAA
 AGAAAAAGAA AAACCTTGAGT TTATCCTTGC AGCGTAATGA TCACTCGAG

Protein Translation

MGILPSPGMPALLSLVSLVLLMGCVA
 IKEEHVIIQAIFYLNPDQSGEFMFDFDGDIEFHVDMAKKETVVRLEEF
 GRFASFEEAQQALANIADV KANLEIMTKRSNYTPITNVPEVTVLTNSP
 VELREPNVLICFDKFTPPVNVTVLWRNGKPVTTGVSETVFLPREDHL
 FRKFHYLPFLPSTEDVDYDCRVEHWGLDEPLKHWEFDT
 SGDDDDKGGSGGLTDLTDLQAETDQLEDEKSA LQTEIANLLKEKEKLEFILAA-

B)

HLA-DR1B*01*01 or HLA-DR1 β

DNA Sequence

GAATTC AAGC TTGCCGCCAC CATGGGGATT CTGCCTTCAC CTGGGATGCC TGCTCTGCTG TCTCTGGTCT CTCTGCTGTC
 AGTCTCTGCTG ATGGGATGCG TCGCTGGAG CCACCCACAG TTCGAGAAGG GAGCACCTGT GTCCAAAATGA
 GAATGGCTAC ACCACTGCTG ATGCAGGCAA GCGGGGGAAG CGGAAGTATT GAGGGGCGGG GATCCGGGGA
 CACCCGACCA CGTTTCTGT GGCAGCTTAA GTTTGAATGT CATTCTTCA ATGGGACGGA GCGGGTGCGG
 TTGCTGGAAA GATGCATCTA TAACCAAGAG GAGTCCGTGC GCTTCGACAG CGACGTGGGG GAGTACCGGG
 CGGTGACGGA GCTGGGGCGG CCTGATGCC AGTACTGGAA CAGCCAGAAG GACCTCTGG AGCAGAGGCG
 GGCCGCGGTG GACACCTACT GCAGACACAA CTACGGGGTT GGTGAGAGCT TCACAGTGCA GCGGCGAGTT
 GAGCCTAAGG TGACTGTGTA TCCTTCAAAG ACCCAGCCCC TGCAGCACCA CAACCTCCTG GTCTGCTCTGT
 GAGTGGTTTC TATCCAGGCA GCATTGAAGT CAGGTGGTTC CGGAACGGCC AGGAAGAGAA GGCTGGGGTG
 GTGTCACAG GCCTGATCCA GAATGGAGAT TGGACCTCC AGACCTGGT GATGCTGGAA ACAGTTCCT
 GGAGTGGAGA GGTTCACACC TGCCAAGTGG AGCACCCAAG TGTGACGAGC CCTCTCACAG TGAATGGAG
 AGCAACCGGT GGCAGCATG ATGACAAGGG TTCAGGGTCT GGGAGAATTG CCGGACTCGA AGAGAAAAGTC
 AAAACGTTGA AAGCGCAAAA CTCGGAGCTG GCTTCAACCG CGAATATGCT CCGTGAACAG GTCGCGCAGT
 TGAAACAGAA GGTGGGAAGC GGTTCGGGAG GGTGGAATGA CATTTCGAA GCGCAGAAGA TCGAGTGGCA
 CGAGGGCTCA GGCCATCATC ATCACCATCA CCACTAATGA TCACTCGAG

Protein Translation

MGILPSPGMPALLSLVSLVLLMGCVAWVSHPPQFEKGA
 PVSKMRMATPLLMQASGGSGSIEGRSGS
 DTRPRFLWQLKFECHFFNGTERVRLLERCIYNQEEVSFRFDSVGEYRAV
 TELGRPDAEYWNQKDLLEQRRAAVDVTCRHNHYGVGESFTVQRRVEP
 KVTVPYSKTQPLQHNLVCSVSGFYPGSIEVRWFRNGQEEKAGVVS
 TGLIQNGDWTFTQLVMLETVPRSGEVYTCQVEHPSVTSPLTVEWRATGG
 DDDDKGGSGGRIARLEEKVKTLKAQNSELASTANMLREQVAQLKQKV
 GSGSGGLNDIFEAQKIEWHEGSGHHHHHHH*

Figure S5 - Sequences of the HLA-DR1 subunits for mammalian expression.

A) cDNA sequence encoding HLA-DR1A*01*01 and amino acid sequence (**Uniprot: p01903**) with a *N*-terminal secretion signal sequence followed by a *C*-terminal enterokinase sequence (DDDDK), a flexible linker and the Fos sequence of the leucine zipper. B) cDNA sequence of HLA-DR1B*01*01 and amino acid sequence (**Uniprot: A9JJF6**). The Strep-tag CLIP-peptide is coupled *N*-terminally to HLA-DR1 β via a flexible linker and can be removed using the factor Xa site. The whole construct has the same *N*-terminal secretion signal sequence. The HLA-DR1 β gene is followed *C*-terminally by an enterokinase site (DDDDK) followed by a flexible linker and the Jun sequence of the leucine zipper. The whole construct has a 7His-tag at its *C*-terminus. Sequences were provided by Prof. Dr. Stephanie Gras.

HLA-DM expression and purification

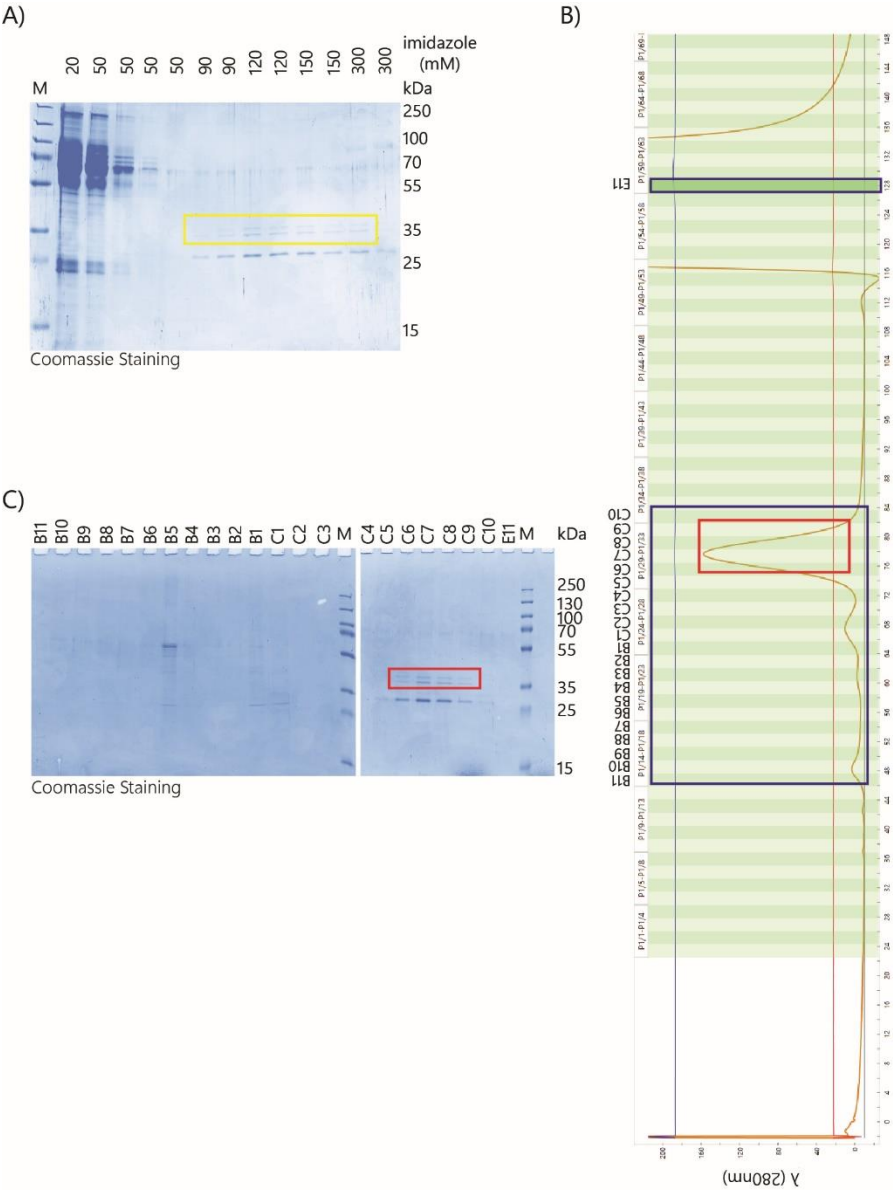


Figure S6 - HLA-DM expression in HEK293s GnT1⁻ and purification.
A) HEK293s GnT1⁻ cells were transfected with DNA encoding the HLA-DM, incubated for 5 days and harvested similar to HLA-DR1. HLA-DM was purified based on its 6His-tag using different concentrations imidazole in Tris/NaCl. B) The fractions indicated with the yellow box in (A) were combined and further purified using an HiLoad Superdex 16/600 200 pg column equilibrated with 10 mM Tris/150 mM NaCl pH 8. The fractions indicated in the blue boxes were analysed on SDS-PAGE (C). The red boxes indicate the fractions containing HLA-DM and correspond to the fractions depicted by the red boxes in (B). The individual subunits of both proteins are about 35-40 kDa.

5

Summary & Future Prospects

This thesis describes the use of 'click-to-release' chemistry for both drug design and in fundamental research. The first part of this thesis described the way in which click-to-release chemistry can be used to get spatiotemporal control over cytokines in an immunocytokine format. The toxicity of these, already existing drugs, is the limiting factor for its application in cancer therapy. Using trans-cyclooctene (TCO) esters, the cytokine can be inactivated, following coupling to a targeting moiety like a nanobody, and be reactivated by tetrazine treatment. For IL-1 β this concept proved to be very functional, however for TNF- α , some improvements still have to be made.

The second part of this thesis covered the first steps of fundamental research that could be done with click-to-release. Using clickable, antigenic peptides, the processing and binding of antigens to MHC-molecules can be researched. The Van Kasteren-group already started this for the murine MHC-I molecule and this work formed the basis for research into the human HLA-molecules. Recombinant overexpression of HLA-DR1 was established in HEK 293s GnT1⁻ cells which allowed for crystallization of the protein. The crystal structure of HLA-DR1 in complex with either a clickable or its native epitope could provide more insight in how binding and consequently T-cell activation is established.

In **Chapter 1** an overview was presented of most immunocytokines (ICs) currently in (pre) clinical trials. Most ICs are based on IL-2, IL-12 and TNF- α coupled to targeting moieties like scFvs which target neovasculature-associated antigens. These are commonly used targets for anti-tumour therapeutics. It is also clear that, even though the cytokines can now be delivered localized, (severe) systemic toxicities remain. Reduction of this systemic toxicity has been attempted by introducing activity-reducing point mutations, applying localized assembly and enzyme-based activation. Until now these are the main methods to reduce this systemic toxicity. However, these methods are not universal applicable for all cytokines and do not completely abolish the cytokine's off-target toxicity.

Therefore, in **Chapter 2** and **Chapter 3**, a new method was introduced in which click-to-release chemistry was proposed as an approach to gain spatiotemporal control over the cytokine activity. Herein NHS-TCO was used to selectively block lysine residues of the cytokines, IL-1 β and TNF- α , respectively, to inactivate the cytokine. Upon addition of a tetrazine, the TCO-moiety was released again, restoring the original lysine and protein folding and consequently restoring the cytokine activity.

For IL-1 β in **Chapter 2**, this worked well, as IL-1 β activity was reduced to <15% of its native activity upon blocking with NHS-TCO ester. Upon treatment with (2PyrH)₂Tz, its activity was restored to >90% of its native activity. With IL-1 β , a covalent construct was obtained by coupling a caged IL-1 β to a CD11c-specific nanobody by means of sortase A. This sequential coupling after the blocking reaction was essential for this immunocytokine design as the caging reaction with NHS-TCO is not specific and can therefore also cage the nanobody lysines, thereby potentially abolishing its targeting capacity.

Nevertheless, the purification of this conjugated protein remained difficult. Increasing the scale of protein before purification would be the initial step to recover more of the caged covalent construct. Also, the addition of (more) NaCl or other salts in the elution buffer during size exclusion chromatography could reduce the interactions of the caged immunocytokine with the excess of nanobody present, thereby separating them in

different fractions. When pure conjugated IL-1 β can be obtained, follow up experiments could include using a targeted *in vitro* assay with CD11c-positive dendritic cells as the target and HEK-Blue IL-1 β cells as reporter cells. When another nanobody can be coupled to IL-1 β this can also be done with relevant cancer models such as SUM229PE, which is an IL-1 β -sensitive triple negative human breast cancer cell line.¹ Eventually an *in vivo* experiment could be performed in which Nude mice carrying a SUM229PE tumour would be used to demonstrate the targeting property of the immunocytokine and the spatiotemporal control over its activity.

TNF- α in **Chapter 3** was also readily inactivated to <15% of its native activity. However, its reactivation proved to be more challenging. Literature study showed that no lysines have direct involvement in receptor interactions nor in the trimerization process.^{2,3} Therefore, significant reactivation was only established using millimolar concentrations of tetrazine in an Eppendorf tube. Translation to reactivation on cells did not prove significant enough for further pursuing this cytokine in this work.

As the exact cause for this limited reactivation remained unknown, some theories could be tested to see whether this reactivation can be established in some other way. TNF- α only functions as a trimer, and even though lysines were not directly involved in trimer formation, their intrinsic charge can be essential for protein folding and unfolding. This charge is removed upon binding of NHS-TCO, possibly resulting in the unfolding of both monomeric but also trimeric TNF- α . Size-exclusion chromatography combined with multi-angle light scattering (SEC-MALS), native mass spectrometry, native page and circular dichroism could be performed to see whether the trimer stayed intact upon treatment with NHS-TCO. If unfolding and/or monomerization indeed takes place, an attempt can be made to make a covalent TNF- α based on research published by Inoue *et al.*⁴ In this research a single-chain trimeric TNF- α variant was designed to selectively inhibit TNFR1 functioning. Three single-chain TNF- α molecules were designed, all with different short peptide linker (GGGGS, GGGSGGG and GGGSGGGSGGG) to couple the individual proteins. As the linkers are present on the upper surface, no disturbance of receptor interactions was predicted. All three single-chain TNF- α variants appeared to have similar biological properties, which were comparable to its non-covalent trimeric counterpart. This could be useful for the research described here as even though the lysines may disrupt initial trimerization (**Figure 1**)², due to covalent bonding between the

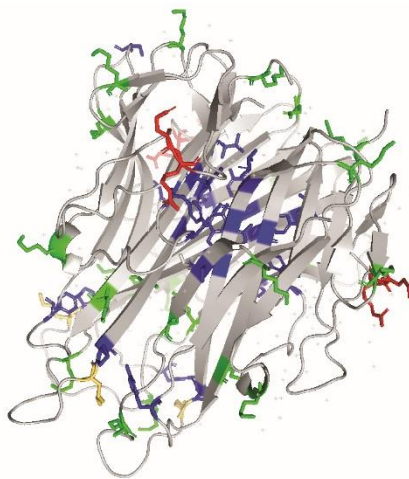


Figure 1 - Crystal structure trimeric murine TNF- α .

Trimeric murine TNF- α . The blue residues are involved in trimer formation. The green residues are the lysines. The red residues (Gln31 and Arg32) are essential for trimer formation. The yellow residue is lysine 112 (Lys112), which is next to proline 113 (Pro113). This residue is involved in trimer formation. Crystal structure was obtained and modified from Baeyens *et al.* (PDB:2tnf).

subunits refolding after decaging should be easier. A final option could be to use amber codon suppression for site-specific incorporation of a TCO-blocked amino acid. However, as the TCO would be exposed for longer periods of time it is expected to convert to cis-cyclooctene (CCO) which cannot be removed using tetrazine. Another aspect to take into account is that the incorporation of this unnatural amino acid is a rather difficult and time consuming process which does not necessarily yield in sufficient homogenous amounts of caged cytokine.

As click-to-release chemistry should be applicable to all molecules with free-amines, also other cytokines should be applicable for this technique. Cytokines contain (a lot of) positively charged lysine residues as these interact with negatively charged glycosaminoglycans (GAGs).⁵ As seen with IL-1 β and TNF- α , having lysines at critical positions in the cytokine structure increases the potential of this technique. These positions include position essential for either receptor binding or multimer formation. Therefore an initial screen could be performed on several (commercial) cytokines – IL-2, IL-10, IL-12, and TGF β , for example – to see whether these cytokines can be inactivated by TCO-treatment and be reactivated upon addition of tetrazine. Initial expression experiments were performed for interleukin-2 (IL-2) and interleukin-10 (IL-10). IL-2 is one of the most commonly used cytokines⁶ in ICs nowadays (see **chapter 1**) and therefore this would be a very important target for this technique. At the same time this cytokine has lysines (K35, K43 and K64) that are essential for, or next to residues, essential for receptor binding.⁷ IL-10 is coming more into focus in the immunocytokine field^{8,9} and is known for having at least two lysines (K99 and K138)^{10–12} in the receptor binding site. Initial expression of IL-2 in bacteria and HEK 293s GnTI⁻ cells (**Figure 2**) and of IL-10 in HEK 293s GnTI⁻ (**Figure 3**) were performed to obtain a substantial amount of cytokine to be used for caging and decaging optimisation.

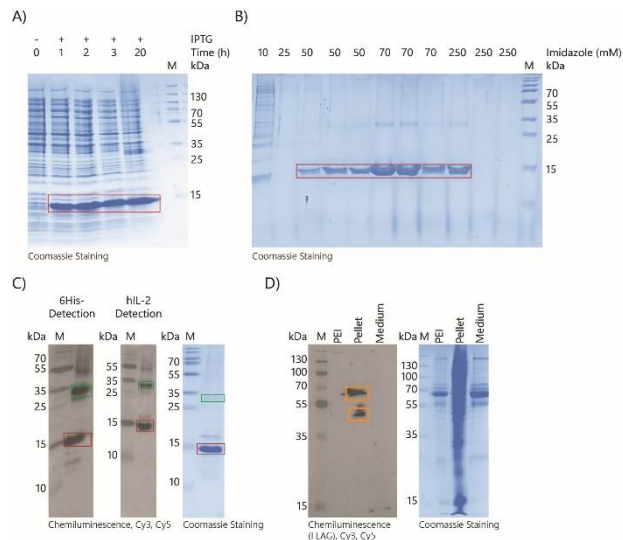


Figure 2 - Expression of human IL-2 (hIL-2) in bacteria and HEK 293s GnT1⁻ cells.

A) Human IL-2 (hIL-2) was expressed by *E. coli* BL21 (DE2) pLysS after IPTG induction for 3 hours. B) In urea dissolved inclusion bodies were loaded onto nickel beads for 6His-tag-based purification. C) Western blot analysis using 6His-tag- and IL-2-based detection. D) Expression of hIL-2 in HEK 293s GnT1⁻ cells. The cells were separated and lysed. Lysate (pellet) and medium were analysed using FLAG-specific Western blot. hIL-2 is about 15.5 kDa (red boxes). Possible dimers are indicated with the green boxes. The orange boxes in D) can be multimers but this was not confirmed.

Human IL-2 (hIL-2) was expressed both in *E. coli* BL21 (DE3) pLysS (**Figure 2A-C**) and HEK 293s GnT1⁻ cells (**Figure 2D**). Expression of hIL-2-6His in *E. coli* BL21 (DE3) pLysS resulted in an unfolded protein produced in inclusion bodies (**Figure 2A**). Protein expression was confirmed using both 6His-tag- and IL-2-based Western blots (**Figure 2C**). Purification using nickel beads resulted in relatively pure hIL-2-6His (**Figure 2B**), however further refolding of hIL-2-6His proved to be difficult (data not shown). Expression without 6His-tag was not established until now (data not shown). Therefore, expression in HEK 293s GnT1⁻ was attempted, which resulted in hIL-2-FLAG (**Figure 2D**). Purification of hIL-2-FLAG was not performed yet.

Both human IL-10 (hIL-10) (**Figure 3A**) and murine IL-10 (mIL-10) (**Figure 3B**) expression were confirmed using Western blot analysis. Transfection with pro-mIL-10 resulted in IL-10 secretion in the medium by the HEK 293s GnT1⁻ cells. The medium was loaded onto a nickel column from which IL-10 was eluted using imidazole in PBS (**Figure 3C**).

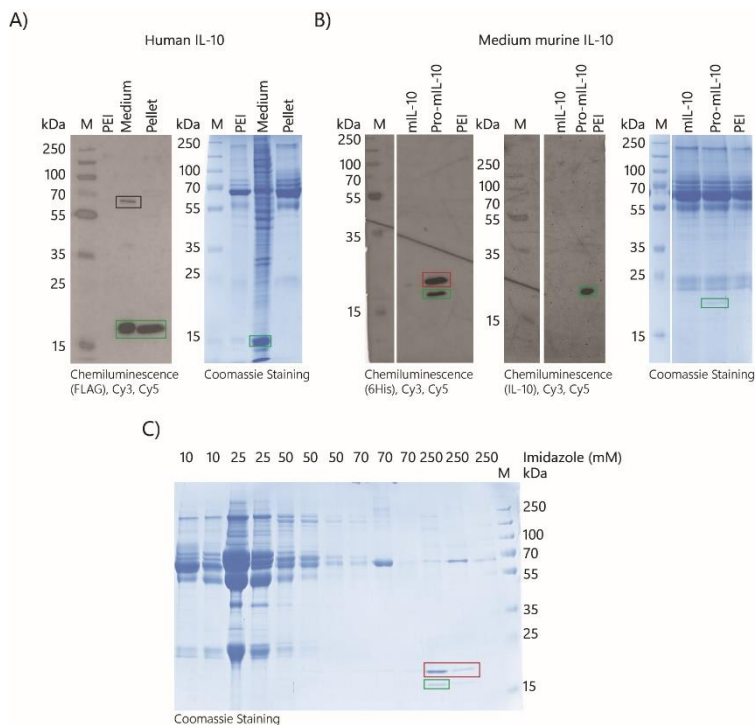


Figure 3 - Initial expression and purification of human and murine IL-10 from HEK 293s GnT1⁻ cells.

A) Human IL-10 (hIL-10) was expressed by HEK 293s GnT1⁻ cells. Medium and pellet were separated and each fraction was analysed using FLAG-specific Western blot. B) Murine IL-10 (mIL-10) was expressed as pro-mIL-10 and active mIL-10 by HEK 293s GnT1⁻ cells. The medium was analysed using 6His- and IL-10-specific Western blot and by coomassie staining. Pro-mIL-10 is about 23 kDa (red boxes) and IL-10 is about 21 kDa (green boxes). C) Medium of pro-mIL-10 transfected HEK 293s GnT1⁻ cells was loaded on nickel beads and eluted with imidazole in PBS.

As well as the cytokine payload also the targeting moiety can be optimised. For this research, an already polyglycine-tagged CD11c nanobody was used to show the general principle of this immunocytokine design and for the ease of continuation of the project. As it seemed that, especially for IL-1 β , the technique of inactivation and reactivation was feasible, alternative nanobodies have to be employed, with more suitable targets both for IL-1 β but also for other potential cytokines. Relevant targets would be targets of the neovasculature, checkpoint inhibitors or other unique antigens present on tumours. A start was made with the expression of five different nanobodies, targeting HER1/EGFR (7D12), HER2 (NB2), VEGF receptor 2 domain 3 (NTV1), human PD-L1 (B1) and murine PD-L1 (C16) (**Figure 4**). Expression was performed in *E. coli* ArcticExpress (DE3) RP upon IPTG induction. C16 and NB2 were readily expressed, 7D12 and NTV1 expression could be confirmed using 6His-tag specific Western blot. Until date no B1 could be expressed. These nanobodies can be purified and after sortase-mediated coupling to IL-1 β (or another cytokine) follow-up studies in relevant cancer models, also *in vivo*, are possible.

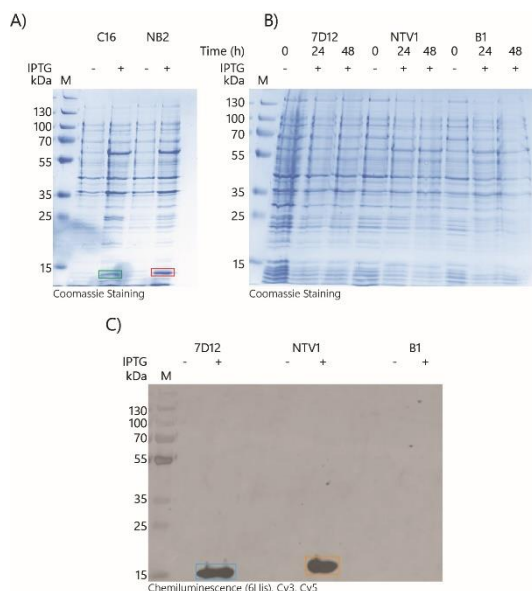


Figure 4 - Bacterial expression of various nanobodies upon IPTG induction.

A) Expression of nanobodies C16 (green box) and NB2 (red box), targeting murine PD-L1 and HER2, respectively, by *E. coli* ArcticExpress (DE3) RP. B) Expression of nanobodies 7D12, NTV1 and B1, targeting HER1/EGFR, VEGF receptor 2 domain 3 and human PD-L1, respectively, by *E. coli* ArcticExpress (DE3) RP. C) Western blot analysis of 7D12 (blue box), NTV1 (orange box) and B1 expression using 6His-specific detection. All, but B1, nanobodies could be expressed. Each nanobody is about 15 kDa.

In **Chapter 4** a different use of click-to-release chemistry was pursued; one geared not at the 'blanket' activation of the innate response, but at controlling the specific activation of specific CD4⁺ T-cells. HLA-DR1, a human MHC-II molecule, was expressed to be crystallized with both clickable and non-clickable peptides to see whether there are changes in HLA-DR1-peptide interactions upon introducing a minor change in the peptide. However, expression of HLA-DR1 proved to be a challenge in itself as it is a human membrane-bound protein complex consisting of two about equal size (molecular weight) subunits. Expression by bacteria, in *E. coli* ArcticExpress (DE3) RP resulted in the large amounts of the individual subunits. Nevertheless, complex formation by refolding did not result in sufficient amounts of correctly folded HLA-DR1. Expression in insect cells, using both *Sf9* and more conventional *High Five* cells, showed signs of folded HLA-DR1 complex. However, this complex remained in the membrane fraction after lysis with different methods. Therefore isolation of the complex without unfolding was rather difficult. Ultimately, HLA-DR1 was expressed by HEK 293s GnT1⁻ cells, which allowed for trimmed glycosylation. This was more favourable for crystallization purposes. An initial crystallization screen was performed with HLA-DR1-CLIP which resulted in quasi crystals. Although these were not applicable for diffraction experiments, these could be used for seeding in later screens. Alternatively, these could function as a starting point for further optimisation based on the current crystallization condition.

Further experiments should include the exchange of the CLIP peptide with another (clickable) peptide. A protocol provided by Prof. Dr. Stephanie Gras could form the basis for this. The initial peptide of choice would be RFYKTLRAEQASQ which originates from the HIV gag protein (Gag₂₉₉₋₃₁₁)^{13,14} and is also used by Szeto *et al.* Clickable peptides should be variants of this peptide in which different positions are replaced, one at the time, by clickable amino acids containing groups such as azides¹⁵ or NHS-TCO.^{16,17} In particular the lysine at position 4 (K4) could be of interest as this residue can be protected and deprotected again as has been described in previous research.¹⁶ Comparing crystal structures of HLA-DR1 with native and clickable peptides could provide insight in why performing click-chemistry on these complexes is more difficult compared to MHC-I. Ultimately, it could provide insight as a tool for studying peptide processing and presentation to T-cells.

Alternatively, research in the last two decades showed that certain sugars, zwitterionic polysaccharides (ZPSs), in the absence of peptides, could induce a T-cell response upon presentation by HLA-DR1.^{18,19} This class of macromolecules could provide a new source for vaccine development next to the already existing peptide- or RNA-based vaccines. However, the actual binding mode of these ZPSs has never been shown directly and also the processing pathway of the ZPSs toward the HLA-DR1 have only been shown in indirect manners (**Figure 5**). Therefore, co-crystal structures with ZPSs such as type 1 capsular polysaccharide from *Streptococcus pneumoniae* (SP1)²⁰ or polysaccharide A1 (PSA)¹⁸, could provide insight in its binding mode. Using clickable versions of these ZPSs could generate additional information about its processing pathway, when click-to-release chemistry proved to be possible under *in vivo* conditions.

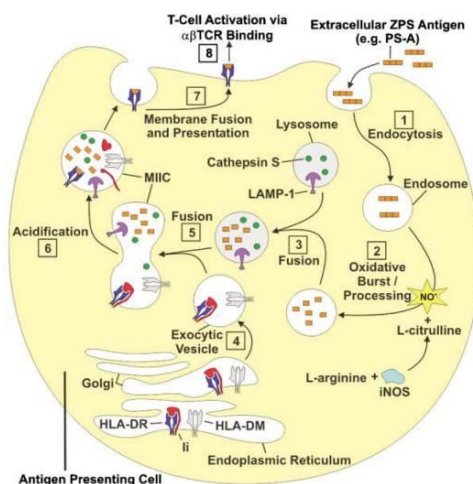


Figure 5 - Proposed processing mechanism of zwitterionic polysaccharides.

Zwitterionic polysaccharides (ZPS) are upon endocytosis (1) processed by the release of reactive oxygen species like hydrogen peroxide (oxidative burst) (2). Lysosome fusion (3) takes place with the MIIC (5) containing HLA-DR1 (4) whereafter it acidifies (6). The invariant chain (Ii) is then cleaved and the remaining CLIP peptide is removed by HLA-DM and replaced by the ZPS. Hereafter, the complexed HLA-DR is transferred to the cell surface to present its content to CD4+ T-cells. The illustration was obtained from Cobb *et al.*¹⁹

Materials & Methods

General reagents and equipment

All donor vectors were purchased from GenScript and primers were ordered at Sigma-Aldrich. All restriction enzymes, polymerases and ligases were purchased from Thermo Fisher Scientific. Benzonase was purchased from Santa Cruz Biotechnology. Sodium deoxycholate monohydrate (CAS:302-95-4) and phenylmethanesulfonyl fluoride (PMSF, CAS:329-98-6) were purchased from Sigma-Aldrich. QIAprep Spin Miniprep Kit (Cat. No. 27104) was purchased from Qiagen. HisPur™ Ni-NTA (Catalog #88222) was purchased from Thermo Fisher Scientific. Amicon® Ultra-4 Centrifugal Filters (#UFC800308) and Amicon® Ultra-15 Centrifugal Filters (#UFC900308) 3K were purchased from Merck. Rabbit anti-6*His (Item No. 600-401-392) was purchased from Rockland and mouse anti-rabbit IgG-HRP (Catalog #sc-2357) was purchased from Santa Cruz Biotechnology. DMEM-medium, L-glutamine, streptomycin and penicillin were all purchased from Sigma-Aldrich (MERCK)

Cell culture

HEK 293s GnT1⁻ cells (#CRL-3022, ATCC) were maintained in Dulbecco's Modified Eagle's Medium – high glucose (DMEM – high glucose, #D6546-500ML) supplemented with 10% Newborn Calf Serum (NCS), 2 mM glutamine, 100 IU/mL penicillin and 50 µg/mL streptomycin at 37°C, 7% CO₂. For each passage, twice a week, the cells were diluted 20 times.

Construct formation

For bacterial expression of human IL-2 NheI restricted (1x Tango Buffer, 10U NheI) pcDNA3.1⁺/C-(K)DYK_IL2 (CloneID: OHu25605, Accession version: NM_000586) was used as template for human IL-2 amplification by PCR (GC Green Buffer, 0.2 mM dNTPs, 0.1 µM of each primer, 50 ng restricted vector, 2U Phusion polymerase) using the primers of **Table 1**. The IL-2 fragments were restricted with XhoI/NcoI (10U each) and ligated into XhoI/NcoI (10U each) restricted pET28a(+)-vector behind the T7 promoter using T4 DNA Ligase (5U) at room temperature for 2 hours. Restriction was performed for 20 hours at 37°C, 300 rpm. The ligation products were transformed into *E. coli* XL10 via heat shock (42°C, 90 seconds) and SOC-medium recovery followed by growth at kanamycin (50 µg/mL) containing LB-agar plates at 37°C overnight. Transformation was checked by colony PCR using the primers of **Table 1**. For mammalian expression of human IL-2 the donor vector pcDNA3.1⁺/C-(K)DYK_IL2 was used.

Table 1 - Primer overview.

Primer Nr.	Construct	Sequence 5'→3'
1	IL-2-6His	ATATTCCATGGCACCTACTTCAAGTTCTACAAA
2		AAAACCTCGAGAGTCAGTGTGAGATGAT

Mammalian expression of human IL-10 was performed using the vector pcDNA3.1⁺/C-(K)DYK_IL10 (CloneID: OHu25319, Accession version: NM_000572.2). Mammalian expression of murine IL-10 (mIL-10) was performed using pcDNA3.1(+) as a vector ordered at GenScript with the cDNA sequence (pro-mIL-10 sequence ID: NM_010548.2) inserted between the NheI/XhoI restriction sites. For mIL-10 the first 54 nucleotides of this cDNA

including the ATG were removed, whereafter ATG was placed back at the *N*-terminus. For both pro-mIL-10 and mIL-10 the cDNA was modified by extending the *C*-terminus with the DNA sequence encoding for a flexible linker and a sortase A recognition site (**Table 2**) and removal of the stop codon. Removal of the stop codon causes the in frame addition of a 6His-tag at the *C*-terminus of the construct.

Table 2 - Extension of the (pro-)mIL-10 gene.

The nucleotides are added to the gene inserted in the pcDNA3.1(+)-vector and translate to a flexible linker and a sortase A recognition site. A *C*-terminal 6His-tag was added by placing the adapted gene without stop codon in frame with the 6His-tag encoded in the vector.

Nucleotide added to <i>C</i> -terminus of the gene	Translation to addition amino acids at <i>C</i> -terminus
GGCGGGGTGGCAGTCTGCCTGAAACAGGGGGT	GGGGS LPETGG

The cDNA of each nanobody (**Table 3**) was ordered in the pET21a(+)-vector in between the *Nde*I/*Xho*I restriction sites and ordered at GenScript. Each nanobody was *N*-terminally modified with a new start codon (ATG), a thrombin cleavage site (LVPRG) followed by a *N*-terminal polyglycine sequence (GGG) and linker sequence (S) (**Table 4, Figure 6**). The modified cDNA was placed in frame with a *C*-terminal 6His-tag.

Table 3 - Overview nanobodies.

Name nanobody	Target	Accession Number sdAb-Db
NB2	HER2	sdAb_2459_Cd
7D12	HER1/EGFR	sdAb_4902_Ca
NTV1	VEGFR-2 D3	sdAb_6905_Sy
B1	Human PD-L1	sdAb_7164_Cd
C16	Murine PD-L1	sdAb_0714_Cd

Table 4 - Overview *N*-terminal extensions of each nanobody.

Name sequence	cDNA sequence	Amino acid sequence added
Thrombin cleavage site	CTGGTCCCGCGC	LVPRG
<i>N</i> -terminal polyglycines	GGCGGAGGAGGT	GGG
Linker	AGT	S

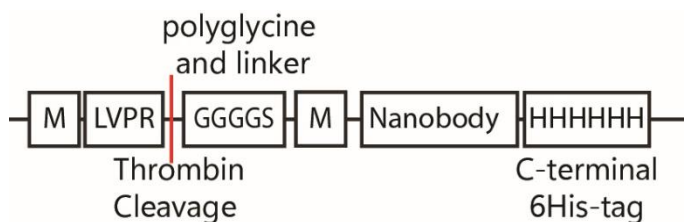


Figure 6 - Schematic overview of the nanobody construct.

The nanobody is *N*-terminally modified with an additional methionine, a thrombin cleavage site (LVPRG) followed by a polyglycine sequence (GGG) and a linker sequence (S). At the *C*-terminus a 6His-tag was introduced by placing the cDNA in frame with the already present sequence.

Protein expression and purification

For bacterial expression of human IL-2, the construct was isolated from *E. coli* XL10 using QIAprep Spin Miniprep Kit. This was used to transform calcium-competent *E. coli* BL21

(DE3) pLysS using heat shock (42°C, 45 seconds) followed by SOC-medium recovery. Colonies were grown on LB-agar plates containing kanamycin (50 µg/mL) and chloramphenicol (35 µg/mL) at 37°C overnight. Colonies were used to grow an overnight culture which was diluted 100 times in kanamycin (50 µg/mL) containing LB-medium for growth at 37°C, until the optical density at 600 nm (OD₆₀₀) reached 0.5-0.6. Expression was induced using 0.5 mM IPTG and took place at 42°C, 130 rpm for 3 hours. The bacteria were harvested by 30 minutes centrifugation at 3400g, 4°C.

5 gram cell pellet was lysed in 5 mL lysis buffer (50 mM Tris pH 8, 25% (w/v) sucrose, 1 mM EDTA, 1 mM PMSF, 2 mM DTT) containing 2 mg/mL lysozyme. Incubation for 30 minutes at 4°C while mixing was followed by addition of 1 mM MgCl₂ and 50U benzonase. 30 minutes incubation at 4°C, constant mixing was followed by lysate sonication (Sonics, Vibra Cell™) for 5 minutes with 5 second pulse of 20% amplitude with 5 seconds intervals on ice. Diluting the lysate three times in detergent buffer (0.2 M NaCl, 1% (w/v) sodium deoxycholate monohydrate, 1% IGEPAL, 20 mM Tris pH 7.5, 2 mM EDTA, 0.02 mM PMSF, 0.04 mM DTT) was followed by another 30 minutes incubation on ice. Centrifugation (30 minutes, 15000g at 4°C) resulted in a pellet which was washed three times using wash buffer (0.5% Triton X-100, 50 mM Tris pH 8, 100 mM NaCl, 1 mM EDTA, 2 mM DTT), a 18G-needle and syringe followed by centrifugation (20 minutes, 15000g at 4°C). The final centrifugation step was followed by dissolving the inclusion bodies in 8 M urea in 10 mM Tris pH 8 containing 10 mM imidazole at 22°C, constant mixing for 30 minutes. Centrifugation (10 minutes, 10000g at 4°C) removed the aggregates. The solubilized inclusion bodies were loaded onto equilibrated HisPur™ Ni-NTA resin. Incubation overnight at 4°C while rolling, was followed by loading onto a reaction syringe and flow through by gravity flow at room temperature. The column was washed using gravity flow with at least two column volumes of various concentrations of imidazole in 8 M Urea in 10 mM Tris pH 8. Samples of each fraction were taken and loaded onto SDS-PAGE for protein content analysis. hIL-2 containing samples were combined and concentrated (3400g for 30 minutes at room temperature) onto an Amicon® Ultra-15 Centrifugal Filter 3K.

For mammalian expression of human IL-2, pcDNA3.1⁺/C-(K)DYK_IL2 was used to transfect HEK 293s GnT1⁻ cells. HEK 293s GnT1⁻ cells were grown until 80% confluence in a T175 flask. Transfection was performed with 60 µg DNA using PEI as transport vehicle in a DNA/PEI w/w-ratio of 1:3. Following 30 minutes room temperature incubation, the DNA/mixture was added to the cells with transfection medium (DMEM-high glucose, 2 mM glutamine, 1% NCS) and 6.7x concentrated master mix (DMEM-high glucose, 40 mM glutamine, 20 mM pyruvate, 200 mM HEPES pH 7.4, 20x non-essential amino acids and 4 µM β-mercaptoethanol) until a total volume of 40 mL. Cells were incubated for 7 days at 37°C, 7% CO₂ before medium and cells were harvested. This suspension was supplied with 50 mM Tris pH 8, 1 mM NiCl₂ and 5 mM CaCl₂, final concentrations. After 30 minutes incubation at 4°C, constant rolling, the suspension was centrifuged for 20 minutes at 3200 rcf, 4°C and the resulting supernatant was filtered using a 0.2 µm filter.

Murine IL-10 (mIL-10) constructs, both pro-mIL10 and mIL-10, and human IL-10 (hIL-10) were also expressed in HEK 293s GnT1⁻ in a similar way as was described above for human IL-2. The filtered resulting supernatant was supplied with 20 mM imidazole for 6His-tag based purification. HisPur Ni-NTA was equilibrated as has been described in the

manufacture's manual. The pro-mIL-10-containing medium was incubated with the resin for 2 hours at 4°C, constant rolling. Following, the proteins were washed and eluted on ice with various concentrations of imidazole in PBS. The protein containing fractions, based on SDS-PAGE, were combined and concentrated using Amicon® Ultra-15 Centrifugal Filters 3K filters equilibrated with PBS (20 minutes at 3200 *rcf*, 4°C).

The nanobody constructs were used to transform calcium competent *E. coli* ArcticExpress (DE3) RP using heat shock (42°C, 45 seconds) and SOC-medium recovery. Colonies were used to inoculate LB-medium containing ampicillin (250 µg/mL) and gentamycin (7 µg/mL) for overnight growth at 37°C, 170 rpm. The overnight culture was diluted 20 times and grown at 37°C, 170 rpm until OD₆₀₀ of 0.6 was reached after which the protein expression was induced with the addition of 0.5 mM IPTG. Expression took place for 24 hours at 18°C, 140 rpm, where after the bacteria were harvested by centrifugation (30 minutes, 3400g at 4°C). Samples before and after IPTG induction were taken and analysed on SDS-PAGE to assess protein expression.

Western blot

Denaturing acrylamide gels (SDS-PAGEs) were blotted onto 0.2 µm PVDF membrane (midi format, single application of Bio-Rad) using the Turbo Trans Blot System (Bio-Rad). Blots were developed using luminol solution (25% (w/v) luminol in 0.1 M Tris pH 8.8), 100x diluted enhancer (1.1 mg/mL p-coumaric acid in DMSO) and H₂O₂. Blots were imaged with the ChemiDoc™ MP Imaging System of Bio-Rad with settings chemiluminescence, Cy3 and Cy5 and analysed using ImageLab Software version 4.1.

6His-specific blot

Blots were washed with TBS (10 minutes) and TBST (3x 5 minutes) (1x TBS pH 7.5; 0.1% Tween-20), respectively before blocking with 5% milk in TBST overnight at 4°C. Washing with TBST (3x 5 minutes) was followed with rabbit anti-6*His incubation (1:1000) in blocking buffer for 3 hours at room temperature. Another wash (3x 5 minutes) with TBST was followed by addition of mouse anti-rabbit IgG-HRP (1:4000) and incubation for 2 hours at room temperature. The blots were washed with TBST (3x 5 minutes) and TBS (10 minutes), respectively, before development with luminol.

FLAG-specific blot

The primary antibody used was mouse anti-FLAG (1:1000, #F3156-5MG, Sigma-Aldrich). The secondary antibody used was goat anti-mouse IgG-HRP conjugate (1:4000, #113-035-003, Jackson).

IL-2- and IL-10-specific blot

Blots were washed with PBS and PBST (1x PBS pH 7.4, 0.5% Tween-80) instead of TBS and TBST, respectively. Blocking was performed with 0.2% BSA in PBST. For hIL-2 the primary antibody used was biotin-conjugate anti-human IL-2 (#88-7025-88, Thermo Fisher Scientific) and for IL-10 the primary antibody used was biotin-conjugate anti-mouse IL-10 (#88-7105-88, Thermo Fisher Scientific). Streptactin-HRP (#2-1502-001, IBA solutions) was used as a secondary antibody or both cytokines.

References

- (1) Martínez-Reza, I.; Díaz, L.; Barrera, D.; Segovia-Mendoza, M.; Pedraza-Sánchez, S.; Soca-Chafre, G.; Larrea, F.; García-Becerra, R. Calcitriol Inhibits the Proliferation of Triple-Negative Breast Cancer Cells through a Mechanism Involving the Proinflammatory Cytokines IL-1 β and TNF- α . *J Immunol Res* **2019**, *2019*, 1–11. <https://doi.org/10.1155/2019/6384278>.
- (2) Baeyens, K. J.; De Bondt, H. L.; Raeymaekers, A.; Fiers, W.; De Ranter, C. J. The Structure of Mouse Tumour-Necrosis Factor at 1.4 Å Resolution: Towards Modulation of Its Selectivity and Trimerization. *Acta Crystallogr D Biol Crystallogr* **1999**, *55* (4), 772–778. <https://doi.org/10.1107/S0907444998018435>.
- (3) Mukai, Y.; Shibata, H.; Nakamura, T.; Yoshioka, Y.; Abe, Y.; Nomura, T.; Tanai, M.; Ohta, T.; Ikemizu, S.; Nakagawa, S.; Tsunoda, S. ichi; Kamada, H.; Yamagata, Y.; Tsutsumi, Y. Structure-Function Relationship of Tumor Necrosis Factor (TNF) and Its Receptor Interaction Based on 3D Structural Analysis of a Fully Active TNFR1-Selective TNF Mutant. *J Mol Biol* **2009**, *385* (4), 1221–1229. <https://doi.org/10.1016/j.jmb.2008.11.053>.
- (4) Inoue, M.; Ando, D.; Kamada, H.; Taki, S.; Niiyama, M.; Mukai, Y.; Tadokoro, T.; Maenaka, K.; Nakayama, T.; Kado, Y.; Inoue, T.; Tsutsumi, Y.; Tsunoda, S. I. A Trimeric Structural Fusion of an Antagonistic Tumor Necrosis Factor- α Mutant Enhances Molecular Stability and Enables Facile Modification. *Journal of Biological Chemistry* **2017**, *292* (16), 6438–6451. <https://doi.org/10.1074/jbc.M117.779686>.
- (5) Fernandez-Botran, R.; Gorantla, V.; Sun, X.; Ren, X.; Perez-Abadia, G.; Crespo, F. A.; Oliver, R.; Orhun, H. I.; Quan, E. E.; Maldonado, C.; Ray, M.; Barker, J. H. Targeting of Glycosaminoglycan-Cytokine Interactions as a Novel Therapeutic Approach in Allotransplantation1. *Transplantation* **2002**, *74* (5), 623–629. <https://doi.org/10.1097/00007890-200209150-00007>.
- (6) Zheng, X.; Wu, Y.; Bi, J.; Huang, Y.; Cheng, Y.; Li, Y.; Wu, Y.; Cao, G.; Tian, Z. The Use of Supercytokines, Immunocytokines, Engager Cytokines, and Other Synthetic Cytokines in Immunotherapy. *Cell Mol Immunol* **2022**, *19* (2), 192–209. <https://doi.org/10.1038/s41423-021-00786-6>.
- (7) Ye, C.; Brand, D.; Zheng, S. G. Targeting IL-2: An Unexpected Effect in Treating Immunological Diseases. *Signal Transduction and Targeted Therapy*. Springer Nature December 1, 2018. <https://doi.org/10.1038/s41392-017-0002-5>.
- (8) Qiao, J.; Liu, Z.; Dong, C.; Luan, Y.; Zhang, A.; Moore, C.; Fu, K.; Peng, J.; Wang, Y.; Ren, Z.; Han, C.; Xu, T.; Fu, Y. X. Targeting Tumors with IL-10 Prevents Dendritic Cell-Mediated CD8+ T Cell Apoptosis. *Cancer Cell* **2019**, *35* (6), 901–915.e4. <https://doi.org/10.1016/j.ccell.2019.05.005>.
- (9) Schwager, K.; Kaspar, M.; Bootz, F.; Marcolongo, R.; Paresce, E.; Neri, D.; Trachsel, E. Preclinical Characterization of DEKAVIL (F8-IL10), a Novel Clinical-Stage Immunocytokine Which Inhibits the Progression of Collagen-Induced Arthritis. *Arthritis Res Ther* **2009**, *11* (5). <https://doi.org/10.1186/ar2814>.
- (10) Walter, M. R. The Molecular Basis of IL-10 Function: From Receptor Structure to the Onset of Signaling; 2014; pp 191–212. https://doi.org/10.1007/978-3-662-43492-5_9.
- (11) Josephson et al 2001 Crystal Structure of the IL-10 IL-10R1 Complex Reveals a Shared Receptor Binding Site.
- (12) Zdanov, A.; Schalk-Hihi, C.; Gustchina, A.; Tsang, M.; Weatherbee, J.; Wlodawer, A. Crystal Structure of Interleukin-10 Reveals the Functional Dimer with an Unexpected Topological Similarity to Interferon γ . *Structure* **1995**, *3* (6), 591–601. [https://doi.org/10.1016/S0969-2126\(01\)00193-9](https://doi.org/10.1016/S0969-2126(01)00193-9).
- (13) Szeto, C.; Bloom, J. I.; Sloane, H.; Lobos, C. A.; Fodor, J.; Jayasinghe, D.; Chatzileontiadou, D. S. M.; Grant, E. J.; Buckle, A. M.; Gras, S. Impact of HLA-DR Antigen Binding Cleft Rigidity on T Cell Recognition. *Int J Mol Sci* **2020**, *27* (19), 1–20. <https://doi.org/10.3390/ijms21197081>.
- (14) Benati, D.; Galperin, M.; Lambotte, O.; Gras, S.; Lim, A.; Mukhopadhyay, M.; Nouël, A.; Campbell, K.-A.; Lemerrier, B.; Claireaux, M.; Hendou, S.; Lechat, P.; de Truchis, P.; Boufassa, F.; Rossjohn, J.; Delfraissy, J.-F.; Arenzana-Seisdedos, F.; Chakrabarti, L. A. Public T Cell Receptors Confer High-Avidity CD4 Responses to HIV Controllers. *Journal of Clinical Investigation* **2016**, *126* (6), 2093–2108. <https://doi.org/10.1172/JCI83792>.
- (15) Pawlak, J. B.; Gentil, G. P. P.; Ruckwardt, T. J.; Bremmers, J. S.; Meeuwenoord, N. J.; Ossendorp, F. A.; Overkleef, H. S.; Filippov, D. V.; van Kasteren, S. I. Bioorthogonal Deprotection on the Dendritic Cell Surface for Chemical Control of Antigen Cross-Presentation. *Angewandte Chemie International Edition* **2015**, *54* (19), 5628–5631. <https://doi.org/10.1002/anie.201500301>.
- (16) Lahav-van der Gracht, A. M. F. Bioorthogonal Deprotection Strategy to Study T-Cell Activation and Cross-Presentation, Universiteit Leiden, Leiden, 2020.
- (17) Van Der Gracht, A. M. F.; De Geus, M. A. R.; Camps, M. G. M.; Ruckwardt, T. J.; Sarris, A. J. C.; Bremmers, J.; Maurits, E.; Pawlak, J. B.; Posthoorn, M. M.; Bongers, K. M.; Filippov, D. V.; Overkleef, H. S.; Robillard, M. S.; Ossendorp, F.; Van Kasteren, S. I. Chemical Control over T-Cell Activation in Vivo Using Deprotection of Trans-Cyclooctene-Modified Epitopes. *ACS Chem Biol* **2018**, *13* (6), 1569–1576. <https://doi.org/10.1021/acscmbio.8b00155>.

Chapter 5

- (18) Kreisman, Iori S.C. Friedman, Julia H. Neaga, Andreea Cobb, B. A. Structure and Function Relations with a T-Cell-Activating Polysaccharide Antigen Using Circular Dichroism. **2007**, *86* (3), 573–579. <https://doi.org/10.1109/TMI.2012.2196707>. Separate.
- (19) Cobb, B. A.; Wang, Q.; Tzianabos, A. O.; Kasper, D. L. Polysaccharide Processing and Presentation by MHC II Pathway. *Cell* **2010**, *117* (5), 677–687. <https://doi.org/10.016/j.cell.2004.05.001>. Polysaccharide.
- (20) Feldman, C.; Anderson, R. Recent Advances in Our Understanding of Streptococcus Pneumoniae Infection. *F1000Prime Rep* **2014**, *6* (September). <https://doi.org/10.12703/P6-82>.

Nederlandse Samenvatting

Deze thesis beschrijft de toepassing van 'click-to-release' chemie in zowel toegepast als fundamenteel onderzoek. De toepassing ligt in het veld van de immunocytokines waarbij deze moleculen selectief geactiveerd kunnen worden na het deactiveren met behulp van chemische groepen. In fundamenteel onderzoek kan het gebruik van deze techniek meer inzicht geven in hoe en waarom bepaalde processen plaatsvinden. In dit werk werd de basis gelegd voor onderzoek naar de aanwezigheid en afwezigheid van T-cel reacties na herkenning van peptiden gepresenteerd op antigeen-presenterende eiwitten.

Hoofdstuk 0 introduceert het concept van 'click-to-release' chemie in de vorm van de inverse-elektron demand Diels-Alder (IEDDA) reactie. Deze reactie is gebaseerd op de ligatie van een elektron-arme diene aan een elektron-rijke dienofiel. Deze bio-orthogonale reactie maakt het mogelijk om selectief moleculaire groepen in, onder andere, eiwitten aan te passen onder fysiologische condities. Enkele toepassingen van deze reactie zijn de ontwikkeling antilichaam-medicijn conjugaten (ADCs), waarbij een antilichaam een zeer toxische stof op een specifieke plek in het lichaam kan loslaten. De binding tussen de toxische stof en het antilichaam wordt gevormd door een *trans*-cyclo-octeen (TCO) die kan reageren met een tetrazine, waardoor de gekoppelde toxische stof loslaat, waarna het bijvoorbeeld tumor cellen kan doden. Een andere toepassing bevindt zich in het veld van fundamenteel onderzoek, waarbij het selectief aan- en uitzetten van een proces inzicht kan geven in het verloop van het proces. Een voorbeeld hiervan is het blokkeren van T-cel activiteit door een peptide met een blokkerende groep (bijvoorbeeld een TCO) te binden aan een antigeen-presenterend eiwit. Met behulp van tetrazine kan de activiteit van de T-cel gereguleerd worden. De IEDDA reactie staat aan de basis van zowel het toegepaste als het fundamentele onderzoek beschreven in dit proefschrift.

Hoofdstuk 1 beschrijft het concept van immunocytokines. Dit zijn cytokines (signaaleiwitten van het immuun systeem) gekoppeld aan een antilichaam of varianten daarvan die gericht zijn op een tumor of de tumor omgeving. Het gebruik van cytokines in kankertherapie is al jaren een belangrijk onderzoeksveld en verschillende cytokines worden inmiddels in de kliniek getest en/of gebruikt. Het grote probleem met cytokines is dat blootstelling aan deze eiwitten op ongewenste plekken in het lichaam, overal behalve bij een tumor of andere infectie, leidt tot onnodige activatie van het immuun systeem, wat leidt tot ernstige bijwerkingen of in sommige gevallen tot de dood. De koppeling van cytokines aan antilichamen die de tumor of het tumormilieu als doelwit hebben reduceert de toxiciteit van de cytokines, maar deze vermindering is nog steeds niet voldoende om de cytokines op grotere schaal toe te passen in kankertherapie. Dit is het gevolg van de activiteit die het betreffende cytokine nog bezit na koppeling met een antilichaam en de aanwezigheid van receptoren die een binding kunnen aangaan met dit cytokine in heel het lichaam. Verschillende methodes zijn onderzocht om deze toxiciteit nog verder te

verminderen, waaronder het aanbrengen van activiteit-verminderende mutaties, het recombineren van cytokines bij de tumor en het gebruik van tumor-geassocieerde enzym-geactiveerde cytokines. Verschillende immunocytokines, gebaseerd op, onder ander interleukine-2, interleukine-12 en tumor necrose factor α (TNF- α), met hun verschillende eigenschappen werden toegelicht in dit hoofdstuk. Tot slot beschrijft dit hoofdstuk de mogelijke applicatie van 'click-to-release' chemie, beschreven in hoofdstuk 0, in het selectief activeren van immunocytokines wanneer deze de tumor (omgeving) bereiken.

Hoofdstuk 2 beschrijft het cytokine interleukine-1 β (IL-1 β) als een model cytokine voor de toepassing van 'click-to-release' chemie in het format van immunocytokines. IL-1 β is een cytokine met zowel pro-inflammatoire als anti-inflammatoire eigenschappen en heeft een dubieuze rol in het ontstaan en behoud van tumoren. Echter heeft IL-1 β ook een aantal lysines op essentiële posities voor receptor interacties, waardoor het blokkeren van deze posities kan leiden tot het deactiveren van het cytokine. IL-1 β werd gereageerd met een lage concentratie TCO op een lagere temperatuur voor een langere periode. Hierbij werden zoveel mogelijk makkelijk toegankelijke lysines geblokkeerd wat leidde tot het blokkeren van interactiemogelijkheden met de IL-1 β receptor op HEK-Blue IL-1 β cellen en RAW-Blue cellen. Door het toevoegen van tetrazine werden deze TCO-groepen verwijderd en werd de IL-1 β activiteit hersteld. Voor de koppeling aan een antilichaam, of in deze studie, een nanobody, werd gebruik gemaakt van het enzym *sortase A* dat een eiwit met de herkenningssequentie LPETG kan koppelen aan een eiwit met een terminale poly-glycine sequentie. IL-1 β met een C-terminale LPETG sequentie werd op deze manier gekoppeld aan een CD11c-specifiek nanobody met een N-terminale poly-glycine sequentie. Alhoewel de zuivering van het geblokkeerde IL-1 β gekoppeld aan het CD11c-specifieke nanobody nog optimalisering vereist, werd wel aangetoond dat dit construct inactief is en gereactiveerd kan worden op cellen met behulp van tetrazine.

Hoofdstuk 3 richt zich op een ander cytokine, tumor necrose factor α (TNF- α). Dit cytokine wordt historisch gezien het meest geassocieerd met het behandelen van kanker en is daarom het onderwerp van verschillende onderzoeken. De technieken beschreven in hoofdstuk 1 en hoofdstuk 2 werden in hoofdstuk 3 toegepast op TNF- α . Het blokkeren van lysines aanwezig in TNF- α resulteerde in het blokkeren van receptor interacties, waardoor TNF- α gevoelige L929 muis fibroblasten overleefden en HEK-Blue TNF- α cellen niet geactiveerd werden. Het reactiveren van geblokkeerd TNF- α met behulp van dimethyl-tetrazine in een Eppendorf buisje kon worden aangetoond door de sterfte van L929 cellen na receptor interacties met TNF- α . Echter kon deze manier van reactiveren niet vertaald worden naar reactiveren in de aanwezigheid van cellen. De mogelijke oorzaken hiervoor liggen in de manier waarop TNF- α bindt aan de receptor. TNF- α functioneert als een trimeer, waarbij de lysine residuen niet direct van belang zijn voor interacties met de receptor of voor de trimeer formatie. Meer onderzoek naar de geblokkeerde TNF- α structuur kan meer inzicht geven in welke lysines reageren met TCO en de bijbehorende gevolgen voor de structuur; valt de trimeer uit elkaar of is er een andere oorzaak.

Hoofdstuk 4 focust zich op een het andere veld waarin 'click-to-release' chemie van grote waarde is: het fundamentele onderzoek. Antigenen (peptide epitoom) worden door immuun cellen gepresenteerd op zogenaamde humaan leukocytenantigeen (HLA-) eiwitten aan immuun cellen zoals T-cellen die zorgen voor de afweerreactie. Voorgaand onderzoek heeft aangetoond dat een kleine modificatie in het gepresenteerde peptide resulteerde in de afwezigheid van een afweerreactie doordat de T-cel het epitoom gebonden aan de muis-variant van HLA (MHC) niet herkende. In dit werk werd de basis gelegd voor onderzoek naar waarom dit het geval is. Hiervoor werd recombinant HLA-DR1 geproduceerd in verschillende eiwit expressie systemen: bacteriën (*E.coli*), insectencellen (*Sf9* en *High Five*) en humane cellen (HEK). Uit dit onderzoek bleek dat productie in bacteriën vereist dat de gevormde eiwitketens opnieuw gevouwen konden worden. Dit gebeurde echter niet of met zeer lage opbrengst, wat deze methode ongeschikt maakte voor vervolgonderzoek. Productie met behulp van insectencellen resulteerde in de productie van gevouwen recombinant HLA. Na analyse bleek echter dat dit gevouwen eiwitcomplex zich bevond in de onoplosbare fractie na het lyseren van de insectencellen. Dit betekende dat zuivering complex zou zijn met het risico dat als gevolg van de zuiveringscondities het complex alsnog zou ontvouwen. Uiteindelijk bleek expressie in een humaan systeem, met behulp van HEK cellen, te resulteren in significante hoeveelheden zuiver HLA-DR1 in een gevouwen staat. Dit zuivere complex werd gebruikt voor kristallisatie experimenten waarbij de structuur van het complex geanalyseerd kan worden. Dit vormt de basis voor toekomstig onderzoek, waarbij het endogene peptide CLIP wordt vervangen door alternatieve peptiden met en zonder blokkerende groepen die geschikt zijn voor click-to-release chemie. Kristalstructuren van deze verschillende peptiden gebonden aan HLA-DR1 kunnen inzicht geven in het waarom T-cellen deze peptiden niet meer herkennen en dus waarom deze cellen geen afweerreactie genereren.

Hoofdstuk 5 betreft een samenvatting van al het werk weergegeven in deze thesis. Daarnaast bevat het suggesties voor toekomstig onderzoek per onderwerp. Dit betreft onder andere het onderzoeken van de toepasbaarheid van 'click-to-release' chemie op verschillende cytokines zoals interleukine-2 en interleukine-10. Initiële experimenten voor de expressie van deze cytokines worden hier al weergegeven. Daarnaast kan meer structuuronderzoek voor TNF- α meer inzicht geven in waarom dit cytokine minder geschikt lijkt voor deze methode dan IL-1 β . Tot slot worden er suggesties beschreven voor experimenten met recombinant HLA-DR1. Naast het co-kristalliseren met verschillende (geblokkeerde) peptiden, worden ook experimenten met zwitterionische polysachariden (ZPSs) beschreven. De laatste 20 jaar werd duidelijk dat deze suikermoleculen een vergelijkbare immuunreactie kunnen genereren via binding aan HLA-DR1. De manier waarop deze binding plaatsvindt is echter nog een punt van discussie. Het co-kristalliseren van deze ZPSs met HLA-DR1 zou meer antwoorden kunnen geven in dit onderzoek.

List of Publications

Patent Submission

Inactivation and reactivation of (immune) cytokines using Click-to-Release chemistry.

A. Barendrecht, T. Shema, M. Verdoes, M. Travis, S.I. van Kasteren. Filing date: January 23, 2024

Manuscript in preparation

Click-to-Release Chemistry as a Tool to Chemically Control Activity of Cytokines in the Immunocytokine Format

A. Barendrecht, D. Torres García, T. Shema, G. Aba, C. LeGall, H. Mikula, M. Travis, M. Verdoes, S. I. van Kasteren

New Insights in Binding Interactions between HLA-DR1 and Zwitterionic Polysaccharides

C. E. J. Sorieul, A Barendrecht, J. C. R. Brzoskowski, S. Gras, Z. W. B. Armstrong, S. I. van Kasteren

Curriculum Vitae

Nederlands

Amber Barendrecht werd geboren op 17 november 1994 te Dirksland. In 2013, na het afronden van de middelbare school (VWO, Maerlant te Brielle), startte zij met de bachelor Life Science & Technology aan de Universiteit Leiden en Technische Universiteit Delft (TU Delft). Het afronden van de propedeuse in 2014 werd beloond met de Young Talent Encouragement Award namens de Koninklijke Hollandsche Maatschappij der Wetenschappen. In 2016 behaalde zij haar bachelor *cum laude*. Tijdens haar bachelor stage in de groep van dr. Sander I. van Kasteren aan de Universiteit Leiden werkte zij aan de kristallisatie van immuun eiwitten (MHC-I) met verschillende peptiden gebonden.

Vervolgens zette zij haar studie voort met de research master Life Science & Technology aan de Universiteit Leiden. Tijdens het eerste jaar van deze master (2016) volgde zij naast het reguliere onderwijs nog een extra-curriculair programma van de Netherlands Research School of Chemical Biology. In het tweede jaar van deze master (2017) volgde zij een onderzoeksstage onder leiding van dr. Sander I. van Kasteren aan de Universiteit Leiden. Dit onderzoek betrof het produceren van humane immuun eiwitten in insectencellen. In 2018 werd het master diploma *cum laude* behaald.

In september 2018 begon zij aan haar PhD aan de Universiteit Leiden in de vakgroep Bio-Organische Synthese onder supervisie van dr. Sander I. van Kasteren en dr. Zach W. B. Armstrong. Het onderzoek verricht tijdens deze periode staat beschreven in dit proefschrift.

In juni 2023 is zij begonnen als postdoc aan de Universiteit Leiden.

Curriculum Vitae

English

Amber Barendrecht was born on November 17th, 1994 in Dirksland. She finished her secondary education (VWO, Maerlant in Brielle, the Netherlands) and started her bachelor Life Science & Technology at Leiden University and Technical University Delft (TU Delft). Her first year was awarded with the Young Talent Encouragement Award by the Koninklijke Hollandsche Maatschappij der Wetenschappen in 2014. In 2016, she obtained her bachelor degree *cum laude*. Her bachelor internship, which she performed under supervision of dr. Sander I. van Kasteren, aimed to obtain crystal structures of immune proteins (MHC-I) bound by various peptides.

She continued her education with the research master Life Science & Technology at Leiden University. During her first year (2016) she followed an extracurricular program of the Netherlands Research School of Chemical Biology. During the second year of the master program she did a research internship in the Bio-organic Synthesis group at Leiden University under supervision of dr. Sander I. van Kasteren. This research involved the recombinant expression of the human proteins in insect cells. In 2018 she obtained her master degree, *cum laude*.

In September 2018 she started her PhD studies at Leiden University in the Bio-Organic Synthesis group under supervision of dr. Sander I. van Kasteren and dr. Zach W. B. Armstrong. The research performed during these studies is described in this Thesis.

In June 2023, she continued working in the Bio-Organic Synthesis group as a postdoc.

Dankwoord

Het doen van onderzoek, het doorlopen van een PhD en alle dingen daarbuiten die veel van ons meemaken zijn een uitdaging, een avontuur. Het is uitdagend, zwaar, uitzichtloos maar vaak ook enerverend, trots-makend en leuk en bovendien een tijd die ik niet had willen missen. Het ging niet altijd makkelijk, dat is *part-of-the-job* in goed Nederlands, maar ik had het nooit kunnen doen zonder de volgende mensen.

Allereerst natuurlijk *Sander van Kasteren*. Toen ik in 2016 begon aan een bachelor stage in jouw groep had ik nooit gedacht dat ik er pakweg 7 jaar later op terug zou kijken als het eigenlijke begin van mijn PhD. Jij gaf mij de kans en het vertrouwen dat ik dingen kon bereiken op een lab, iets waar ik voor die tijd altijd hard van weggerend zou hebben. Dank daarvoor. Gedurende laatste 4-5 jaar hebben we veel discussies gehad hoe een project te vervolgen, waarbij ik het niet altijd (direct) met je eens was, maar uiteindelijk is dit proefschrift er toch gekomen, met werk waar echt nog veel potentie in zit en wat ik nooit had kunnen bereiken zonder dat tomeloze enthousiasme en de onvoorwaardelijke steun van jou. Daarnaast wil ik ook *Zach Armstrong* bedanken voor zijn begeleiding en kritisch oog tijdens het opschrijven van al dit werk. Een frisse blik op soms 4 jaar oude ideeën kan tot veelbelovende nieuwe experimenten leiden.

Het is een cliché, maar onderzoek doe je niet alleen. Misschien werk je wel vaak alleen in het lab, maar de meetings, de koffiepauzes en de lunchtafels zijn bronnen van nieuwe ideeën, ontspanning en de soms broodnodige klaagmuren als er iets niet goed ging. Therefore I would like to thank the following former and current group members: *Alexi, Anouk, Chan, Charlotte, Diana, Eva, Kas, Luuk, Mark, Michel, Mikkel, Mirjam, Nina, Shimrit, Thijmen, Thomas, Tyrza, Ward and Yixuan*. In het bijzonder wil ik Anouk, Diana en Shimrit bedanken. *Anouk* voor alle tips-en-tricks die ik in alle jaren van je heb mogen leren en het luisterend oor dat ik soms echt even nodig had. *Diana* for all the help with statistics and the more relevant experiments at the end of my PhD. Your knowledge about cytokines and in vivo models were not only a win for me, but for the whole group. And *Shimrit*, my partner in crime during the start of my PhD, for starting up the initial experiments with the cytokines that eventually led to this thesis and all the brainstorm sessions we had about getting this to work.

Buiten de groep, maar binnen de universiteit zijn er een aantal mensen die mij altijd geholpen hebben: *Floor, Hedwich, Max* en *Noëlle* voor een luisterend oor of die ene opmerking waardoor ik een project weer in gang kon trekken; *Hellen, Annelies* en *Sebastiaan* voor het verzorgen van faciliteiten zodat experimenten zomaar dezelfde dag gestart konden worden, wat uiteraard niet voor alle labs of universiteiten geldt; *Patrick* en *Anneloes* voor hun hulp bij het kristalliseren en zuiveren van eiwitten.

Zelfs met al deze mensen om mij heen kon ik het niet alleen. Ze zeggen veel handen maken licht werk en dat geldt zeker voor onderzoek. Tijdens de afgelopen jaren heb ik veel studenten mogen begeleiden tijdens hun verschillende stages. Ieder heeft zijn bijdrage kunnen leveren aan deze thesis, zelfs als jouw specifieke werk niet direct de eindversie gehaald heeft. Alles wat jullie gedaan hebben heeft bijgedragen aan dit werk en daar ben ik jullie dankbaar voor: *Maxim, Rick, Daniël, Martin, Sergio, Joris, Göktuğ, Thierry, Irene en Rachel*.

Tot slot, een PhD is geen 9-tot-5 baan. Natuurlijk, je kan thuis geen experimenten uitvoeren, maar al-dan-niet bewust heb je je experimenten altijd in je achterhoofd. En soms is dat vervelend, maar soms leidt dat ook tot nieuwe ideeën. *Yordy, ma, pa, oma, opa, Mark, Jeannette, Joep, Robin, Mariska* en *Geert*: jullie waren er altijd om mijn gedachten te verzetten. *Sanne*, altijd al mijn beste maatje geweest en nu ook nog de enige buiten de universiteit die een beetje wist waar ik met mijn hoofd kon zitten en mij daar ook van kon afleiden. Tot slot *Jorrik*, dankjewel voor je onvoorwaardelijke steun, het aanhoren van mijn dilemma's en het meevieren van (kleine) succesjes. Dit alles was een groot avontuur, en ook al waren de dalen diep en de toppen niet altijd heel erg hoog, ik had het voor geen goud willen missen.